The mechanisms underlying mechanical cell competition and leader cell migration in mammalian epithelia

Katarzyna Kozyrska

University of Cambridge

Girton College

This dissertation is submitted for the degree of **Doctor of Philosophy**

September 2018

Preface

This dissertation is the result of my own work and includes nothing which is the outcome of work done in collaboration except as declared in the Preface and specified in the text.

It is not substantially the same as any that I have submitted, or, is being concurrently submitted for a degree or diploma or other qualification at the University of Cambridge or any other University or similar institution except as declared in the Preface and specified in the text. I further state that no substantial part of my dissertation has already been submitted, or, is being concurrently submitted for any such degree, diploma or other qualification at the University of Cambridge or any other University or similar institution except as declared in the Preface and specified in the text

It does not exceed the prescribed word limit of 60,000 words, as set by the Biological Sciences Degree Committee.

The majority of the data on the role of E-cadherin in leader cell migration and loser cell status has been published in (Wagstaff et al. 2016). The bulk of the data describing the role of p53 and p21 in leader cell migration has been compiled into a manuscript for publication in late 2018 (Kozyrska et al. 2018 – see Appendix 1).

The cell tracking quantifications in Figure V.2I-K and Figure VI.1H-J were performed by Medhavi Vishwakarma in the Piddini lab.

Katarzyna (Kasia) Kozyrska

Acknowledgements

Firstly, I would like to thank Eugenia Piddini for accepting an awkwardly timed student like me into her lab. I am grateful for the supervision, guidance, and advice she offered throughout my PhD. While it has not always been plain sailing, I think I emerged from the process a better scientist and a stronger individual.

Thank you so much to Laura Wagstaff for her supervision at the beginning of my PhD and, more recently, taking the time to give invaluable feedback on this thesis. She has been both a great supervisor and remains a fantastic friend (even though she did delete our group chat at one point to free up space on her phone – brutal!). It is no underestimation that I have learnt everything I know about cell culture from Laura, for which I am eternally grateful. She was also always there to listen, offer advice, and attend painful gym classes.

I would also like to thank the other half of the 'Crazies' duo – Yasmin Paterson – for bringing a bucket and a half of madness into the lab. She was also the first one to put her foot down when it came to a healthy work/life balance and I massively respect her for that.

A huge thank you to Mike Dinan for sharing the #phdlife rollercoaster with me. He was a crucial source of bants and often the only one to understand my lab frustrations. I could also always rely on Mike for a cheeky Nando's, many of which were consumed during the four years to keep us just about sane.

I would like to thank Goli Kolahgar for 'getting down with the kids' once she was stranded in the lab with just Mike and me. Her understanding nature, kindness, and science expertise made her a great 'lab mother' to both of us before our move to Bristol. Her appreciation of a good glass of wine and a chat made her a great friend.

A massive thank you to the other Cambridge ex-Piddinis: Iwo Kuciński, Kathy Oswald, Saskia Suijkerbuijk, and Silvia Vivarelli. They made the lab a warm and welcoming place when I first arrived and they still offer a sympathetic ear for my endless moaning and stories from The Motherland.

On the Bristol side, I would like to thank Lizzie Lawrence and Nat Osborne for being a top-notch lunch crew and a pair of great friends. They have infinitely enriched my time in Bristol, partly by generating some of the most epic face swaps known to man.

I would also like to thank the Cambridge faction of the Piddini lab for playing a key role in me meeting Ash Coleman. I will remain forever grateful to Ash for keeping my Eastern European pessimism in check and offering the best hugs around. I doubt I would have finished this PhD without him. <3

Finally, I would like to thank my family for not asking “are you done with this PhD yet?” too many times. Jokes aside, their love and support (and supplies of coffee and snacks) have made my PhD journey a lot more bearable. Kocham Was!

Abstract

Cell competition is a form of cell-cell signalling that results in the elimination of less fit cells from a tissue by their fitter counterparts. I take advantage of an established *in vitro* model of cell competition using Madin-Darby canine kidney (MDCK) cells to shed insight into the molecular basis of cell competition in epithelial cells. In this system, silencing of the tumour suppressor *scribble* (*scrib*^{KD}) results in a 'loser' phenotype whereby *scrib*^{KD} cells are specifically eliminated from the monolayer by surrounding wild-type cells. More specifically, *scrib*^{KD} cells are compacted into tight clones through activation of a directed, collective migration in the wild-type population: *scrib*^{KD} are 'mechanical losers' and delaminate and die due to an intrinsic hypersensitivity to high cell density. Remarkably, p53 activation is both necessary and sufficient for this mechanical loser cell status.

I first investigate the role of E-, N-, and P-cadherin in the directed migration between *scrib*^{KD} and wild-type cells and in *scrib*^{KD} cell loser status. I show that differential expression of E-cadherin between *scrib*^{KD} losers and wild-type winners is required but not sufficient for directed migration and has no impact on loser cell status. I also show that elevation of neither E-cadherin nor N-cadherin is sufficient to induce directed migration or loser status, but that P-cadherin may play a role in both.

I next focus on translating findings about the molecular details of competition from the *scrib*^{KD} set-up into a system where p53 differences alone drive the formation and elimination of mechanical losers. I show that the ROCK – P-p38 – p53 pathway activated in response to mechanical compaction in *scrib*^{KD} cells is conserved in p53-driven losers.

In the latter part of my thesis, I characterise the directed migration observed during MDCK competition by drawing parallels to canonical leader-follower migration. Canonical leader cells emerge when epithelial sheets are wounded and, by becoming migratory, drive collective cell migration of follower cells, which results in wound closure. It was not known what confers the leader cell fate. I show that p53 and its effector p21 (and potentially other cyclin-dependent kinase inhibitors) are the key drivers of leader cell migration. I demonstrate that p53-induced leaders use the same molecular pathways that have been shown to drive leader cell migration during wound healing and, in fact, p53 and p21 are also elevated in leaders generated by wounding. Importantly, I establish that p53 activity drives efficient wound closure. Lastly, I show that leader cells are often eliminated by cell competition in the final stages of wound closure, as their elevated p53 mediates their hypersensitivity to density. The model incorporating these data proposes that cellular damage during wounding generates cells with elevated p53, which become leaders and drive wound healing, but these are then cleared once the wound is closed because their high p53 levels cause them to become mechanical losers.

Table of contents

Chapter I: Introduction

Cell competition

Cell competition is a form of cell-cell communication conserved from arthropods to mammals, the result of which is the specific elimination of less fit cells from a tissue. Cell competition is triggered when two cell populations of differing fitness levels come into contact: 'loser' (less fit) cells are removed from the tissue usually, but not exclusively, through induction of apoptosis by 'winner' (more fit) cells (Figure I.1) (reviewed in Di Gregorio et al. 2016). Following loser elimination, tissue homeostasis is maintained by winner cells undergoing compensatory proliferation or hypertrophy to replace the lost cells or fill the space vacated by losers, respectively (de la Cova et al. 2004; Simpson & Morata 1981; Tamori & Deng 2013). Importantly, loser populations can survive in a homotypic situation, although they often display slower proliferation rates (reviewed in Di Gregorio et al. 2016).

Elimination of weak, damaged, or otherwise potentially harmful cells from a tissue through cell competition allows re-population by healthy, wild-type cells both during development (Morata & Ripoll 1975) and in adult tissue maintenance (Kolahgar et al. 2015). It has therefore been suggested that cell competition helps maintain overall tissue health and can have a role in delaying the onset of pathologies and ageing. On the flipside, cells harbouring some tumour-promoting mutations (e.g. high levels of Myc) exhibit a 'super-competitor' phenotype whereby they outcompete their wild-type neighbours (Figure I.1) (Moreno & Basler 2004; de la Cova et al. 2004; Sancho et al. 2013; Clavería et al. 2013). Similar observations have highlighted the potential importance of cell competition in cancer and this has recently been demonstrated *in vivo*: tumour growth in the adult *Drosophila melanogaster* (*Drosophila*) gut is accelerated due to elimination of wild-type tissue by adenomas resulting from mutations in *adenomatous polyposis coli* (*APC*) genes (Suijkerbuijk et al. 2016).

Despite the discovery of cell competition in the 1970s (Morata & Ripoll 1975), its mechanistic basis is only beginning to be understood. It remains unclear how cells compare fitness within a tissue and how detection of loser cells translates into their

elimination. In the following sections, I will summarise the current knowledge of the field that led up to my PhD project and discuss the importance of cell competition in both physiology and pathology.

Minute cell competition

The first report of cell competition came from studies in *Drosophila* wing imaginal discs (Morata & Ripoll 1975). The authors were investigating *Minute* genes, which encode ribosomal proteins: *Minute* mutations result in impaired translation and slower growth. While homozygous *Minute* mutations are lethal, heterozygous *Minute* flies ($Minute^{+/-}$) are viable, if slightly developmentally delayed compared to wild-type animals. Clones of $Minute^{+/-}$ tissue induced in a wild-type background are much smaller than would be predicted by the slower proliferation of $Minute^{+/-}$ cells alone. In fact, it was shown that $Minute^{+/-}$ cells undergo apoptosis and are actively eliminated when surrounded by wild-type cells (Morata & Ripoll 1975). Conversely, wild-type clones in $Minute^{+/-}$ wing discs can take over the entire compartment at the expense of $Minute^{+/-}$ tissue (Simpson & Morata 1981). $Minute^{+/-}$ cells can therefore be classed as loser cells: while viable in a homotypic environment, they are less fit and eliminated by the fitter winner cells (in this case, wild-type cells) around them.

Minute competition highlights two additional important features of cell competition. Firstly, cellular fitness is relative, as slower growing *Minute* mutant cells can be outcompeted by faster growing cells originating from a distinct, milder *Minute* mutation. Secondly, loser and winner cells must be in close proximity for cell competition to occur, but proximity itself is not sufficient for competition, as competition does not cross the anterior-posterior compartment boundary in *Drosophila* wing discs (Simpson & Morata 1981).

Molecularly, $Minute^{+/-}$ cells have a reduced ability to transduce decapentaplegic (Dpp, the *Drosophila* homologue of bone morphogenetic proteins, BMPs) signalling in the presence of wild-type cells, which results in the upregulation of the c-Jun N-terminal kinase (JNK) pathway (Moreno et al. 2002). However, it was later shown that the JNK pathway is

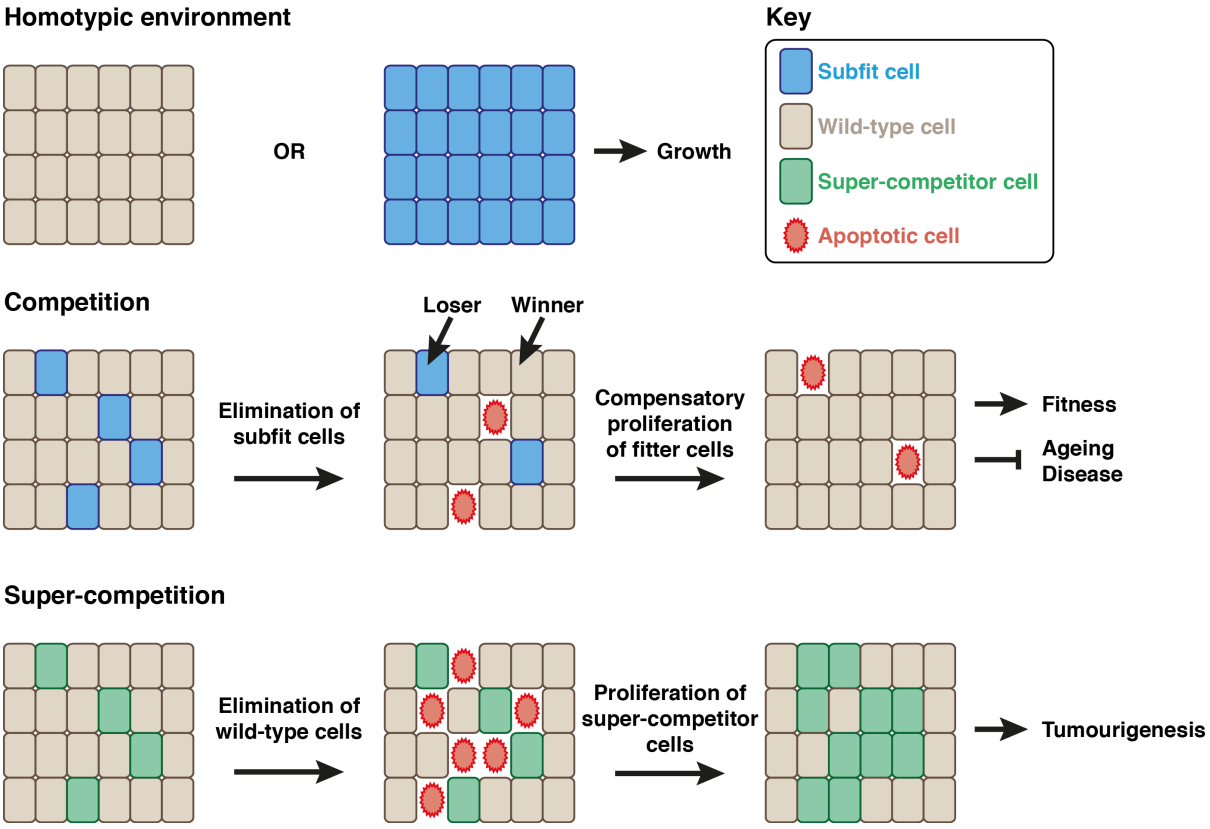

Figure I.1: Schematic representation of cell competition. Top panel: both wild-type cells (beige) and cells harbouring loser mutations (blue) can thrive in a homotypic environment. Middle panel: upon confrontation with fitter wild-type cells, less fit loser cells are eliminated through the induction of apoptosis. Elimination of losers is accompanied by compensatory proliferation/hypertrophy of winners. Bottom panel: super-competitor cells (green) are fitter than wild-type cells and induce elimination of the latter from the tissue.

Adapted from (Di Gregorio et al. 2016).

constitutively active in *Minute*$^{+/-}$ cells, even prior to competition (Tamori & Deng 2011; Kucinski et al. 2017). JNK upregulation in *Minute*$^{+/-}$ losers was originally thought to simply provide a pro-apoptotic signal (Moreno et al. 2002), but it has now become apparent that JNK also stunts the proliferation of *Minute*$^{+/-}$ cells, putting them at a further growth disadvantage on top of their translational impairment (Kucinski et al. 2017). Simultaneously, JNK activity drives secretion of Unpaired ligands, which are sensed by surrounding wild-type cells promoting their compensatory proliferation. Interestingly, oxidative stress has shown to be the underlying cause of the loser status of both *Minute*$^{+/-}$ and a functionally distinct loser, *mahjong* cells (Kucinski et al. 2017).

While *Minute* competition remains the archetypal model of cell competition, many more mutations have since been identified to play a role in cell competition. Pathways that trigger cell competition can be broadly classified into metabolic or structural pathways, although there are also some outliers. It is now becoming apparent that there are most likely many mechanisms of cell competition, which all lead to the common outcome of loser cell elimination, although this is still somewhat controversial in the field.

Metabolic cell competition

Impaired translation of *Minute*$^{+/-}$ cells can be classed as a metabolic defect, as mutant cells have lower anabolic activity than their neighbours. In fact, many mutations reducing a cell's anabolic potential also confer the loser status (reviewed in Amoyel & Bach 2014). This makes perfect sense at an organismal level, as cells with defective metabolism may be detrimental to the development or function of the whole tissue or organ, and their elimination is therefore beneficial to promote overall health. Interestingly, cells with overactive anabolic pathways often become super-competitors and can outcompete surrounding wild-type tissue, suggesting that metabolic potential is a key determinant of cellular fitness.

One important metabolic regulator in both flies and mammals is the transcriptional factor Myc, which promotes a plethora of processes, including cell growth and proliferation, ribosome and mitochondrial biogenesis, as well as glucose and glutamine metabolism (Dang 2013). Cells with lower levels of Myc are outcompeted by cells with higher levels

of Myc in a similar way to the interaction between *Minute*$^{+/-}$ and wild-type cells. Strikingly, cells with higher but non-tumourigenic levels of Myc have the ability to outcompete surrounding wild-type tissue in a process known as super-competition (Johnston et al. 1999; de la Cova et al. 2004; Moreno & Basler 2004). Importantly, differential growth rates are not sufficient to trigger cell competition, as wild-type cells juxtaposed with cells overexpressing growth-promoting factors Dp110 or CDK4/Cyclin D are not outcompeted (de la Cova et al. 2004). Mosaic Myc activation has also been shown to induce cell competition in mammalian models, including *in vivo* during early mouse development (Clavería et al. 2013; Sancho et al. 2013).

Other metabolic pathways have been shown to have cell competition phenotypes similar to Myc, whereby their inactivation creates loser cells when juxtaposed with wild-type cells, while their over-activation results in a super-competitor phenotype that eliminates surrounding wild-type tissue. Some examples include pathways regulating proliferation, growth, and patterning: Janus kinase/signal transducer and activator of transcription (JAK/STAT); Ras/Raf/mitogen-activated protein kinase (MAPK); and Wnt (reviewed in Amoyel & Bach 2014).

Interestingly, Myc activation lies downstream of many metabolic pathways that induce cell competition. For instance, while *ras* mutant clones are eliminated from mosaic *Drosophila* wing discs, this can be partially rescued by expression of Myc (Prober & Edgar 2000). Similarly, cells with misregulated Hippo pathway signalling, which is responsible for organ size control, are super-competitors because the pathway effector Yorkie (*Drosophila* homologue of YAP/TAZ) directly upregulates Myc expression (Ziosi et al. 2010; Neto-Silva et al. 2010). In contrast, Wnt pathway activation results in lower Myc than the surrounding tissue and yet still confers the super-competitor phenotype (Duman-Scheel et al. 2004; Vincent et al. 2011), while JAK/STAT activation partially rescues Myc mutant clone outcompetition (Rodrigues et al. 2012). Wnt and JAK/STAT pathways therefore affect cell competition in a Myc-independent manner. Taken together, these experiments suggest that there are multiple parallel pathways that define a cell's fitness and drive competitive interactions.

Structural cell competition

The second major class of factors involved in cell competition includes molecules involved in the determination and maintenance of apico-basal polarity, including Lethal giant larvae (Lgl), Scribble, Discs large (Dlg), and Mahjong. Lgl, Scribble, and Dlg are classed as neoplastic tumour suppressors in *Drosophila*, as their loss results in disorganisation of the epithelium, differentiation failure, and neoplastic growth (reviewed in Clavería & Torres 2016). Juxtaposition of *lgl*, *scribble*, and *dlg* mutant cells with wild-type tissue is sufficient to limit the growth and lead to the elimination of the mutant cells. Interestingly, while Mahjong lies downstream of Lgl and *mahjong* mutant cells are also losers, loss of Mahjong does not affect cell polarity (Tamori et al. 2010). In fact, as mentioned earlier, the underlying cause of loser status of *mahjong* cells is oxidative stress rather than a loss of polarity (Kucinski et al. 2017).

scribble competition was the initial focus of my PhD. As such, I further discuss the molecular details of this type of competition in subsequent sections in this chapter.

p53 in cell competition

The tumour suppressor p53 coordinates cellular responses to many types of stresses, including DNA damage, nutrient deprivation, and hypoxia. The best studied effects of p53 activation are cell cycle arrest, senescence, and apoptosis. Four p53 molecules form the active p53 tetramer, which exerts its downstream effects mainly by modulating transcription, although it is becoming increasing clear that p53 also has transcription-independent roles in the cytoplasm and mitochondria. Because of its widespread influence, p53 activity is tightly regulated through multiple mechanisms e.g. post-translational modifications, subcellular localisation, and protein stability. One of the key p53 regulators is the E3 ubiquitin ligase mouse double minute 2 (Mdm2), which suppresses p53 activity by continually targeting it for degradation in the absence of cellular stress (reviewed in Vousden & Lane 2007).

Differences in p53 activity can trigger cell competition (Figure I.2). For example, when a mixture of sub-lethally irradiated (90%) and non-irradiated (10%) bone marrow cells

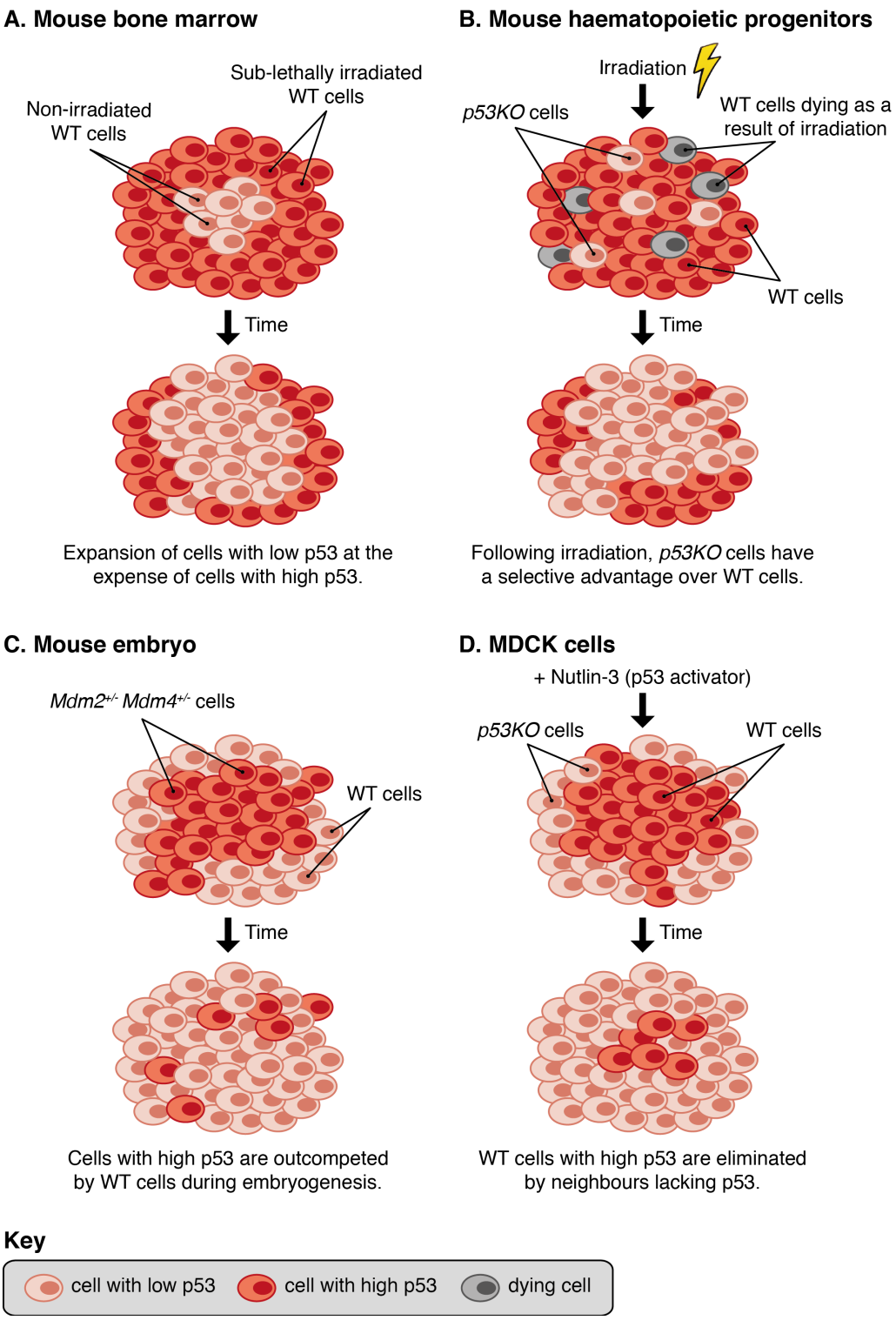

Figure I.2: Diagram summarising the role of p53 in various models of cell competition. (**A**) Non-irradiated (low p53) mouse bone marrow cells can colonise more of the tissue at the expense of irradiated cells with higher p53 levels (Bondar & Medzhitiv 2010). (**B**) Irradiation directly induces the death of a sub-

population of wild-type (WT) haematopoietic cells, while simultaneously conferring a selective advantage on cells lacking p53 over the surviving wild-type cells. This promotes the tissue colonisation ability of cells mutant for p53 (Marusyk et al. 2010). (**C**) Cells deficient in p53 inhibitors Mdm2 and Mdm4 have elevated p53 levels and are eliminated by wild-type tissue (low p53) during mouse embryogenesis (Zhang et al. 2017). (**D**) In the presence of Mdm2 inhibitor Nutlin-3, wild-type MDCK cells activate p53 while *p53KO* cells maintain low p53. Over time, wild-type MDCKs are eliminated by the surrounding *p53KO* cells (Wagstaff et al. 2016).

---

was transplanted into a lethally irradiated donor mouse, the contribution of non-irradiated cells to the tissue increased over several weeks to approximately 40%. The absolute numbers of bone marrow cells were comparable between experimental (irradiated/non-irradiated mixture) and control (irradiated cells only) conditions, suggesting that the expansion of the non-irradiated population happens at the expense of the irradiated cells. The outcompetition of irradiated cells is mediated by p53, as the 90 : 10 seeding ratio of irradiated heterozygous p53 mutant cells to non-irradiated wild-type cells was still maintained at the end of the experiment. Moreover, genetic mosaics of bone marrow cells with a dominant negative *p53* allele have a competitive advantage over wild-type cells following irradiation (Bondar & Medzhitiv 2010). Similarly, irradiation confers a selective advantage on haematopoietic cells deficient in p53 and promotes their tissue colonisation ability (Marusyk et al. 2010). Unlike in canonical models of competition, apoptosis is not induced in loser cells in the mouse bone marrow system: instead, losers adopt a senescence-like state and are replaced over time by fitter cells (Bondar & Medzhitiv 2010). Importantly, p53-mediated competition in these models is only triggered following an external stressor such as irradiation.

p53-mediated competition has also recently been reported in the developing mouse embryo. In this system, mild p53 activation triggered by partial loss of p53 regulators Mdm2 and Mdm4 is sufficient to confer a competitive disadvantage on mutant cells in mutant/wild-type mosaic embryos (Zhang et al. 2017). Another study later showed that elevated p53 in mouse embryos represses the mechanistic target of rapamycin (mTOR) pathway, a crucial growth and metabolism regulator. Loss of mTOR signalling in loser cells is necessary and sufficient for their elimination. Interestingly, excessive mTOR activation results in a super-competitor phenotype, suggesting it is a key determinant of relative fitness levels (Bowling et al. 2018).

Importantly, the Piddini lab recently showed that p53 activation is the underlying cause of the loser status of MDCK cells lacking *scribble*. In fact, mild p53 elevation itself is sufficient to confer hypersensitivity to cell density on otherwise wild-type MDCK cells and this results in their elimination by surrounding cells with lower p53 in a process termed 'mechanical cell competition' (Wagstaff et al. 2016). I will further discuss these findings in subsequent sections, as they are fundamental to my PhD work. Please note that I personally contributed to the (Wagstaff et al. 2016) publication: the majority of the data

on the role of E-cadherin in leader cell migration and loser cell status was generated by me and is described in this thesis.

Interestingly, MDCK and mouse intestinal epithelial cells harbouring oncogenic p53 variants with mutations in the DNA-binding domain (e.g. p53 R175H) are competitively eliminated from wild-type epithelia. Cells with mutant p53 are basally extruded from the monolayer and this is often accompanied by nuclear and cell body fragmentation. However, MDCKs harbouring p53 mutations are not eliminated from Ras^{V12}-transformed epithelia. This is particularly striking considering that p53 mutations are not usually detected at the initial stage of carcinogenesis, but only in mid to late stages. Cell competition may therefore play an instructive role in the sequence of cancer progression: the order in which oncogenic mutations appear could determine whether mutant cells can be cleared through cell competition or not (Watanabe et al. 2018).

While most studies have focussed on the role of p53 in loser cells, p53 has also been shown to play a vital role in winners. As discussed previously, Myc overexpression triggers a super-competitor phenotype in *Drosophila*. In a non-competitive *Drosophila* cell culture model, Myc overexpressing cells increase glycolysis and concomitantly activate p53, which acts to balance their metabolism and promote fitness by boosting the more energy-efficient oxidative phosphorylation. When confronted with wild-type cells, Myc super-competitors undergo additional p53-dependent changes: they further boost glycolysis, gain a proliferative advantage, and secrete a 'killing factor' to eliminate surrounding wild-type cells. Crucially, p53 activity is necessary for Myc overexpressing cells to detect the change from a homotypic environment to a competitive one (de la Cova et al. 2014).

Molecular mechanisms of cellular fitness comparison

Cell competition can be divided into three phases: a trigger that confers a fitness disadvantage on one cell population, a fitness comparison stage that leads to the recognition of losers, and an execution stage whereby losers are eliminated and winners undergo compensatory proliferation/hypertrophy. In previous sections, I have described some of the pathways that label cells as less fit than their neighbours, and hence confer the loser status. Below, I discuss three models of cellular fitness comparison: surface

contact, diffusible signal, and mechanical models (Figure I.3). These are not exhaustive and may also work in combination.

(i) Surface contact model

In the surface contact model for fitness comparison, molecules on a cell's surface report its fitness status to its neighbours. Evidence for this model first came from studies in *Drosophila* wing imaginal discs. The authors showed that all cells express an isoform of Flower (fwe^{ubi}), a transmembrane protein proposed to be a calcium ion channel, while loser cells simultaneously express two further isoforms ($fwe^{Lose\text{-}A}$ and $fwe^{Lose\text{-}B}$). The relative amounts of fwe^{ubi} and the loser isoforms of Flower determine which population will be eliminated. Indeed, Flower is required for *Minute* competition and Myc super-competition (Rhiner et al. 2010).

Importantly, upregulation of Flower isoforms only occurs following confrontation between winner and loser cells: it is not a pre-existing difference prior to competition onset. Pre-existing differences in the surface proteomes of loser and winner cells have not yet been demonstrated to constitute a fitness comparison mechanism, but this remains an attractive hypothesis, especially considering cell-cell contact has been shown to be required for loser cell elimination in several models of cell competition (Clavería et al. 2013; Portela et al. 2010; Wagstaff et al. 2016; Levayer et al. 2015; Li & Baker 2007). That said, others have shown that direct cell-cell contact is not required for cell competition using both *in vivo* (de la Cova et al. 2004) and *in vitro* models (Senoo-Matsuda & Johnston 2007; Sancho et al. 2013).

(ii) Diffusible signal model

In the diffusible signal model, a cell's fate is determined by its response to secreted factors. One example of this is Spätzle, a diffusible ligand that activates the Toll-related receptor (TRR). In *Drosophila* wing discs, TRR activation is necessary for the elimination of *Minute* cells and those with low Myc levels. In fact, loser cells express more TRR and are hence more responsive to Spätzle, which leads to higher nuclear factor kappa-light-chain-

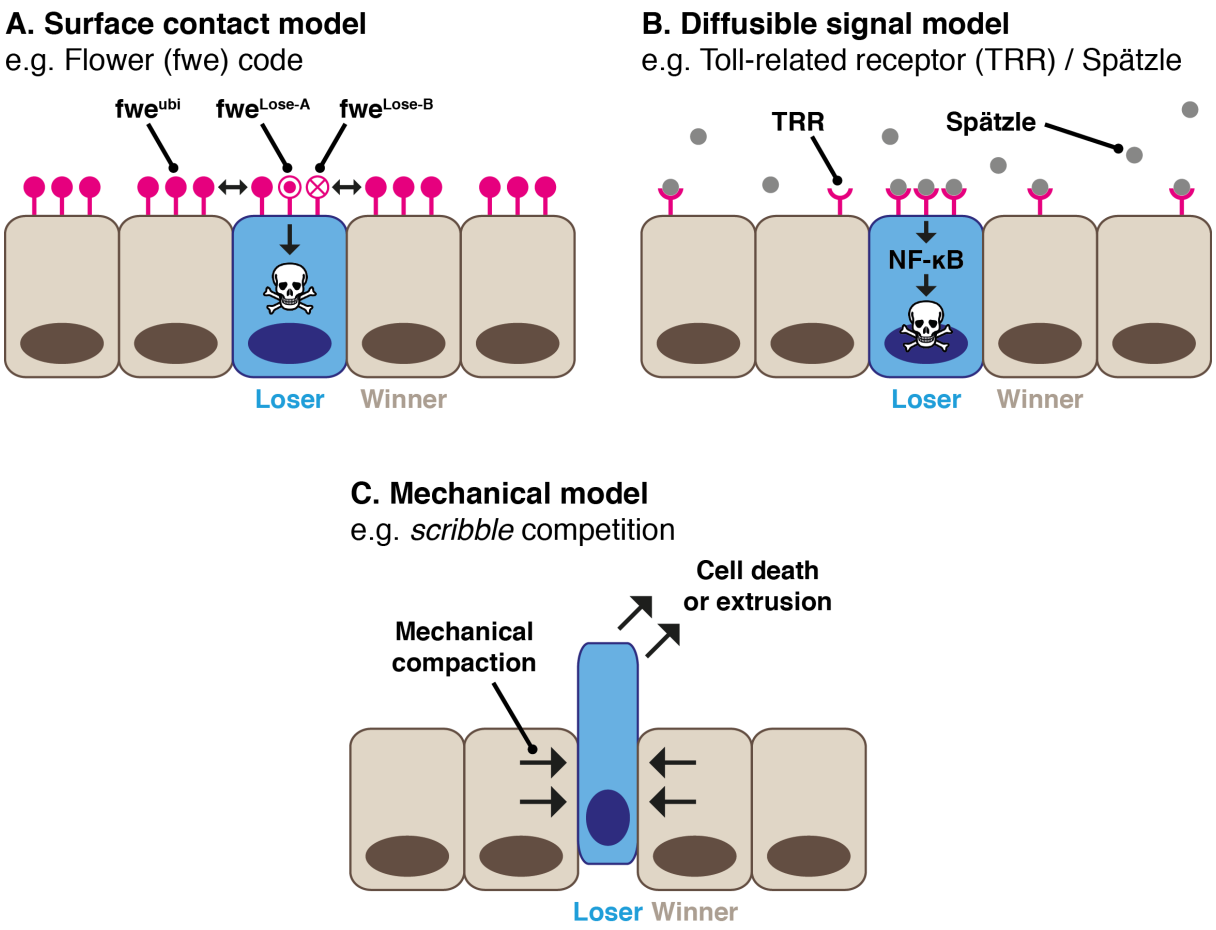

Figure I.3: Schematic representation of three models of cellular fitness comparison. (**A**) Surface contact model. Example: differences in the expression pattern of Flower (fwe) isoforms between winner cells (beige) and cells harbouring loser mutations (blue) result in the elimination of the mutant cells. (**B**) Diffusible signal model. Example: losers express more Toll-related receptor (TRR) and are hence more responsive to Spätzle, a diffusible ligand that activates TRR. TRR activation leads to higher NF-κB activity, which results in loser cell apoptosis. (**C**) Mechanical model. Example: mechanical compaction of cells lacking *scribble* leads to their death and delamination.

Adapted from (Di Gregorio et al. 2016).

enhancer of activated B cells (NF-κB) activity. NF-κB is a protein complex involved in the cellular response to stress; in the context of competition, NF-κB activity leads to loser cell apoptosis (Meyer et al. 2014).

Similarly, transwell experiments in *Drosophila* cell culture demonstrated that contact is not required for elimination of wild-type cells by cells overexpressing Myc. Furthermore, conditioned media from competing cultures, but not homotypic cultures of cells overexpressing Myc, is sufficient to induce wild-type cell death while boosting the proliferation of winner cells. This implies that the two populations must sense each other before the competition 'signal' is produced: loser cells respond to it by undergoing apoptosis, while winners increase their proliferation (Senoo-Matsuda & Johnston 2007). The identity of this signal remains unknown.

Others have argued against the diffusible signal model. In the early mouse embryo, for example, conditioned media from cultures of competing Myc-overexpressing and wild-type cells is not sufficient to trigger loser cell apoptosis (Clavería et al. 2013). This further demonstrates that, depending on the context, there are most likely multiple mechanisms mediating cell competition.

(iii) Mechanical model

The third aspect that may determine cellular fitness is a cell's response to mechanical stress. Epithelia must at all times maintain continuous, cohesive sheets, so elimination of cells that disrupt this morphology, such as mechanically weak or supernumerary cells, is a beneficial strategy. In fact, epithelia are capable of extruding live cells in response to overcrowding; this has been shown in a number of different systems, including *Drosophila* imaginal discs, mammalian cell culture, and zebrafish development (Marinari et al. 2012; Eisenhoffer et al. 2012). It remains unclear why some cells are preferentially extruded over others. One possibility could be that cells with weaker attachments to the substrate are the ones selected for extrusion.

Mechanical cell competition was recently demonstrated in MDCK cells (Wagstaff et al. 2016), while mechanical super-competition has been described in the *Drosophila* pupal

notum (Levayer et al. 2016). Please refer to the "*scribble* competition in MDCK cells" section in this chapter for a closer description of these findings.

Roles of cell competition: from quality control to cancer

During an organism's lifetime, each of its constituent cells is subjected to different biochemical and physical stresses. Each cell thus accumulates a unique set of insults, some of which may be detrimental to its fitness. Cell competition leads to the elimination of these less fit cells from tissues and can therefore be regarded as a quality control mechanism that promotes the overall health of the organism. In *Drosophila*, cell competition has been implicated in improving tissue fitness during development by removing slowly proliferating cells (Moreno et al. 2002), regulating organ size by changing the cellular composition of a tissue without affecting its size (de la Cova et al. 2004; Moreno & Basler 2004), and in adult tissue homeostasis to maintain tissue health and delay the onset of ageing (Kolahgar et al. 2015; Merino et al. 2015). It has also been proposed that cell competition may act as a protective mechanism against aneuploidy (Sancho et al. 2013).

Cell competition has also been shown to play a role in tissue regeneration *in vivo* in mammalian models e.g. in the mouse heart (Villa del Campo et al. 2014) and the rat liver (Oertel et al. 2006). In the latter study, for example, it was shown that rapidly proliferating foetal liver cells transplanted into an adult animal with partial hepatectomy contribute at a much higher proportion to the regeneration response. This is not just due to faster proliferation of the foetal cells but also through induction of apoptosis in the host liver cells (Oertel et al. 2006). Enhancing cell competition exogenously is therefore an attractive therapeutic goal, which could be used to promote self-regeneration or boost the success of cell replacement strategies.

Cell competition can have a tumour suppressive role in promoting tissue fitness. As discussed, loss of polarity factors results in neoplastic overgrowth but polarity-defective cells are losers in a heterotypic context and are cleared from the epithelium. What is more, overexpression of Ras^{V12} or v-Src oncogenes in MDCK cells leads to cell transformation, which is thought to be the first step of carcinogenesis (Hogan et al. 2009; Kajita et al. 2010). Strikingly, Ras^{V12}- or v-Src-transformed cells are extruded from the epithelium by

surrounding wild-type MDCKs in a competitive 'epithelial defence against cancer' mechanism (Ohoka et al. 2015). That said, extrusion of Ras^{V12} cells can be independent of their death: basally extruded cells can survive and invade surrounding tissues. In fact, additional factors like loss of E-cadherin or reduced Cdc42 activity can promote basal extrusion of Ras^{V12}-transformed cells and therefore boost their invasive potential (Hogan et al. 2009). This highlights the context-dependence of cell competition as a tumour suppressor and demonstrates how malignant cells may be able to evade cell competition in the presence of secondary oncogenic mutations.

There are also examples of cell competition being able to promote tumour formation independently of secondary mutations. For instance, loss of *APC*, a Wnt pathway inhibitor, is highly correlated with human colon cancers and also leads to formation of intestinal adenomas in *Drosophila* (Wang et al. 2013). The Piddini lab has recently shown that adenoma growth in the *Drosophila* gut is dependent on the *APC* tumour cells being able to outcompete the surrounding wild-type tissue. Importantly, preventing cell competition from taking place by expressing apoptosis inhibitors in the wild-type cells is sufficient to constrain adenoma growth (Suijkerbuijk et al. 2016). Similar observations were made in *Drosophila* wing discs, where co-expression of epidermal growth factor receptor (EGFR) and microRNA miR-8 gives rise to aggressive tumours with super-competitor qualities. The growth of these tumours can be restricted by inhibiting apoptosis in the tissue (Eichenlaub et al. 2016). Together, these findings suggest that removal of wild-type tissue by apoptosis is not a by-product of tumour expansion but is actively required for it.

scribble **competition in** ***Drosophila***

Just like Dlg and Lgl, Scribble is a polarity factor localised asymmetrically in wild-type epithelia. In *Drosophila*, the Scribble protein is enriched at the cell cortex at septate junctions (*Drosophila* homologue of mammalian tight junctions), which are localised basally to the adherens junctions (Bilder & Perrimon 2000). Scribble is a large protein containing several protein-protein interaction domains, many of which play a role in the establishment and maintenance of its asymmetrical localisation; it is classified as a LAP, a protein containing leucine-rich repeats (LRR) and PSD-95, ZO-1 and Disc large (PDZ) domains (reviewed in Humbert et al. 2008).

Homozygous *scribble* mutant (*scribble*$^{-/-}$) larvae develop normally due to maternal stores of the wild-type Scribble protein. However, once these supplies are exhausted, *scribble* mutant cells, while viable, lose their polarity and regular shape. As development continues, mutant cells become multi-layered and have difficulties differentiating, which results in overproliferation and tumour formation: this phenotype classifies *scribble* as a neoplastic tumour suppressor. Ultimately, *scribble* mutant larvae cannot progress through pupariation and die as giant larvae (Bilder & Perrimon 2000).

Importantly, while *scribble* mutant clones in *Drosophila* imaginal eye discs show the same overgrowth phenotype as homotypic mutant tissues, their growth is halted through JNK-dependent induction of apoptosis by the surrounding wild-type tissue. By the time the larvae reach adulthood, very few *scribble*$^{-/-}$ cells remain in the mosaic eye, as they have been eliminated through cell competition. Strikingly, outcompetition of *scribble*$^{-/-}$ cells in a mosaic context can be prevented by concomitant expression of oncogenic versions of genes such as Ras or Notch, highlighting the importance of the tumour microenvironment in cancer progression (Figure I.4) (Brumby & Richardson 2003; Pagliarini & Xu 2003).

It was later shown that Eiger, a tumour necrosis factor (TNF) superfamily ligand, is required for the JNK-dependent elimination of *scribble*$^{-/-}$ cells. *scribble* mutant cells show increased rates of endocytosis specifically when surrounded by wild-type neighbours. One of the endosome cargos in *scribble* mutant cells is in fact Eiger, which also co-localises with phosphorylated (activated) JNK staining in endosomes (Igaki et al. 2009). Endosomes have been previously described as hubs that cells exploit to compartmentalise and regulate/enhance signalling (Miaczynska et al. 2004). The authors therefore propose that increased endosomal uptake of Eiger in *scribble*$^{-/-}$ cells results in enhanced Eiger-JNK signalling that is responsible for triggering their apoptosis, and ultimately elimination, in a competition scenario (Igaki et al. 2009).

That said, others argue that apoptosis of *scribble* mutant cells in heterotypic tissues is not sufficient on its own to overcome their overproliferation phenotype and result in their complete elimination (Chen et al. 2012). The enhanced proliferation of *scribble*$^{-/-}$ cells is due to overactivation of Yorkie, a pro-growth transcriptional coactivator whose activity is suppressed by activation of the Hippo pathway (Doggett et al. 2011). Chen et al. go on to show that JNK signalling in *scribble*$^{-/-}$ cells suppresses their Yorkie activity during

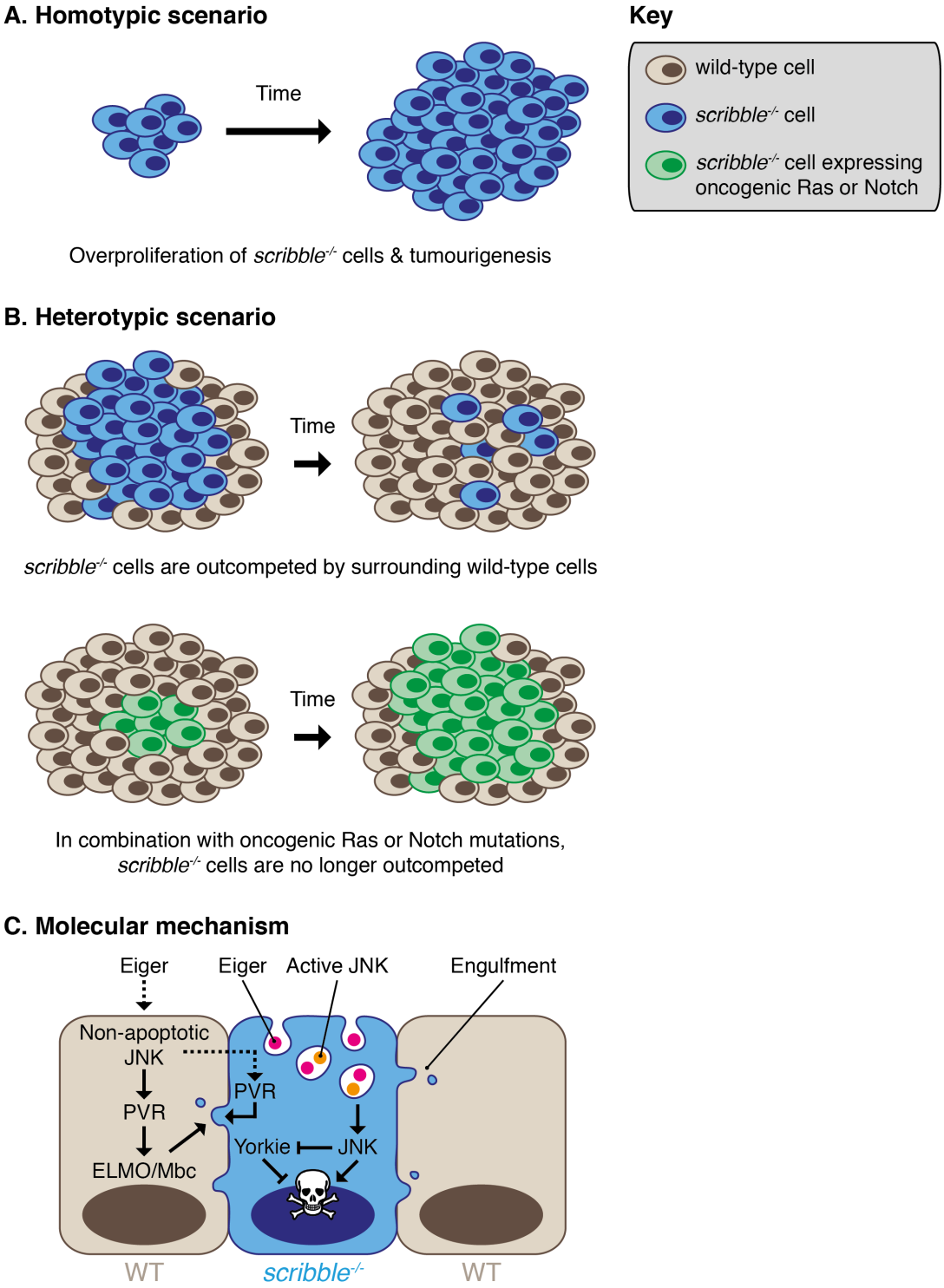

Figure I.4: Diagram summarising the behaviour of *scribble*$^{-/-}$ cells in *Drosophila* cell competition models. (**A**) In *Drosophila* larvae, homotypic populations of *scribble*$^{-/-}$ cells overproliferate, which leads to

tumour formation (Bilder & Perrimon 2000). (**B**) In a mixed population of wild-type and *scribble*$^{-/-}$ cells in *Drosophila* imaginal eye discs, *scribble* mutant cells are eliminated through cell competition. *scribble*$^{-/-}$ cells harbouring oncogenic Ras or Notch mutations are no longer outcompeted and drive tumourigenesis (Brumby & Richardson 2003; Pagliarini & Xu 2003). (**C**) *scribble*$^{-/-}$ cells display higher rates of endocytosis in the presence of wild-type cells. This drives increased endosomal uptake of Eiger, which boosts JNK signalling (Igaki et al. 2009). JNK directly triggers *scribble*$^{-/-}$ cell apoptosis, while simultaneously inhibiting pro-growth factor Yorkie. Yorkie suppression stunts *scribble*$^{-/-}$ cell proliferation and is essential for their elimination (Chen et al. 2012). Eiger-dependent, non-apoptotic JNK signalling is also required in the wild-type population, where it upregulates PVR in both cell populations. Increased PVR expression drives the activity of ELMO/Mbc, which promotes the engulfment of *scribble*$^{-/-}$ cells by their wild-type neighbours (Ohsawa et al. 2011).

competition and this suppression is essential for *scribble*$^{-/-}$ cell elimination (Chen et al. 2012). Oncogenes can also modulate Yorkie activity in *scribble*$^{-/-}$ cells, but this yields a very different outcome. For example, combining *scribble* mutation with an active form of the Ras oncogene (Ras^{V12}) stops their outcompetition. This is most likely because Ras^{V12} feeds into Yorkie activation and both of these proteins boost Myc levels, which increases cellular fitness (Brumby & Richardson 2003; Pagliarini & Xu 2003).

Eiger-dependent JNK signalling is also required in wild-type cells during *scribble* competition. Wild-type cells surrounding *scribble* mutant clones activate non-apoptotic JNK, which in turn upregulates the *Drosophila* PDGF/VEGF receptor (PVR) in both populations. The JNK-PVR signalling then induces the activity of engulfment and cell motility (ELMO) and myoblast city (Mbc), which are proteins involved in the cytoskeletal rearrangement during phagocytosis. This results in the mutant population being actively eliminated through engulfment by the wild-type population (Figure I.4). It is currently unknown if JNK activation in winners and losers is part of the same pathway (Ohsawa et al. 2011).

Scribble in mammalian models and cancer

There is only one homolog of *Drosophila scribble* in mammals, encoded by the *SCRB1* gene (Su et al. 2013). In Madin-Darby canine kidney (MDCK) cells, the Scribble protein is localised at adherens junctions and extends more basally from them along the basal and lateral domains (Navarro et al. 2005). Unlike in *Drosophila*, knockdown of *scribble* (*scrib*^{KD}) in MDCKs does not cause polarity defects (Qin et al. 2005). This is also largely consistent with observations from two- and three-dimensional cultures of *scrib*^{KD} human mammary epithelial MCF10A cells, where no or very subtle polarity defects are reported (Dow et al. 2007; Zhan et al. 2008). Also in contrast to the *Drosophila* system, MCF10A cells lacking *scribble* do not exhibit increased proliferation rates (Zhan et al. 2008). Similarly, *scrib*^{KD} MDCK cells do not form multi-layered structures and in fact have slower division rates than wild-type cells (Qin et al. 2005; Norman et al. 2012; Wagstaff et al. 2016).

Despite these differences, both *Drosophila* and mammalian Scribble function as tumour suppressors *in vivo*. Loss of *scribble* results in hyperplastic growth within the mouse mammary gland and prostate. In mammary epithelia, *scribble* loss results in abnormal epithelial morphogenesis and, combined with hyperproliferation caused by an oncogene, it can also inhibit apoptosis to promote tumorigenesis (Zhan et al. 2008). In prostate epithelia, loss of *scribble* promotes overproliferation through de-repression of the Ras/MAPK cascade (Pearson et al. 2011).

Mislocalisation and deregulation of Scribble have been associated with several human epithelial cancers, for example colorectal and breast cancer (Gardiol et al. 2006; Navarro et al. 2005). Scribble itself is a target for ubiquitin-mediated degradation during high-risk human papilloma virus (HPV) infection, which is linked to a high percentage of uterine cervical carcinomas (Nakagawa & Huibregtse 2000; Burd 2003). Taken together, these data support a tumour suppressive role for *scribble* both in mammalian *in vivo* models and in cancer.

scribble competition in MDCK cells

MDCK cells were first isolated in 1958 by Madin and Darby from kidney tubules of a phenotypically normal female cocker spaniel, although this does not seem to have been published (Dukes et al. 2011). MDCKs have a regular, cobblestone morphology *in vitro* and can be grown as flat epithelial sheets, which makes them very amenable to live imaging. Clones grow as tight colonies and there is minimal cell mixing between distinct islands of cells. All experiments described in this thesis have been performed in two-dimensional cultures of MDCKs grown on either plastic or glass. One should bear in mind that such 2D cultures, while widely used and recognised in the scientific community, have their limitations: cells *in vivo* exist in a three-dimensional environment, which is molecularly and mechanically much more varied and complex, so their behaviour may differ substantially from observations made *in vitro*.

scrib^{KD} MDCK cells generated using a short hairpin RNA (shRNA) construct are viable and display a flattened, mesenchymal-like morphology. That said, the distribution of apical marker gp135 is unaffected in *scrib*^{KD} MDCKs and their tight junction assembly is only

slightly delayed, implying they maintain apico-basal polarity at least to some degree. MDCKs lacking *scribble* also display an enhanced ability to migrate through filters and migrate faster, but more chaotically, than wild-type cells in two-dimensional wound healing assays (Qin et al. 2005).

Strikingly, juxtaposing *scrib*^{KD} and wild-type MDCK cells at a 1 : 10 ratio in a confluent culture results in the death and apical extrusion of the *scribble* mutant cells. As mentioned before, *scrib*^{KD} cells are viable in homotypic cultures and are not eliminated if confronted by other *scrib*^{KD} cells, defining this phenomenon as cell competition (Figure I.5) (Norman et al. 2012; Wagstaff et al. 2016). Cells lacking *scribble* undergo Bcl-2 homologous antagonist/killer (Bak) and Bcl-2 associated X protein (Bax)-dependent mitochondrial apoptosis that is independent of their extrusion. Unlike in *Drosophila*, *scribble* competition in MDCKs does not involve JNK activity or phagocytosis; instead, p38 MAPK activates the apoptosis pathway in *scrib*^{KD} losers (Norman et al. 2012).

The Piddini lab further characterised MDCK *scribble* competition in our (Wagstaff et al. 2016) publication, which I describe in detail below and in subsequent sections. The bulk of the data constituting this thesis is either part of or builds on the work within this paper.

Wagstaff et al. first demonstrated that while contact is required, it is not sufficient for elimination of *scrib*^{KD} cells. Neither conditioned media from competing *scrib*^{KD} : wild-type cultures added to *scrib*^{KD} cells, nor media exchanged between *scrib*^{KD} cells and competing cultures through a transwell system is sufficient to induce loser cell death. What is more, only fully surrounded *scrib*^{KD} cells are efficiently eliminated; loser clones that are in prolonged contact with winners, but are not surrounded, survive for much longer.

The most striking difference between *scrib*^{KD} clones fully surrounded by wild-type cells and *scrib*^{KD} clones only in contact with (but not surrounded by) wild-type cells is their density: the density of surrounded *scrib*^{KD} clones is around 4.5 times higher than their homotypic density and it is also higher than that of the surrounding wild-type cells. This suggests that *scrib*^{KD} cells are actively compacted and their increased density does not just reflect the density of the surrounding culture. In fact, compaction of *scrib*^{KD} cells in the absence of wild-type cells is sufficient to induce apoptosis in the loser population, showing that they are hypersensitive to density. Taken together, *scrib*^{KD} cells are

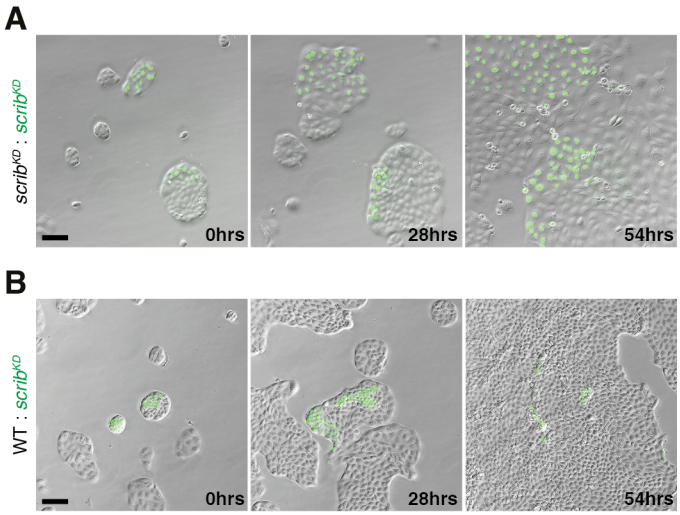

Figure I.5: *scrib*^{KD} cells are viable in homotypic cultures but are eliminated in the presence of wild-type cells via cell competition. (**A**) Stills from movies of a co-culture of unlabelled and GFP-labelled *scrib*^{KD} cells. (**B**) Co-culture of GFP-labelled *scrib*^{KD} cells and unlabelled wild-type cells. *scrib*^{KD} cells are eliminated over the course of the movie.

Scale bars = 100 μm. Adapted from (Wagstaff et al. 2016).

outcompeted through compaction induced by surrounding winners in a process termed mechanical cell competition, where loser cell elimination relies on mechanical insults rather than molecular exchange (Wagstaff et al. 2016).

Prior to initiation of competition, *scrib*^{KD} cells show elevated activity of the tumour suppressor p53. Mechanical stress caused by compaction is sufficient to further boost p53 levels in loser cells, which ultimately results in their death and delamination. Consistently with this, genetic knockout of *p53* (*p53KO*) in *scrib*^{KD} cells rescues their low homeostatic density and hypersensitivity to density, and hence prevents their outcompetition. The Piddini lab further showed that p53 in compacted *scrib*^{KD} cells is activated by p38, which in turn lies downstream of Rho-associated protein kinase (ROCK) (Wagstaff et al. 2016).

Perhaps the most striking finding emerging from the work described in (Wagstaff et al. 2016) is the fact that p53 activation alone is sufficient to confer the mechanical loser status on cells. Wild-type MDCKs were treated with a mild dose of Nutlin-3 (from here on referred to as Nutlin), a chemical inhibitor of Mdm2, which normally targets p53 for ubiquitin-mediated degradation. As a consequence of Nutlin treatment, wild-type cells accumulate sub-lethal levels of p53, which is sufficient to replicate flattening, low homeostatic density, and compaction hypersensitivity seen in *scrib*^{KD} cells. Remarkably, confronting wild-type and *p53KO* MDCK populations in the presence of Nutlin results in the elimination of the former population through mechanical cell competition. What is more, p53-induced hypersensitivity to density and mechanical competition are also conserved in mouse tracheal epithelial cells.

Nutlin was used to exacerbate the difference in p53 levels between the two populations in both the MDCK and mouse tracheal system, as competition does not happen in the absence of Nutlin (Figure I.6) (Wagstaff et al. 2016). In fact, external stimuli are also necessary to induce p53-mediated competition in other systems (Bondar & Medzhitiv 2010; Marusyk et al. 2010). This implies that variable cellular responses to external insults may be required to generate a sufficiently steep p53 imbalance before competition can occur.

It is worth noting that mechanical cell competition has also recently been described in *Drosophila*. It was shown that local tissue crowding in the midline region of the pupal

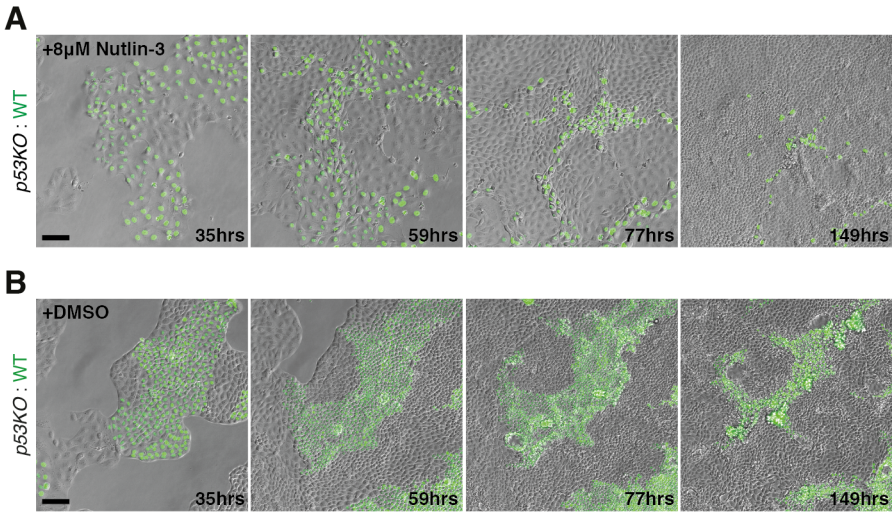

Figure I.6: p53 elevation is sufficient to induce mechanical cell competition. (**A-B**) Movie stills of a co-culture of GFP-labelled wild-type cells and cells lacking p53 (*p53KO*) in the presence of a sub-lethal dose of Mdm2 inhibitor, Nutlin-3 (A), or the solvent, DMSO (B). Nutlin-3 treatment elevates p53 specifically in the wild-type cells and enables their elimination via mechanical cell competition.

Scale bars = 100 μm. Adapted from (Wagstaff et al. 2016).

notum is both sufficient and necessary to induce delamination. In accordance with this, mechanical stress induced by rapidly growing Ras-transformed clones on their non-transformed neighbours is sufficient to result in the elimination of wild-type tissue; the authors term this process 'mechanical super-competition' (Levayer et al. 2016).

Scribble and E-cadherin

'Classical' cadherins are a subfamily of cell-cell adhesion receptors. Members include epithelial, neural, and placental cadherin (E-, N-, and P-cadherin, respectively), named after the tissues they were first identified in, but their expression is not restricted to those tissues (reviewed in Saito et al. 2012). Each classical cadherin molecule is composed of five extracellular cadherin (EC) domains, a single transmembrane anchor, and an intracellular domain. The extracellular regions of cadherins on one cell recognise and bind cadherins on neighbouring cells, predominantly in a homotypic fashion. The intracellular domain is responsible for transducing extracellular signals through mediator proteins (e.g. catenins) to many intracellular processes, including cell-cell adhesion, cytoskeleton rearrangement during locomotion, and changes in gene expression. Importantly in the context of mechanical cell competition, cadherin complexes have also been shown to act as force sensors capable of triggering intracellular in response to changes in intercellular tension (reviewed in Leckband & de Rooij 2014).

Because cadherins have such wide-ranging cellular effects in a physiological context, it is not surprising that their misregulation has been implicated to have a role in cancer progression. As most solid tumours arise from epithelial tissue, the link between E-cadherin in particular and cancer has been the focus of much investigation. Tumours have been shown to often lose or mislocalise E-cadherin, and this is associated with a more invasive/metastatic phenotype (reviewed in Jeanes et al. 2008). Interestingly, E-cadherin expression is downregulated during the epithelial-to-mesenchymal transition (EMT) in normal development; EMT is a process during which epithelial cells lose their apico-basal polarity and cell-cell junctions to acquire a more motile, mesenchymal phenotype associated with increased N-cadherin expression (reviewed in Lamouille et al. 2014). It has therefore been suggested that aberrant EMT activation may contribute to tumourigenesis.

In *Drosophila*, cells mutant for *scribble* in conjunction with a secondary oncogenic Ras mutation have low E-cadherin expression, which results in a more invasive phenotype (Brumby & Richardson 2003; Pagliarini & Xu 2003). Similarly, loss of *scribble* in MDCKs has been reported to result in an approximately threefold drop in the number of homophilic E-cadherin adhesions, as assessed by the ability of cells to bind surfaces coated with the extracellular domain of E-cadherin. This was shown to be because Scribble is required for the cortical stabilisation of α- and β-catenin, which associate with the cytoplasmic tail of E-cadherin to bridge its interaction with the cytoskeleton and transduce extracellular signals (Qin et al. 2005; Tian et al. 2011).

Despite the drop in E-cadherin adhesion numbers, it has been reported that *scrib*^{KD} MDCKs have the same amount of E-cadherin as wild-type cells, as shown by Western blotting and pull-down of biotinylated surface proteins (Qin et al. 2005). Another group reported no increase in E-cadherin levels in *scrib*^{KD} MDCKs by Western blotting, but the immunofluorescence images presented suggest that *scrib*^{KD} cells have elevated E-cadherin (Norman et al. 2012). In contrast, the Piddini lab has found that *scrib*^{KD} MDCKs have elevated total (shown by Western blot and immunofluorescence, Figure I.7A and B) and cell surface levels of E-cadherin (shown by surface immunostaining, Figure I.7C) (Wagstaff et al. 2016). Two of these publications also describe E-cadherin knockdown (*E-cad*^{KD}) MDCK lines: one has a flattened, *scrib*^{KD}-like morphology (Qin et al. 2005) and the other has a more wild-type morphology (Wagstaff et al. 2016). Importantly, the *E-cad*^{KD} MDCK line used in (Wagstaff et al. 2016) was generated as part of the work presented in (Hogan et al. 2009). Hogan et al. do not describe any morphological changes of *E-cad*^{KD} cells and the micrographs they present imply that *E-cad*^{KD} cells have a wild-type morphology (Hogan et al. 2009). An explanation for these discrepancies could be the use of two distinct MDCK subtypes and antibodies with different epitopes or sensitivity in the conflicting reports.

Perhaps more consistently, E-cadherin localisation has been shown to be perturbed in *scrib*^{KD} MDCKs. Upon *scribble* knockdown, E-cadherin shifts from cell-cell boundaries to the basal side (Norman et al. 2012). In fact, by visualising E-cadherin-GFP, it was shown that E-cadherin accumulates in intracellular vesicles primarily found around the perinuclear region of *scrib*^{KD} cells (Lohia et al. 2012). One of the ways cells regulate E-cadherin signalling is by its endocytosis, followed by recycling back to the cell surface or

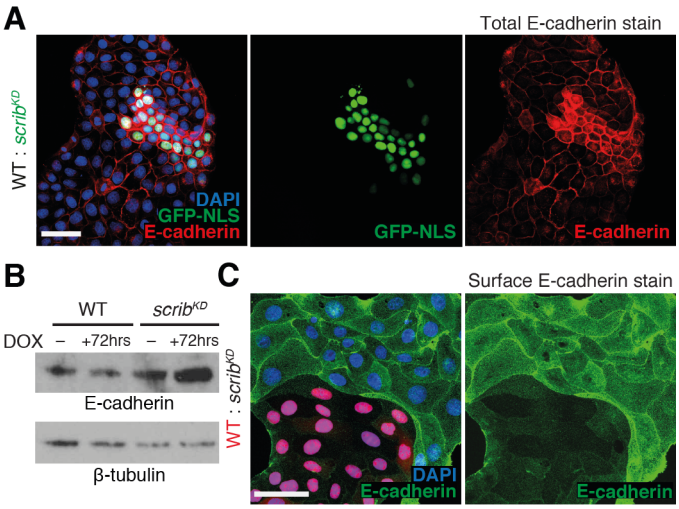

Figure I.7: E-cadherin is upregulated in *scrib*^{KD} cells. (**A**) Immunofluorescence images showing total E-cadherin levels in a co-culture of unlabelled wild-type cells and GFP-labelled *scrib*^{KD} cells. DAPI is used to label the nuclei. (**B**) Western blot against E-cadherin in wild-type and *scrib*^{KD} cells in the presence or absence of doxycycline (DOX), which induces *scribble* knockdown. β-tubulin was used as loading control. This Western blot was generated by me. (**C**) Immunofluorescence images showing surface E-cadherin levels in a co-culture of RFP-labelled wild-type cells and unlabelled *scrib*^{KD} cells.

Scale bars = 50 μm. Adapted from (Wagstaff et al. 2016).

lysosomal degradation. Loss of *scribble* promotes E-cadherin internalisation in MDCKs through destabilisation of the E-cadherin/p120 interaction, which normally maintains E-cadherin at the cell surface. Increased retromer complex binding in the absence of *scribble* causes E-cadherin to be redirected from lysosome-bound endosomes to the Golgi apparatus, resulting in its accumulation in *scrib*^{KD} cells (Lohia et al. 2012).

Directional cell migration in *scribble* competition

As described in an earlier section, compaction of *scrib*^{KD} MDCKs during competition is an active process, as compacted clones reach a density higher than the surrounding wild-type culture. Plating competing *scrib*^{KD} : wild-type cultures at lower densities revealed that this is a consequence of a remarkable migratory behaviour triggered upon contact between the two populations (Figure I.8A), which is not observed in homotypic cultures of *scrib*^{KD} or wild-type cells (Figure I.8B and Wagstaff et al. 2016). Following contact, both *scrib*^{KD} and wild-type cells engage in highly directional collective migration: *scrib*^{KD} cells are always at the migrating front with wild-type cells behind them. Further analysis of this migration suggested that wild-type cells are the first to start migrating towards *scrib*^{KD} cells before the mutant cells begin moving away. Both populations then become locally compressed at the contact site, but it remains unclear whether this is due to wild-type cells 'pushing' on *scrib*^{KD} cells or *scrib*^{KD} cells self-compacting to avoid the interaction. As migration progresses with *scrib*^{KD} cells being followed by wild-type cells, *scrib*^{KD} clones eventually encounter other wild-type cells, which also start migrating. This ultimately results in *scrib*^{KD} cells being corralled into tight clones for elimination (Wagstaff et al. 2016).

Perhaps unsurprisingly, adhesion molecules including cadherins have been implicated in collective cell migration (reviewed in Theveneau & Mayor 2012). Knockdown experiments have shown that cadherins are to some extent functionally redundant but play distinct roles when co-expressed. For example, when both P- and E-cadherin are present, P-cadherin is sensitive to the levels of intercellular force while E-cadherin responds to the rate at which intercellular force builds up. In the absence of E-cadherin, P-cadherin can take over the mechanotransducing properties of E-cadherin (Bazellières et al. 2015).

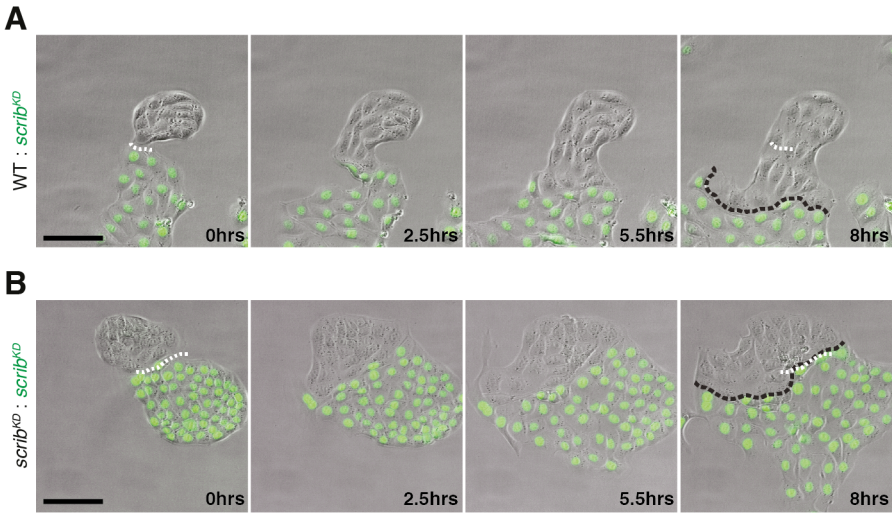

Figure I.8: Collective, directional migration is triggered upon collision between wild-type and *scrib*^{KD} clones. (**A**) Movie stills of a co-culture of GFP-labelled *scrib*^{KD} cells and unlabelled wild-type cells. White dashed lines mark the initial contact point; black dashed lines mark the final contact point here and in (B). (**B**) Stills from movies of a homotypic co-culture of GFP-labelled and unlabelled *scrib*^{KD} cells.

Scale bars = 100 μm. Adapted from (Wagstaff et al. 2016).

Considering its misregulation in *scribble* mutant cells, the Piddini lab investigated if E-cadherin was involved in the directional migration observed during MDCK competition. I describe the experiments I did to help address this question in Chapter II. Other members of the Piddini lab had previously used an E-cadherin blocking antibody and low calcium conditions to disassemble E-cadherin-mediated junctions in both *scrib*^{KD} and wild-type cells, which abolished the directional migration (Figure I.9A and B). Lack of directional migration prevented the active compaction of *scrib*^{KD} cells and this delayed their elimination (Figure I.9C and D) (Wagstaff et al. 2016). However, cultures with the blocking antibody can eventually reach densities high enough to induce *scrib*^{KD} cell death. Taken together, while the directional migration triggered during *scribble* competition is not essential for *scrib*^{KD} cell elimination, it makes their outcompetition much more efficient.

The directional migration triggered during *scribble* competition in MDCKs is somewhat similar to the chase-and-run migration described between neural crest (NC) and placodal cells in *Xenopus laevis* embryos. In this system, NC cells use chemotaxis to chase placodal cells, which secrete the chemoattractant Sdf1. Following collision, a contact inhibition of locomotion response, mediated by Wnt/planar cell polarity (PCP) and N-cadherin, is triggered in both populations. This results in a transient collapse of cell protrusions and localised loss of focal adhesions. The resulting asymmetry triggers placodal cells to migrate away from NC cells, restarting the cycle (Theveneau et al. 2013). Despite the similarities shared with NC/placodal cell chase-and-run behaviour, directional migration in MDCK *scribble* competition does not rely on secreted factors: contact between *scrib*^{KD} and wild-type cells is essential (Wagstaff et al. 2016). This has two interesting implications:

Firstly, there must be a recognition event triggered upon loser : winner contact that directs the migration of winners towards the loser population and/or vice-versa. Since cell-cell contact is required, any such signal is most likely to be on the surface of either or both populations. For example, one population may express an extracellular protein that is absent or reduced in the other. Alternatively, the two populations may expose different splice variants of the same protein (Rhiner et al. 2010), or have distinct post-translational modifications on a protein common to both. Such asymmetry could then be a trigger for the ensuing directional migration. It is unlikely that transcription or translation are

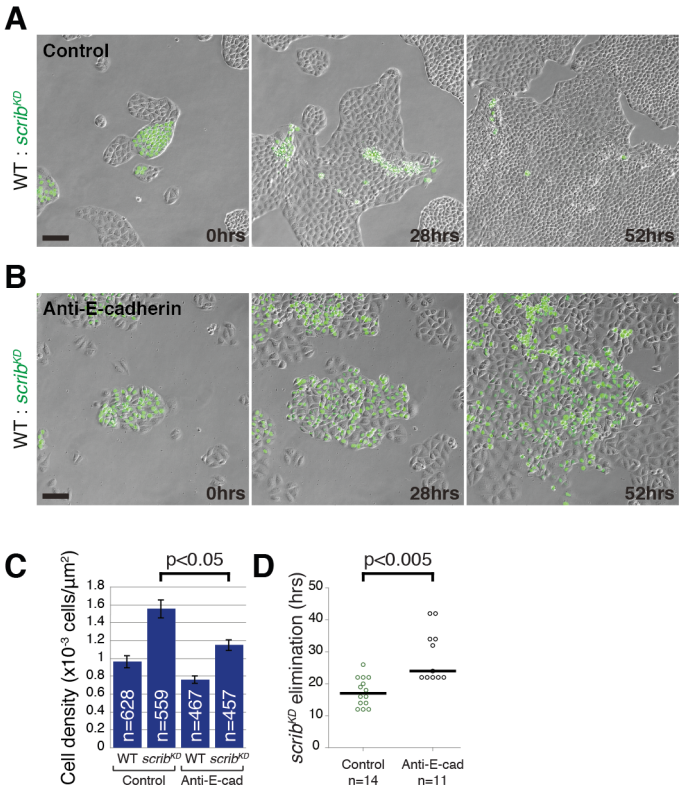

Figure I.9: Functional E-cadherin-based junctions are required for directional migration between wild-type and *scrib*^{KD} cells. (**A-B**) Disrupting cell junctions using an E-cadherin blocking antibody and low calcium conditions (B) prevents contact-induced migration compared with control conditions (A). (**C**) Compaction of *scrib*^{KD} cells is significantly reduced in the presence of the E-cadherin blocking antibody. Error bars ± standard error of the mean (SEM). p values were calculated using the Kolmogorov-Smirnov (K-S) test here and in (D). n = number of cells. (**D**) Elimination of *scrib*^{KD} cells is delayed in the presence of the E-cadherin blocking antibody. This was defined as the number of hours from the point at which a *scrib*^{KD} clone became fully surrounded by wild-type cells to the complete elimination of that *scrib*^{KD} clone. n = number of clones.

Scale bars = 100 μm. Adapted from (Wagstaff et al. 2016).

involved, as the onset of migration happens almost immediately after initial contact. I therefore propose that there is a pre-existing difference in the surface molecule signature of *scrib*^{KD} and wild-type cells and that this is the trigger for the subsequent directed migration.

Secondly, *scrib*^{KD} cells without fail migrate away from wild-type cells and are intrinsically more motile, suggesting they are always poised for migration and contact from winners might be providing the symmetry breaking cue to initiate it. Wild-type MDCKs do not share this predisposition to migrate, as contact between two populations of wild-type cells does not result in either of the populations moving away from the other (Wagstaff et al. 2016). It would be important to find out which molecular pathways confer this directional migratory response upon contact between wild-type and *scrib*^{KD} cells, and whether the same pathways are also responsible for the loser status of *scrib*^{KD} cells.

Collective cell migration and leader cells

Importantly for this thesis, *scrib*^{KD} cells during directed migration are always observed at the front of the collective, with wild-type cells behind them (Wagstaff et al. 2016). This is very reminiscent of a phenomenon called 'leader cell migration', with *scrib*^{KD} cells acting as 'leaders' and wild-type cells acting as 'followers'. I describe leader cell migration in more detail here and in subsequent sections.

Single cell migration relies on the establishment of a front-to-rear polarity axis. Cytoskeletal rearrangements driven by the activity of small GTPases Rac and Cdc42 at the front of a migrating cell lead to the formation of protrusions, such as lamellipodia and filopodia, and engagement of integrins with the substrate. As the lamellipodium reaches forward in the direction of migration, integrin-based adhesions (that eventually mature into focal adhesions) are formed, to which acto-myosin cables are anchored. The activity of small GTPase Rho at the rear of the cell promotes acto-myosin contractility, which retracts the rear end of the cell. Focal adhesions are disassembled as the retracting edge reaches them, resulting in net movement forwards (reviewed in Mayor & Etienne-Manneville 2016). This type of migration is classed as mesenchymal, in contrast to amoeboid migration, a 'crawling' type of movement driven by distinct molecular and

physical mechanisms (not discussed in this thesis) (reviewed in Lämmermann & Sixt 2009).

Collective cell migration can be broadly defined as the coordinated migration of two or more cells, which occurs as a result of communication between them, be it mechanical, chemical, or physical (reviewed in Theveneau & Linker 2017). The molecules that govern single cell migration are also implicated in collective migration. Importantly, front-to-rear polarity is established at a 'supra-cellular' level (from the front to the rear of the migrating collective rather than within an individual cell) thanks to adhesion and communication enabled by intact cell-cell junctions (reviewed in Khalil & Friedl 2010). Collective migration is crucial in many physiological processes, such as morphogenesis, wound healing, and angiogenesis, but has also been implicated in tumour cell migration. Deeper understanding of the processes underlying this mode of migration could therefore form the basis for therapeutic approaches promoting wound healing or preventing cancer metastasis.

The directionality and efficiency of collective migration is mostly determined by two regions: the leading and trailing edge. Single or multiple 'leader' cells are localised to the front of a collectively migrating group, with 'follower' cells migrating behind them (Figure I.10A). Leader cells are characterised by a mesenchymal-like front edge and a rear end with a more epithelial identity: this polarisation is achieved mainly through integrin β1 (ITGβ1)-mediated protrusion formation and cadherin-based junctions with follower cells at the rear (reviewed in Khalil & Friedl 2010). Leaders are not always initially present at the front of the collective: they can be transported to the outer edge of a colony from a few rows behind by flows within the collective (Poujade et al. 2007).

Canonically, leaders have been thought to sense the microenvironment, direct the migration of the collective, generate traction forces, and proteolytically degrade the extracellular matrix (ECM) to create tracks through which the cells can migrate (reviewed in Khalil & Friedl 2010). This was challenged by more recent evidence that suggests that directionality is not always determined by the cells at the leading edge, traction force generation and proteolytic activities are not necessarily confined to leaders, and that protrusive and guidance abilities are independent of each other (reviewed in Theveneau & Linker 2017).

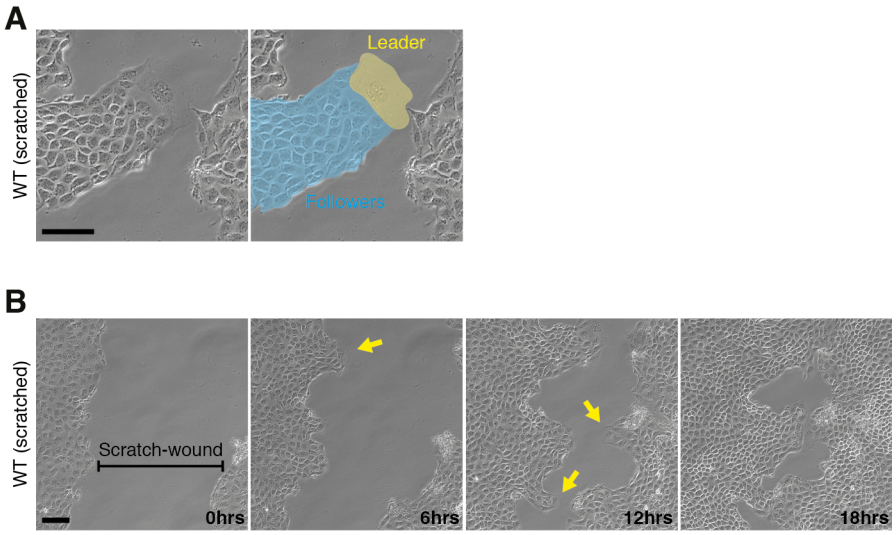

Figure I.10: Finger-like protrusions, each capped by a leader cell, emerge in MDCK cultures following scratching of a confluent monolayer. (**A**) An MDCK leader cell (highlighted in yellow) displaying the characteristic flattened morphology and an active lamellipodium with the follower cells (highlighted in blue) trailing behind it. (**B**) Scratching of a wild-type MDCK monolayer results in the emergence of a finite number of leader cells, some of which are indicated by the yellow arrows. The scratch-wound area decreases over time as cells migrate to close the wound gap.

Scale bars = 100 μm.

This data was generated by me.

Mammalian *in vitro* models of leader cell migration

In mammalian epithelial *in vitro* models of leader migration (e.g. MDCKs), cell monolayers are grown to confluency before scratching or releasing a barrier to generate space for migration. These manipulations trigger the emergence of a finite number of leader cells from the colony edges (Figure I.10B, leaders are marked with yellow arrows). Barrier release experiments are generally accepted to be a more controlled way of generating leaders, as they avoid the formation of barriers of cell debris, release of intracellular material into the media, and detectable damage to the edge cells (Poujade et al. 2007). Leader cells drive the formation of migration 'fingers' in which follower cells make up the stem and a leader cell caps the tip. I will refer to leaders generated by wounding and barrier release as 'canonical leaders' to distinguish them from other types of leader that I describe in this thesis.

While MDCKs dominate the leader cell migration field, leaders have also been described in other cell lines. In fact, leaders were first described in the rat liver epithelial line IAR-2 and their formation was shown to depend on reduced RhoA activity (Omelchenko et al. 2003). Interestingly, leaders emerging from wounds in monolayers of invasive breast cancer MCF-7 cells emerge through a different mechanism. Wounding of MCF-7 cultures reduces mechanical tension, which triggers expression of the Notch ligand Dll4 at the wound edge. The frequency of leader appearance is regulated by lateral inhibition, whereby cells with high Dll4 inhibit Dll4 upregulation in neighbouring cells (Riahi et al. 2015).

I will now focus on findings established using MDCKs as a model for leader cell migration.

Leader cells are essential for collective migration of MDCK cells (Yamaguchi et al. 2015). MDCK leaders are morphologically distinct from follower cells: they display a characteristic half-moon shape, are larger than follower cells, and have active lamellipodia and large focal adhesions (Poujade et al. 2007; Omelchenko et al. 2003). Leaders have also been shown to often have multiple nuclei and not to divide (Reffay et al. 2011). Molecularly, leaders generated by barrier release have high levels of phosphoinositide 3-kinase (PI3K), ITGβ1, and Rac1, whose activities are indispensable for leader migration. PI3K and Rac1 are in a positive feedback loop in leader cells while ITGβ1 regulates Rac1 individually (Yamaguchi et al. 2015). I will term PI3K, ITGβ1, and

Rac1 ‘canonical leader markers’ and use them as a benchmark for characterisation of other types of leader in this thesis. It is also important to note that cell division does not contribute to wound closure in MDCK leader migration (Farooqui & Fenteany 2005) and that the initial speed of migration depends on plating density (Rosen & Misfeldt 1980): I control for the latter in my experiments by seeding cells at the lowest possible density that still results in a confluent monolayer.

Other researchers have used techniques like traction force microscopy and FRET to characterise leader cell migration from a more biophysical perspective. For instance, micropatterning experiments have shown that increased membrane curvature promotes leader formation (Rausch et al. 2013). Similarly, particle image velocimetry was used to show that axis alignment of cells perpendicularly to the wound edge precedes leader cell appearance, although these experiments were largely observational in nature (Reffay et al. 2011). In another study, it was shown that a contractile acto-myosin ‘cable’ runs uninterrupted along the outer edge of the cells making up a migratory finger. The cable is kept under tension and its laser ablation is sufficient to increase the probability of a leader emerging, suggesting that the cable mechanically inhibits leader cell formation in the vicinity of an existing leader (Reffay et al. 2014). Finally, mathematical models assuming that a cell’s shape determines its motility, which leads to surface instability at the wound edge, have successfully recapitulated leader formation, implying leaders can emerge in the absence of biochemical cues (Mark et al. 2010).

Despite the body of work on leader cells, there has so far been no evidence to show that leader cells are initially distinct from the cells around them (Poujade et al. 2007; Petitjean et al. 2010; Reffay et al. 2014). Even if the reduced mechanical tension or exposure of a free edge after wounding provide the mechanical cues for leader formation, only a few cells become leaders from the mass of phenotypically homogeneous cells, implying that other factors are also at play. Ultimately, it is not yet clear how individual cells are singled out and instructed to acquire the leader cell fate. I attempt to address this question in the last part of this thesis.

Leader cell migration in wound healing and cancer

Collective and leader cell migration have been implicated in physiological processes such as wound healing but have also been shown to be active in pathological migration e.g. in invasive carcinoma. I will discuss examples from both physiology and pathology to highlight how findings from the leader cell migration field could be exploited for potential therapeutic uses in the future.

The importance of leader migration in wound healing has been mainly described in the skin and corneal epithelium. Following a wound to the epithelium, keratinocytes collectively migrate over the wound bed to quickly close the wound and restore the epithelial barrier. Proliferation is suppressed in cells at the leading edge so that the integrity of the moving sheet is not compromised by cells rounding up during mitosis; meanwhile, the proliferation of follower cells is boosted to compensate for cell loss. Just like canonical leader cells, the front row of migrating keratinocytes uses integrin-based attachments to generate traction force on the ECM while maintaining cell-cell junctions with the cells behind them. Additionally, growth factor signalling at the wound site (e.g. from stromal fibroblasts) helps boost migration efficiency. Importantly, a new basement membrane is deposited during keratinocyte migration and this is key for re-epithelisation. Multi-layered stratification of the keratinocyte monolayer hours or days after wound closure ensures that an epidermis is fully reformed (reviewed in Zelenka & Arpitha 2008 and Friedl & Gilmour 2009).

In vitro studies using MDCKs and MCF-7 have directly demonstrated that collective migration driven by leader cells is necessary for efficient scratch-wound closure (Riahi et al. 2015; Yamaguchi et al. 2015). In fact, *in vitro* studies were also particularly useful in characterising some of the molecular players involved. In MDCK wound healing models, extracellular regulated kinase 1/2 (ERK1/2) MAPK activity is essential for coordinated cell migration and its levels are directly proportional to the speed of migration. Wounding has been shown to generate reactive oxygen species (ROS) and activate a rapid, transient wave of ERK1/2 signalling in the edge cells. A second, slower and more sustained wave of ERK1/2 signalling is then activated, most likely by locomotion of individual cells within the monolayer. Importantly, only the second wave is activated in a constraint removal assay, a completely injury-free barrier release assay, showing that injury provides a vital signal for MDCK migration into the wound area. The second wave is important for sheet

movement and depends on Src activity. Upon wound closure, ERK1/2 activity dissipates from the opposing edges (Matsubayashi et al. 2004; Nikolic et al. 2006). While these studies address collective migration at the wound edge and not leader cell migration *per se*, leader cells are present at MDCK wound edges and I would therefore expect their migration to at least partially rely on ERK1/2 activity.

Later studies in keratinocytes showed that transforming growth factor β (TGFβ) lies upstream of wound-induced ERK1/2 activation. TGFβ is a secreted cytokine that can signal to activate a plethora of intracellular responses, including p38, RhoA, and PI3K that, interestingly, also play roles in *scribble* competition and canonical leader cell migration. TGFβ reduces cell density at the leading edge, which is a prerequisite for and the driver of ERK1/2 activation. This induces efficient collective migration towards regions of lower density and therefore presumably into the wound area. Sensing of cell density is hence proposed to be the way leaders are defined in the keratinocyte system (Chapnick & Liu 2014).

The processes underlying collective and leader cell migration have also been implicated in the migration of cancer cells away from a primary tumour during metastasis. Cancer cells can adopt several types of migratory behaviour, from single cell migration to multicellular streaming (reviewed in Friedl et al. 2012). Importantly, cancer cells often migrate as a collective, at the front of which are leader cells. Leader cells can emerge from the tumour itself and usually have a mesenchymal-like phenotype, but non-tumour cells such as cancer-associated fibroblasts (CAFs) can also become leaders during metastasis. CAFs can provide directional cues to the migrating tumour cells and generate tracks for the cancer cells to follow by remodelling the ECM (reviewed in Theveneau & Linker 2017).

CAFs leading cancer cells away from a primary tumour in both 2D and 3D migration assays look remarkably like finger-like protrusions observed in canonical leader cell migration. As they migrate, CAFs generate pulling forces on cancer cells through mechanosensitive, heterotypic E-cadherin / N-cadherin adhesions. N-cadherin is also important for the repolarisation of CAFs following their interaction with the tumour mass so that they migrate away from it. Taken together, invasive cancer cells can direct CAF migration away from the tumour mass and into the surrounding tissue. Cell-cell adhesions between the two populations then result in CAFs physically pulling cancer cells away from the primary tumour to promote their metastasis (Labernadie et al. 2017).

Mechanical stress at tumour sites has also been implicated in the progression of metastasis. When mammary epithelial cancer cell lines were subject to compression similar to that in a breast tumour microenvironment, the migration of more invasive lines in a scratch-wound assay was enhanced. In contrast, compression suppressed the migration of non-invasive lines. More specifically, compression was shown to promote the formation of an increased number of leader-like cells at the edges of the scratched invasive cancer cell monolayers. The authors propose that in an uncompressed situation, only a few cells become leaders in response to other cues (e.g. increased membrane curvature at the edge), but compression provides pro-migratory mechanical cues to all border cells. This results in the formation of many more leaders in a compressed scenario, many of which can migrate away from the primary tumour (Tse et al. 2012).

In summary, leader cell migration plays an important role in epithelial wound healing. Leader cells guide the migration into the wound area while maintaining cell-cell contacts that keep the epithelial barrier intact. On the flipside, aspects of leader cell migration can often be exploited by malignant cells to promote their invasion into the surrounding tissue. Cancer cells are able to form and maintain cell-cell junctions and thus migrate as a collective following leader cells. Leader cells, be it CAFs or ones originating from the tumour itself, display properties of canonical leaders e.g. the ability to generate traction forces at the front while maintaining adhesions at the rear. Using leader cell migration models to understand more about what mechanisms drive leader-follower migration may therefore help identify therapy targets also applicable to migration during cancer metastasis.

Thesis objectives

The work I describe in this thesis aims to broaden our understanding of three distinct aspects of cell competition and leader cell migration in the MDCK system.

(i) What roles do surface molecules play in the directional migration and mechanical loser status observed during *scribble* competition?

It remains unclear which molecular pathways drive the directional migration between wild-type and *scrib*^{KD} cells during MDCK *scribble* competition. It is also unknown whether the molecular players that drive contact-induced migration also play an active role in *scrib*^{KD} cell elimination. This is an attractive hypothesis: the same pathway could trigger the directional migration to drive loser cell compaction while simultaneously conferring the density hypersensitivity on losers, leading to their robust elimination.

The Piddini lab has recently shown that the contact is required for *scrib*^{KD} cell elimination. Moreover, the directional migration phenotype is triggered almost immediately after contact between loser and winner clones (Wagstaff et al. 2016). It is therefore highly likely that the molecules orchestrating the migratory response reside on the cell surface of either or both cell populations. Should this be the case, these molecules could also conceivably transduce 'kill' signals from the winner cells (or the environment) to the loser cells.

Following leads from exploratory immunofluorescence and RNA sequencing experiments done by others in the Piddini lab, I aimed to characterise the involvement of several surface molecules in the directional migration triggered between wild-type winners and *scrib*^{KD} losers. I also set out to test the role of these surface molecules in the mechanical loser status.

(ii) Is the molecular cascade responsible for the density hypersensitivity of *scrib*^{KD} cells conserved in mechanical losers triggered by p53 activation alone?

Recent work from the Piddini lab identified elevated p53 as the underlying cause of mechanical loser status of *scrib*^{KD} cells. In fact, most *scrib*^{KD} cell phenotypes, such as lower homeostatic density and hypersensitivity to compaction, can be replicated by chemically elevating p53 in otherwise wild-type cells (Wagstaff et al. 2016). What remained unaddressed is whether the ROCK – P-p38 – p53 molecular cascade leading to density hypersensitivity in compacted *scrib*^{KD} cells is also conserved in losers induced by mild p53 activation alone. It remained possible that *scrib*^{KD} and p53-driven losers activate parallel pathways in response to compaction and that these signalling events only converge further downstream to drive the same outcome in both types of mechanical loser.

In the second part of this thesis, I aimed to determine to what extent the ROCK – P-p38 – p53 molecular cascade was conserved between *scrib*^{KD}- and p53-mediated competition.

(iii) What are the molecular drivers of the directional migration observed during MDCK competition? Are the same molecules involved in leader cell migration?

The directional migration preceding compaction and elimination of *scrib*^{KD} cells had not been further characterised past the experiments described in (Wagstaff et al. 2016), which left several open questions about the molecular drivers behind this phenomenon. The third part of this thesis aimed to further characterise the directional migration observed during MDCK competition and pinpoint the signalling pathways involved.

As I mentioned previously, the contact-induced collective migration occurring during *scribble* competition is reminiscent of canonical leader cell migration described in the context of wound healing. It is therefore an interesting possibility that the same molecular markers might be involved in driving both processes. I therefore also aimed to test whether any parallels can be drawn between directional migration during MDCK competition and leader cell migration. Should this be the case, any findings could be more significant from a therapeutic point of view and help develop methods of boosting wound healing *in vivo*.

Chapter II: E-cadherin is necessary but not sufficient for the directional migration observed in *scribble* competition and its loss does not ameliorate *scrib^{KD}* cell loser status

---

In the first part of my thesis (Chapters II and III), I investigate the role of three candidate molecules (E-, N-, and P-cadherin) in the directional migration between *scrib^{KD}* and wild-type cells and in the mechanical loser status of *scrib^{KD}* cells.

Contact-induced migration following contact between *scrib^{KD}* and wild-type cells is initiated almost immediately after clone collision (Wagstaff et al. 2016). As I postulated earlier, it is likely that there is a difference in the surface molecule repertoire of *scrib^{KD}* and wild-type cells even prior to initiation of directional migration or competition. Among other (not mutually exclusive) possibilities, a pre-existing difference in surface molecules may be responsible for loser cell recognition, providing a directional cue for winner cell migration, and even transducing pro-apoptotic signals from winners into losers. One candidate for this is E-cadherin, a cell surface molecule involved in collective cell migration and mechanotransduction (reviewed in Theveneau & Mayor 2012 and Leckband & de Rooij 2014).

Multiple lines of evidence suggest that E-cadherin might play a role in directional migration during *scribble* competition in MDCKs. For one, *scrib^{KD}* cells have elevated levels of both total and surface E-cadherin compared to wild-type cells, even before competition (Figure I.7) (Wagstaff et al. 2016). What is more, the Scribble protein is directly implicated in E-cadherin regulation (Lohia et al. 2012). Disruption of E-cadherin junctions using a blocking antibody is sufficient to abolish contact-induced migration, as is shRNA-mediated knockdown of E-cadherin in the wild-type population alone (Wagstaff et al. 2016). Functional E-cadherin junctions and the presence of E-cadherin in the wild-type population are therefore necessary for contact-induced migration. This set of experiments however does not address the role of elevated E-cadherin in *scrib^{KD}* cells, as E-cadherin was never manipulated in this population alone. I therefore aimed to test if E-cadherin elevation in *scrib^{KD}* cells itself was important in contact-induced migration.

E-cadherin, as well as other cadherins, has mechanotransductive properties: cadherins bear force and translate it into intracellular responses through interaction with molecules like α-catenin, whose function is altered by force (reviewed in Yap et al. 2017). Consistently with this, disruption of E-cadherin-mediated junctions with a blocking antibody delays the mechanical outcompetition of *scribble* mutant cells (Wagstaff et al. 2016). I therefore also aimed to address the role of E-cadherin in the mechanical loser status of *scrib*^{KD} cells. It is conceivable that elevated surface E-cadherin, or E-cadherin misregulation due to loss of *scribble*, could result in aberrant extracellular signal transduction, which could ultimately drive loser cells' hypersensitivity to density. The E-cadherin blocking antibody experiments performed in the Piddini lab suggested that loss of functional E-cadherin junctions delays, but does not prevent, *scrib*^{KD} cell elimination. However, the possibility remained that excessive/aberrant E-cadherin-mediated signalling prior to blocking antibody addition had already triggered the density hypersensitivity of *scrib*^{KD} cells and 'sealed' their fate as losers.

Elevated E-cadherin in *scrib*^{KD} cells is necessary for directional migration but does not impact loser status

To test the role of E-cadherin elevation in *scrib*^{KD} cells, I generated a clonal, stable MDCK cell line where both *scribble* and *E-cadherin* could be silenced (*scrib*^{KD} *E-cad*^{KD}) in a tetracycline (TET)-inducible manner. I did this by generating a modified version of a published silencing vector: I adapted the antibiotic resistance cassette to allow selection using hygromycin and introduced a previously described shRNA against *E-cadherin* (Hogan et al. 2009; Norman et al. 2012). I then stably transfected this *E-cad*^{KD} construct (Appendix 2A) into a *scrib*^{KD} cell line. The knockdown efficiency of *E-cadherin* was very variable within the hygromycin-selected pool, with most cells displaying negligible or only partial knockdown, as determined by comparing immunofluorescence images in the presence and absence of TET (data not shown). I therefore deemed it necessary to isolate single clones from the stably transfected pool. The clone I used in subsequent experiments could be induced to silence *E-cadherin* in *scrib*^{KD} cells down to levels reminiscent of wild-type MDCKs (Figure II.A and B, yellow dotted line indicates the boundary between wild-

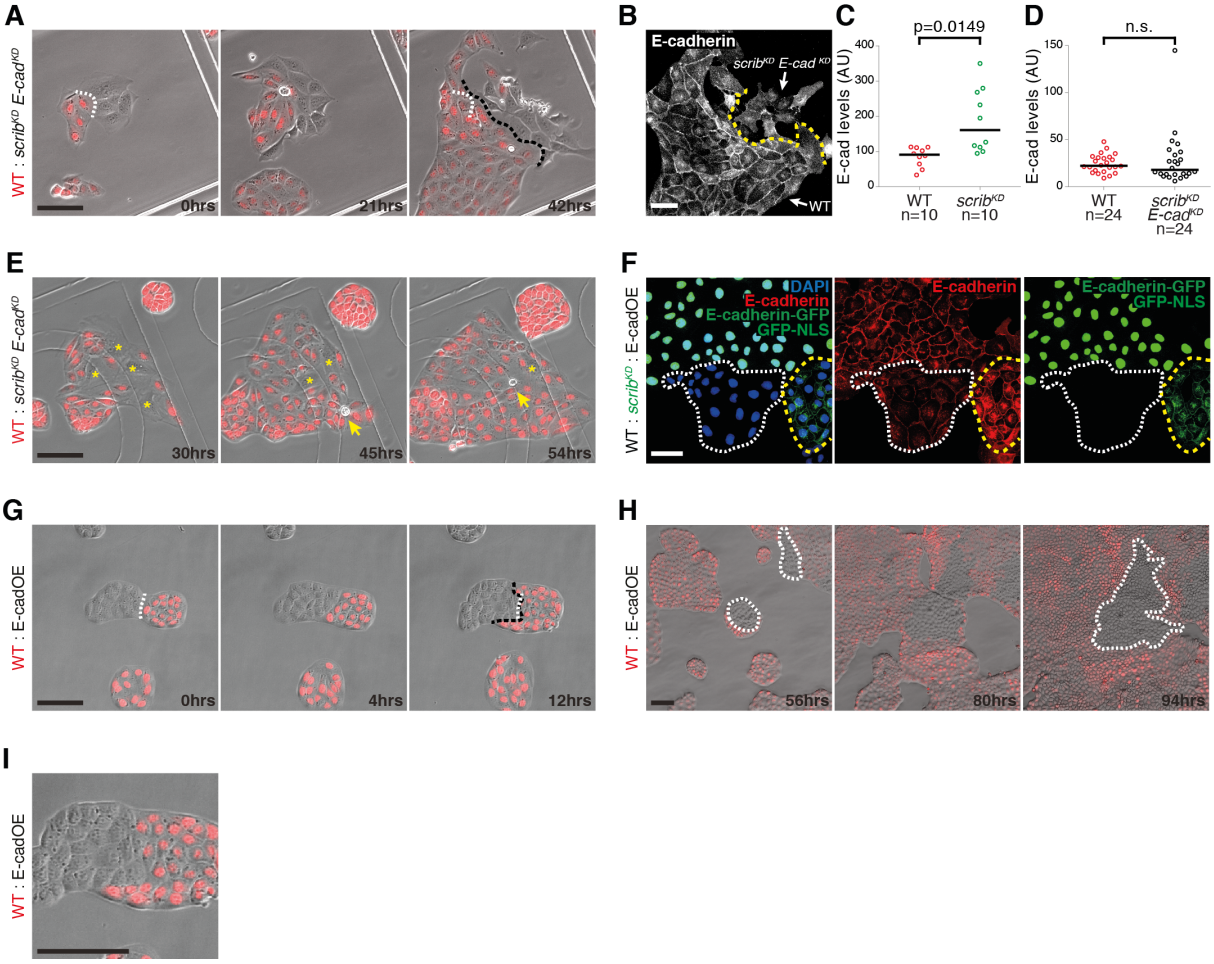

Figure II: Elevated E-cadherin is necessary but not sufficient for the directional migration observed in *scribble* competition and does not play a role in the mechanical loser status. (**A**) Directional migration is abolished between RFP-labelled wild-type cells and unlabelled *scrib*^{KD} cells expressing an shRNA against *E-cadherin* (*scrib*^{KD} *E-cad*^{KD}). White dashed lines mark initial contact point; black dashed lines mark final contact point here and in (G). (**B**) Anti-E-cadherin immunofluorescence at end of movie in (A). The yellow dashed line separates wild-type (bottom part) cells from *scrib*^{KD} *E-cad*^{KD} cells (top part). (**C-D**) Quantification of single-cell E-cadherin intensities from one representative set of confocal images as in (B). E-cadherin levels of wild-type cells are compared to *scrib*^{KD} cells (C) or *scrib*^{KD} *E-cad*^{KD} cells (D). Black bars represent the median. p values were calculated using the K-S test. AU = arbitrary units. n = number of cells. (**E**) *scrib*^{KD} *E-cad*^{KD} cells (marked by yellow asterisks) are still mechanical losers in co-culture with RFP-labelled wild-type cells. Yellow arrows mark cell death events. (**F**) Immunofluorescence showing total E-cadherin levels in wild-type MDCKs (white dashed line), wild-type cells overexpressing GFP-labelled E-cadherin (E-cadOE; yellow dashed line), and *scrib*^{KD} cells (nuclear GFP). (**G**) Directional migration does not occur between unlabelled E-cadOE cells and RFP-labelled wild-type cells. (**H**) E-cadOE clones (white dashed lines) are not outcompeted and display a similar response to increased cell density as surrounding RFP-

labelled wild-type cells. (**I**) 2x zoom of the third panel in (G) showing that E-cadOE cells are not significantly flatter than RFP-labelled wild-type cells.

Scale bars = 100 μm for movie sequences and 50 μm for immunofluorescence images.

Here and throughout all figures:

Unless otherwise specified in the figure legend or text, all quantifications, immunofluorescence images, movie sequences, and Western blots shown are from a single representative experiment taken from a minimum of three independent repeats per experiment. For live imaging and immunofluorescence experiments, at least 10 fields of view were analysed per condition.

---

type and *scrib^{KD} E-cad^{KD}* cells), thus abolishing the E-cadherin gradient between the two populations.

I did not observe directed cell migration in co-cultures of unlabelled *scrib^{KD} E-cad^{KD}* and wild-type cells labelled with nuclear RFP (Figure II.A, white and black dashed lines indicate initial and final points of contact, respectively), suggesting that elevated E-cadherin in losers is required for this process. At the end of each experiment, I fixed the co-cultures and confirmed by immunofluorescence that the total E-cadherin levels of *scrib^{KD} E-cad^{KD}* clones not displaying directed migration had been brought down to those of wild-type cells (Figure II.B and quantifications in C and D).

Despite the inhibitory effect on directed migration, *E-cadherin* knockdown did not rescue *scrib^{KD}* cell outcompetition by wild-type cells in higher density co-cultures (Figure II.E, yellow arrows indicate cell death events). This clearly demonstrated that high levels of E-cadherin are not responsible for *scrib^{KD}* cells' hypersensitivity to compaction and suggested that E-cadherin signalling does not feed into the ROCK – p38 – p53 cascade responsible for the acute response of loser cells to high density.

Taken together, I have shown that elevated E-cadherin in *scrib^{KD}* cells is required for directional migration after confrontation with wild-type cells, but it does not contribute to *scrib^{KD}* cells' mechanical loser status.

E-cadherin elevation is not sufficient for contact-induced migration or loser status

Having established that elevated E-cadherin in *scrib^{KD}* cells is required for contact-induced migration following confrontation with wild-type cells, I next investigated whether high levels of E-cadherin alone are sufficient to trigger this behaviour. Using a previously published construct as a template (Adams et al. 1998), I sub-cloned E-cadherin fused to GFP at its C terminus into a doxycycline (DOX)-inducible pTRIPZ RFP-NLS lentiviral vector. The main advantage of using a lentiviral vector is that target sequences are integrated into the genome and therefore passed onto daughter cells during division (Durand & Cimarelli 2011). I also added a P2A 'self-cleaving' peptide in between the E-cadherin-GFP and RFP-NLS reading frames so that both proteins were expressed at an equimolar ratio from the same promoter (Appendix 2B) (Kim et al. 2011). Please note

that I use variations of this DOX-mediated overexpression strategy in several chapters of this thesis. The overexpression construct is always inserted into the pTRIPZ vector and its architecture is as follows: protein of interest – P2A – RFP/GFP-NLS, plus a puromycin resistance cassette for antibiotic selection.

I then generated lentiviruses containing the E-cadherin overexpression construct and used them to transduce an otherwise wild-type MDCK cell line. I used antibiotic selection to generate a puromycin-resistant pool, which I plated at a very low density in 96-well plates to isolate single clones. I used immunofluorescence in the presence or absence of DOX to select clones with strong, uniform expression of E-cadherin-GFP. The resulting clonal cell line (E-cadOE) overexpressed E-cadherin-GFP to levels comparable to or even surpassing those of *scrib*^{KD} cells (Figure II.F, compare wild-type and E-cadOE cells in white and yellow dashed lines, respectively, and *scrib*^{KD} cells with nuclear GFP).

I next used live cell imaging to monitor interactions between clones of wild-type and E-cadOE cells and found that directional migration was not triggered following contact between the two populations. This showed that differential levels of E-cadherin are not sufficient to induce directional migration (Figure II.G). Moreover, E-cadOE cells were not outcompeted by their wild-type counterparts: at densities which induce *scrib*^{KD} cell elimination, E-cadOE cells did not appear compacted and responded to high density similarly to wild-type cells (Figure II.H, EcadOE clones are marked with the white dashed lines).

I therefore conclude that elevated E-cadherin is not sufficient to trigger directional cell migration and does not confer the loser cell status.

Discussion

The data I generated and present in this chapter have been published as part of (Wagstaff et al. 2016). Other members of the Piddini lab have shown that directional migration between *scrib*^{KD} and wild-type cells requires functional E-cadherin-based adhesions and the presence of E-cadherin in the wild-type population. My data demonstrates that directional migration relies on *scrib*^{KD} cells maintaining their E-cadherin levels above those of wild-type: if the E-cadherin gradient is 'flattened', contact-induced migration no

longer occurs. However, I have also shown that E-cadherin elevation itself is not sufficient to drive migration, suggesting other players must be involved, either in concert with or parallel to E-cadherin.

It also remains unclear whether E-cadherin is part of a more complex signal required by the winner population to recognise and migrate directionally towards losers and/or whether it is required for a more mechanical aspect of the migration. Maintenance of cell-cell contacts between leader and follower cells is crucial for cohesive, collective cell migration and polarisation of the migrating group (reviewed in Mayor & Etienne-Manneville 2016). This explains why directional migration is abolished in the E-cadherin blocking experiments. However, I have demonstrated that reducing the E-cadherin in *scrib*^{KD} cells to wild-type levels also abolishes directed migration, implying that E-cadherin does more than simply maintain the integrity of the collective. Since overexpression of E-cadherin alone is not sufficient to trigger contact-induced migration, I propose that elevated E-cadherin is part of a more complex molecular signature in *scrib*^{KD} losers that is responsible for their migratory behaviour.

While I have implied that surface molecules like E-cadherin may be playing a role in the recognition event between loser and winner cells, this has proven difficult to address directly. In the migration assays I present, the readout for a wild-type cell recognising a *scrib*^{KD} cell as a loser is directed migration. I therefore cannot distinguish whether elevated E-cadherin in *scrib*^{KD} cells is necessary for their recognition as losers or the directional migration phenotype (or both). This can only be addressed once there is a way to disentangle recognition from contact-induced migration e.g. by tracking a molecular response within winner cells that only occurs upon contact with losers.

Considering that E-cadherin elevation is necessary but not sufficient for directional cell migration, there are most likely other molecules acting alongside it. Many of these are likely to be localised on the cell surface because of the requirement for contact between *scrib*^{KD} and wild-type cells. One could therefore screen for candidates by comparing the surface proteomes of the two populations. A way to do this would be by using membrane-impermeable biotin to label all cell surface proteins of *scrib*^{KD} and wild-type cells grown as homotypic cultures (in the absence of competition), purifying the proteins on streptavidin beads, and using mass spectrometry to identify any differentially expressed molecules (Elia 2008).

That said, one cannot disregard alternative possibilities that would not be detected using the surface biotinylation approach. For instance, loser cells might traffic a molecule to the membrane in response to collision, which triggers winners to follow them. Trafficking of proteins from intracellular vesicles to the cell surface would fall well within the timeframe of contact-induced migration: for example, vesicles containing the GLUT4 glucose transporter can be translocated to the cell membrane in response to insulin in under 15 minutes (Lampson et al. 2000). I have also not formally tested whether soluble factors are involved in directional migration in *scribble* competition, but neither I nor others in the Piddini lab have ever observed wild-type clones directionally migrating toward *scrib*^{KD} cells prior to collision (Piddini lab, unpublished). The two populations proliferate in their individual clones until they collide, which is only when the directed migration begins. It is therefore unlikely that directional migration is triggered by soluble factors in the MDCK system.

Lastly, I have shown that elevated E-cadherin alone does not induce loser status. I have also demonstrated that high E-cadherin in *scrib*^{KD} cells does not contribute to their loser cell status, discounting the possibility that elevated E-cadherin feeds into the signalling cascade responsible for *scrib*^{KD} cells' hypersensitivity to density. There must therefore be other molecular players bridging the mechanical stress a *scrib*^{KD} cell experiences and its acute response to density. An interesting corollary emerging from this data is that directional migration and density hypersensitivity of loser cells seem to be distinct processes. Consistently with this, others in the Piddini lab have shown that *scrib*^{KD} *p53KO* cells have elevated E-cadherin levels and exhibit contact-induced migration, but are not mechanical losers when co-cultured with wild-type cells (Wagstaff et al. 2016). I will revisit this in Chapters V, VI, and VIII.

It is worth noting that cells overexpressing E-cadherin are morphologically very similar to wild-type cells (Figure II.I, compare unlabelled E-cadOE cells and RFP-labelled wild-type cells) and do not flatten like *scrib*^{KD} cells As I will discuss in later chapters, cell flattening is not sufficient for directional cell migration but the two are closely linked in the MDCK experimental system. Whether a cell is flat is therefore a good predictor of its migratory behaviour: E-cadOE cells not flattening is consistent with these cells not engaging in contact-induced migration. Flattening is less well correlated with hypersensitivity to cell density (see Chapters VI and VIII), further indicating that

directional migration and mechanical loser status are most likely driven by distinct factors.

Chapter III: N-cadherin is not sufficient for directional migration or mechanical loser cell status, but P-cadherin may be involved in driving both

---

Having established that E-cadherin elevation itself is not sufficient for directed cell migration or loser status, I investigated two further candidate molecules that could be involved in these processes: N-cadherin and P-cadherin. Just like E-cadherin, both N- and P-cadherin are classical cadherins and have been implicated in collective cell migration, generation and transmission of mechanical forces, and polarisation of cells towards the direction of migration (reviewed in Plutoni et al. 2016). This made them attractive candidate molecules that could potentially be involved in the migration and density hypersensitivity of *scrib*^{KD} cells.

During EMT, when epithelial cells acquire a more motile, mesenchymal phenotype, loss of E-cadherin is associated with increased expression of N-cadherin: this is termed the 'cadherin switch'. Homotypic N-cadherin junctions are less robust than E-cadherin junctions and this promotes the migratory and invasive phenotypes (reviewed in Theveneau & Mayor 2012). What is more, N-cadherin induces contact inhibition of locomotion behaviour in cells undergoing EMT, resulting in their repolarisation and migration away from the cell mass (Scarpa et al. 2015). In MDCK cells, hepatocyte growth factor (HGF) has been shown to induce 'cadherin switching' and promote an invasive phenotype in 3D collagen matrices. In this system, N-cadherin has been shown to be required for cohesion within the migrating collective, as well as pro-migratory signalling. In contrast, N-cadherin cell-cell adhesions are too weak and/or transient on a stiff 2D substrate, so HGF-treated MDCKs migrate faster but as single cells in 2D (Shih & Yamada 2012). I therefore had reason to believe that N-cadherin may be involved in driving contact-induced migration between *scrib*^{KD} and wild-type cells, with E-cadherin perhaps helping maintain the collective nature of the migration on the stiff glass and plastic substrates used to culture the cells.

N-cadherin expression has been associated with numerous hallmarks of cancer, including increased proliferation, metastasis, an invasive phenotype, and resistance to chemotherapy. N-cadherin expression also correlates with poor cancer patient prognosis (reviewed in Yan et al. 2015). However, many tumours classed as invasive do not undergo

a full EMT switch and maintain some E-cadherin expression. In fact, many highly aggressive breast cancers have a wild-type pattern of E-cadherin expression but simultaneously express abnormally high levels of P-cadherin. Overexpression of P-cadherin, alongside wild-type E-cadherin levels, has been shown to promote invasion, motility, and migration of MCF-7 breast cancer cells (Ribeiro et al. 2010). Moreover, RNA sequencing experiments comparing transcripts from homotypic cultures of wild-type and *scrib*^{KD} cells showed that the latter express slightly more P-cadherin (Wagstaff et al. 2016), suggesting a similar mechanism may be involved in the directed migration of *scrib*^{KD} cells.

Please note that the experiments I describe in this section are not exhaustive and of a preliminary nature. I include them because they provide interesting leads to follow up in the future.

N-cadherin elevation is not sufficient for directional migration or loser status

Consistent with observations that elevated N-cadherin is correlated with a more motile, mesenchymal phenotype (like that of *scrib*^{KD} cells), I found that inducing *scribble* knockdown with TET resulted in the upregulation of N-cadherin expression, as visualised by Western blotting of whole cell lysates (Figure III.1A). In fact, *scrib*^{KD} cells expressed more N-cadherin than wild-type MDCKs, as I show by immunofluorescence (Figure III.1B). This was very reminiscent of the E-cadherin gradient between *scrib*^{KD} and wild-type cells. I therefore decided to test whether N-cadherin upregulation also played a role in contact-induced migration and mechanical loser status in MDCKs.

To address this, I used MDCK cDNA as a template to amplify canine N-cadherin and cloned it into the DOX-inducible pTRIPZ RFP-NLS vector, as I had done for E-cadherin (Appendix 2C). I used the resulting lentiviral construct to transduce unlabelled, wild-type cells and isolated a single clone that overexpressed N-cadherin (N-cadOE) to levels above those of *scrib*^{KD} cells (Figure III.1C). Similarly to E-cadOE cells, N-cadOE cells retained a wild-type morphology and did not flatten (Figure III.1D, compare unlabelled N-cadOE cells and GFP-labelled wild-type cells). I juxtaposed N-cadOE cells with wild-type cells and showed that there was no directed cell migration, as would be predicted by the lack of flattening

(Figure III.1E, first two panels). At the end of each migration experiment, I also verified that the N-cadherin levels of imaged N-cadOE cells were higher than those of surrounding wild-type cells (Figure III.1E, last two panels). An N-cadherin gradient between two MDCK populations is therefore not sufficient to drive contact-induced migration.

To test the involvement of N-cadherin in the mechanical loser status, I co-cultured N-cadOE cells and wild-type cells expressing nuclear GFP until the cultures reached densities at which *scrib*^{KD} cells would have been eliminated. Even at such high densities, N-cadOE cells remained in the monolayer and looked non-compacted and healthy, just like the surrounding wild-type cells (Figure III.1F, N-cadOE clones are labelled in white dashed lines). Due to the heterogeneous nature of GFP expression in the wild-type population, it was sometimes difficult to identify the unlabelled N-cadOE clones at the end of the experiment, but there was little to no cell death and no active clone compaction throughout the movies. I am therefore confident in concluding that N-cadherin overexpression is not sufficient to drive the mechanical loser phenotype.

Taken together, I have shown that increased N-cadherin expression alone is not sufficient to drive contact-induced migration or confer the mechanical loser status on cells.

Elevated P-cadherin levels may be necessary for contact-induced migration and loser cell status

I next investigated the role of P-cadherin in directional migration and mechanical loser status. The experiments described in this section are preliminary in nature, so any conclusions must be drawn with caution.

I used a cDNA library from *scrib*^{KD} cells, which transcriptionally elevate P-cadherin, to amplify P-cadherin cDNA. As before, I cloned the cDNA into the DOX-inducible pTRIPZ RFP-NLS overexpression vector (Appendix 2D) and transduced unlabelled wild-type cells with the resulting lentivirus. I then generated a pool population overexpressing P-cadherin (P-cadOE) using puromycin; I used this P-cadOE pool in all subsequent experiments. The pool nature of the P-cadOE cells is an important consideration, as will become apparent below.

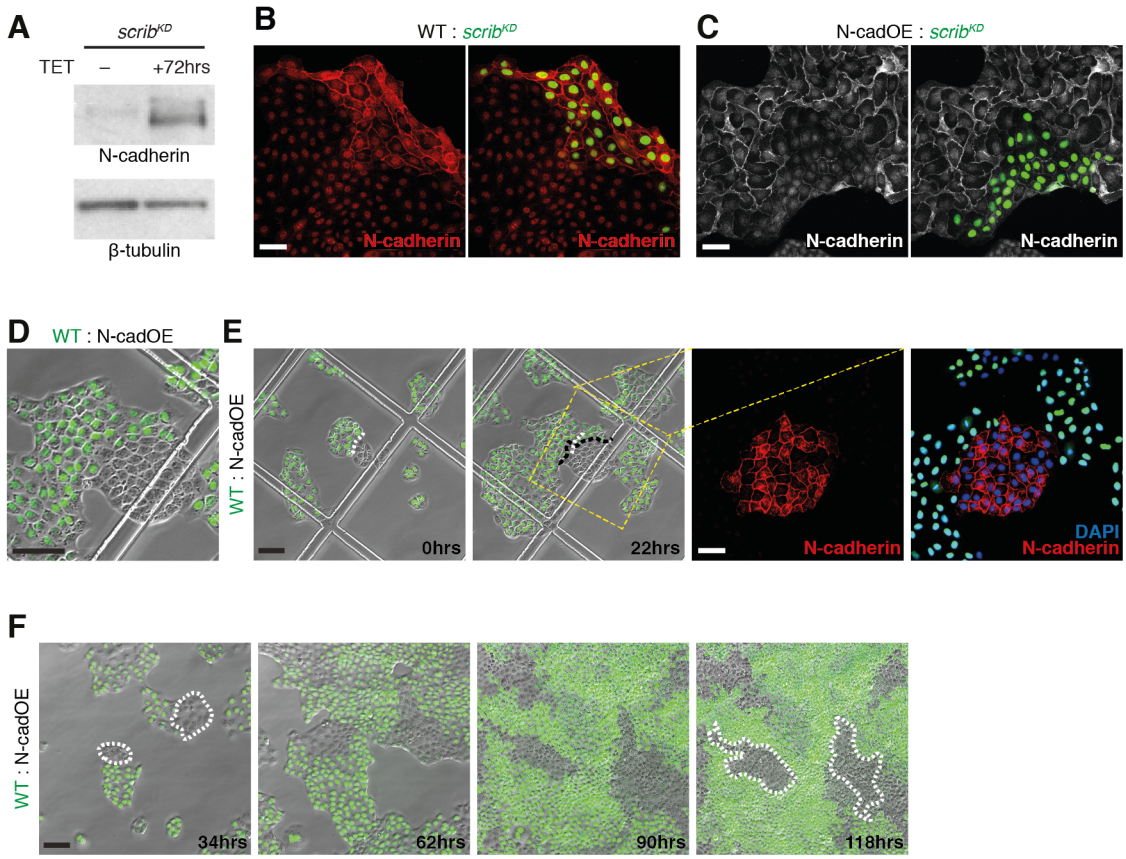

Figure III.1: N-cadherin is elevated in *scrib*^{KD} cells but is not sufficient to trigger directional migration or confer the mechanical loser status. (**A**) Western blot against N-cadherin in *scrib*^{KD} cells in the presence or absence of tetracycline (TET). β-tubulin was used as a loading control. (**B**) Immunofluorescence against N-cadherin of co-cultures of unlabelled wild-type cells and GFP-labelled *scrib*^{KD} cells. (**C**) Immunofluorescence against N-cadherin of co-cultures of GFP-labelled *scrib*^{KD} cells and wild-type cells overexpressing N-cadherin (N-cadOE). (**D**) 2x zoom of second panel in (E) demonstrating that N-cadOE cells (unlabelled) are not significantly flatter than wild-type cells (GFP-labelled). (**E**) Directional migration does not occur between GFP-labelled wild-type cells and unlabelled N-cadOE cells (left two panels). White dashed line marks initial contact point; black dashed line marks final contact point. N-cadherin immunofluorescence at the end of live imaging (right two panels) confirms elevated N-cadherin levels in N-cadOE cells. (**F**) Clones of unlabelled N-cadOE cells (white dashed lines) do not display mechanical loser features in co-culture with GFP-labelled wild-type cells.

Scale bars = 100 μm for movie sequences and 50 μm for immunofluorescence images.

While performing single clone selections of E-cadOE and N-cad OE lines, I had noticed that there was a lot of variability in construct expression in the parent pools, with some cells barely expressing any protein of interest (data not shown). Cadherins are large, multi-domain proteins, and increasing construct size has been correlated with lower lentiviral titres (Kumar et al. 2001). I therefore generated clonal populations from E-cadOE and N-cadOE to avoid heterogeneity of expression resulting from low titre lentiviruses. Unfortunately, I did not generate a clonal population of P-cadOE cells due to time constraints. It was therefore not surprising that I observed a mixed response to DOX in the P-cadOE pool: many cells remained morphologically wild-type but some clones flattened in a way similar to *scrib*^{KD} cells (Figure III.2A and B, blue and yellow arrows, respectively). It remains to be confirmed whether cell flattening within the P-cadOE pool corresponds to higher P-cadherin expression, which could be established by immunofluorescence.

Interestingly, in co-cultures of P-cadOE cells and wild-type cells expressing nuclear GFP, flat P-cadOE cells exhibited directional migration (Figure III.2C). In fact, flat P-cadOE cells also showed indications of density hypersensitivity: P-cadOE cells trapped between two wild-type clones died, suggesting they may not be able to tolerate high local cell density (Figure III.2C, yellow arrows indicate death events). Flattening of P-cadOE cells was infrequent and the cells were quickly dispersed through activation of the migratory response, so I could not observe whether larger P-cadOE clones were in fact compacted and eliminated at higher densities.

Considering the incomplete nature of these experiments, I tentatively propose that elevated P-cadherin is most likely sufficient to induce directed migration. High P-cadherin may also confer lower homeostatic density and density hypersensitivity on cells, both of which are hallmarks of mechanical losers.

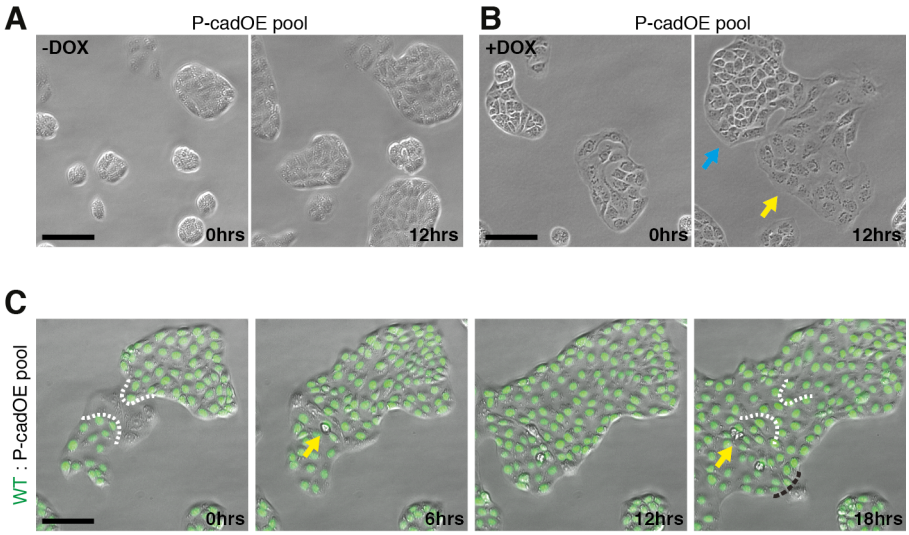

Figure III.2: P-cadherin overexpression flattens a subpopulation of cells and may be sufficient for directional migration and mechanical loser status. (**A-B**) Movie stills of MDCKs overexpressing P-cadherin in a DOX-inducible manner (P-cadOE) in the absence (A) or presence (B) of DOX. Flattened cells are indicated with the yellow arrow; cells with standard epithelial morphology are indicated with the blue arrow. (**C**) Movie stills of co-cultures of GFP-labelled wild-type cells and unlabelled P-cadOE cells. The flat P-cadOE clone is trapped between two wild-type clones that appear to corral it into a high density configuration that it cannot tolerate (death events are marked with the yellow arrows). White dashed lines mark the initial contact point; black dashed lines mark the final contact point.

Scale bars = 100 μm.

Discussion: the cadherin conundrum

I have shown that elevated N-cadherin is not sufficient for either directed cell migration or mechanical loser status during *scribble* competition. The requirement of N-cadherin in these processes was not investigated in the scope of this thesis. Addressing this would require the generation of an *N-cadherin* and *scribble* double knockdown/knockout cell line.

I also provide preliminary evidence that P-cadherin upregulation may be sufficient to both drive directional migration and confer the mechanical loser status on cells. Interestingly, P-cadherin overexpression has been shown to induce flattening and a more motile phenotype in pancreatic ductal adenocarcinoma cells (Taniuchi et al. 2005), supporting my preliminary findings. To further substantiate my observations, the priority would be to isolate a monoclonal P-cadOE population, verify its uniform P-cadherin overexpression, and determine whether high P-cadherin correlates with cell flattening. This would allow one to repeat and expand on my experiments with a 'clean' P-cadOE population. If my conclusions hold true, one could then generate *P-cadherin* and *scribble* double knockdown/knockout lines to test the requirement of elevated P-cadherin in $scrib^{KD}$ cell migration and mechanical loser status.

Based on observations and findings described so far and in subsequent chapters, I hypothesise that cells engaging in directed migration activate a plethora of potentially interlinked factors that constitute a 'migratory signature'. Most if not all of these factors are essential for directed migration, but are not sufficient to drive it on their own. I propose that E- and N-cadherin are part of this molecular signature. Please refer to Chapter VI where I discuss the migratory signature in light of data I describe in the rest of this thesis.

P-cadherin seems to play a more instructive role in the migratory signature, but I can only speculate on it based on the evidence presented: P-cadherin may activate a positive feedback loop that leads to the expression of other components of the migratory signature, or lies upstream of the whole signature, or drives migration in a completely independent way. While beyond the scope of this thesis, there are several key questions that it would be important to tackle. Does P-cadherin overexpression upregulate E-cadherin, which I have shown is necessary for the directed migration, or vice versa? Are

elevated P- and N-cadherin in *scrib*^{KD} cells necessary for contact-induced migration? Is boosting E-, N-, or P-cadherin (alone or in combination) in wild-type cells enough to 'flatten' the cadherin gradient and stop migration towards *scrib*^{KD} cells?

The cadherin expression pattern in *scrib*^{KD} cells does not reflect the classical cadherin switch where E-cadherin expression is lost in favour of N-cadherin to drive a migratory phenotype. *scrib*^{KD} cells express elevated levels of all three cadherins, E-, N-, and P-cadherin. On the other hand, wild-type MDCKs express very low levels of junctional N-cadherin (Figure III.1B and Shih & Yamada 2012), while E- and P-cadherin are expressed at a roughly equimolar ratio at levels higher than N-cadherin (Wu et al. 1993). Because of this, there is a gradient of all three cadherins between *scrib*^{KD} and wild-type cells. The cadherin gradient may therefore be part of a symmetry breaking cue to direct the migration of *scrib*^{KD} cells away from the wild-type population (or wild-type cells towards *scrib*^{KD} cells), as well as conferring a more motile phenotype on the former. In fact, I have discussed an example where E- and P-cadherin co-expression is sufficient to drive an invasive phenotype in breast cancer cells (Ribeiro et al. 2010). In addition, N-cadherin overexpression in the BT-20 breast cancer cell line that maintains high E-cadherin expression is sufficient to drive a more motile, invasive phenotype (Nieman et al. 1999). A similar non-EMT mechanism could therefore be responsible for directed cell migration in *scribble* competition.

The role of cadherins in the mechanical loser status appears less convoluted, but I must first express a word of caution. While my observations from competition assays are valid, it would be advisable to formally test whether N-cadOE and E-cadOE cells are not mechanical losers and that P-cadOE cells are. This could be done by compacting the cells in the absence of competition using a 'stretcher assay', where cells are plated either at confluence or at a low density on a stretched PDMS membrane. The membrane stretch is then released, mechanically compacting the confluent cells (experimental condition), but not significantly affecting the cells at lower density (control condition) (Eisenhoffer et al. 2012; Wagstaff et al. 2016). A density-dependent increase in cleaved caspase-3 staining above wild-type levels indicates a hypersensitivity to density that is characteristic of mechanical losers. That said, overexpression of neither N- nor E-cadherin resulted in cell flattening, another feature of mechanical losers. As I have discussed, *scrib*^{KD} cells (and potentially P-cadOE cells) have a lower homeostatic density, which contributes to their mechanical loser status. Based on this, I would therefore predict that E-cadOE and N-

cadOE cells are not hypersensitive to density, even in a stretcher assay, but that P-cadOE cells may be.

The molecular details of how P-cadherin may be conferring density hypersensitivity should only be investigated if my preliminary findings can be confirmed using a monoclonal P-cadOE population in the stretcher assay. One way to shortlist candidate molecules would be to compare targets regulated either only by P-cadherin activity (and not E- or N-cadherin) or those affected by P-cadherin in a uniquely identifiable way (e.g. P-cadherin engagement results in the phosphorylation of a target at a site that is not phosphorylated as a result of E- or N-cadherin activity). It should be possible to achieve this by using mass spectrometry to compare the proteomes of MDCKs lines individually silenced/knocked-out for E-, N-, and P-cadherin.

Chapter IV: p53-mediated competition shares molecular features of *scribble* competition

---

In the second part of my thesis (Chapter IV), I test whether the signalling cascade leading to *scrib*^{KD} cell elimination upon compaction is also conserved in mechanical losers generated through p53 activation alone.

In the *scribble* competition system, losers have elevated p53 even prior to the start of competition. Compaction-mediated ROCK activation triggers phosphorylation of the stress kinase p38 at T180 and Y182 (P-p38), which boosts p53 levels further still and ultimately leads to *scrib*^{KD} cell death through induction of apoptosis. Importantly, a p53 imbalance between losers (high p53) and winners (low p53) is sufficient to replicate mechanical cell competition. Experimentally, this is done by mildly elevating p53 in wild-type cells using sub-lethal doses of Nutlin and juxtaposing them with *p53KO* cells, which are unresponsive to Nutlin and maintain minimal p53 levels (Wagstaff et al. 2016).

It is clear that sub-lethal Nutlin treatment of wild-type cells replicates most of the phenotypic features of *scrib*^{KD} mechanical losers: Nutlin-treated cells flatten, their homeostatic density is lowered, and they display density hypersensitivity. However, it remained unaddressed whether the molecular cascade leading to loser cell outcompetition was conserved between the two mechanical competition systems. It is important to establish how similar *scrib*^{KD}- and p53-mediated competition models are because p53-mediated competition is, arguably, more broadly relevant from both a physiological and a clinical perspective. For instance, mechanical cell competition may lead to the elimination of cells with activated p53 as a result of injury or other cellular stress *in vivo*: exogenously boosting competition could therefore promote tissue fitness following damage. Moreover, cells lacking functional p53 (*p53KO*) are insensitive to mechanical competition, suggesting p53 loss in cancer is permissive for tumourigenesis, as potentially malignant cells escape elimination. In this case, reactivating signalling pathways responsible for the mechanical loser status in *p53KO* cells, and hence bypassing the requirement for p53, could offer a potential therapeutic approach.

I therefore investigated if key findings from the *scribble* competition system are also conserved in p53-mediated competition. If they are, I would argue that future work on characterising mechanical cell competition should mostly focus on the p53-mediated system, as it is free of any competition-independent effects of *scribble* knockdown. That said, p53 itself is a master regulator of many cellular processes and may therefore confer its own set of competition-independent phenotypes, so any conclusions should still be drawn with appropriate caution.

The ROCK – p38 – p53 signalling pathway is activated in p53-mediated mechanical losers

To determine whether the ROCK – p38 – p53 signalling cascade is conserved in p53-based competition, I quantified the nuclear p53 signal intensity of each cell within a pure population of wild-type cells treated with a sub-lethal dose of Nutlin, where the cells could reach their low homeostatic density (Figure IV.A). I compared these p53 intensities to those recorded for wild-type clones in a competing co-culture: *p53KO* cells versus wild-type in the presence of the same dose of Nutlin as homotypic cultures. I found that competing wild-type cells appeared more compacted than in a monoculture and had significantly elevated levels of p53 (Figure IV.B and C). This indicated that the initial p53 elevation as a result of Nutlin treatment is further boosted in response to compaction during competition.

In the *scribble* competition system, phosphorylation (activation) of p38 lies upstream of compaction-dependent p53 elevation (Wagstaff et al. 2016). I therefore used an antibody against phosphorylated p38 to compare the nuclear P-p38 intensities of Nutlin-treated homotypic wild-type cultures and compacted wild-type cells in a p53-mediated competition scenario. I found that P-p38 levels were significantly higher in compacted wild-type cells during competition (Figure IV.D-F). While these experiments do not demonstrate that phosphorylation of p38 is upstream of p53 activation, Nutlin-treated wild-type cells exhibit compaction-dependent elevation of both p53 and P-p38, mirroring the *scribble* competition system. I therefore propose that it is highly likely that the directional P-p38 -> p53 interaction is also conserved in the Nutlin competition system.

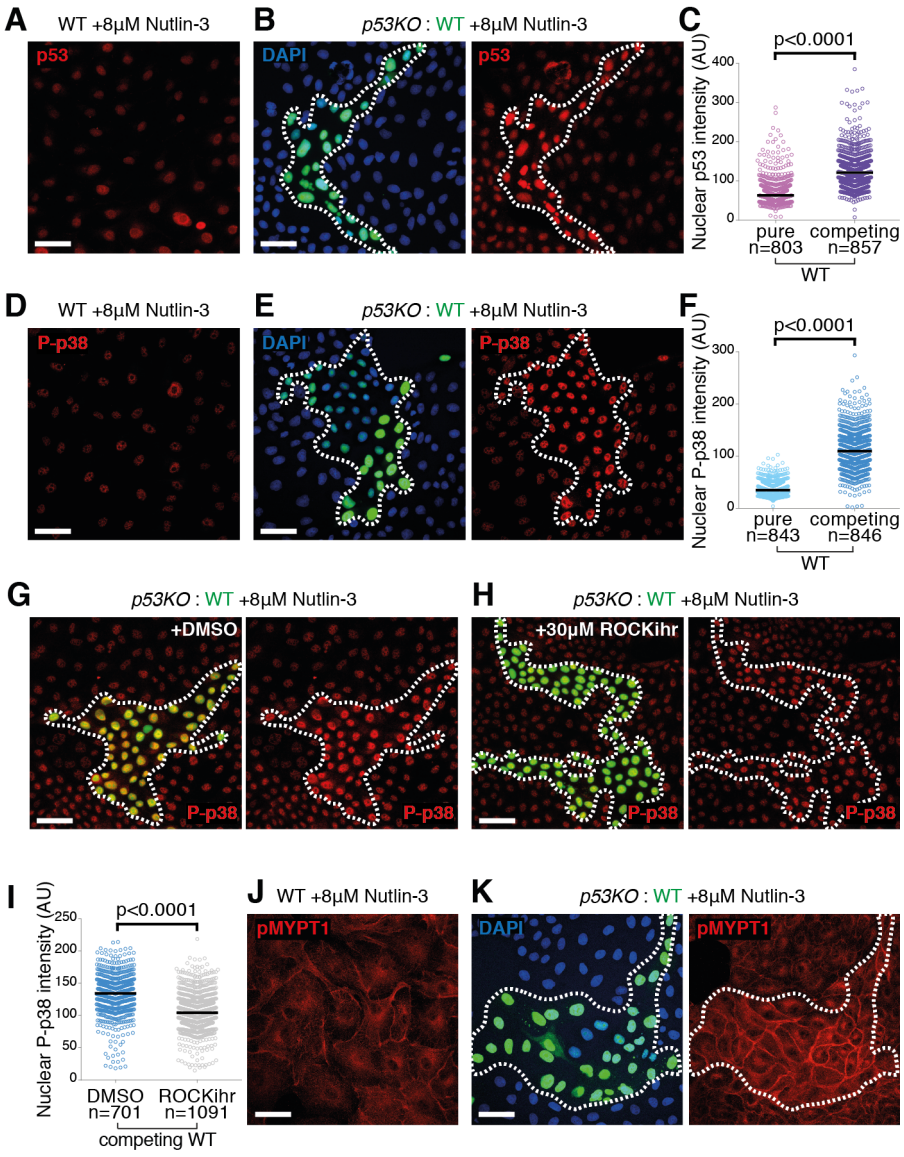

Figure IV: The molecular hallmarks of *scribble* competition are conserved in p53-mediated competition. (**A-B**) Immunofluorescence images (sum projections in z) showing p53 levels of wild-type cells treated with a sub-lethal dose of Nutlin-3 in a monoculture (A) and in a competing co-culture with *p53KO* cells (B). The GFP-labelled WT clone is outlined by the white dashed line here and in (E), (G), (H), and (K). (**C**) Quantification of single-cell nuclear p53 intensities from a single representative experiment as in (A-B). Here and in (F) and (I): black bars represent the median, p values were calculated using the K-S test, and n = number of nuclei. (**D-F**) Same as (A-C) but for phosphorylated p38 (P-p38) levels. (**G-H**) P-p38 levels in wild-type cells under competing conditions (G) are higher than in competing co-cultures treated with ROCK inhibitor Y27632 (H). (**I**) Quantification of single-cell nuclear P-p38 intensities from a single representative experiment as in (G-H). (**J-K**) Single immunofluorescence section showing phosphorylated

MYPT1 (pMYPT1) levels of Nutlin-3-treated wild-type cells grown as a monoculture (J) and in competing conditions (K).

Scale bars = 50 μm.

To test whether ROCK is activated in compacted wild-type cells during p53-mediated competition and, if so, lies upstream of P-p38, I used a chemical inhibitor of ROCK (Y27632). I treated competing co-cultures of wild-type and *p53KO* cells with ROCK inhibitor or the solvent (DMSO) and measured the nuclear P-p38 signal of compacted wild-type cells. I found that compaction-induced elevation of nuclear P-p38 was significantly reduced upon ROCK inhibitor treatment (Figure IV.G-I). Moreover, I immunostained compacted wild-type losers during Nutlin competition against Thr853-phosphorylated myosin phosphatase target subunit 1 (pMYPT1), a regulatory subunit of myosin phosphatase phosphorylated by ROCK specifically at this residue (Khromov et al. 2009; Qiao et al. 2014). pMYPT1 levels therefore provide an indirect but specific readout of ROCK activity: I showed that compacted wild-type losers have elevated pMYPT1, and hence more ROCK activity, compared to the surrounding *p53KO* winners (Figure IV.J-K).

Taken together, these findings indicate that p53-mediated competition in MDCK cells shares the key molecular hallmarks of *scribble* competition. Upon confrontation with *p53KO* winners, ROCK activity is detectably boosted in Nutlin-generated losers, as are the downstream signalling components P-p38 and p53.

Discussion

The data I describe in this chapter strongly support the hypothesis that the ROCK – p38 – p53 pathway responsible for the acute response of mechanical losers upon compaction is conserved between *scrib*^{KD}- and Nutlin-induced competition. I have shown that Nutlin-treated wild-type cells elevate nuclear p53 and P-p38 following compaction in competing cultures. I have also shown that ROCK activity is increased in compacted Nutlin-generated losers and is required for and likely upstream of p38 phosphorylation. If these key milestones are conserved in the Nutlin-based competition system, I believe it is highly likely that so is the rest of the cascade described in the *scrib*^{KD}-mediated system. Namely, that elevated P-p38 results in increased p53 and that compaction itself is sufficient to increase ROCK, P-p38, and p53.

What my experiments do not formally demonstrate is the connection between P-p38 and p53 or its directionality. This could be addressed by measuring nuclear p53 levels of

Nutlin-treated wild-type cells following compaction and p38 inhibitor treatment or the introduction of the catalytically inactive *p38K53N* allele (Wang et al. 1998). Following this, it would be worthwhile testing that compaction itself is responsible for elevation of ROCK, P-p38, and p53 in Nutlin-generated losers by compacting the cells in the absence of competition using the stretcher system. Considering the vast similarities between $scrib^{KD}$- and Nutlin-mediated losers, I suggest that the whole compaction-activated signalling cascade is likely conserved in the latter.

It is interesting to note that increased ROCK activity (and the resultant MYPT inactivation) in loser cells may also have a more direct, mechanical effect on competition. Broadly speaking, ROCK promotes cellular contractility (reviewed in Amano et al. 2010). Increased ROCK signalling in response to p53 activation could therefore mean that loser cells contribute to their own elimination by 'self-compacting'. The forces generated during this 'self-compaction' may be interpreted by a loser cell as surrounding cells pushing inwards on its membrane in a crowded tissue. This could help explain why mechanical losers have such an acute response to seemingly normal cell densities: loser cells may perceive densities to be higher than they are.

Further research should focus on understanding how mechanical compaction is translated into ROCK activation and how p53 confers density hypersensitivity. It would also be of great interest to test whether elevated p53 is also responsible for mechanical cell competition *in vivo*. It is easy to envisage how imbalances in p53 expression might occur in tissues e.g. as a result of stress, injury, or mutation in a subset of cells. If changes in p53 expression are sufficient to determine whether a cell is eliminated or gains a competitive advantage also *in vivo*, manipulation of this process may be of great therapeutic relevance. In theory, p53-mediated competition could be boosted to promote endogenous clearance of damaged cells, or reactivated in malignant cells escaping mechanical elimination.

Chapter V: p53 drives leader cell migration

In the third and final part of my thesis (Chapters V to VIII), I investigate the molecular mechanisms underlying the directional migration between *scrib*^{KD} and wild-type cells. I draw molecular parallels between migration occurring during competition and leader cell migration in wound healing. I also re-discuss data from Chapters II and III regarding the determinants of contact-induced migration in light of these new findings.

While live imaging untreated, sub-confluent cultures of wild-type MDCKs, Laura Wagstaff in the Piddini lab noticed the spontaneous emergence of cells with a distinctive, flattened morphology (Figure V.1A, yellow arrows). Laura noticed that these flattened cells were more motile than the surrounding wild-type cells with standard, epithelial morphology, but their movement lacked directionality. Following contact between these flat cells and cells with classical, epithelial morphology, the flat cells' migration acquired directionality. These flat cells would then lead the collective migration of the entire colony (Figure V.1A) in a behaviour reminiscent of contact-induced migration previously described for interactions between *scrib*^{KD} and wild-type cells (Figure I.8A). In fact, the supra-cellular finger-like structures formed as migration progressed, with the leader cell at the tip and other cells following it, were also remarkably similar to leader cell migration in a wound healing context (Poujade et al. 2007). As discussed, little is known about the mechanisms that allow leader cells to emerge from a seemingly homotypic culture. Considering how leader-like these flat cells were, I hypothesised that characterising them could offer an orthogonal strategy to study not only directed migration in *scribble* competition, but also wound-induced leader cell migration, which would make any findings more therapeutically relevant.

Spontaneous leaders in MDCK cultures have elevated p53

I first asked how pervasive the migration of spontaneously emerging flat cells was. I plated untreated, wild-type cells and imaged them over several days. When I analysed the behaviour of 112 spontaneously emerging flat cells, I found that around 90% of them

showed leader behaviour (Figures V.1A and B). I will refer to these cells as 'spontaneous leaders', as they emerge in the absence of external stimuli like wounding. Laura Wagstaff also noticed that spontaneous leaders often had two or even more nuclei: I confirmed this observation by live imaging wild-type cells expressing nuclear GFP. Spontaneous leaders did in fact tend to have multiple nuclei (Figure V.1C), although this was not always the case. The 'tetraploidy checkpoint' triggered upon cytokinesis failure and subsequent binucleation has been shown to induce cell cycle arrest in a p53-dependent manner (Andreassen et al. 2001), so I next tested whether spontaneous leaders continue dividing after they emerge. During the timeframe of my movies (≥48 hours), almost all (97.5%) of the 89 spontaneous leaders I analysed did not divide, while the surrounding cells with standard epithelial morphology did (Figure V.1D). This implied that spontaneous leaders might activate p53 signalling.

To assess the p53 status of spontaneous leaders, I seeded wild-type MDCKs in optically clear, gridded cell culture dishes that allowed me to identify and track spontaneous leaders during live imaging and locate them again on a confocal microscope after fixation and staining. Following anti-p53 immunofluorescence, I quantified the nuclear p53 signal intensity of spontaneous leaders and showed that they tend to have higher nuclear p53 levels than neighbouring non-leader cells (Figure V.1E and F). I next asked if p53 activity played an active role in driving the migration of leader cells.

p53 activation is sufficient and necessary for leader cell migration

Considering that spontaneous leaders elevate p53, I asked whether p53 activation itself is sufficient to generate leader cells. I did this by establishing an assay to irreversibly activate p53 in one cell population and confront it with another untreated, genetically similar population. More specifically, I used mitomycin C (MMC) to induce DNA damage in a wild-type population expressing nuclear GFP; MMC crosslinks complementary DNA strands, so the damage is irreversible (Tomasz 1995). I then seeded the MMC-treated cells in tissue culture dishes containing unlabelled, wild-type cells seeded a day earlier (Figure V.2A). This approach both prevented MMC carryover and generated larger clones of untreated cells to better visualise any leader-follower behaviour. As expected, DNA

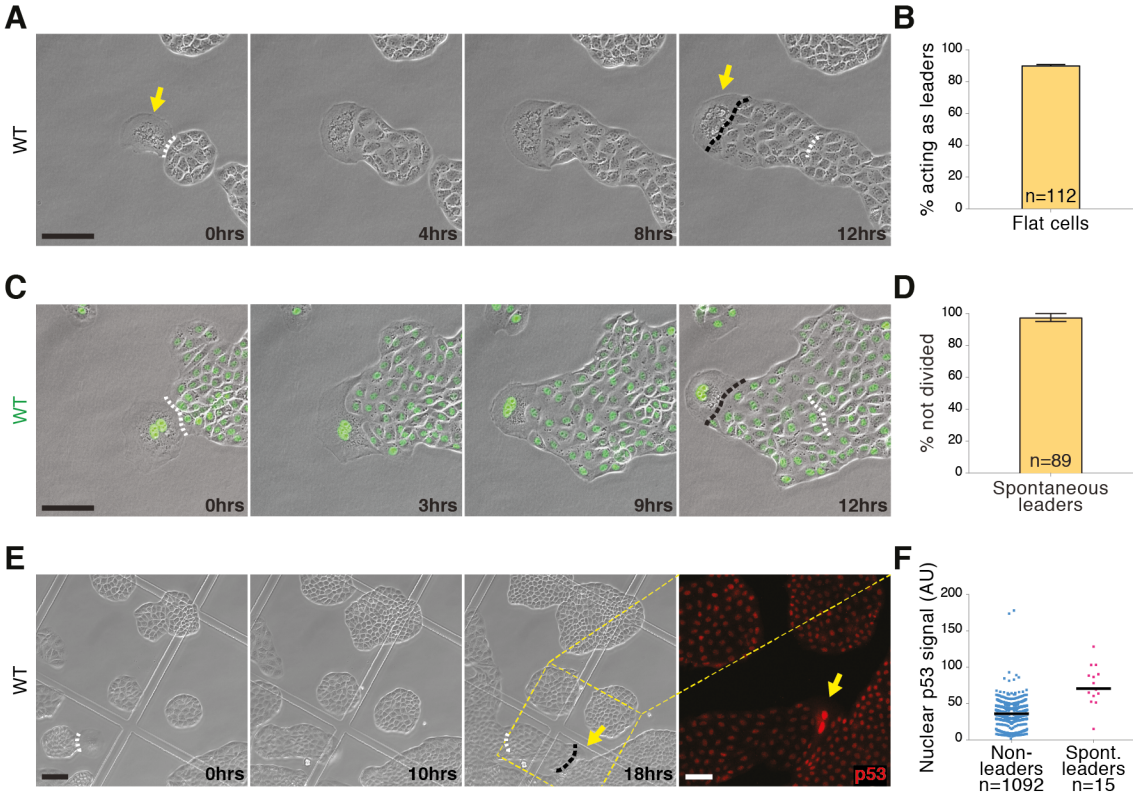

Figure V.1: Flat cells spontaneously emerging from untreated wild-type MDCK cultures show leader behaviour, are often binucleated, and have higher p53 levels than surrounding cells with standard epithelial morphology. (**A**) Time-lapse movie stills of untreated wild-type MDCK cultures in which a cell with flattened morphology (yellow arrow) has spontaneously emerged and displays leader behaviour following contact with neighbouring cells. I term such cells 'spontaneous leaders'. Here and in (C) and (E): white dashed lines mark the initial contact point; black dashed lines mark the final contact point. (**B**) Quantification of the frequency at which cells with flattened morphology act as leaders. Here and in (D): n = number of cells pooled from three independent repeats; error bars ± SEM. (**C**) Time-course movie stills of a binucleated spontaneous leader emerging from a wild-type MDCK population that expresses nuclear GFP. (**D**) Quantification of the number of spontaneous leaders that did not divide during the course of movie acquisition. (**E**) Movie stills (first three panels) following the migration of a spontaneous leader (yellow arrows). Fourth panel shows the confocal image of that same spontaneous leader following p53 immunostaining. (**F**) Quantification of single-cell nuclear p53 intensities of spontaneous leaders versus surrounding non-leaders. n = number of cells. A sample size of at least 212 leaders would be required to perform statistical analysis.

Scale bars = 100 μm for movie sequences and 50 μm for immunofluorescence images.

damage triggered stabilisation of p53 specifically in the MMC-treated population (Figure V.2B) (reviewed in Mirzayans et al. 2012).

I was careful to select a dose of MMC that would activate p53 to sub-lethal levels. At a dose of 7.5 μg/ml MMC, MDCK cells arrested their division and took on a flattened morphology, but remained viable for the duration of the experiment (Figure V.2C and D). MMC-treated cells also became slightly more motile than untreated cells but their migration was not directional (Figure V.2D, yellow and blue dashed lines indicate the trajectories followed by two cells during the experiment). The flattening was particularly intriguing, as *scrib*^{KD} cells and spontaneous leaders are both also flat, intrinsically more motile, and exhibit leader-like directional migration following collision with cells of classical, epithelial morphology. Canonical leaders have also been reported to have lost their classical epithelial morphology and be much larger and flatter than follower cells (Poujade et al. 2007). These observations drew me to hypothesise that cell flattening is potentially a prerequisite for leader fate; I will further discuss this in Chapter VIII.

Strikingly, when I co-cultured MMC-treated wild-type cells expressing nuclear GFP with unlabelled, untreated wild-type cells, the MMC-treated cells acted as leaders and guided the migration of untreated follower cells (Figure V.2E). I did not observe any directional migration following collisions between two untreated populations (Figure V.2F). Unpublished work in the Piddini lab also showed that p53 elevation following sub-lethal Nutlin treatment of wild-type cells was sufficient to trigger a leader phenotype after confrontation with *p53KO* cells. Together, this suggested that p53 elevation alone is sufficient to trigger the leader cell phenotype.

I next asked if p53 activation was necessary for the leader phenotype. I treated a *p53KO* population with MMC and found that a significantly lower proportion of cells behaved as leaders: following MMC treatment, only ~20% of *p53KO* cells behaved as leaders, compared to ~80% of wild-type cells (Figure V.2G and H). This trend can be visualised in the cell tracking analysis performed by Medhavi Vishwakarma in the Piddini lab (Figure V.2I-K). This suggested that p53 activity is required for the bulk of leader cell migration, Interestingly, MMC-treated *p53KO* cells still flattened but did not become leaders, suggesting flattening is not sufficient for the leader phenotype.

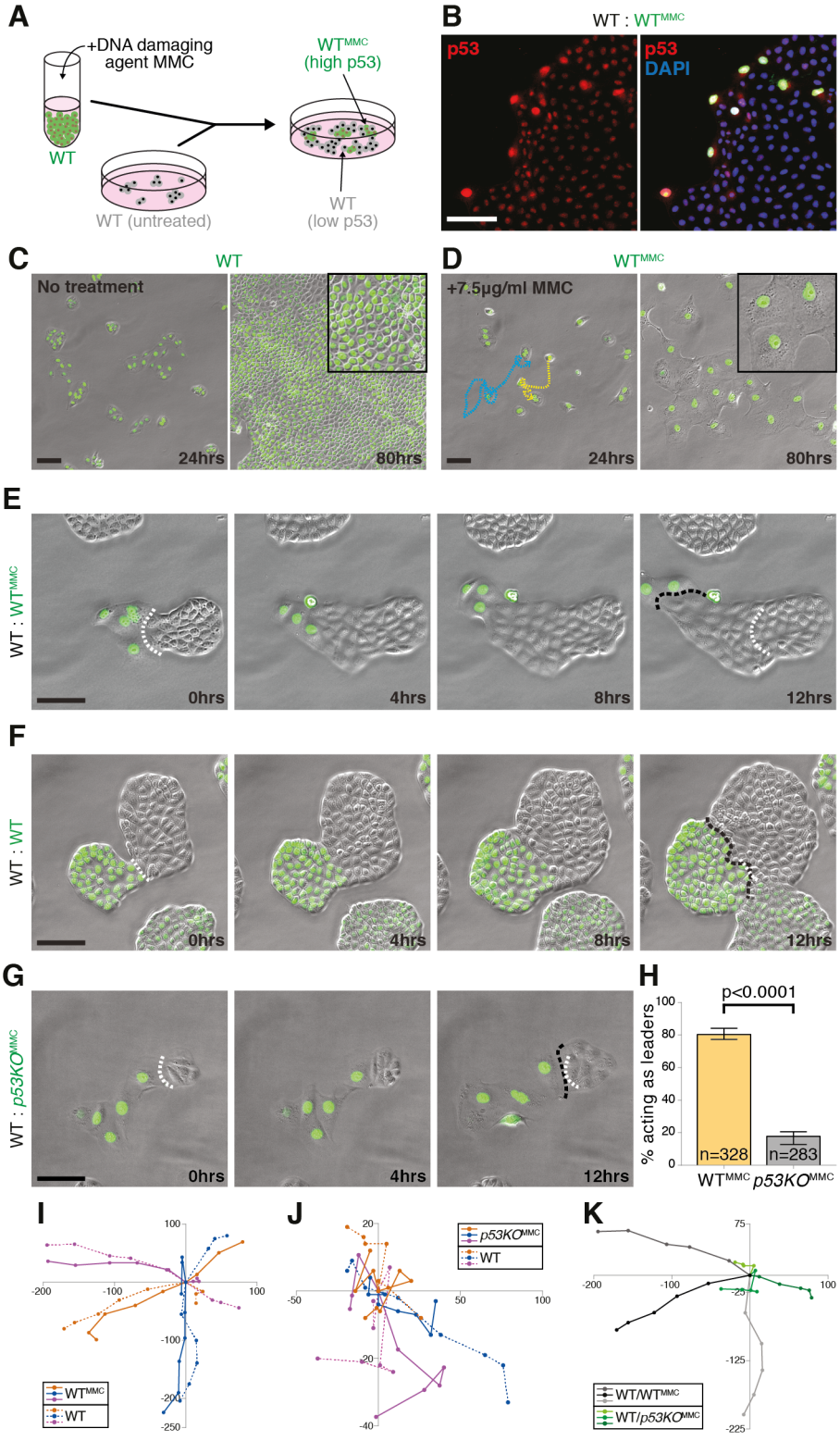

Figure V.2: p53 activation is both necessary and sufficient for leader cell behaviour. (**A**) Schematic illustrating the experimental design to test whether p53 is sufficient for leader cell fate, shown in (E). (**B**) Confocal images of a co-culture of unlabelled wild-type cells and mitomycin C (MMC)-treated wild-type

cells expressing nuclear GFP immunostained against p53. (**C-D**) MMC treatment (D) induces cell cycle arrest and flattening in GFP-labelled wild-type cells, compared to untreated control cells (C). MMC-treated cells are also more mobile: the yellow and blue dashed lines in (D) indicate trajectories of two cells during the experiment. The insets are 2x zooms of the two cell populations at 80 hours to demonstrate cell flattening in the MMC-treated condition. (**E-F**) Movie stills of co-cultures of unlabelled wild-type cells and MMC-treated (E) or untreated (F) wild-type cells labelled with nuclear GFP. Leader behaviour only occurs if one of the populations has been MMC-treated. Here and in (G): white dashed lines mark the initial contact point; black dashed lines mark the final contact point. (**G**) Movie stills from co-cultures of unlabelled wild-type cells and MMC-treated *p53KO* cells expressing nuclear GFP. (**H**) Quantification showing the percentage of MMC-treated wild-type or *p53KO* cells acting as leaders when confronted with untreated wild-type cells. p values were calculated using the K-S test. Error bars ± SEM. n = number of cells pooled from three independent repeats. (**I-J**) Coordinates of pairs of untreated wild-type and MMC-treated wild-type cells (I) or untreated wild-type and MMC-treated *p53KO* cells (J) plotted over time after they first establish contact at point 0,0. (**K**) Coordinates of untreated wild-type cells in two scenarios: where they are contacted by MMC-treated wild-type cells (grey shades) or MMC-treated *p53KO* cells (green shades). Untreated wild-type cells migrate much further following interaction with an MMC-treated wild-type leader.

Scale bars = 100 μm for movie sequences and 50 μm for immunofluorescence images.

The quantifications in (I-K) were performed by Medhavi Vishwakarma in the Piddini lab.

Taken together, I have shown that p53 activation is both sufficient and necessary to confer the leader cell fate on most leader cells.

Canonical leader cell markers are upregulated in spontaneous, *scrib*^{KD}-, and p53-driven leaders

Leader cells induced by scratching or barrier release are the gold standard in the leader cell migration field. These canonical leaders have been reported to be frequently binucleated, have an increased surface area, and divide more slowly compared to surrounding cells with standard epithelial morphology (Poujade et al. 2007; Reffay et al. 2011). All these features are shared by spontaneous leaders, while *scrib*^{KD} and MMC-treated cells only exhibit the latter two. These similarities led me to hypothesise that the p53 elevation present in spontaneous leaders, *scrib*^{KD} cells, and MMC-generated leaders may induce leader cell behaviour using the same factors required for the migration of scratch- or barrier release-induced leaders. Molecularly, leaders generated by barrier release upregulate Rac1, ITGβ1, and PI3K and require their activities to drive cell migration (Yamaguchi et al. 2015). I therefore tested whether these canonical leader markers were also upregulated and required in spontaneous leaders and those induced by *scribble* loss and p53 activation.

I used optically clear, gridded dishes and immunofluorescence to show that PI3K and ITGβ1 were both upregulated in spontaneous leaders (Figure V.3A-D). Interestingly, I also showed that *scrib*^{KD} cells expressed higher levels of PI3K and ITGβ1 than their wild-type neighbours (Figure V.3E-G), as did MMC-generated leaders (Figure V.4A-C). Consistently with this, when I treated actively migrating p53-driven leaders with PI3K or Rac1 inhibitors, their migration stalled (Figure V.4D-F). This strongly suggested that p53 lies upstream of PI3K and ITGβ1 activation and that migration of p53-driven leaders relies on the activity of PI3K and Rac1. I therefore propose that elevation of these markers in spontaneous leaders is a consequence of their elevated p53 levels.

scrib^{KD} upregulate canonical leader markers PI3K and ITGβ1, display a flattened morphology similar to spontaneous leaders, and engage in directional migration when confronted by wild-type cells. I therefore suggest that, during contact-induced migration,

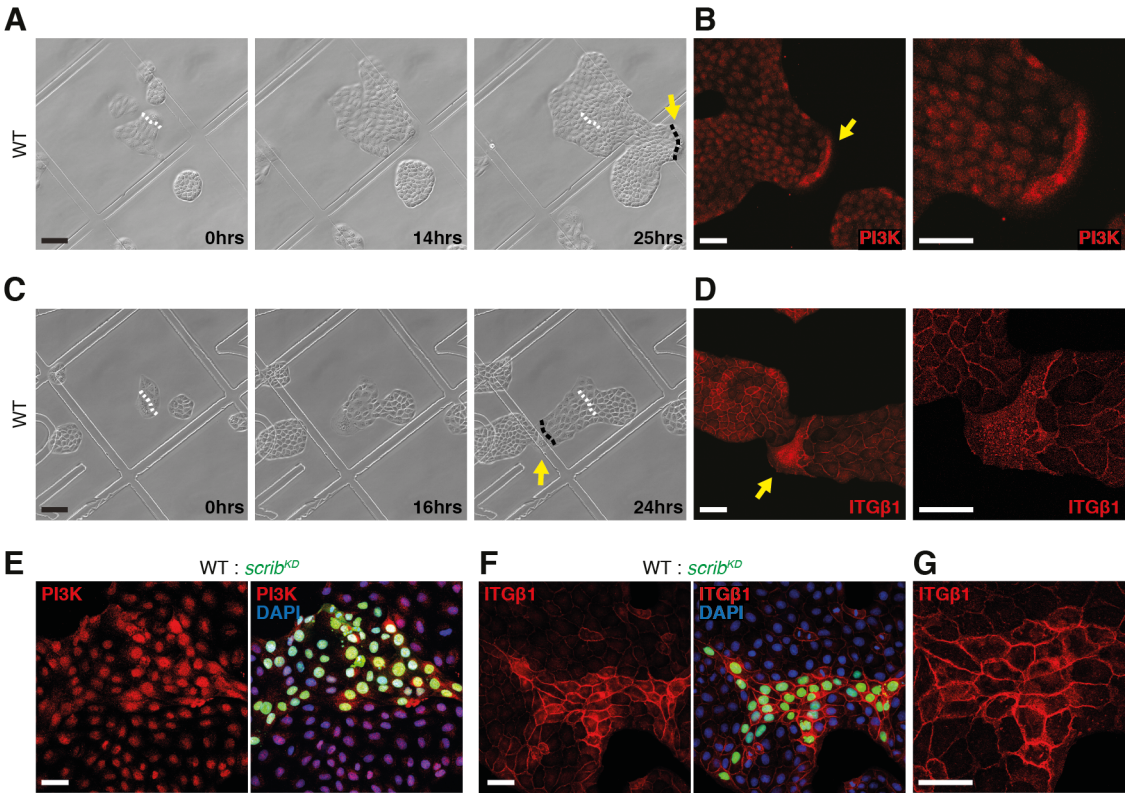

Figure V.3: Spontaneous and *scrib*^{KD} leaders have elevated canonical leader cell markers. (**A-B**) Movie stills (first three panels) following the migration of a spontaneous leader (yellow arrow). White dashed lines mark the initial contact point; black dashed lines mark the final contact point. The first panel in (B) shows a confocal image (maximum projection in z) of the same spontaneous leader following immunostaining against phosphoinositide 3-kinase (PI3K). The second panel in (B) is a 2x zoom of a single z slice taken from the stack in the first panel to better show PI3K localisation. (**C-D**) Same as (A-B) but for integrin β1 (ITGβ1). (**E-F**) Confocal images of co-cultures of unlabelled wild-type cells and GFP-labelled *scrib*^{KD} cells immunostained against PI3K (E) and ITGβ1 (F). (**G**) 2x zoom of a single z slice taken from the leftmost image in (F) to better show ITGβ1 localisation.

Scale bars = 100 μm for movie sequences and 50 μm for immunofluorescence images.

scrib^{KD} cells can be classified as leaders and wild-type cells as followers. As with spontaneous leaders, p53 may also drive PI3K and ITGβ1 expression in *scrib*^{KD} leaders, but the situation is less clear-cut because *scrib*^{KD} *p53KO* cells exhibit directional migration (Wagstaff et al. 2016). In other words, *scrib*^{KD} *p53KO* cells can still become leaders without functional p53. I will discuss this in Chapters VI and VIII in light of experiments I describe there: I propose that *scrib*^{KD} *p53KO* cells activate a pathway parallel to p53 to drive their migration.

Altogether, I have shown that spontaneously occurring flattened cells, *scrib*^{KD} cells, and MMC-treated cells all display the molecular hallmarks of canonical leaders and engage in leader cell migration. I also propose that elevated p53 in leaders lies upstream of PI3K and ITGβ1 upregulation.

Discussion

I have characterised spontaneously occurring leaders in untreated, wild-type MDCK cultures and shown that they have elevated p53 levels. I then demonstrated that p53 activation is both sufficient and necessary for leader cell migration, suggesting that p53 may be a universal driver of leader cell migration in MDCKs. I have also shown that spontaneous, *scrib*^{KD}-, and MMC-mediated leaders all upregulate both p53 and canonical leader cell markers PI3K and ITGβ1. p53 may lie upstream of canonical leader cell markers, but this needs to be further verified by immunostaining MMC-treated *p53KO* cells against PI3K and ITGβ1, for example.

p53 activation using MMC mimics many hallmarks of canonical leaders: flattening, cell cycle arrest, migratory phenotype, and expression of specific molecular markers. It is therefore likely that p53 elevation may also be instrumental in the migration of canonical leaders during wound healing; I will test this hypothesis in Chapter VII. Should this be the case, it could molecularly explain how only some cells are singled out to become leaders from a phenotypically homogeneous wound edge.

The most striking feature that spontaneous, *scrib*^{KD}-, and MMC-mediated leaders have in common is that they have significantly higher p53 levels than follower cells. Importantly,

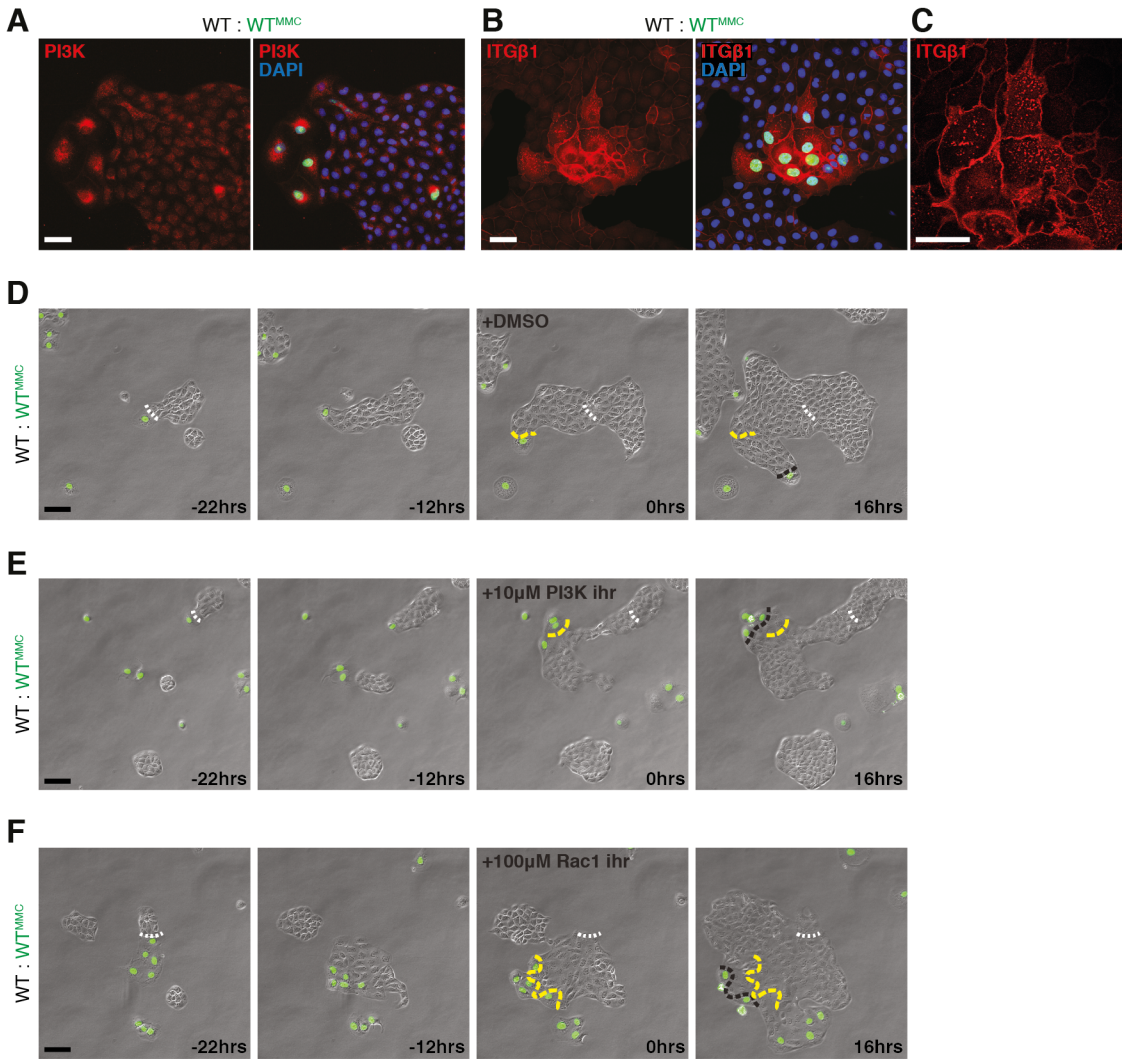

Figure V.4: MMC-driven leaders have elevated canonical leader markers, whose function they rely on for their migration. (**A-B**) Confocal images of co-cultures of unlabelled wild-type cells and MMC-treated wild-type cells expressing nuclear GFP immunostained against PI3K (A) and ITGβ1 (B). (**C**) 2x zoom of a single z slice taken from the leftmost image in (B) to better show ITGβ1 localisation. (**D-F**) Movie stills from co-cultures of unlabelled wild-type cells and MMC-treated wild-type cells labelled with GFP. White dashed lines mark the initial contact point; yellow dashed lines mark the contact point at which treatments were added; black dashed lines mark the final contact point. The addition of DMSO (D) does not affect the migration of MMC leaders, but acute chemical inhibition of PI3K (E) or Rac1 (F) stalls leader cell migration.

Scale bars = 100 μm for movie sequences and 50 μm for immunofluorescence images.

MDCKs with high p53 in homotypic cultures (e.g. MMC-treated cells) are more motile than wild-type cells, but their migration is random. It is only upon contact with a population with lower p53 that their migration becomes directional, heading away from the collision site. It is possible that p53 elevation induces cytoskeletal changes resulting in cells being 'poised' for migration but an imbalance in p53 activity is further required to provide a symmetry breaking cue to initiate leader cell behaviour.

These observations may be considered difficult to reconcile with the canonical role of p53 as a tumour suppressor, as it has been widely reported that wild-type p53 has anti-metastatic properties. For example, p53 promotes cell-cell adhesion by boosting E-cadherin expression and suppresses motility via inhibition of focal adhesion kinase (reviewed in Powell et al. 2014). Conversely, loss of p53 has been associated with increased migration in mouse embryonic fibroblasts, while tumours produced by experimental p53 inactivation are particularly invasive (reviewed in Roger et al. 2006). That said, tumours in *p53KO* mice are often not invasive and tend not to metastasise, suggesting that loss of p53 is not sufficient to drive the migration of malignant cells. In fact, there is increasing evidence to suggest that dominant negative, gain-of-function mutations in p53 are primarily responsible for its role in the context of migration and metastasis in cancer. Mutant variants of p53 are thought to exert their effects through binding and activating non-p53 promoters and potentially modifying the function of other p53 family proteins (reviewed in Powell et al. 2014).

Despite this apparent contradiction, pro-migratory effects of wild-type p53 have been described in other contexts, which are potentially more relevant to MDCK leader cell migration than cancer models. For example, human pulmonary fibroblasts become more proliferative and migratory following silicone dioxide treatment. Ablation of p53 activity inhibits migration in a scratch-wound assay in the presence of silicone dioxide (Wang et al. 2015). Similarly, p53 protein and mRNA levels are boosted at the migrating edges of mouse skin wounds, both in keratinocytes and in the recruited inflammatory cells. The role of p53 in this model was only investigated in the context of apoptosis of the inflammatory cells beneath the leading edge of the migrating epithelium, rather than in the migration itself (Kane & Greenhalgh 2000), but it remains plausible that p53 at the wound edge may also be contributing to the migration in this system.

Ultimately, it would be important to recapitulate the instructive role of wild-type p53 in migration in a system other than MDCKs. Firstly, conservation of a mechanism across multiple model systems would give more significance to the research, as it remains possible that my observations are a phenomenon restricted to a single cell line. Secondly, as the ultimate goal is to use any findings in a clinical setting, it would be important to be able to validate them in an *in vitro* or *ex vivo* human cell system. Lastly, there are far more tools available for non-canine systems (e.g. commercial antibodies and verified shRNA sequences) that could make further research quicker and more efficient.

In fact, our lab has recently started a collaboration with Stephane Gross (Aston University) to investigate whether p53-driven migration may be conserved during placental implantation. Preliminary results suggest that there may be an enrichment of p53 (and its effector p21) in the cells at the tip of the implantation structures in human trophoblast sections (unpublished data). This would be an interesting observation to follow up, as it could be a great model for non-pathological, physiologically relevant migration.

Chapter VI: The p53 effector p21 is the key driver of leader cell migration

Having shown that p53 drives leader cell migration, I next wanted to find out which downstream p53 targets are involved in this process. The major clue came from the observation that both spontaneous and MMC-driven leaders are cell cycle arrested and *scrib*^{KD} cells divide at a reduced rate (Wagstaff et al. 2016). One of the main transcriptional targets of p53 involved in cell cycle arrest is Cyclin-Dependent Kinase Inhibitor 1A (CDKN1A), also known as p21$^{WAF1/Cip1}$ (from here on referred to as p21) (Dulić et al. 1994). RNA sequencing experiments have previously shown that the *p21* transcript is more highly expressed in *scrib*^{KD} cells than in wild-type cells (Wagstaff et al. 2016). I therefore decided to investigate the involvement of p21 in leader cell migration.

p21 is sufficient for leader cell migration but not mechanical loser status

Using the same approach as for p53, I tracked the migration of spontaneous leaders using live imaging and then fixed the samples for immunostaining. Using a polyclonal anti-p21 antibody, I showed that spontaneous leaders have higher levels of p21 than surrounding non-leader cells (Figure VI.1A and B). It is worth noting that the p21 antibody and/or the expression pattern of p21 gives much more binary readouts than the p53 antibody.

I next asked if elevated p21 is instructive of leader cell fate. To address this, I constructed a lentiviral vector from which the concomitant expression of p21 and nuclear RFP could be driven by the addition of DOX (in a similar way to the construct I used to overexpress E-cadherin in Chapter II, see Appendix 2E). I transduced wild-type cells with the resulting lentivirus and generated a monoclonal cell line strongly and uniformly overexpressing p21 in a DOX-inducible manner (p21OE; Figure VI.1C and D). As expected, p21OE cells displayed cell cycle arrest specifically in the presence of DOX and, remarkably, adopted a flat leader-like morphology (Figure VI.1E and F). p21OE cells in homotypic cultures were also slightly more migratory than wild-type cells, similarly to *scrib*^{KD} and MMC-treated cells (Figure VI.1F, yellow arrows indicate the position of the same cell at the start and end of the experiment).

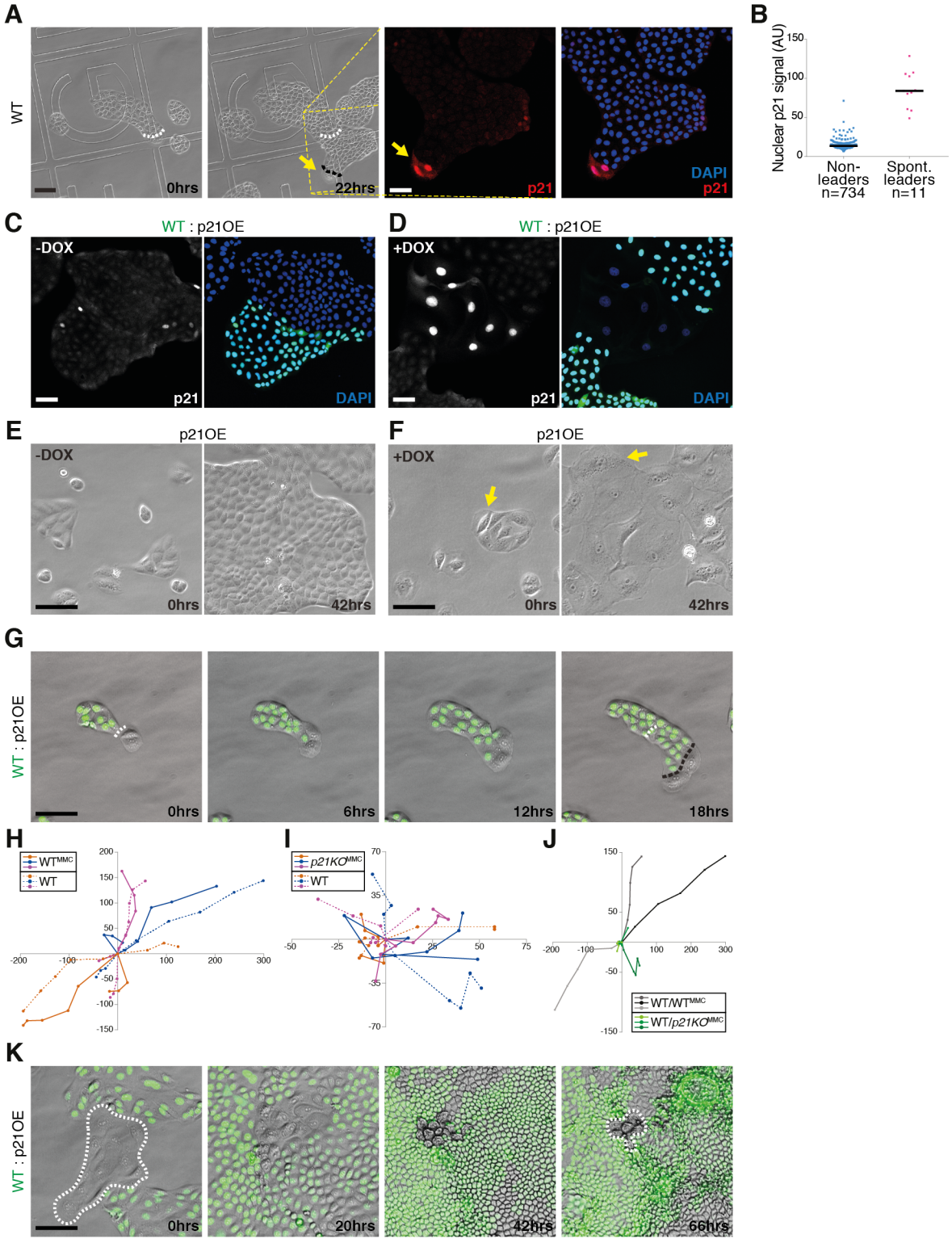

Figure VI.1: p53 target p21 is both necessary and sufficient to drive leader cell migration but does not confer mechanical loser status. (**A**) Movie stills (first two panels) of a migrating spontaneous leader (yellow arrows). Last two panels show confocal images of the same spontaneous leader following p21 immunostaining. Here and in (G): white dashed lines mark the initial contact point; black dashed lines mark

the final contact point. (**B**) Quantification of single-cell nuclear p21 intensities of spontaneous leaders versus surrounding non-leaders. n = number of cells. A sample size of at least 47 leaders would be required to perform statistical analysis. (**C-D**) Confocal images of co-cultures of GFP-labelled wild-type cells and unlabelled cells overexpressing p21 (p21OE) in a DOX-inducible manner. Immunostaining against p21 in the absence (C) or presence (D) of DOX shows strong, DOX-dependent induction of p21 expression in p21OE cells. (**E-F**) p21 overexpression induces cell cycle arrest and flattening of p21OE cells (F), compared to DOX-free conditions (E). p21OE cells are also more motile: yellow arrows in (F) indicate the position of the same cell at the beginning and end of the experiment. (**G**) Movie stills from co-cultures of GFP-labelled wild-type cells and unlabelled p21OE cells. (**H-I**) Coordinates of pairs of untreated wild-type and MMC-treated wild-type cells (H) or untreated wild-type and MMC-treated *p21KO* cells (I) plotted over time after they first establish contact at point 0,0. (**J**) Coordinates of untreated wild-type cells in two scenarios: where they are contacted by MMC-treated wild-type cells (grey shades) or MMC-treated *p21KO* cells (green shades). Untreated wild-type cells migrate much further following interaction with an MMC-treated wild-type leader. (**K**) Unlabelled p21OE clones (white dashed line) are compacted but not eliminated by surrounding GFP-labelled wild-type cells.

Scale bars = 100 μm for movie sequences and 50 μm for immunofluorescence images.

The quantifications in (H-J) were performed by Medhavi Vishwakarma in the Piddini lab.

When I co-cultured p21OE cells with wild-type cells expressing nuclear GFP, I found that the p21OE population became leaders and led the migration of wild-type followers (Figure VI.1G). This observation is corroborated by the cell tracking analysis performed by Medhavi Vishwakarma in the Piddini lab (Figure VI.1H-J). The leader/follower migration resulted in the compaction of p21OE clones by wild-type neighbours to densities at which *scrib*^{KD} cells would be eliminated. Unexpectedly, p21OE were often not outcompeted (Figure VI.1K), suggesting that p53-mediated density hypersensitivity of losers is not driven through p21. This demonstrated that p21 activation is sufficient to drive leader cell migration but does not confer the mechanical loser status. It would be important to verify whether p21OE cells are indeed not mechanical losers using stretcher experiments where cells can be compacted in the absence of competition. If compaction is insufficient to elevate the p53 in p21OE cells, then this could explain why they are not eliminated during competition.

I next wanted to establish whether p21 activity was also necessary for the leader phenotype.

Construction of the *p21KO* MDCK cell line

In order to test the requirement of p21 in leader cell migration, I constructed a *p21* knockout (*p21KO*) cell line using CRISPR/Cas9 technology. I designed two short guide RNA (sgRNA) target sequences targeting the 5' end of exon 2 of canine *CDKN1A*, which is the first translated exon (Figure VI.2A). I cloned these target sequences individually into a previously published vector encoding the Cas9 D10A 'nickase' variant of the Cas9 nuclease derived from *Streptococcus pyogenes* and the sgRNA scaffold (Appendix 2J) (Wyman et al. 2013). Thanks to the nickase mutation, only a single DNA strand is cleaved at each of the positions in the genomic DNA specified by the sgRNA, which results in a staggered double-stranded break (DSB). The advantage of the nickase system over the wild-type Cas9, which creates DSBs directly, is that generates fewer off-target hits. Error-prone DNA repair mechanisms activated in response to DSBs can occasionally lead to insertions and/or deletions of base pairs at the targeted locus. This ultimately disrupts the coding region of the target protein and creates a non-functional allele (reviewed in Sander & Joung 2014).

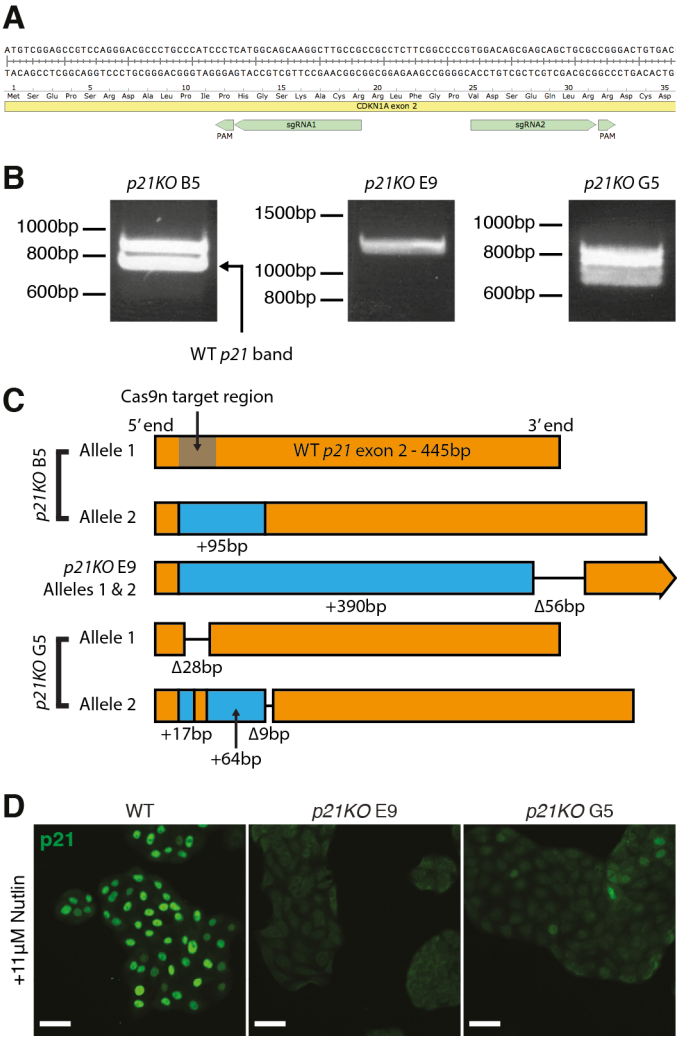

Figure VI.2: Construction and verification of the *p21KO* MDCK lines. (**A**) Target region for CRISPR/Cas9 mutagenesis in exon 2 of canine *CDKN1A* (*p21*). sgRNA1 and sgRNA2 indicate the target sequences used to guide a pair of Cas9 nickase enzymes. PAM = protospacer adjacent motif. (**B**) Agarose gel containing the PCR products from a reaction amplifying a ~800bp region around the *CDKN1A* locus from the genomic DNA of clones B5 (heterozygous mutant, leftmost panel), E9 (pseudo-homozygous mutant with only one *CDKN1A* allele, middle panel), and G5 (homozygous mutant with two different mutant alleles, rightmost panel). (**C**) Schematic representation of the sequencing analysis of the three mutant clones. (**D**) Confocal images of homotypic cultures of wild-type cells (leftmost panel), or *p21KO* clones E9 (middle panel) and G5 (rightmost panel) treated with a mild dose of Nutlin-3 and stained against p21.

Scale bars = 50 μm.

Normally, Nutlin treatment activates p53 and hence its transcriptional targets, including the cell cycle inhibitor p21. By definition, *p21KO* cells lack functional p21, so they should not be growth-inhibited in the presence of Nutlin. I followed this logic to enrich for a pool of MDCKs lacking functional p21 by culturing cells transfected with the Cas9 nickase vectors for six days at a moderate dose of Nutlin. I split the surviving cells at a low density to isolate single clones. I then pre-screened the clones using p21 immunofluorescence in the presence and absence of Nutlin (data not shown) and chose the following for further characterisation: two clones that did not show Nutlin-induced p21 elevation (E9 and G5) and one that expressed p21 as a negative control for *p21* knockout (B5).

To verify whether I had generated true *p21KO* clones, I used PCR to amplify a region containing exon 2 of *CDKN1A* (just under 800 bp) from the genomic DNA of the three clones. Visualisation of the PCR products on an agarose gel showed that the 'negative' control B5 clone had two bands: one of the expected size, and one around 100 bp larger (Figure VI.2B, leftmost panel). This implied that only one of the *p21* alleles was truly wild-type and the other most likely contained an insertion. Clone B5 was therefore a heterozygous *p21KO* clone and was still able to drive p21 expression (data not shown). In contrast, clone E9 only had one band, much larger than the predicted size for a wild-type band (Figure VI.2B, middle panel). Clone G5 had two bands: one at the 800 bp mark, and one slightly smaller than that (Figure VI.2B, rightmost panel). The minute size difference between the larger G5 band (800 bp) and the wild-type band (just under 800 bp) implied that there might have been a small insertion in that allele of clone G5. In fact, sequencing revealed this was exactly the case. Clone G5 returned two sequences: one with a 28 bp deletion and one with a mixture of deletions and insertions but a net size increase; both of these mutations generated frameshifts at the *p21* locus. Clone B5 gave two sequences: one wild-type and one with a 95 bp insertion, as I predicted from the PCR. Clone E9 only had one sequence with a large insertion and a small deletion, implying it had completely lost the other allele or potentially duplicated the mutated one. These results are summarised in Figure VI.2C.

Having established that clones E9 and G5 were disrupted at both *p21* loci by sequencing, I formally tested their loss of functional p21 by immunofluorescence in the presence of Nutlin. Rather than using the heterozygous *p21KO* clone B5 as a control, I reverted to wild-

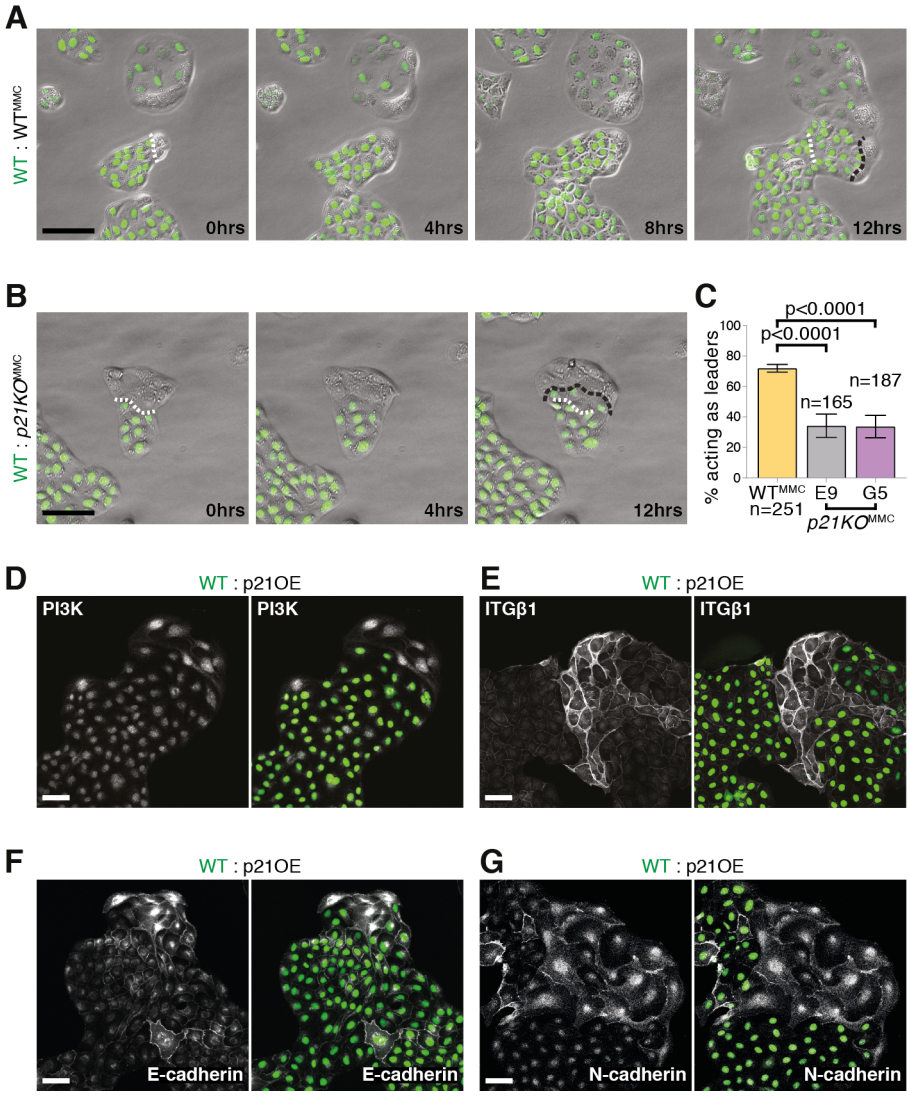

Figure VI.3: p21 activity is necessary for leader migration and lies upstream of canonical leader cell markers, E-cadherin, and N-cadherin. (**A-B**) Stills from movies of GFP-labelled wild-type cells co-cultured with unlabelled, MMC-treated wild-type (A) or p21 knockout (*p21KO*) cells (B). White dashed lines mark the initial contact point; black dashed lines mark the final contact point. (**C**) Quantification showing the percentage of MMC-treated wild-type or *p21KO* cells acting as leaders when confronted with untreated wild-type cells. n = number of cells. p values were calculated using the K-S test. Error bars ± SEM. (**D-G**) Unlabelled p21OE cells display higher levels of PI3K (D), ITGβ1 (E), E-cadherin (F), and N-cadherin (G) than GFP-labelled wild-type cells.

Scale bars = 100 μm for movie sequences and 50 μm for immunofluorescence images.

type cells as the benchmark for p21 activity. In agreement with the sequencing analysis, I found that both *p21KO* clones E9 and G5 showed minimal p21 activity in response to Nutlin (Figure VI.2D).

p21 is necessary for leader migration and lies upstream of canonical leader markers, E-cadherin, and N-cadherin

Having confirmed that I had generated two functional *p21KO* clones, I next asked whether p21 is necessary for leader cell behaviour. As discussed earlier, MMC treatment of wild-type cells is sufficient to drive leader migration when confronted with their untreated counterparts (Figure VI.3A). Strikingly, MMC-treated *p21KO* cells behaved as leaders less often but still displayed a rather flat, leader-like morphology (Figure VI.3B and C). Taken together, the data I describe in Chapter V and here suggest that p53 drives leader cell migration through activation of its transcriptional target p21.

I have previously shown that p53-driven leaders activate canonical leader cell markers PI3K and ITGβ1, implying that they lie downstream of p53. I therefore tested where canonical leader marker expression lies with respect to p21 activation. Using immunofluorescence, I showed that p21 overexpression alone may be sufficient to upregulate both PI3K and ITGβ1 (Figure VI.3D and E). Interestingly, p21OE cells also tended to display higher levels of E- and N-cadherin, markers upregulated in *scrib*^{KD} cells, which also display leader behaviour (Figure VI.3F and G). *scrib*^{KD} cells have high p21 levels (Wagstaff et al. 2016), which would imply that PI3K, ITGβ1, E-cadherin, and N-cadherin are expressed downstream of p21 also in *scrib*^{KD} leaders. That said, this hypothesis would need to be formally tested using a *scrib*^{KD} *p21KO* line.

Taken together, these experiments suggest that leaders upregulate multiple markers as part of a 'leader cell signature' and that these markers are activated downstream of p53 signalling via p21.

Discussion: the leader cell signature

So far, I have described four types of MDCK leaders: *scrib*^{KD} cells, spontaneous leaders, MMC-induced leaders, and p21OE cells. The expression pattern of and requirement for published and novel leader cell markers in these four types of leaders and canonical leaders is summarised in Table 1. Because of the morphological and molecular similarities between all described types of MDCK leaders, I suggest that one may be able to extrapolate findings from one type of leader to others. For example, it is possible that the E-cadherin gradient is also required for the migration of spontaneous and p53-driven leaders, not just *scrib*^{KD} cells. It would be interesting to experimentally verify this in the future.

	Leader marker											
	E-cadherin		**N-cadherin**		**P-cadherin**		**PI3K**		**ITGβ1**		**Rac1**	
Type of leader	↑	Req.	↑	Req.	↑	Req.	↑	Req.	↑	Req.	↑	Req.
Canonical barrier release							✓	✓	✓	✓	✓	✓
scrib^{KD}	✓	✓*	✓*		✓		✓*		✓*			
Spontaneous							✓*		✓*			
p53-mediated							✓*		✓*			✓*
p21OE	✓*		✓*				✓*		✓*			

Table 1: Molecular markers upregulated in different types of MDCK leader, based on (Yamaguchi et al. 2015), (Wagstaff et al. 2016), and data presented in this thesis. P-cadherin is included for completeness but its involvement requires further testing.

"↑" indicates whether a given marker is upregulated; "Req." indicates whether a given marker is required for leader migration. Asterisks (*) indicate experiments I have done myself and present in this thesis; blank spaces indicate that that combination has not been tested yet.

Taking together observations from all investigated types of leaders, I propose the existence of a multi-component leader cell signature shared by all leaders in the MDCK system. The leader signature includes, but is not necessarily limited to, elevated

expression of PI3K, ITGβ1, Rac1, E-cadherin, and N-cadherin. Neither E- nor N-cadherin are sufficient to drive leader migration on their own and appear to be activated alongside PI3K and ITGβ1 (as demonstrated in *scrib*^{KD} cells). Moreover, PI3K and ITGβ1 have been shown to regulate Rac1 in the context of leader migration independently of each other (Yamaguchi et al. 2015). I therefore suggest that leader signature components may be acting in parallel pathways and that their concerted activities are required for the coordinated, directed migration of leader cells, even though the evidence for this is still incomplete (Table 2).

Molecularly, the leader signature is likely promoting cytoskeletal changes predisposing cells for migration or actively participating in it, and may be responsible for leader cell flattening. The boosted expression of multiple intracellular and extracellular molecules may also be responsible for generating asymmetry cues that can be sensed by leaders and/or followers to promote the directionality of leader cell migration. It would be interesting to determine whether there is any interplay between the signature components and what processes lies downstream of each of them.

Molecule	Necessary for leader migration	Sufficient for leader migration
PI3K	Yes	[not tested]
ITGβ1	Yes	[not tested]
Rac1	Yes	[not tested]
E-cadherin	Yes*	No*
N-cadherin	[not tested]	No*
P-cadherin	[not tested]	Yes*
p53	Yes*	Yes*
p21	Yes*	Yes*

Table 2: The requirement for different molecules in the migration of MDCK leaders, based on data extrapolated from (Yamaguchi et al. 2015), (Wagstaff et al. 2016), and this thesis. Proposed leader signature molecules are italicised.

Asterisks (*) indicate experiments I have done myself and present in this thesis.

The data I present here and in Chapter V suggests that p53 drives MDCK leader cell migration through its transcriptional target p21. Increased p21 activity leads to

expression of the leader signature, implying that p53/p21 activity lies upstream of leader cell marker expression. Interestingly, density hypersensitivity of mechanical losers does not seem to be mediated by p21, suggesting it is part of a separate, p21-independent pathway downstream of p53. This is particularly interesting, as it could explain how cells with elevated p53 may be eliminated by mechanical competition in non-migratory tissues like homeostatic adult epithelia.

I have shown that p53 activation is both sufficient and necessary for leader cell behaviour, but an important exception to this are *scrib^{KD} p53KO* cells, which are not mechanical losers but still act as leaders (Wagstaff et al. 2016). To reconcile these data, I propose the following. Loss of *scribble* affects multiple pathways, one of which is p53, responsible for *scrib^{KD}* cells' hypersensitivity to density and, through p21, for their leader behaviour. *scrib^{KD} p53KO* cells have little p21 activity but maintain high expression of E-cadherin, a leader signature marker (Wagstaff et al. 2016). While I have not tested this, I would hypothesise that *scrib^{KD} p53KO* cells also express high levels of other leader signature markers e.g. PI3K and N-cadherin. This would imply that loss of *scribble* simultaneously feeds into a pathway parallel to or downstream of p21 to drive leader signature expression, or that *scrib^{KD} p53KO* cells have a p53- and p21-independent way of activating those markers. As I will discuss in Chapter VIII, one possibility is that *scrib^{KD} p53KO* cells activate other cell cycle inhibitors (e.g. p16) that lie upstream of the leader signature, parallel to p21.

Chapter VII: p53 and p21 activity drive migration of leader cells during wound healing, many of which become mechanical losers and are eliminated at wound closure

---

In Chapters V and VI, I established that increased p53/p21 activity is both sufficient and necessary for leader cell migration. I also demonstrated that p53- and p21-driven leaders share the same molecular mechanisms as canonical leaders. I therefore next asked whether p53 and p21 may also play an instructive role in the migration of canonical leaders, both during scratching and barrier release. This was an attractive hypothesis because it could potentially explain how only some cells are singled to become leaders from a superficially homogeneous environment at wound edges. What is more, a better understanding of the factors that drive cell migration during wound healing could help identify future treatments to accelerate wound closure *in vivo*.

Scratch-induced and barrier release leaders elevate p53 and p21

Historically, leader cell migration has been studied using one of two assays: scratching of a lawn of cells or releasing a barrier from around a confluent monolayer. Both of these manipulations are used to generate space for migration to proceed into, as physical damage is not required to trigger leader migration. Barrier release is generally more accepted, as it minimises the damage element at the colony edge (Poujade et al. 2007), but I expected scratching may be more relevant from a physiological wound healing perspective. I therefore set out to assess the p53/p21 status of canonical leaders generated using both methods.

Using a P1000 pipette tip, I generated scratch-wounds in confluent monolayers of wild-type MDCKs. I followed the emergence and migration of leaders using live imaging, and then fixed the samples for immunofluorescence. I found that both p53 (Figure VII.1A and B) and p21 (Figure VII.1C and D) tended to be upregulated in scratch-generated leaders, although this could not be statistically tested for significance due to an insufficient sample

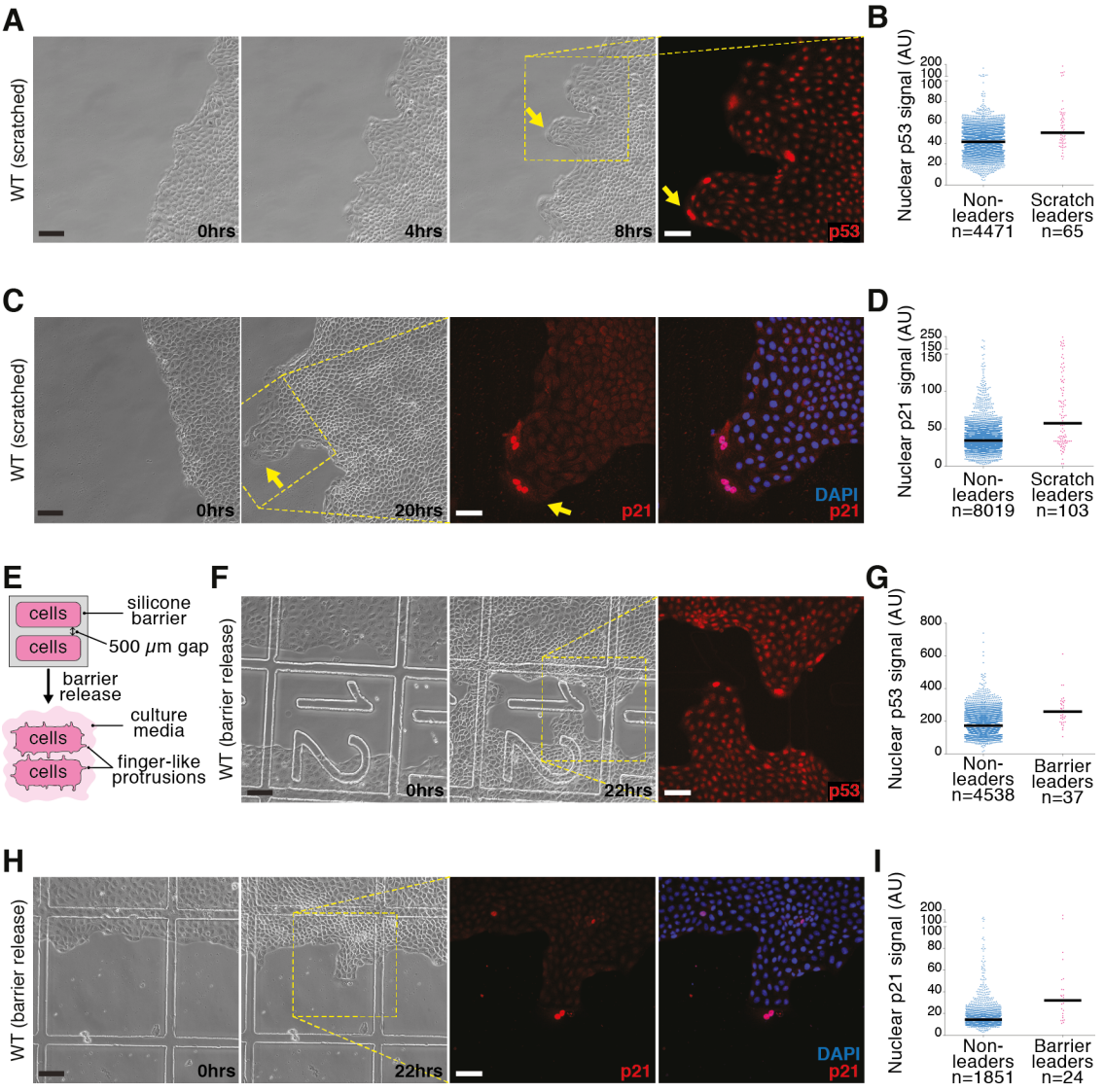

Figure VII.1: p53 and p21 are elevated in MDCK leaders generated by scratching and barrier release. (**A**) Movie stills following a scratch-wound to a confluent wild-type MDCK monolayer (first three panels) show emergence of leader cells (an example one is indicated using the yellow arrows). The last panel shows a confocal image of that same leader cell after p53 immunostaining. (**B**) Quantification of single-cell nuclear p53 intensities in scratch-induced leaders versus non-leaders. Here and in (D), (G), and (I): black bars represent the median; n = number of cells. (**C**) Movie stills following a scratch-wound to a confluent wild-type MDCK monolayer (first two panels). Last two panels are confocal images of that same leader cell (yellow arrows) after p21 immunostaining. (**D**) Quantification of single-cell nuclear p21 intensities of scratch-induced leaders versus surrounding non-leaders. (**E**) Schematic of the barrier release experiment shown in (F) and (H). (**F**) Movie stills (first two panels) following the migration of leaders generated by barrier release. The last panel shows a confocal image of those same leaders following p53 immunostaining. (**G**) Quantification of single-cell nuclear p53 intensities of barrier release-induced leaders versus

surrounding non-leaders. (**H**) Movie stills (first two panels) following the migration of a leader generated by barrier release. Last two panels show confocal images of that same leader following p21 immunostaining. (**I**) Quantification of single-cell nuclear p21 intensities of barrier release-induced leaders versus surrounding non-leaders.

A sample size of at least 1200, 942, 867, and 1057 leaders would be required to perform statistical analysis in (B), (D), (G), and (I), respectively.

Scale bars = 100 μm for movie sequences and 50 μm for immunofluorescence images.

---

size of leaders. Next I plated two pools of wild-type cells into a twin-chambered silicone mould with a barrier separating the two populations (schematic in Figure VII.1E). When the cells reached confluence, I removed the barrier and followed the migration of subsequently formed leaders. Upon fixation and immunostaining, I showed that leaders generated by barrier release also indicated a slight increase in both p53 (Figure VII.1F and G) and p21 (Figure VII.1H and I).

Taken together, I demonstrated that p53 and p21 are activated in leaders generated by scratching and barrier release, suggesting their involvement in canonical leader cell migration.

p53 activity drives migration at the wound edge

I next tested whether the p53/p21 pathway plays an active role in leader cell migration during wound healing. I hypothesised that inhibiting the pathway should decrease the speed of wound healing, as fewer leaders would be formed and thus make wound closure less efficient. Conversely, activating p53 in cells at the wound edge should boost the number of leaders and hence also increase wound closure rates.

I had initially performed wound healing assays with *p53KO* cells, which developed finger-like protrusions and closed the wound comparably to wild-type cells (data not shown). I hypothesised that the *p53KO* line may have acquired background mutations due to its compromised tumour suppressor activity and was therefore able to overcome the requirement for p53 in leader migration. To avoid any such genetic background effects, I chose to inhibit the p53 pathway more acutely and use a dominant negative peptide, GSE-22.

The GSE-22 peptide is derived from full length p53 and has been reported to have a dominant negative effect on p53 function: GSE-22 stabilises p53 but the latter is rendered functionally inactive (Ossovskaya et al. 1996). The original construct was made up of amino acids 312-391 from rat p53. I amplified the sequence encoding the homologous canine amino acids (302-381) from a cDNA library obtained from *scrib*^{KD} MDCKs, which express p53 at high levels. In accordance with the original publication, I cloned an adaptor with three start ATG codons in front of the GSE-22 coding sequence and a fragment

containing three stop codons behind it to account for all three reading frames. I then introduced this into a DOX-inducible lentivirus expressing GFP-NLS in tandem with GSE-22 (Appendix 2F). I transduced wild-type cells with the GSE-22 lentivirus and selected an antibiotic-resistant pool.

While I could not verify GSE-22 expression directly due to loss of the anti-p53 antibody epitope, I could detect quite uniform levels of GFP-NLS in the antibiotic-selected pool, which was a proxy for GSE-22 expression (Figure VII.2A and B). Remarkably, scratch-wounds of cells expressing GSE-22 closed at a significantly slower rate than control scratches in the absence of DOX, as quantified (Figure VII.2C-E). This suggests that p53 activity is essential for efficient wound closure in MDCKs. That said, it would be important to additionally use an indirect readout for p53 activity to confirm whether increased GSE-22 expression translates into impaired p53 signalling by, for example, comparing p21 levels of Nutlin-treated cultures in the presence and absence of GSE-22.

To complement this finding, I next sought to specifically activate p53 at the edge of scratch-wounds. The localisation of p53 activity just to the edge cells was crucial, as I have previously shown p53 activity is only elevated in leader cells, while followers have low p53, and that this imbalance in p53 expression is crucial for leader migration. I used a 405 nm laser to induce sub-lethal DNA damage exclusively in the front row of cells of a scratch-wound (Figure VII.2F). I used immunostaining against γH2AX, a form of histone H2AX specifically phosphorylated in response to DSBs (Kuo & Yang 2008), to verify that DNA damage was indeed generated in response to UV treatment (Figure VII.2G). It remains to be formally demonstrated whether p53 is elevated in the irradiated cells under these experimental conditions, which could be assessed by anti-p53 immunofluorescence.

Importantly, I only irradiated the top half of one side of a scratch-wound and not the bottom half. I then compared the migration speeds of the irradiated and non-irradiated halves within the same wound: this helped control for other factors that may have influenced the migration speed e.g. cell density or soluble factors leaking into the media from damaged cells. Using this technique, I showed that laser-mediated p53 activation in cells at the wound edge resulted in significantly faster migration and wound closure rates than those observed for untreated edges (Figure VII.2H-J).

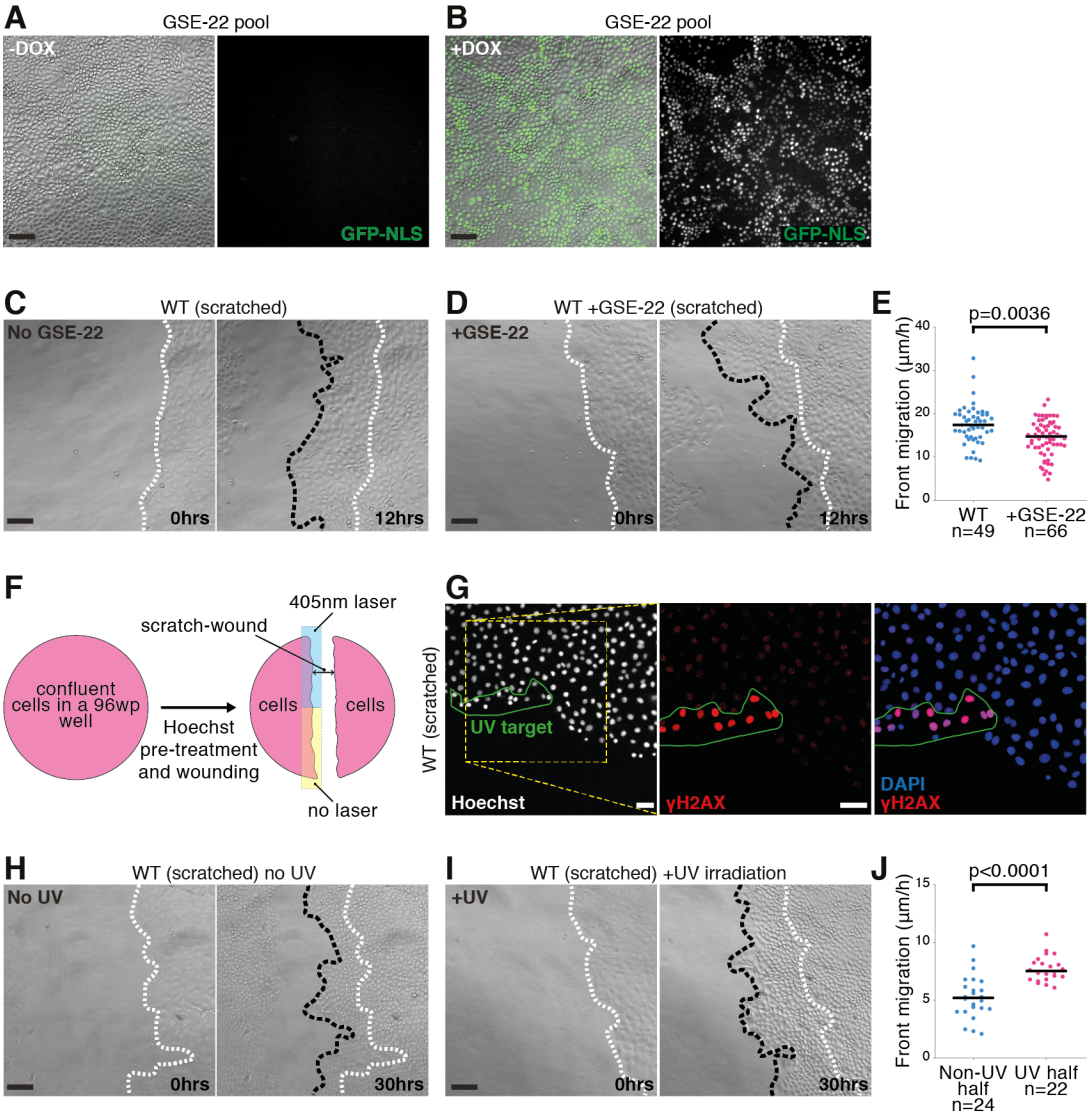

Figure VII.2: p53 activity drives leader cell migration during wound healing. (**A-B**) Homotypic cultures of wild-type cells overexpressing GSE-22, a dominant negative p53 peptide, and nuclear GFP in a DOX-inducible manner. (**C-E**) Movie stills of uninduced wild-type cultures (C) or cultures induced to overexpress the GSE-22 peptide (D) following a scratch-wound. The fields were chosen to be representative of the median front migration speeds of each population, quantified in (E). Here and in (H) and (I): white dashed lines mark the wound edge at the beginning of the experiment; black dashed lines mark the wound edge at the end of the experiment. Here and in (J): black bars represent the median; p values were calculated using the K-S test; n = number of fields. (**F**) Schematic illustrating the experimental design to test whether p53 activation through UV irradiation is sufficient to accelerate wound healing, shown in (H-I). (**G**) The first panel is a confocal image of a scratch-wound edge generated in a Hoechst-treated wild-type MDCK monolayer prior UV irradiation of the left half of the edge cells; the UV target region is marked using the green line. The last two panels are confocal images of a γH2AX immunostaining of the same scratch area

approximately 2 hours post UV treatment. (**H-J**) Movie stills of non-irradiated wild-type cultures (H) or wild-type cultures treated with a sub-lethal dose of UV (I) following a scratch-wound. The fields were chosen to be representative of the median front migration speeds of each population, quantified in (J).

Scale bars = 100 μm for movie sequences and 50 μm for immunofluorescence images.

Taken together, I have shown that p53 activity is likely both necessary and sufficient to drive efficient wound closure in the MDCK scratch-wound model.

Spontaneous and scratch-induced leaders are mechanical losers due to increased p53 activity

As I have discussed previously, elevated p53 levels confer the mechanical loser status on cells. Considering that wound-generated leaders have elevated p53 signalling, I next investigated what happens to leader cells upon wound closure. I imaged the closure of wild-type MDCK scratch-wounds and found that many leaders are eliminated when the two wound edges meet (Figure VII.3A, yellow and blue arrows). In fact, almost 40% of scratch-induced leaders were eliminated at wound closure, compared to under 2% of non-leader cells present at the wound edge at the same cell density (Figure VII.3B).

Moreover, when I followed the fate of spontaneous leaders that had been surrounded by neighbours with standard epithelial morphology, I found that around 70% of the former were eliminated (Figure VII.3C and D). The binucleation frequently observed in spontaneous leaders implies that they maintain high p53 throughout their lifetime, which is consistent with their elimination at a higher frequency than scratch-induced leaders. I suggest that p53 levels in wound-mediated leaders are lower and/or less 'terminal' than those of spontaneous leaders, which explains why fewer scratch-induced leaders are eliminated.

Taken together, I show that while elevated p53 signalling drives the migration of both wound-generated and spontaneous leaders, it also turns them into mechanical losers. At higher densities achieved through corralling by surrounding cells or wound closure, sustained high p53 activity results in leaders' hypersensitivity to cell density and their consequent elimination.

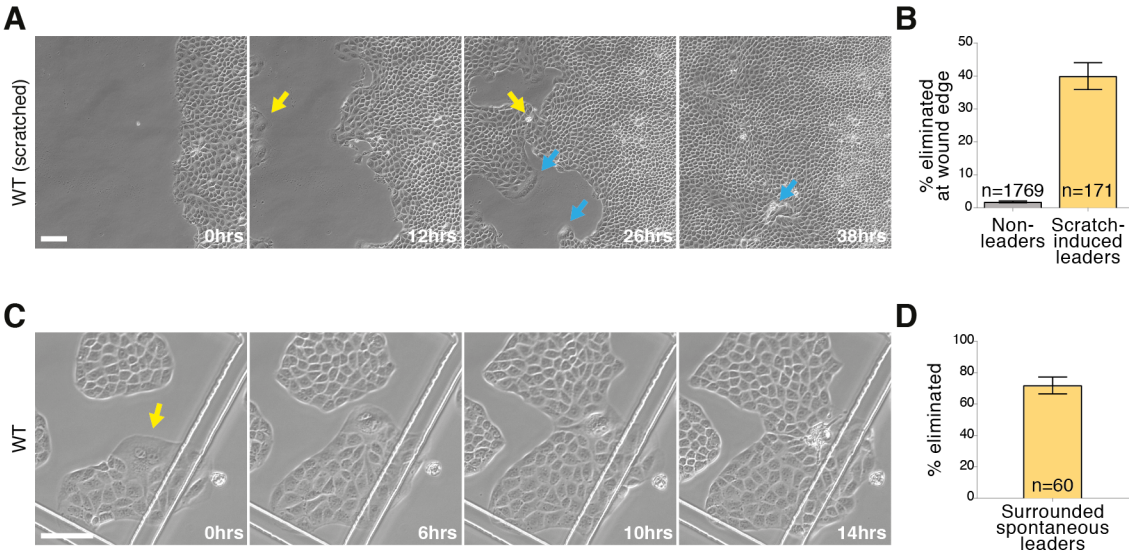

Figure VII.3: Wound-generated and spontaneous leaders are often eliminated at higher cell densities. (**A**) Movie stills following the closure of a wild-type scratch-wound. Leaders indicated in yellow and blue arrows are being eliminated. (**B**) Quantification of the number of leader cells that are eliminated at wound closure, compared to non-leader cells present at the wound edge. The comparison was made at cell densities where leaders tend to get eliminated. Here and in (D): n = number of cells pooled from three independent repeats; error bars ± SEM. (**C**) Movie stills following the migration of a spontaneous leader (yellow arrow) that is eliminated once the local cell density increases. (**D**) Quantification of the number of spontaneous leaders that are eliminated when surrounded by wild-type neighbours.

Scale bars = 100 μm.

Construction of a fluorescent p21 reporter

An important question raised by my finding that ~40% of wound-generated leaders are eliminated by mechanical cell competition concerns the fate of the other ~60%. I propose the two following hypotheses to explain why some scratch-induced leaders are not eliminated. Either p53 elevation in non-eliminated leaders may only reach a level high enough to trigger their migration via p21 activation, but too low for mechanical loser status. Alternatively, p53-inducing damage sustained by these leaders during wounding may be repaired by the time the wound closes, lowering their p53 back to levels insufficient for density hypersensitivity.

One way to correlate the p53 status of leader cells with their fate would be to use a live reporter for p53 activity. Rather than using a labelled version of p53, I modified a previously published reporter for p21 activity (Paek et al. 2016). This was because of the binary nature of p21 expression, which I had noticed myself and was also described in (Paek et al. 2016): their p21 sensor has very little background fluorescence and is capable of responding quickly to stimuli with a very bright signal. The original p21 sensor consisted of destabilised CFP-NLS driven by the human *p21* promoter; I used the same principle to clone a GFP-NLS version of the p21 reporter (Appendix 2G), which was more compatible with the live imaging set up in the Piddini lab (Figure VII.4A).

I transfected the GFP-NLS p21 reporter construct into wild-type MDCK cells. After generating an antibiotic-resistant pool, I used immunofluorescence to identify three clones with very low background signal that responded to Nutlin treatment by strong induction of nuclear GFP, as assessed by confocal microscopy (Figure VII.4B-D).

Unfortunately, due to time constraints, I did not have the chance use these p21 reporter clones in an experimental setting. The next step would be to verify whether the fluorescence produced in response to Nutlin treatment (and hence p53 activation) is bright enough for the live imaging set up in the Piddini lab. Following this, it should be possible to visualise the emergence of GFP-positive leaders and correlate their GFP intensities with their fate at wound closure. Considering that GFP expression is driven directly by the p53-responsive *p21* promoter, it might be possible to determine whether the threshold of p53 activity that triggers leader migration is lower than that conferring

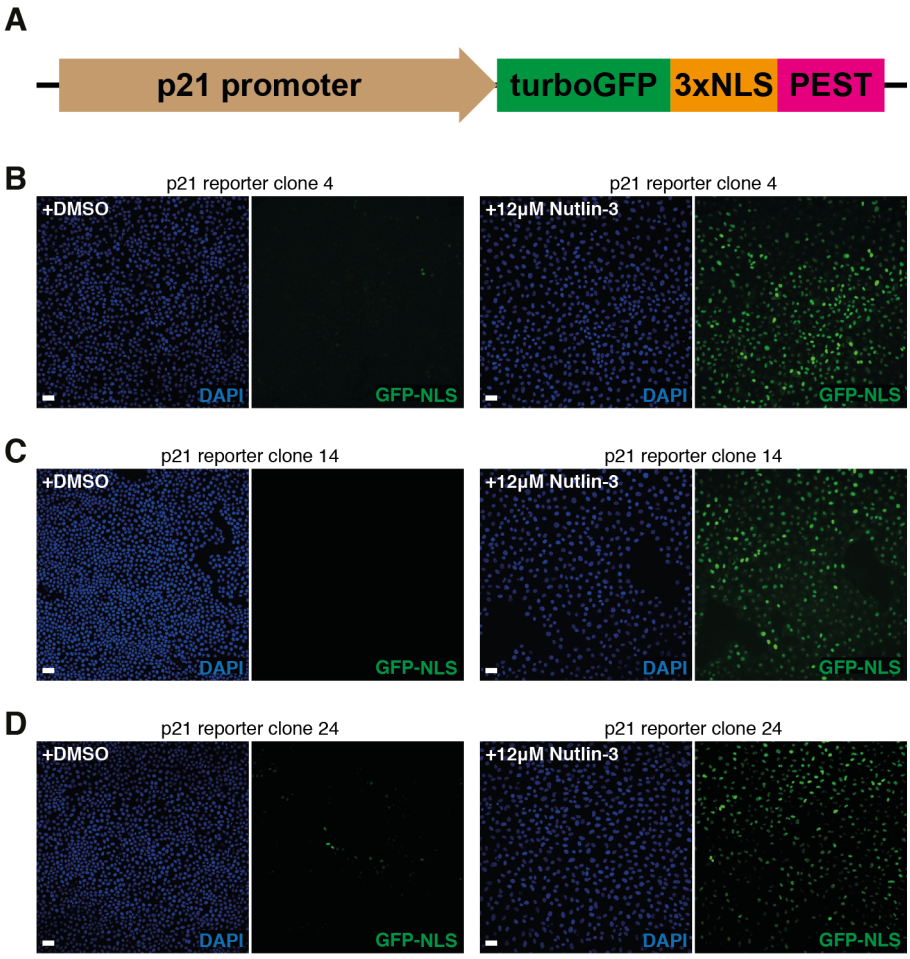

Figure VII.4: Construction and testing of the p21 GFP reporter lines. (**A**) Schematic representation of the architecture of the p21 reporter construct. NLS = nuclear localisation sequence. PEST = destabilisation sequence rich in proline (P), glutamate (E), serine (S), and threonine (T). (**B-D**) Confocal images of three candidate p21 reporter clones in the absence (left two panels) and presence (right two panels) of a mild dose of Nutlin-3. Nutlin-3 addition induces a reduction in cell density and expression of GFP-NLS, driven by the *p21* promoter.

Scale bars = 50 μm.

mechanical loser status: if this were true, eliminated leaders would have consistently brighter GFP signal than their non-eliminated counterparts. Alternatively, the GFP signal might spike early in the wound healing process and then fall back down, as some leaders reduce their p53 activity through induction of repair mechanisms.

In summary, I have generated and verified three p21 reporter clones that could be used as a proxy to measure p53 activity of leader cells during live imaging. This could help address questions regarding the p53 status of non-eliminated leaders.

Discussion

I have shown that leaders generated by barrier release and scratching have elevated p53 and p21. I further demonstrated that the speed at which an MDCK wound front migrates is directly dependent on p53 activity, implying that p53 is crucial for efficient wound healing. Lastly, I presented evidence to suggest that elevated p53 signalling in scratch-induced and spontaneous leaders results in their hypersensitivity to density and, ultimately, their elimination.

It is important to note that the migration speed of scratch-wound fronts was measured by manually drawing freehand lines outlining the wound edge at the first and final time points. If any wound edges were not parallel to the y axis, the images were adequately rotated. The median x position for each line was recorded to calculate the median x displacement in μm, which was then divided by the duration of the experiment in hours to generate a speed value in μm/h. An important consideration of this approach is that it masks the individual speeds at which the cells in the front are migrating by assigning a single speed value to the whole front within a field of view. Calculating the rate of wound area shrinkage, for example, could have provided a more accurate representation of the speed of wound closure. Similarly, one could have calculated the rate of increase in the area between the initial and final wound front positions to give a measure of front advancement. All of these approaches would have also benefitted from stitching together fields of view to create one continuous image of the whole wound, rather than individually analysing subsections of it.

The p53/p21 upregulation observed in leaders generated by barrier release or scratching can be explained by one of two not mutually exclusive theories: wound-induced damage either triggers a stress response that elevates p53/p21, or simply exposes cells with pre-existing high levels of p53/p21. While it has been reported that barrier release does little damage to cells in contact with the barrier walls (Poujade et al. 2007), it is possible that cells can sense minute mechanical distortions and translate them into an elevated p53 response even if no gross damage can be detected through experimental means. In support of the pre-existing leader theory, it has been reported that leader cells do not always emerge from the first row of cells (Poujade et al. 2007). As I have shown in the case of spontaneous leaders, cells with elevated p53/p21 levels occur naturally within wild-type populations and are viable at lower densities. It is therefore conceivable that wounding simply provides the space for the migration of pre-existing spontaneous leaders present in the first few rows of cells.

One of the tools that could be used to distinguish between these two possibilities are the MDCK p21 reporter lines that I generated to indirectly measure p53 activity. It should be possible to use live imaging techniques to test whether and how often cells with elevated GFP levels pre-wounding become leaders, or whether wounding generates cells with high GFP signal that then become leaders. In fact, I expect these cell lines will also help answer other important questions: is there a threshold of p53 activity that drives leader migration, but results in leader elimination if exceeded? Does the p53 activity of non-eliminated leaders fall back down to 'normal' levels prior to wound closure or do they never reach levels high enough for elimination? Do all cells with high p21 and space to migrate into become leaders? Do all leaders show elevated p53/p21 activity?

Although useful, the p21 reporter line has an important limitation. While p21 transcription is mainly regulated by p53 (reviewed in Sullivan et al. 2017), p21 can also be activated in p53-independent ways (reviewed in Karimian et al. 2016). For example, TGFβ can activate p21 transcription through elements in its promoter distinct from the p53 response elements (Datto et al. 1995). In MDCK leader cell migration, I suggest that p21 is mainly activated through a p53-dependent pathway: p21 activation is necessary for leader cell migration, but MMC-treated *p53KO* cells do not behave as leaders, suggesting the presence of p53 is required for p21 activation. However, I have also established in this thesis that the role of p53 in mechanical loser status is separate from

its p21-dependent role in leader migration. One should therefore be cautious when making conclusions about p53 activity in the mechanical loser status based solely on the p21 reporter.

Taken together, I suggest a model where damage during wounding induces p53/p21 activity in several cells at the scratch edge or exposes cells with pre-existing p53/p21 elevation. Elevation of the p53 pathway drives the leader cell phenotype through p21 and promotes migration. The free space in the wound bed and the discontinuity of high to low p53/p21 between leaders and followers both contribute symmetry breaking cues that drive migration into the wound gap. The imbalance of p53/p21 activity may be especially important to give directionality to the migration of leaders not immediately at the wound edge. Importantly, sustained high p53 ensures elimination of cells with irreparable damage through mechanical cell competition once the wound is sealed. All in all, p53/p21 activity drives leader cell migration into the wound gap to promote efficient wound healing and ensures the elimination of cells damaged beyond repair from the epithelium (Figure VII.5).

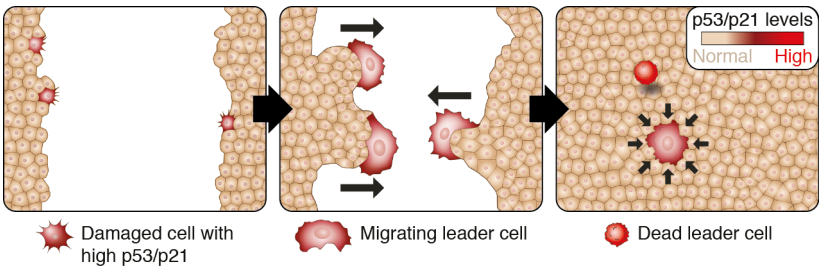

Figure VII.5: Schematic diagram summarising the role of p53/p21 in wound healing. Cells with elevated p53/p21 activity emerge as a consequence of damage during wounding or because scratching opens up space for the migration of cells with pre-existing p53/p21 elevation (the latter option is not portrayed). Increased p53/p21 activity drives the migratory phenotype, while the imbalance of p53/p21 activity between leaders and followers helps direct leaders into the wound gap. Upon wound closure, the local cell density increases and leaders with persisting p53 elevation are eliminated via mechanical cell competition.

Adapted from images commissioned by Eugenia Piddini from Veronique Juvin of SciArtWork.

Chapter VIII: Cell cycle inhibitors may be the universal drivers of leader cell migration

---

Cell cycle arrest is a common feature of many types of MDCK leader: canonical leaders, spontaneous leaders, MMC-treated cells, and p21OE cells. That said, cell cycle arrest is not a prerequisite for leader cell fate, as *scrib*^{KD} cells and Nutlin-treated cells are both leaders but continue dividing, if at a slower rate than untreated wild-type cells. Importantly, slow division implies that *scrib*^{KD}- and Nutlin-mediated leaders maintain some cell cycle inhibitor activity and, in fact, p21 (and potentially other cell cycle inhibitors) is expressed in both types of leader (Wagstaff et al. 2016 and Figure VI.2D, respectively). I therefore decided to investigate whether elevated cell cycle inhibitor activity could be a common factor that induces leader migration.

The activity of cyclin/cyclin-dependent kinase (CDK) complexes is crucial for cell cycle progression. One way in which CDKs are regulated is by interaction with CDK inhibitors (CKIs). CKIs have been classified into two families, INK4 and Cip/Kip, each of which have different specificities and mechanisms of CDK inhibition. p21$^{WAF1/Cip1}$ and p27^{Kip1} (from here on referred to as p27) are part of the Cip/Kip CKI family and share a common N-terminal motif responsible for binding to cyclin/CDK complexes, but they also have their own distinct functions. For example, p21 has been shown to inhibit DNA replication by binding to a DNA polymerase processivity factor, proliferating cell nuclear antigen (PCNA). In contrast, p27 does not bind PCNA but has been reported to interact with and inhibit a helicase subunit at the replication fork to stall DNA replication (reviewed in Besson et al. 2008).

p16^{INK4A} (from here on referred to as p16) is part of the INK4 CKI family and therefore evolutionarily distinct from p21 and p27 (reviewed in Besson et al. 2008). p16 specifically inhibits CDK4 and CDK6 but can also stop cell cycle progression in CDK-independent ways, just like p21 and p27. For instance, p16 has been shown to inhibit phosphorylation of a subunit of RNA polymerase II, which contributes to cell cycle arrest (reviewed in Li et al. 2012).

While p21 is a direct transcriptional target of p53, this has not been shown for the structurally related p27 (Zhang et al. 2005). There is also little evidence for the relationship between p53 and p16: so far, it has only been reported that p53 is necessary but not sufficient for the repression of p16 (Leong et al. 2009). I would therefore argue that both the regulation and the downstream targets of the three CKIs in question are quite distinct. Consequently, I used manipulation of p27 and p16 to achieve two largely independent ways of cell cycle arrest (alongside p21 overexpression discussed in Chapter VI) to test the requirement for cell cycle inhibition in leader cell migration.

Cell cycle inhibitors p27 and p16 are elevated in various types of MDCK leaders

I first wanted to know if p27 and p16 are expressed and/or upregulated in MDCK leader cells, as this could indicate their potential involvement in the leader status. Interestingly, nuclear p27 tended to be higher in spontaneous leaders than in wild-type follower cells (Figure VIII.1A and B), but the statistical power was not sufficient to be completely conclusive. I only took nuclear signal into consideration, as that is where the CDKs are localised and can be inhibited by p27. Moreover, I noticed that nuclear p16 was also elevated in spontaneous leaders (Figure VIII.1C), but this was just a preliminary finding, as I only performed this immunostaining once. Further pilot experiments also showed that nuclear p27 appeared to be increased in scratch-induced leaders (Figure VIII.D) and in leaders generated by p21 overexpression (Figure VIII.E), but this needs further confirmation.

Assuming these observations can be reproduced, both p27 and p16 appear elevated in different types of leader cell and might therefore be contributing to the leader phenotype.

p27 and p16 independently drive leader cell migration but are not responsible for mechanical loser status

In order to test whether p27 and/or p16 have an instructive role in leader status, I generated two DOX-inducible, lentiviral overexpression constructs: canine p27 and

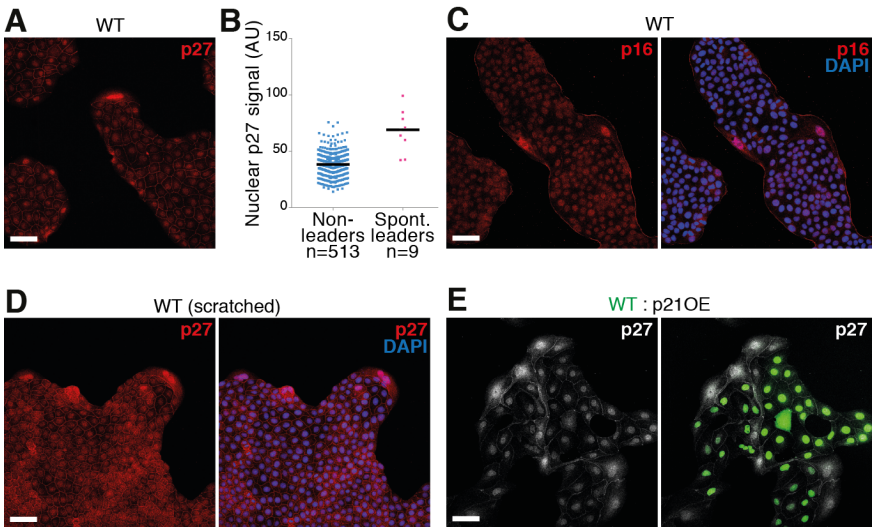

Figure VIII.1: CDK inhibitors p27 and p16 are elevated in different types of MDCK leader. (**A**) Nuclear p27 is elevated in spontaneous leaders emerging from wild-type cultures. (**B**) Quantification of single-cell nuclear p27 intensities in spontaneous leaders versus surrounding non-leaders. Black bars represent the median. n = number of cells. A sample size of at least 138 leaders would be required to perform statistical analysis. (**C**) Confocal images following immunostaining against p16 on spontaneous leaders. (**D**) p27 immunostaining on leaders generated by scratching of a wild-type MDCK monolayer. (**E**) Co-cultures of GFP-labelled wild-type cells and unlabelled p21OE cells following immunostaining against p27.

Scale bars = 50 μm.

human p16, each expressed in tandem with nuclear RFP (Appendix 2H and I, respectively). I used human p16 because it was available in a plasmid backbone and therefore easier to amplify by PCR. This was justified, as there is 83% sequence identity between human and canine p16 (Altschul et al. 1997). I individually transduced wild-type MDCKs with the lentiviral p27 and p16 constructs and used antibiotic selection to make pool populations overexpressing p27 (p27OE) or p16 (p16OE). Remarkably, both p27OE and p16OE cells flattened in the presence of DOX (Figure VIII.2A-D), much like p21OE cells and a subpopulation of P-cadOE cells. It is worth noting that the p27OE and p16OE pools flattened much more uniformly than the P-cadOE pool, most likely due to the smaller size of the constructs and hence more efficient packaging into the lentiviral particles (Kumar et al. 2001).

Strikingly, when I co-cultured wild-type cells expressing nuclear GFP with p27OE, I found that p27OE cells displayed leader behaviour (Figure VIII.2E). Similarly, p16OE cells juxtaposed by wild-type cells also behaved as leaders (Figure VIII.2F). I could also show that neither p27OE (Figure VIII.2G) nor p16OE clones (Figure VIII.2H) were eliminated at higher cell densities in competing cultures, but this should be confirmed in a stretcher assay. Taken together, I show that elevation of p27 or p16 (just like p21) is sufficient for leader cell behaviour but not mechanical loser status.

Chemical cell cycle inhibition may be sufficient for leader cell fate

p21, p27, and p16 have all been shown to have functions outside their role as CKIs. For example, p21 and p27 can inhibit the Rho/ROCK/LIMK/cofilin signalling pathway, which normally stabilises actin filaments and maintains stress fibres (reviewed in Besson et al. 2008). I therefore wanted to test whether p21, p27, and p16 induce leader fate through activation of their CDK inhibitory role or another function that, for instance, affects the cytoskeleton directly.

To address this, I performed pilot experiments using a chemical inhibitor of CDK1 on actively migrating leaders generated by scratching wild-type MDCK monolayers. As expected, cells treated with CDK1 inhibitor stopped proliferating and, interestingly, acquired a more flattened morphology than their untreated counterparts (Figure VIII.3A).

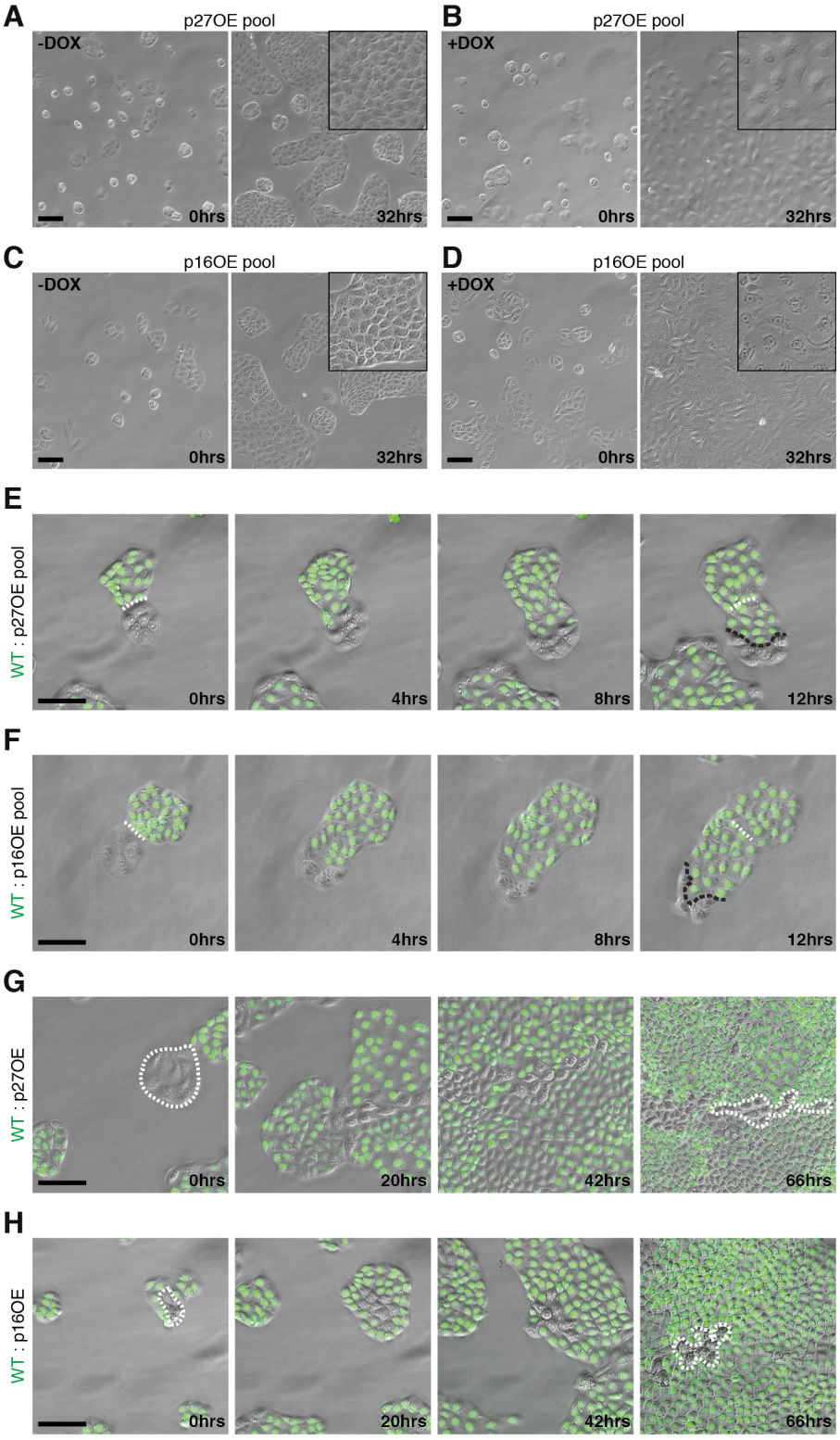

Figure VIII.2: Overexpression of CDK inhibitors p27 and p16 is sufficient to drive the leader phenotype but does not confer the mechanical loser status. (**A-D**) Homotypic cultures of unlabelled cells overexpressing p27 (p27OE) (A-B) or p16 (p16OE) (C-D) in a DOX-inducible manner. Overexpression

of either p27 or p16 induces cell cycle arrest and flattening (B, D), compared to DOX-free conditions (A, C). The insets are 2x zooms of the cell populations at 32 hours to better demonstrate cell flattening in the +DOX conditions. (**E-F**) Movie stills from co-cultures of GFP-labelled wild-type cells and p27OE (E) or p16OE (F) cells. White dashed lines mark the initial contact point; black dashed lines mark the final contact point. (**G-H**) Neither p27OE (G) nor p16OE (H) clones (marked in white dashed lines) are eliminated at higher densities when surrounded by GFP-labelled wild-type cells.

Scale bars = 100 μm.

Strikingly, acute CDK1 inhibition was sufficient to halt leader cell migration following scratching (Figure VIII.3B and C). Based on these observations, I hypothesised that CDK1 inhibition caused follower cells to become more leader-like and the asymmetry between leaders and followers was lost. This meant that leader cell migration could no longer proceed directionally into the wound gap. This suggests that the free space generated after scratching is not sufficient to drive efficient, directional leader migration across the wound bed: a molecular imbalance between leaders and followers is also required.

These experiments strongly suggest that CDK1 inhibition is sufficient to confer the leader cell fate. The next step would be to irreversibly inhibit CDK1 in one population and confront it with wild-type cells to test if the CDK1-deficient population becomes migratory. It is also important to note that because of the preliminary nature of these data, I cannot exclude the possibility that chemical CDK1 inhibition activates one of the known drivers of leader migration e.g. p21. It is possible that acutely activating p21 in all cells within a scratch-wound would have a similar effect of the leader cell migration as CDK1 inhibition: wound closure would stall because of loss of asymmetry between leaders and followers. Without further investigation, I cannot conclusively say that CDK1 inhibition confers the leader cell status independently of other leader cell drivers.

My preliminary experiments imply that cell cycle inhibition itself is sufficient for the leader cell status. If this can be confirmed, I would like to investigate if there is common pathway activated downstream of cell cycle arrest factors that drives expression of the leader signature.

Discussion

The data I present in this chapter supports the role of cell cycle inhibition being a universal driver of leader cell fate in MDCK cells. p27 and p16 are elevated in many types of MDCK leader and independently overexpressing them is sufficient to trigger leader cell migration. What is more, chemical CDK1 inhibition stalls the migration of scratch-induced leaders by (potentially) eradicating the asymmetry between leaders and followers that is necessary for the directional progression of leaders across the wound gap.

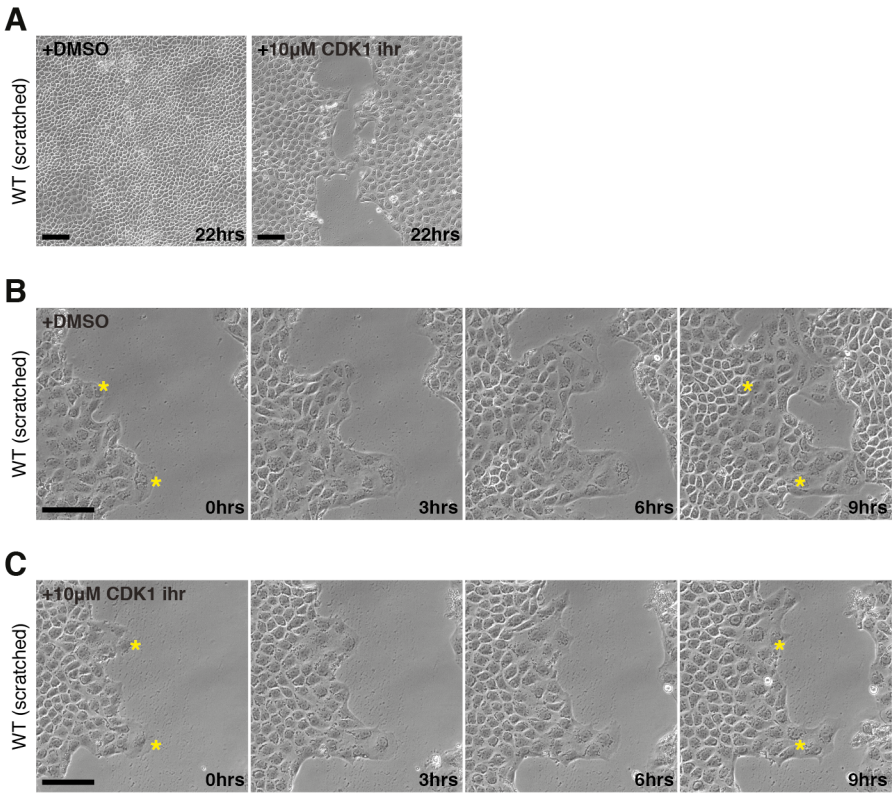

Figure VIII.3: Chemical CDK1 inhibition is sufficient to stall leader cell migration following a scratch-wound to an MDCK monolayer. (**A**) CDK1 inhibition using RO-3306 (right panel) results in cell cycle arrest and flattening, compared to the solvent-only condition (left panel). (**B-C**) Addition of the CDK1 to actively migrating scratch-induced leaders results in their stalling. The yellow asterisks indicate the positions of two leaders when treatments were added at the beginning of the experiment.

Scale bars = 100 μm.

Considering these observations and that p21OE cells are also leaders, it is likely that mediators of cell cycle inhibition activate a common set of targets responsible for the leader cell phenotype. If chemical CDK1 inhibition can be shown to be independent of p21, p27, and p16 and confer the leader cell fate in co-culture assays, this would demonstrate that the cell cycle inhibitory role of the three CKIs tested is the driving factor behind leader cell fate, rather than any of their alternative roles (e.g. direct modification of the cytoskeleton). I therefore propose that p21, p27, and p16 all likely lie upstream of leader signature expression and thus leader cell fate. Alternatively, p27 and p16 may activate distinct factors, which are responsible for the increased motility and other cytoskeletal changes permissive to leader status in parallel to those downstream of p21. Testing whether p27OE and p16OE cells express leader cell markers would help distinguish between these hypotheses.

In light of the findings and hypotheses discussed in this chapter, I would like to re-discuss several aspects of leader cell migration and the mechanical loser status:

(i) *scrib^{KD} p53KO* cells and the leader signature

Firstly, p53/p21 activity is necessary for leader cell migration but *scrib^{KD} p53KO* cells behave as leaders despite having no p53 or p21 activity. In Chapter VI, I suggested that *scrib^{KD} p53KO* cells may be activating a p53- and p21-independent pathway upstream of the leader cell signature that this induces their leader behaviour. While I have not tested whether p27OE and p16OE cells express leader cell markers like PI3K and E-cadherin, I would expect that they do, based on their flattened morphology and leader behaviour. If so, activation of other CKIs like p27 and p16 may be driving *scrib^{KD} p53KO* cell migration; this could be tested by immunostaining of *scrib^{KD} p53KO* cultures against p27 and p16.

That said, *scrib^{KD} p53KO* cells are an exception, as I have shown in Chapter V that the bulk of leader cell migration is p53-dependent (~80%, Figure V.2H). I therefore propose that the MDCK leader cell phenotype is, in majority of cases, a consequence of p53-dependent p21 activation. In the absence of p53, p53-independent activation of other CKIs like p27 and p16 may be responsible for leader migration and feed into leader signature expression. To test this hypothesis, one could for example use the p21 reporter cell line I generated to ask what percentage of scratch-induced leaders have elevated p21, and

whether any that do not upregulate p21 elevate p27 and/or p16 instead. It would also be important to find out what factors lie upstream of p27 and p16 activation and whether there is any interplay between them, as p27 expression in p21OE cells would suggest. It also remains unknown how CKIs mediate leader cell signature expression.

(ii) Flattening

Secondly, I have shown that flattening is a common feature of most leaders: *scrib*^{KD} cells, P-cadOE cells, spontaneous leaders, MMC-generated leaders, p21OE cells, p27OE cells, and p16OE cells. Wound-induced leaders have also been described as having a larger surface area (Poujade et al. 2007). This implies that cell flattening may be a prerequisite for leader behaviour. I have however shown that MMC-treated *p53KO* and *p21KO* cells are flat but do not behave as leaders. I would therefore argue that flattening may be necessary but is not sufficient for leader cell fate; this hypothesis would need testing experimentally. Micropatterning could be used to prevent cell flattening upon, for example, p21 overexpression. It would however be difficult to test if cells manipulated in this way became leaders because generating space for migration would also allow flattening. To test whether flattening is sufficient for the leader phenotype, one could use an established method to induce cell flattening (e.g. trapping cells between glass and a sheet of agar and then wicking away some of the media to lower the agar sheet) and ask whether this is sufficient for expression of leader signature markers (Westendorf et al. 2010).

(iii) Leader cell migration and mechanical loser status

Thirdly, p21OE, p27OE, and p16OE cells are all leaders in co-culture with wild-type cells but they are not eliminated as cell density increases, suggesting they are not mechanical losers. Mechanical losers have three defining features in the MDCK system: flattening, lower homeostatic density, and hypersensitivity to density (Wagstaff et al. 2016). While overexpression of p21, p27, or p16 is correlated with cell flattening and therefore a lower homeostatic density, it does not appear to be sufficient for cells' hypersensitivity to density. If these observations are confirmed using stretcher experiments, and immunoblotting of p21OE, p27OE, and p16OE cells shows that p53 is indeed inactive, it

would argue that p53 elevation confers density hypersensitivity independently of leader cell migration. It remains unknown what factors downstream of p53 are involved in conferring density hypersensitivity. This could be investigated using chemical inhibitors of known downstream p53 effectors to pinpoint which of its signalling branches may play a part.

(iv) Senescence and wound healing

Many of the MDCK leaders described in this thesis share many features with cells undergoing senescence. Senescence can be triggered by cellular damage (e.g. telomere loss, ROS, oncogene activation) and some developmental processes (e.g. polyploidy, cell fusion). Senescence plays a role in physiological processes that promote clearance of damaged or ageing cells and boost tissue regeneration, as well as in the removal of transient developmental structures and pre-malignant cells. However, senescent cells can accumulate after persistent damage, or due to ageing that compromises their clearance, and this can have detrimental effects on the tissue (reviewed in Muñoz-Espín & Serrano 2014).

Senescent cells are cell cycle arrested and can be characterised by several molecular and morphological markers, although they do not always display all of these features. Senescent cells *in vitro* can be multinucleated, tend to be flat, and have large vacuoles, although *in vivo* their morphology is determined by their host tissue. They have also been shown to express a multitude of tumour suppressors and cell cycle inhibitors, including p53, p21, p16, and p27. Increased lysosomal activity in senescent cells allows for detection of arguably the most common senescence marker, senescence-associated β-galactosidase (SAβGAL). Additionally, senescent cells secrete extracellular proteins as part of a senescence-associated secretory phenotype (SASP), which acts in an autocrine and paracrine manner to reinforce and promote senescence (reviewed in Muñoz-Espín & Serrano 2014). The SASP is also responsible for attracting immune cells, which clear senescent cells from tissues (reviewed in Lujambio 2016).

Many senescent cells are not migratory and it has been hypothesised that ECM degradation by SASP components may impair wound healing (reviewed in Burton 2009).

More recently, however, it was demonstrated the presence of senescent fibroblasts and endothelial cells accelerates wound repair in mouse models. This depends on PDGF-AA secretion that promotes wound contraction, rather than migration (Demaria et al. 2015). Interestingly, senescent cells can also be detected at invasive borders in papilliary thyroid carcinoma samples; the invasive area is also characterised by increased E-cadherin expression. Senescent cells in the thyroid were shown to attract cancer cells and promote their survival through a chemokine gradient, which hence promotes cancer invasion (Kim et al. 2017). Similarly to MDCK leaders, senescent cells can therefore play a role in migration and wound healing, although this is mediated by soluble factors and does not appear to require cell contact.

Clearly, MDCK leaders are very similar to senescent cells, both morphologically and molecularly. It would be of great importance to determine whether MDCK leaders also express SAβGAL, the hallmark of most senescent cells. On the other hand, I would not expect leaders to secrete many SASP components, as I have never observed a propagation of the leader phenotype to follower cells, as might be expected if soluble senescence-promoting factors were present. This should however be tested experimentally. If MDCK leaders are shown to be senescent, findings from one system could be translated into the other. For example, p53-mediated mechanical competition may have a role in the elimination of senescent cells from tissues *in vivo* in the absence of an immune response.

(v) Quantifications

It is important to point out that all cell migration within this thesis was assessed qualitatively by analysing movie sequences from at least three independent repeats with at least 10 fields per experiment. While I took great care to minimise bias and subjectivity in my analyses, my conclusions could be further strengthened by performing new quantifications and improving on the ones presented.

Firstly, it would be advisable to quantify whether two populations are engaging in collective, directional migration. One way to do this would be to track the paths taken by cells in each population over time and overlay them. The migration of each population before and after leader/follower collision should be tracked: migration would

presumably be random prior to collision and more coordinated afterwards. If one population could be shown to start migrating directionally first, one could also demonstrate which, if either, population was leading the migration. Quantifications like these were done by Medhavi Vishwakarma for some of my data (Figure V.2I-K and Figure VI.1H-J) and it would be prudent to do them for all other migration data presented.

Secondly, several of my quantifications have a large imbalance in the numbers of leader and follower cells analysed because the two populations exist at very different numbers in the culture (e.g. Figure VII.1B). As discussed earlier, this poses a problem for the statistical analysis and prevents one from determining whether there is a significant difference between the two samples. One way to balance out the numbers of leaders and followers would be to only count non-leader cells at the wound edge as followers, rather than all the non-leader cells in the field of view. Naturally, the minimum sample size of leaders required for this new follower sample size would still have to be calculated before any statistical tests could be performed.

Thirdly, it would be useful to establish a non-biased way for identifying leaders in wound healing assays. For example, one could use pre-defined criteria to establish what constitutes a finger-like protrusion, such as a minimum length and diameter. One could then define a pre-specified number of cells at the tip of a finger-like protrusions as leaders. These leaders could be compared to followers defined as cells at the edge of the trough between fingers. This approach would also help balance out the leader vs. non-leader numbers, so that quantifications could be analysed statistically.

Chapter IX: Conclusions and perspectives

In this thesis, I further characterised three aspects of cell competition in MDCK cells. Firstly, I investigated the roles of E-, N-, and P-cadherin in the directed migration triggered following encounters between wild-type and *scrib*^{KD} cells; I later demonstrated this migration is most likely a manifestation of leader behaviour. I also briefly probed the roles of classical cadherins in the mechanical loser status. Secondly, I showed that the signalling pathway responsible for the acute response of compacted *scrib*^{KD} cells is also conserved in p53-mediated competition. This is especially significant, because findings from the *scribble* competition system can now be more easily translated to other situations where discontinuities in p53 expression are present, some of which are of prime therapeutic interest (e.g. tumourigenesis). Thirdly, I further characterised the molecular drivers of leader cell migration and showed that p53/p21 elevation is the key driver of the leader cell phenotype. This is the first time (to my knowledge) that activation of a single pathway was shown to result in the formation of leader cells. I propose that the p53/p21 imbalance drives the migratory phenotype, provides a symmetry breaking cue for efficient migration across the wound bed, and results in the elimination of cells with sustained damage at wound closure. My findings also provide an explanation as to how only some cells are singled out to become leaders. Lastly, I explored the possibility that cell cycle arrest may be the common trigger of leader fate, which could constitute an alternative pathway for the clearance of senescent-like cells *in vivo*.

Please refer to Figure IX for a model integrating the findings I describe in this thesis.

Cadherins in loser recognition and leader migration

scrib^{KD} cells display a migratory phenotype when confronted with wild-type cells and express a range of markers also present in other types of MDCK leader. I therefore propose that *scrib*^{KD} cell migration is in fact another manifestation of leader migration and that findings in the *scribble* system are applicable to MDCK leader migration as a whole.

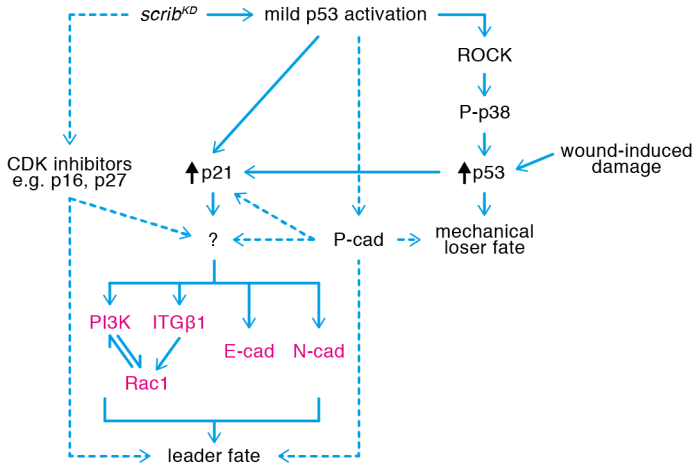

Figure IX: Model summarising the molecular interactions governing leader cell migration in MDCKs. p53 activation as a result of wound-induced damage, *scribble* knockdown, or Nutlin treatment ('mild p53 activation') leads to increased p21 activity. p21 drives expression of a number of markers comprising the leader cell signature (highlighted in magenta) through a currently uncharacterised mechanism. The leader signature is required for the leader cell fate downstream of p21 activation; the list of leader signature components is not necessarily exhaustive. Elevated p53 simultaneously confers the mechanical loser status independently of p21 activity.

I represent conclusions and implications from pilot experiments using dashed lines to indicate more tentative connections that require further testing. Firstly, loss of *scribble* may feed into both p53/p21 activation, as well as a parallel pathway like p27 or p16, which would explain how *scrib*^{KD} *p53KO* maintain the leader phenotype. Secondly, P-cadherin overexpression may be sufficient for both leader cell fate and mechanical loser status: how this links into what is already known about both processes still needs to be established. Thirdly, cell cycle inhibition through expression of CDK inhibitors other than p21 appears sufficient for the leader fate, but it remains unclear if this depends on leader signature components.

In the first part of my thesis, I investigated the role of E-, N-, and P-cadherin as potential candidates driving *scrib*^{KD} cell recognition and their directed migration away from winner cells.

E-, N-, and P-cadherin are all elevated in *scrib*^{KD} cells and I showed that at least E-cadherin is necessary for their migration following contact with wild-type cells. Neither E- nor N-cadherin elevation is sufficient to drive leader migration. Preliminary experiments with P-cadherin suggested it may play a more active role in leader migration, but this needs further confirmation. I propose that E- and N-cadherin are part of the leader cell signature downstream of p21, the components of which work together to enable leader migration. It remains to be determined what role each of the leader signature factors plays, whether there is any interaction between them, and how increased p21 activity leads to their upregulation.

It was not possible to determine whether the three cadherins are part of a winner/loser recognition event, as the assay readout was ambiguous: no migration following E-cadherin knockdown in *scrib*^{KD} cells could simply mean that the cells have lost the cytoskeletal changes permissive for migration or are incapable of generating forces to migrate, rather than evading recognition by followers. Combined with the available RNA sequencing data highlighting the difference between the transcriptomes of MDCK winners and losers (Wagstaff et al. 2016), a screen for surface molecules differentially expressed between loser and winner cells would shortlist more candidates for recognition molecules. However, the difficulty remains in defining a recognition event. If the molecular change that happens in winner cells upon loser cell recognition can be pinpointed, one could test which molecule(s) on the surface of losers is/are sufficient to trigger it. These experiments could ultimately define what differences winner cells can sense in loser cells (or vice versa) that triggers the cascade of events leading to loser cell elimination in a mammalian system.

p53-mediated competition

In the second part of my thesis, I demonstrated that the ROCK – P-p38 – p53 signalling pathway activated during compaction of *scrib*^{KD} cells is also conserved in competition

induced by mild p53 elevation. This allows for findings from the *scribble* mechanical competition system to be extrapolated into contexts where only a p53 imbalance is present. For example, does p53 loss during tumourigenesis enable cells to stop responding to mechanical cues and evade elimination? Conversely, are damaged/less fit cells removed *in vivo* by mechanical cell competition if they display chronic p53 elevation below levels that directly induce their apoptosis and, if so, how prevalent is this? If p53-mediated mechanical cell competition proves to be relevant in *in vivo* systems, one could envisage that it could become a therapeutic target. For instance, ectopic reactivation of p53 selectively in cells harbouring p53 mutations could enable their clearance by an intrinsic mechanical cell competition mechanism and restore epithelial health.

The mechanism of ROCK activation by compaction, as well as the downstream effectors of p53 responsible for density hypersensitivity also remain to be determined. The more is unveiled about the factors governing mechanical cell competition, the more directed any future therapies targeting it can be.

Leader cell migration in wound healing

The most significant findings described in this thesis concern the role of leader cells in MDCK wound healing, described in the third part of my thesis. I propose that p53 is activated in some cells at the wound edge as a result of cellular damage, or that the wound gap opens up space for the migration of cells with pre-existing p53 elevation: the p21 reporter line that I generated may help distinguish between these two possibilities. Increased p53 activity drives expression of p21, which is both sufficient and necessary to drive leader cell migration across the wound bed. In fact, I suggest that the p53/p21 imbalance between leader and follower cells actively contributes to directing cell migration into the wound area by providing a symmetry breaking cue.

p21 lies upstream of the leader cell signature (E-cadherin, N-cadherin, PI3K, ITGβ1, and Rac1), which is necessary for leader migration. Other CKIs like p27 and p16 may also lie upstream of these signature markers and contribute to the leader status alongside p21. Members of the leader signature are highly expressed in all types of MDCK leader tested. Most signature components are necessary for leader migration but are not sufficient,

suggesting they work in concert to drive the migratory phenotype of leaders. It remains unclear how expression of the leader signature contributes to the leader phenotype e.g. does it confer a more motile phenotype on cells? Does it drive formation of cell-cell contacts necessary for follower migration? Does it enable faster cell repolarisation upon detection of symmetry breaking cues in a mechanism akin to contact inhibition of locomotion? Moreover, I cannot discount the possibility that there are members of the leader signature that have not yet been identified. One example may be P-cadherin, which is upregulated in *scrib*^{KD} cells and may drive leader cell migration either as part of the leader signature or independently from it, but this needs further investigation.

I show that increased p53/p21 activity is sufficient to drive leader cell migration in MDCKs. This is a key finding in the leader cell migration field, as it is the first time leader cells have been generated 'on demand' through activation of a single pathway. In fact, p53 pathway activation could also explain the upregulation of Notch ligand Dll4 demonstrated to play a role in MCF-7 leader formation: p53 has been shown to directly regulate Dll4 expression in cancer cell lines, including MCF-7 cells (Yao & Sherif 2016). What is more, I show that activation of cell cycle inhibitors is likely the universal driver of the leader status. Stochastic or damage-induced CKI activation may therefore explain how only some cells are singled out to acquire the leader fate over others.

Interestingly, my findings shed a new light on a previously described experiment where the acto-myosin cable lining the border of finger-like protrusions was cut with a laser (Reffay et al. 2014). This manipulation frequently generates a new leader at the cut site, which the authors claim is a result of mechanical de-inhibition of leader formation. I would argue that the laser simultaneously induces cellular damage and activates a p53/p21 response, which promotes leader emergence. In fact, other factors implicated in the formation of leaders (e.g. increased membrane curvature) may also contribute by feeding into p53 activation through a yet-unidentified mechanism. Alternatively, p53 activation may pre-determine a cell's response to an external cue and make it respond like a leader when cells with lower p53 might not.

Mechanical loser status

It has previously been shown that p53 elevation converts cells into mechanical losers (Wagstaff et al. 2016). I have demonstrated situations where leader migration is uncoupled from mechanical loser status (p21OE, p27OE, and p16OE cells), strongly suggesting that p53 elevation confers the mechanical loser status on cells independently of leader cell behaviour. Spontaneous leaders with 'terminal' p53 upregulation are eliminated at a higher frequency than scratch-induced leaders. I therefore suggest that mid-level p53 activity results in p21 activation and leader behaviour, but p53 elevation above this level also additionally triggers factors responsible for density hypersensitivity. This would make sense from an organismal point of view, as only cells with irreparable damage would be destined for elimination. If this theory were true, it should be possible to isolate cells that are mechanical losers but do not act as leaders.

During wound healing, I propose that persistent p53 elevation in migrating leaders results in their elimination at wound closure when the cell density increases. Meanwhile, any cells that do not reach as high p53 levels or reduce them by repairing the damage by the time the wound shuts are deemed healthy enough to remain in the epithelium. Taken together, this model places p53 as a key player in MDCK scratch-wound healing: p53 is the driver of the directional migration that seals the gap and also ensures the elimination of cells damaged beyond repair. While migration has been implicated in wound healing in mammalian corneal epithelia and rat skin (reviewed in Li et al. 2013), wound healing *in vivo* is a very complex process additionally involving the immune response, a 3D environment, soluble factors, cell proliferation, and many other variables (reviewed in de Oliveira Gonzalez et al. 2016). p53/p21 activity may therefore contribute to wound healing *in vivo*, but it is unlikely it is the sole driver of the process.

p53-mediated density hypersensitivity is conserved in an *ex vivo* mouse tracheal model (Wagstaff et al. 2016), but due to the nature of the experimental set-up, it could not be determined whether p53 elevation also triggered a leader-like migratory phenotype. It hence remains unclear if there is a role for p53/p21-driven leader migration in systems other than MDCK cells. It is therefore imperative that findings are translated from the MDCK system into other mammalian models, especially if they are to form the foundations for future therapeutic approaches.

Antibodies and drugs

For immunofluorescence, the following antibodies were used:

Epitope	Species	Dilution	Catalogue number	Supplier
Alexa Fluor conjugated secondary antibodies	various	1:1,000	various	Thermo Fisher Scientific
DAPI	N/A	1 µg/ml in water	D3571	Thermo Fisher Scientific
E-cadherin	mouse	1:600	rr1	DSHB
ITGβ1	rat	1:200	AIIB2	DSHB
N-cadherin (13A9)	mouse	1:200	14215	Cell Signalling Technology
p-MYPT1 (Thr 853)	goat	1:50	sc-17432	Santa Cruz Biotechnology
P-p38 MAPK (T180/Y182)	rabbit	1:50	9215	Cell Signalling Technology
p16	rabbit	1:5,000	10883	Proteintech Europe
p21	rabbit	1:200	sc-397	Santa Cruz Biotechnology
p27	mouse	1:200	610241	BD Biosciences
p53	rabbit	1:750	9382	Cell Signalling Technology
PI3K	mouse	1:200	610045	BD Biosciences
γH2AX (Ser 139)	rabbit	1:200	9718	Cell Signalling Technology

For Western blotting, the following antibodies were used:

Epitope	Species	Dilution	Catalogue number	Supplier
E-cadherin	mouse	1:1,000	rr1	DSHB
HRP conjugated secondary antibodies	various	1:3,000	various	BioRad
N-cadherin (13A9)	mouse	1:1,000	14215	Cell Signalling Technology
p21	rabbit	1:500	sc-397	Santa Cruz Biotechnology
p53	rabbit	1:1,000	9382	Cell Signalling Technology
β-tubulin	rabbit	1:50,000	ab6046	Abcam

Treatments used:

Treatment	Final concentration	Solvent	Supplier
Blasticidin	5 μg/ml	water	Sigma
CDK1 inhibitor RO-3306	10 μM	DMSO	Calbiochem
Doxycycline (DOX)	1 μg/ml	water	Merck
Hoechst 33342	3 μg/ml	water	Thermo Fisher Scientific
Hygromycin B	75 μg/ml	water	Thermo Fisher Scientific
Mitomycin C (MMC)	7.5 μg/ml	water	Merck
Nutlin-3	as specified in text	DMSO	Cambridge Bioscience
PI3K inhibitor LY294002	10 μM	DMSO	Merck
Puromycin (puro)	0.65 μg/ml	water	Merck
Rac1 inhibitor Z62954982	100 μM	DMSO	Merck
ROCK inhibitor Y27632	30 μM	DMSO	Sigma
Tetracycline (TET)	5 μg/ml	water	Sigma

Cell culture – MDCK cells

Wild-type MDCK and MDCK-pTR *scribble* shRNA (*scrib*^{KD}) cells were provided by Yasuyuki Fujita (Norman et al. 2012). MDCK cells were maintained in Dulbecco's Modified Eagle media (DMEM, Thermo Fisher Scientific) supplemented with 10% TET-free foetal bovine serum (FBS) in a humidified incubator at 37°C / 5% CO_2. Unless stated otherwise, MDCK culture media was not supplemented with any antibiotics. Cells were cultured at sub-confluence and split twice a week at ratios varying between 1:8 and 1:15, depending on growth rates. Passaging was performed as follows: cells were washed once in phosphate buffered saline (PBS) and then once in 0.05% trypsin-EDTA (Thermo Fisher Scientific). Fresh 0.05% trypsin-EDTA was then added and the culture dishes were incubated for 10-15 min at 37°C / 5% CO_2 until all cells had detached. At least two volumes of DMEM + 10% FBS were then used to quench the trypsin and the suspension centrifuged at 200 rcf for 3.5 min. Cell pellets were resuspended in fresh DMEM + 10% FBS (with appropriate antibiotics, if required) and plated into fresh cell culture dishes.

scrib^{KD} cells were maintained in media supplemented with 800 µl/ml G418 (Thermo Fisher Scientific) and 5 µg/ml blasticidin (Sigma); media for *scrib*^{KD} GFP-NLS cells additionally contained 0.65 µg/ml puromycin (Sigma).

Wild-type clones expressing either nuclear GFP or RFP were generated by my colleagues in the Piddini lab using a modified pGIPZ-turboGFP-Puro (Thermo Scientific) plasmid, in which turbo-GFP was replaced with either turbo GFP-NLS or turbo RFP-NLS (Wagstaff et al. 2016). The MDCK *p53KO* lines were generated by others in the Piddini lab using CRISPR/Cas9 technology (Wagstaff et al. 2016).

MDCK transfection

On day 1, 80,000 MDCK cells per well were seeded in a 6-well plate. On day 2, two solutions were prepared as follows:

Solution 1: 250 µl Opti-MEM (Thermo Fisher Scientific) + 10 µl Lipofectamine 2000 (Thermo Fisher Scientific)

Solution 2: 250 µl Opti-MEM + 4 µg of plasmid DNA

Solution 1 was incubated at RT for 5 min. Solution 2 was then pipetted into Solution 1, the tube tapped to mix, and incubated at RT for 20 min. The media on the cells was changed to 2 ml of fresh DMEM + 10% FBS. The transfection mix was then added drop-wise to the cells and incubated at 37°C / 5% CO_2 for 6 hours before the media was changed to fresh DMEM + 10% FBS. The media was changed again on the morning of day 3. If required, antibiotic selection was begun on day 4 and continued until no cells were left in the non-transfected well.

Cell culture – HEK293T cells

HEK293T cells were maintained in DMEM supplemented with 10% FBS in a humidified incubator at 37°C / 5% CO_2. Cells were cultured at sub-confluence and split twice a week at a ratio of around 1:10. Passaging was performed as follows: HEK293T cells were washed once in PBS, then 0.05% trypsin-EDTA was added and the culture dishes were incubated for 1-3 min at 37°C / 5% CO_2 until all cells had detached. At least two volumes of DMEM + 10% FBS were then used to quench the trypsin and the suspension centrifuged at 200 rcf for 3.5 min. Cell pellets were resuspended in fresh DMEM + 10% FBS and plated into fresh cell culture dishes.

Lentivirus production

On day 1, 2 x 10^6 HEK293T cells were seeded in a 10 cm dish. On day 2, the following solution was made up:

600 µl Opti-MEM + 2 µg psPAX2 + 2 µg pMD2G + 3 µg of transfer vector of choice (pTRIPZ/pGIPZ backbone – second generation vectors)

The DNA mix was then supplemented with 20 µl FuGENE HD (Promega), the tube tapped to mix, and incubated at RT for 15 min. The media on the cells was changed to 8 ml of fresh DMEM + 10% FBS. The transfection mix was then added drop-wise to the cells and

the plates incubated at 37°C / 5% CO_2 overnight. The media was changed on the morning of day 3 to fresh DMEM + 10% FBS. Lentiviruses were harvested on days 4 and 5 as follows: the HEK293T media was collected and centrifuged at 200 rcf for 5 min. The supernatant was filtered through a 0.45 μm filter, aliquoted into cryovials, and used immediately or frozen at -80°C.

Lentiviral transduction

On day 1, 80,000 MDCK cells per well were seeded in a 6-well plate. On day 2, lentiviral aliquots were thawed on ice. The media on the cells was then replaced with pure lentiviral suspension or just DMEM + 10% FBS in the negative control well. On the morning of day 3 (approximately 24 hours later), the media was changed to fresh DMEM + 10% FBS. If required, antibiotic selection was begun on day 4 and continued until no cells were left in the non-transduced well.

Freezing cells

To generate frozen cell stocks, cells were passaged as normal. The cell pellet was resuspended in a solution of 90% FBS and 10% DMSO to make a cell suspension at a concentration of 10^6 cells per ml. 1 ml aliquots of this suspension were then frozen in cryovials placed in a Styrofoam rack at -80°C. A minimum of 24 hours later, vials were moved into liquid nitrogen for long-term storage.

MDCK cell lines generated as part of this work

Name	Description	Associated fluorophore	Antibiotic(s) in media
scrib^{KD} E-cad^{KD}	TET/DOX-inducible knockdown of Scribble and E-cadherin	N/A	G418*, blasticidin, hygromycin
E-cadOE	DOX-inducible overexpression of E-cadherin	RFP-NLS	Puromycin
N-cadOE	DOX-inducible overexpression of N-cadherin	RFP-NLS	Puromycin
P-cadOE (pool)	DOX-inducible overexpression of P-cadherin	RFP-NLS	Puromycin
p21OE	DOX-inducible overexpression of p21	RFP-NLS	Puromycin
p21KO	CRISPR/Cas9-mediated knockout of p21	N/A	None
p21 reporter	Destabilised GFP-NLS expression controlled by the p21 promoter to report p21 activity	GFP-NLS	G418*
GSE-22 (pool)	DOX-inducible overexpression of dominant negative p53 peptide, GSE-22	GFP-NLS	Puromycin
p27OE (pool)	DOX-inducible overexpression of p27	RFP-NLS	Puromycin
p16OE (pool)	DOX-inducible overexpression of p16	RFP-NLS	Puromycin

Antibiotic concentrations used: 5 μg/ml blasticidin, 75 μg/ml hygromycin, 0.65 μg/ml puromycin.

* Cells with *scrib^{KD}* in their genetic background were cultured in media containing 800 μg/ml G418; 400 μg/ml G418 was used in all other cases.

Generation of the *scrib^{KD} E-cad^{KD}* construct and cell line

To knockdown E-cadherin expression in MDCK *scribble* shRNA cells (*scrib^{KD} E-cad^{KD}*), I modified a plasmid provided by Yasuyuki Fujita, pSUPERIOR.neo+gfp E-cadherin shRNA (Hogan et al. 2009), which that already contained an shRNA against canine E-cadherin. I excised the neomycin/G418 antibiotic resistance cassette and used In-Fusion to replace it with a hygromycin resistance cassette amplified from pCMV-LacI (Agilent Genomics). This created pSUPERIOR.hygro+gfp E-cadherin shRNA, which I transfected into recipient *scrib^{KD}* cells and selected for positive double knockdown clones using hygromycin B (75 μg/ml). The knockdown efficiencies of Scribble and E-cadherin were verified by Western blotting and immunofluorescence, respectively.

Generation of the E-cadherin, N-cadherin, P-cadherin, p27, and p16 overexpression constructs and cell lines

I amplified the E-cadherin-GFP sequence from a plasmid provided by James Norman (Adams et al. 1998). For N- and P-cadherin, the respective cDNA sequences were amplified from a cDNA library obtained from MDCK *scribble* shRNA cells treated with tetracycline to induce *scribble* knockdown, as these cells have elevated levels of both N- and P-cadherin (Piddini lab, unpublished and Wagstaff et al. 2016). I amplified p27 cDNA from the same canine cDNA library. I amplified human p16 from pLenti CMV p16 Neo (w111-1) (Addgene #22260); I modified the forward primer to reintroduce eight N-terminal amino acids that were missing from the p16 construct in the plasmid when compared to the full-length human p16 sequence (transcript ENST00000304494.9, Ensembl).

I designed the reverse primers used for amplification such that they contained a 'self-cleaving' P2A peptide sequence (Kim et al. 2011). Using In-Fusion cloning, I individually introduced the three cadherin, p27, and p16 cDNAs into pTRIPZ-RFP-NLS-Puro, a lentiviral backbone where protein expression was induced by addition of doxycycline.

The final constructs were as follows:

pTRIPZ E-cadherin-GFP-P2A-RFP-NLS = EcadOE cell line

pTRIPZ N-cadherin-P2A-RFP-NLS = NcadOE cell line

pTRIPZ P-cadherin-P2A-RFP-NLS = PcadOE cell line

pTRIPZ p27-P2A-RFP-NLS = p27OE cell line

pTRIPZ p16-P2A-RFP-NLS = p16OE cell line

These constructs express E-cadherin-GFP/N-cadherin/P-cadherin/p27/p16 and RFP-NLS as a single transcript in a doxycycline-inducible manner. I then generated lentiviruses from the final constructs and used them to (individually) transduce wild-type MDCKs. Selection following infection was carried out with puromycin (0.65 μg/ml). I then plated the E-cadOE and N-cadOE pools at one cell per well in 96-well plates to generate single clones; I verified the expression levels of the relevant cadherins by immunofluorescence. The P-cadOE, p27OE, and p16OE antibiotic-selected pools were used as pool populations.

Generation of the *p21KO* construct and clones

I generated MDCK *p21KO* clones G5 and E9 using Cas9 D10A CRISPR technology. I manually designed the sgRNA target sequences against canine *CDKN1A* following published methods (Ran et al. 2013). I made sure that the two target sequences were ≤20nt apart and that their respective PAM sequences were pointing away from each other. I used the following target sequences in exon 2 of *CDKN1A*:

5'-CGGCAAGCCTTGCTGCCATG(AGG)-3'

5'-TGGACAGCGAGCAGCTGCGC(CGG)-3'

I cloned the target sequences individually into PX461 vectors (Appendix 2J) containing the Cas9 D10A nickase enzyme and the sgRNA scaffold (Ran et al. 2013), as described in the 'Molecular Biology' section of this work, and co-transfected 2 μg of each plasmid into wild-type MDCK cells. I treated the transfected cells with 11 μM Nutlin for 6 days to enrich for *p21KO* cells, as these would not be growth-inhibited as a result of Nutlin-mediated p53 (and hence p21) elevation. I then plated the pool at one cell per well in 96-well plates; I

expanded the resulting clones and verified them by immunofluorescence in the presence or absence of Nutlin and sequencing.

Generation of the p21OE construct and cell line

To overexpress p21, I amplified the p21 cDNA a cDNA library obtained from MDCK *scribble* shRNA cells treated with tetracycline to induce *scribble* knockdown, as these cells have been shown to express high levels of p21 (Wagstaff et al. 2016). I used In-Fusion to introduce the resulting PCR product into doxycycline-inducible pTRIPZ-RFP-NLS-Puro with a P2A peptide bridging the two proteins to make pTRIPZ-p21-P2A-RFP-NLS. I then made lentiviruses from the final construct and transduced wild-type MDCK cells. I then selected positive clones using 0.65 μg/ml puromycin, and plated the pool out at one cell per well in 96-well plates to isolate single clones that I verified by immunofluorescence.

Generation of the p21 reporter construct and clones

To generate a cell line reporting p21 activity through the dynamics of GFP-NLS, I modified a reporter for p21 activity described in (Paek et al. 2016). The original reporter contained a destabilised version of CFP-NLS whose expression was driven by the human p21 promoter. I first excised the CMV promoter, CMV enhancer, and eGFP from pcDNA3.3 d2eGFP (Addgene #26821) using MluI and HindIII (this left behind the PEST destabilisation signal in the backbone). Meanwhile, I amplified turbo GFP-NLS from pTRIPZ GFP-NLS-Puro and used In-Fusion to insert it into MluI/HindIII-digested pcDNA3.3 d2eGFP. This generated a vector containing a destabilised version of turbo GFP-NLS, pcDNA3.3 d2turbo GFP-NLS. I then amplified the p21 promoter from a modified version of the original reporter, p273, supplied by Andrew Paek. Finally, I used In-Fusion to add the p21 promoter into MluI-digested pcDNA3.3 d2turbo GFP-NLS.

The final construct contained a destabilised version of turbo GFP-NLS whose expression is driven by the human p21 promoter. I transfected this construct into wild-type MDCKs and selected for stably transfected cells using G418 (400 μg/ml). From the pool, I isolated

three clones that had very low background signal and responded to Nutlin treatment by strong induction of nuclear GFP, as assessed by confocal microscopy.

Generation of the GSE-22 construct and cell line

The dominant negative GSE-22 peptide was first described for the rat in (Ossovskaya et al. 1996). To overexpress the dominant negative GSE-22 peptide in MDCK cells, I amplified the sequence encoding amino acids 302-381 of canine p53 (homologous to the original rat sequence) from the MDCK cDNA library used in p21OE cloning above. I used a forward primer carrying an adaptor with three start ATG codons and a reverse primer containing three stop codons to account for all three reading frames, as was done in the original publication. I used In-Fusion to introduce the resulting PCR product into doxycycline-inducible pTRIPZ-GFP-NLS-Puro with a P2A peptide bridging the two proteins to make pTRIPZ-GSE-22-P2A-GFP-NLS. I then generated lentiviruses with this construct and tranduced wild-type MDCK cells. I selected positive transformants using 0.65 μg/ml puromycin to generate a pool population.

Competition and directed migration assays using the 'fences' system

Cell competition and directed migration assays were carried out in 24 well plates using 'fences' (Aix Scientifics, http://www.aix-scientifics.co.uk/en/fences.html). 'Fences' allow two different cell populations to be seeded on either side of a silicone barrier, thus allowing for an internal control for any treatments and/or immunostainings. Control, pure cultures were plated on the inside of the 'fence'; competition co-cultures were seeded on the outside of the 'fence'. To distinguish the two cell populations, one cell line was always labelled with a fluorescent nuclear marker, GFP-NLS or RFP-NLS.

Cell numbers were as follows:

Experiment	Inside	Outside
Competition	1000 loser cells	800 loser cells : 7200 winner cells
Directed migration	1000 loser cells	400 loser cells : 3600 winner cells
Nutlin competition	1000 WT GFP-NLS	900 WT GFP-NLS : 1900 *p53KO*

'Fences' were removed ~5 hours after plating for all experiments. For most competition and directed migration experiments, the culture medium was replaced at this point with media containing TET or DOX, and replaced again 20 hours later. For Nutlin-induced competition, the culture medium was replaced with fresh DMEM + 10% FBS after 'fence' removal; Nutlin/DMSO was only added ~30 h after 'fence' removal. Live imaging was started 2–4 h after the last media change and was continued for at least 3 days with media changes every 2 days.

Gridded dishes for *scrib^{KD} E-cad^{KD}* directed migration assays

6,250 cells were plated per gridded tissue culture plate (μ-Dish 35 mm Grid-500, Ibidi). This allowed for live imaging of specific clones that could be located again for immunofluorescence analysis. Co-cultures were plated at a ratio of 1:10 loser : winner and imaged every 2-4 hours using the Nikon BioStation CT system. Cells at the end of live imaging were fixed in 4% PFA in PBS for 10 min at RT and processed using the immunofluorescence protocol described below.

Mitomycin C (MMC) assays

On day 1, 2,500 untreated wild-type MDCK cells (labelled with GFP-NLS or unlabelled, as appropriate) were seeded per well in 24-well plates; 5,000 of that same population was also plated in a separate well as a pure population. On day 2, a second population of MDCK cells was trypsinised, and 1 x 10^6 of these were incubated in suspension in 5 ml complete media containing 7.5 μg/ml MMC for 1 hour at 37°C / 5% CO_2. The cells were then washed at least three times in complete media (spinning down the cells after each wash) to reduce

MMC carryover. 5,000 MMC-treated cells (or 2,500 untreated cells for the negative control) were then plated on top of the 2,500 untreated cells; 10,000 MMC-treated cells (or 5,000 untreated cells for the negative control) were also plated as a pure population in an otherwise empty well. Live imaging was begun on day 3 and continued for at least 2 days; samples were imaged every 2 hours.

It is worth noting that I tested MMC concentrations ranging from 1 to 50 μg/ml (data not shown). Many cells in ≤5 μg/ml MMC did not display cell cycle arrest, while concentrations above 10 μg/ml MMC resulted in rapid cell death. I chose 7.5 μg/ml MMC, as all cells stopped dividing at this MMC concentration, but still survived for many days, which enabled assays to be run.

Spontaneous leader assays

5,000 wild-type MDCK cells were seeded in a 24-well plate or, if immunofluorescence was to be performed at end of live imaging, in a gridded tissue culture plate (μ-Dish 35 mm Grid-500, ibidi). Approximately 48 hours later, cells with the flattened spontaneous leader morphology were manually selected on the Nikon BioStation CT and imaged every 2 hours. Where applicable, cells at the end of live imaging were fixed in 4% PFA in PBS for 10 min at RT and processed using the immunofluorescence protocol described below.

Wound healing and barrier release assays

27,000-33,000 wild-type MDCK cells were seeded in the middle of a 'fence' placed in a 24-well plate or straight into a well of a 96-well plate (no 'fence'). If immunofluorescence was to be performed after live imaging, optically clear plates (μ-Plate 24 well, ibidi or CellCarrier-96, PerkinElmer) were used. The 'fence' was removed approximately 5 hours after seeding and the culture medium changed to fresh DMEM + 10% FBS (supplemented with DOX for experiments with the GSE-22 line). Approximately 20 hours later, a P1000 pipette tip was used to generate a scratch-wound through the middle of the now-confluent monolayer and the culture medium changed. Imaging of the wound edge was started approximately 1 hour after scratching and imaged every 1-2 hours.

UV irradiation experiments

On day 1, 25,000-30,000 wild-type cells per well were plated in an optically clear 96-well plate (CellCarrier-96, PerkinElmer). The cells were left to adhere overnight. On day 2, a scratch-wound was generated through the middle of each well in the 96-well plate using a P1000 tip and returned to the 37°C / 5% CO_2 incubator for approximately 30 min. Cells were then treated in the incubator with 3 μg/ml Hoechst diluted in complete media for 10 min. The cells were washed three times in complete media. UV irradiation along the top half of the wound edge was performed using a 20× air objective on a Leica SP8 confocal microscope, which was set up to keep the samples at 37°C / 5% CO_2 during imaging; the bottom half of the wound was not irradiated. UV treatment settings used: 30 frames at 100% 405 nm laser with the FRAP booster on. The samples were then imaged using the BioStation CT every hour for at least 24 hours. For γH2AX staining, samples were fixed and processed using the phospho-antibody protocol described below 2-4 hours after UV irradiation.

Immunofluorescence

Depending on the assay, cells were cultured on glass coverslips or optically clear tissue culture dishes. Cells were fixed in 4% PFA (Electron Microscopy Sciences) in PBS for 10 min at RT, quenched for 10 min at RT in 50 mM in NH_4Cl in PBS, and permeabilised for 10 min at RT in 0.1% Triton X-100 in PBS. Samples were blocked for at least 30 min in 2% BSA, 2% FBS in PBS at RT. Both primary and secondary antibodies were diluted in blocking solution diluted 1 : 1 with PBS. Primary antibody incubations were either a minimum of 1 hour at RT or overnight at 4°C. Following 4 x 5 min washes in PBS, secondary antibodies were incubated for 1 hour at RT, then washed 4 x 5 min in PBS. Coverslips were mounted in FluorSave (Merck). Optically clear dishes were either flooded with FluorSave and sealed with a coverslip or imaged directly in the last PBS wash. For immunostaining against phosphorylated proteins, fixing solution was supplemented with PhosSTOP (1 tablet per 10ml, Sigma), all PBS solutions were substituted with TBS, and blocking solution was substituted with 5% BSA in TBS.

Imaging and image analysis

Imaging of fixed samples was primarily done at RT on Leica SP5 or SP8 confocal microscopes using a 40× oil objective. The PerkinElmer Opera LX system with a 20× water objective and the Yokogawa Electric Corporation CellVoyager 7000 system with a 20× air objective were also used for high-throughput screening of clonal cell lines. UV irradiation experiments were done on a Leica SP8 confocal microscope set up to keep the samples at 37°C / 5% CO_2 during imaging. All live imaging was done on a Nikon BioStation CT system at 37°C / 5% CO_2 using 10× or 4× air objectives with an imaging frequency every 1-4 hours (indicated in movie time stamps); media was changed every 2–3 days.

Unless stated otherwise in the figure legends, all confocal images are displayed as sum projections in z.

E-cadherin staining intensities were measured using Fiji (Schindelin et al. 2012). Individual cells were selected manually on an average z stack projection and their integrated densities values were recorded and plotted.

Mean intensities of nuclear p53, P-p38, and p21 were measured using DAPI as a mask to segment the nuclear volumes in Volocity (PerkinElmer). This script was written by Richard Butler from the Imaging Facility at the Gurdon Institute, University of Cambridge.

The migration speed of scratch-wound fronts was measured in Fiji by manually drawing freehand lines outlining the wound edge at the first and final time points. If any wound edges were not parallel to the y axis, the images were adequately rotated. The median x position for each line was recorded to calculate the median x displacement in μm, which was then divided by the duration of the experiment in hours to generate a speed value in μm/h.

Statistical analysis was performed using Prism 7 (GraphPad). All p values were obtained using the Kolmogorov-Smirnov (K-S) test.

Prism 7 was used to plot all graphs. Brightness and contrast adjustments were made in Fiji. Figures were made using Adobe Illustrator CS6.

Statistical analysis

Every experimental condition and treatment was carried out alongside an untreated or solvent-only (e.g. DMSO) control. Unless otherwise specified in the figure legend or text, all quantifications, immunofluorescence images, movie sequences, and Western blots shown are from a single representative experiment taken from a minimum of three independent repeats per experiment. For live imaging and immunofluorescence experiments, at least 10 fields of view were analysed per condition.

When analysing the migration of MMC-treated *p53KO* and *p21KO* cells (and their respective controls), the experiments were randomised by another lab member before being analysed blind by me.

Where indicated in the text and figure legends, some quantifications could not have statistical tests performed due to uneven sample sizes. In these instances, I used the means and standard deviations of the two populations to calculate the minimum sample size required to be conclusive about saying there is a significant difference between them (Chow et al. 2008).

Western blotting

To lyse cell samples, 1% SDS diluted in PBS was added to the culture dish and the cells scraped with the wide end of a P1000 tip. Lysates were incubated at 100°C for 5 min and then passed through a 25G needle ten times to shear the DNA. Lysates were then frozen at -20°C, thawed and the DNA shearing process repeated. The freezing-shearing process was repeated once more such that each lysate had been passed through a needle a total of 30 times. Samples were made up with 10-20 μg of protein, 3 μl dithiothreitol (DTT), 7.5 μl 4× SDS loading dye (Invitrogen), and topped up to 30 μl with PBS. Samples were then separated on a 4-12% Bis-Tris gradient gel (Invitrogen) in MOPS SDS running buffer (Invitrogen) at 175V for approximately 1 hour. Proteins were then transferred from the gel onto a methanol-activated PVDF membrane (Anachem) using a semi-dry blotter (Bio-Rad) at 13V for 45-60 min. Membranes were blocked with 5% skimmed milk diluted in 0.05% Tween-20 in PBS (PBST) for 1 hour at RT, incubated in primary antibodies (in 2%

skimmed milk in PBST) overnight at 4°C, washed in PBST, and incubated in secondary HRP-conjugated antibodies diluted in 2% skimmed milk in PBST for 1 hour at RT. After washes in PBST, membranes were developed using ECL (GE Healthcare) and radiographic film.

Molecular biology

I designed all cloning strategies and primers in SnapGene (GSL Biotech) and cDNA sequences obtained using the Ensembl genome browser (Zerbino et al. 2018). I also used SnapGene to analyse sequencing data and draw the plasmid maps presented in Appendix 2.

All forward primers used to amplify mammalian coding regions contained the Kozak consensus sequence GCCACC just upstream of the first ATG codon.

The pTRIPZ-RFP-NLS-Puro and pTRIPZ-GFP-NLS-Puro plasmids were generated by Silvia Vivarelli, a colleague in the Piddini lab, by modifying the commercially available pTRIPZ-turboGFP-Puro (Thermo Scientific).

(vi) cDNA library preparation

The RNA template was prepared by colleagues in the Piddini lab from MDCK *scribble* shRNA cells treated with tetracycline to induce *scribble* knockdown. I then used this RNA to make an MDCK cDNA library using Superscript III Reverse Transcriptase (Thermo Fisher Scientific) according to the manufacturer's instructions. I used the resulting cDNA library for further cloning, as described in the relevant sections.

(vii) PCR amplification

PCR amplification of desired genes was performed using Phusion High-Fidelity DNA Polymerase (New England Biolabs) and construct-specific DNA oligonucleotides (Sigma) in the following reaction mix:

Component	Volume per 50 µl reaction (µl)
5× Phusion GC buffer	10
dNTPs (10 mM each)	1
Forward primer (10 µM)	2.5
Reverse primer (10 µM)	2.5
Template: cDNA (100 ng) or plasmid (<30 ng)	1
DMSO	2.5
Phusion enzyme	0.5
ddH_2O	30

If needed, the above reaction mix was optimised by changing to 5× Phusion HF buffer, varying the DMSO concentration (0-5% final concentration), or screening a range of annealing temperatures.

The PCR reaction mix was then cycled in a thermocycler under the following conditions:

Stage	Temperature	Duration	
Initial denaturation	98°C	30 sec	
Denaturation	98°C	10 sec	30 cycles
Annealing	Primer-specific T_m	10 sec	
Extension	72°C	30 sec per kb of expected product	
Final extension	72°C	7 min	
Hold	15°C	∞	

Presence and size of expected PCR products were verified by agarose gel electrophoresis (1% w/v agarose in 1× TAE buffer). Bands of interest were cut out from the gel and purified using a QIAquick Gel Extraction Kit (Qiagen).

(viii) Restriction digestion

Plasmid backbones were linearised by restriction digestion overnight at 37°C to minimise the amount of uncut plasmid. The whole reaction was then run on an agarose gel and the bands of interest cut out and purified using a QIAquick Gel Extraction Kit (Qiagen).

(ix) sgRNA target sequence cloning for CRISPR strategies

The PX461 backbone, encoding Cas9 D10A ('nickase') and GFP, was linearised overnight using BbsI/BpiI. The whole reaction was run on an agarose gel; the band was cut out and purified using a QIAquick Gel Extraction Kit (Qiagen).

Two DNA oligos per sgRNA target sequence were designed such that, once annealed, they formed a fragment with sticky ends compatible with the BbsI/BpiI-linearised PX461 backbone:

5'	CACCG – NNNNNNNNNNNNNNNNNNN	3' top (guide sequence)
3'	C – NNNNNNNNNNNNNNNNNNN – CAAA	5' bottom

The following reaction was set up to first phosphorylate their 5' ends of the DNA oligos and then anneal them:

Component	Volume per 10 µl reaction (µl)
Oligo 1 (100 µM)	1
Oligo 2 (100 µM)	1
10× T4 polynucleotide kinase (PNK) buffer	1
T4 PNK	1
ddH_2O	6

The reaction was placed in a thermocycler with the following programme: 30 min at 37°C to allow the T4 PNK to work, followed by gradient from 95°C to 25°C dropping 5°C every minute to enable oligo annealing.

The following ligation mix was then set up:

Component	Volume per 20 µl reaction (µl)
50 ng BbsI/BpiI digested PX461 backbone	x
Annealed oligos (1:200 dilution in ddH_2O)	1
10× T4 ligase buffer	1
T4 ligase	1
ddH_2O	make up to 20

The ligation reaction was incubated for approximately 1 hour at RT. 2 µl of the reaction mix was then transformed into 20 µl of chemically competent Stbl3 *E. coli*.

(x) In-Fusion cloning

The In-Fusion HD Cloning Kit (Clontech) was used for all cloning, unless specified, according to the manufacturer's instructions. I designed In-Fusion primers such that they had a 20 nt overlap with the linearised vector (rather than the suggested minimum of 15 nt).

(xi) Bacterial transformation and culture

To amplify plasmid DNA, an appropriate volume of In-Fusion reaction mix, ligation reaction mix, or purified plasmid was transformed into chemically competent *E. coli* cells. For In-Fusion reactions, Stellar cells were used; for large plasmids like pTRIPZ or PX461, Stbl3 cells were used to prevent recombination events; for any other purposes, TOP10 cells were used. The DNA was incubated with 20-50 µl of cells for 20 min on ice. Cells were then heat shocked at 42°C for 42 sec, followed by 2 min on ice. 1 ml of LB broth was then added to the transformation mix and the samples incubated in a ThermoMixer (Eppendorf) for 1 hour at 37°C with shaking. 100 µl of the cell suspension was then plated on an LB agar plate containing appropriate antibiotics (100 µg/ml ampicillin or 50 µg/ml kanamycin). The remainder of the solution was pelleted (16,000 rcf, 30 sec), most of the supernatant tipped out such that the pellet could be resuspended in approximately 100 µl of liquid, and spread on another LB plate containing antibiotics. This produced two plates per transformation, one with approximately 10% of the cells and the other with the remaining ~90%. Plates were incubated at 37°C for 16-20 hours.

Plasmids were recovered from an overnight culture in 2 ml LB broth containing appropriate antibiotics (100 µg/ml ampicillin or 50 µg/ml kanamycin) using a QIAGEN Plasmid Mini Kit (Qiagen). If larger quantities of plasmid were required, the overnight culture was scaled up to 50-100 ml and a QIAGEN Plasmid Midi Kit (Qiagen) was used for plasmid recovery. Plasmids were eluted in ddH_2O and the DNA concentration measured using a NanoDrop spectrophotometer (Thermo Fisher Scientific).

(xii) Verification by 'diagnostic digest' and sequencing

Correct fragment insertion was verified by performing a 'diagnostic digest': a small-scale restriction digestion (≤5 µl of the recovered plasmid) followed by agarose gel electrophoresis. Clones with correct digestion patterns were diluted to 50 ng/µl in 15 µl and sent for sequencing (Eurofins Genomics) with plasmid-specific primers at 10 µM.

List of abbreviations

°C	Degrees Celsius
APC	Adenomatous polyposis coli
AU	Arbitrary units
Bak	Bcl-2 homologous antagonist/killer
Bax	Bcl-2 associated X protein
BNPs	Bone morphogenetic proteins
bp	Base pair(s)
BSA	Bovine serum albumin
CAFs	Cancer-associated fibroblasts
CDK	Cyclin/cyclin-dependent kinase
CDKN1A	Cyclin-Dependent Kinase Inhibitor 1A, $p21^{WAF1/Cip1}$, p21
cDNA	Complementary DNA
CFP	Cyan fluorescent protein
CKI	Cyclin/cyclin-dependent kinase inhibitor
cm	Centimetre(s)
CO_2	Carbon dioxide
DAPI	4′,6-diamidino-2-phenylindole
ddH_2O	Double-distilled water
Dlg	Discs large
DMEM	Dulbecco's Modified Eagle media
DMSO	Dimethyl sulphoxide
DNA	Deoxyribonucleic acid
dNTPs	Deoxyribonucleotide triphosphates
DOX	Doxycycline
Drosophila	*Drosophila melanogaster*
DSB	Double-strand break
DTT	Dithiothreitol
E-cad/E-cadherin	Epithelial cadherin
E-cad^{KD}	*E-cadherin* knockdown
E. coli	*Escherichia coli*

EC domain	Extracellular cadherin domains
ECM	Extracellular matrix
EDTA	Ethylenediaminetetraacetic acid
EGFR	Epidermal growth factor receptor
ELMO	Engulfment and cell motility
EMT	Epithelial to mesenchymal transition
ERK1/2	Extracellular regulated kinase 1/2
FBS	Foetal bovine serum
GEF	Guanosine exchange factor
GFP	Green fluorescent protein
h/hrs	Hour(s)
HEK-293T cells	Human embryonic kidney cells 293 transformed with the SV40 large T antigen
HGF	Hepatocyte growth factor
Hoechst	Hoechst 33342
HRP	Horseradish peroxidase
ITGβ1	Integrin β1
JAK/STAT	Janus kinase / signal transducer and activator of transcription
JNK	c-Jun N-terminal kinase
K-S test	Kolmogorov–Smirnov test
KO	Knockout
LAP protein	LRR and PDZ domains protein
LB	Lysogeny broth
Lgl	Lethal giant larvae
LRR	Leucine-rich repeats
MAPK	Mitogen-activated protein kinase
Mbc	Myoblast city
MDCK cells	Madin-Darby canine kidney cells
Mdm2	Mouse double minute 2
min	Minute(s)
ml	Millilitre(s)
mm	Millimetre(s)
mM	Millimolar

MMC	Mitomycin C
MOPS	3-(N-morpholino)propanesulphonic acid
mRNA	Messenger ribonucleic acid
N-cad/N-cadherin	Neural cadherin
NC	Neural crest
NF-κB	nuclear factor kappa-light-chain-enhancer of activated B cells
ng	Nanogram(s)
NLS	Nuclear localisation sequence
nt	Nucleotide(s)
OE	Overexpression
oligo	DNA oligonucleotide
P-cad/P-cadherin	Placental cadherin
p16	$p16^{INK4A}$
p21	$p21^{WAF1/Cip1}$
p21KO	*p21* knockout
p27	$p27^{Kip1}$
P2A	Porcine teschovirus-1 2A
p53KO	*p53* knockout
PAM	Protospacer adjacent motif
PBS	Phosphate buffered saline
PBST	Phosphate buffered saline + 0.05% Tween-20
PCNA	Proliferating cell nuclear antigen
PCP	Planar cell polarity
PCR	Polymerase chain reaction
PDGF	Platelet-derived growth factor
PDMS	Polydimethylsiloxane
PDZ	PSD-95, ZO-1 and Disc large
PEST	Peptide sequence rich in proline (P), glutamate (E), serine (S), and threonine (T)
PFA	Paraformaldehyde
PI3K	Phosphoinositide 3-kinase
pMYPT1	Phosphorylated myosin phosphatase target subunit 1
PNK	Polynucleotide kinase

Puro	Puromycin
PVDF	Polyvinylidene difluoride
PVR	PDGF/VEGF receptor
rcf	Relative centrifugal force
RFP	Red fluorescent protein
RNA	Ribonucleic acid
ROCK	Rho-associated protein kinase
ROS	Reactive oxygen species
RT	Room temperature
SAβGAL	Senescence-associated β-galactosidase
scribble$^{-/-}$	*scribble* knockout (in *Drosophila*)
scrib^{KD}	*scribble* knockdown (in mammalian systems)
SDS	Sodium dodecyl sulphate
sec	Second(s)
SEM	Standard error of the mean
sgRNA	Short guide RNA
shRNA	Short hairpin RNA
SV40	Simian virus 40
TAE buffer	Tris-acetate-EDTA buffer
TBS	Tris buffered saline
TET	Tetracycline
TGFβ	Transforming growth factor β
T_m	Melting temperature
TNF	Tumour necrosis factor
Tris	Tris(hydroxymethyl)aminomethane
TRR	Toll-related receptor
UV	Ultraviolet
V	Volt(s)
VEGF	Vascular endothelial growth factor
WT	Wild-type
µg	Microgram(s)
µl	Microlitre(s)
µM	Micromolar

References

Adams, C.L. et al., 1998. Mechanisms of Epithelial Cell–Cell Adhesion and Cell Compaction Revealed by High-resolution Tracking of E-Cadherin–Green Fluorescent Protein. *The Journal of Cell Biology*, 142(4), pp.1105–1119.

Altschul, S.F. et al., 1997. Gapped BLAST and PSI-BLAST: A new generation of protein database search programs. *Nucleic Acids Research*, 25(17), pp.3389–3402.

Amano, M., Nakayama, M. & Kaibuchi, K., 2010. Rho-kinase/ROCK: A key regulator of the cytoskeleton and cell polarity. *Cytoskeleton*, 67(9), pp.545–554.

Amoyel, M. & Bach, E.A., 2014. Cell competition: how to eliminate your neighbours. *Development*, 141(5), pp.988–1000.

Andreassen, P.R. et al., 2001. Tetraploid State Induces p53-dependent Arrest of Nontransformed Mammalian Cells in G1. *Molecular Biology of the Cell*, 12(5), pp.1315–1328.

Bazellières, E. et al., 2015. Control of cell-cell forces and collective cell dynamics by the intercellular adhesome. *Nature Cell Biology*, 17(4), pp.409–420.

Besson, A., Dowdy, S.F. & Roberts, J.M., 2008. CDK Inhibitors: Cell Cycle Regulators and Beyond. *Developmental Cell*, 14(2), pp.159–169.

Bilder, D. & Perrimon, N., 2000. Localization of apical epithelial determinants by the basolateral PDZ protein Scribble. *Nature*, 403(6770), pp.676–80.

Bondar, T. & Medzhitiv, R., 2010. p53-Mediated Hematopoietic Stem and Progenitor Cell Competition. *Cell Stem Cell*, 6(4), pp.309–322.

Bowling, S. et al., 2018. A p53/mTOR signalling axis drives fitness selection through cell competition during early mouse embryonic development. *Nature Communications*, 1763(9).

Brumby, A.M. & Richardson, H.E., 2003. scribble mutants cooperate with oncogenic Ras or Notch to cause neoplastic overgrowth in Drosophila. *The EMBO journal*, 22(21), pp.5769–79.

Burd, E.M., 2003. Human Papillomavirus and Cervical Cancer. *Clinical Microbiology Reviews*, 16(1), pp.1–17.

Burton, D.G.A., 2009. Cellular senescence, ageing and disease. *Age*, 31(1), pp.1–9.

Chapnick, D.A. & Liu, X., 2014. Leader cell positioning drives wound-directed collective migration in TGF - stimulated epithelial sheets. *Molecular Biology of the Cell*, 25(10), pp.1586–1593.

Chen, C.-L. et al., 2012. Tumor suppression by cell competition through regulation of the Hippo pathway. *Proceedings of the National Academy of Sciences*, 109(2), pp.484–489.

Chow, S., Shao, J. & Wang, H., 2008. Sample Size Calculations in Clinical Research. In *Chapman & Hall/CRC Biostatistics Series*. p. 58.

Clavería, C. et al., 2013. Myc-driven endogenous cell competition in the early mammalian embryo. *Nature*, 500(7460), pp.39–44.

Clavería, C. & Torres, M., 2016. Cell Competition: Mechanisms and Physiological Roles. *Annual Review of Cell and Developmental Biology*, 32(1), pp.411–439.

Dang, C. V, 2013. MYC, metabolism, cell growth, and tumorigenesis. *Cold Spring Harbor perspectives in medicine*, 3(8), p.a014217.

Datto, M.B. et al., 1995. Transforming growth factor beta induces the cyclin-dependent kinase inhibitor p21 through a p53-independent mechanism. *Proceedings of the National Academy of Sciences of the United States of America*, 92(12), pp.5545–9.

Demaria, M. et al., 2015. An Essential Role for Senescent Cells in Optimal Wound Healing through Secretion of PDGF-AA. *Developmental Cell*, 31(6), pp.722–733.

Doggett, K. et al., 2011. Loss of the Drosophila cell polarity regulator Scribbled promotes epithelial tissue overgrowth and cooperation with oncogenic Ras-Raf through impaired Hippo pathway signaling. *BMC Developmental Biology*, 11.

Dow, L.E. et al., 2007. The tumour-suppressor Scribble dictates cell polarity during directed epithelial migration: Regulation of Rho GTPase recruitment to the leading edge. *Oncogene*, 26(16), pp.2272–2282.

Dukes, J.D., Whitley, P. & Chalmers, A.D., 2011. The MDCK variety pack : choosing the right strain. *BMC Cell Biology*, 12(1), p.43.

Dulić, V. et al., 1994. p53-dependent inhibition of cyclin-dependent kinase activities in human fibroblasts during radiation-induced G1 arrest. *Cell*, 76(6), pp.1013–1023.

Duman-Scheel, M., Johnston, L.A. & Du, W., 2004. Repression of dMyc expression by Wingless promotes Rbf-induced G1 arrest in the presumptive Drosophila wing margin. *Proceedings of the National Academy of Sciences*, 101(11), pp.3857–3862.

Durand, S. & Cimarelli, A., 2011. The Inside out of Lentiviral Vectors. *Viruses*, 3(2), pp.132–159.

Eichenlaub, T., Cohen, S.M. & Herranz, H., 2016. Cell competition drives the formation of metastatic tumors in a drosophila model of epithelial tumor formation. *Current Biology*, 26(4), pp.419–427.

Eisenhoffer, G.T. et al., 2012. Crowding induces live cell extrusion to maintain homeostatic cell numbers in epithelia. *Nature*, 484(7395), pp.546–9.

Elia, G., 2008. Biotinylation reagents for the study of cell surface proteins. *Proteomics*, 8(19), pp.4012–4024.

Farooqui, R. & Fenteany, G., 2005. Multiple rows of cells behind an epithelial wound edge extend cryptic lamellipodia to collectively drive cell-sheet movement. *Journal of Cell Science*, 118(1), pp.51–63.

Friedl, P. et al., 2012. Classifying collective cancer cell invasion. *Nature Cell Biology*, 14(8), pp.777–783.

Friedl, P. & Gilmour, D., 2009. Collective cell migration in morphogenesis, regeneration and cancer. *Nature Reviews Molecular Cell Biology*, 10(7), pp.445–457.

Gardiol, D. et al., 2006. Human discs large and scrib are localized at the same regions in colon mucosa and changes in their expression patterns are correlated with loss of tissue architecture during malignant progression. *International Journal of Cancer*, 119, pp.1285–1290.

Di Gregorio, A., Bowling, S. & Rodriguez, T.A., 2016. Cell Competition and Its Role in the Regulation of Cell Fitness from Development to Cancer. *Developmental Cell*, 38(6), pp.621–634.

Hogan, C. et al., 2009. Characterization of the interface between normal and transformed epithelial cells. *Nature cell biology*, 11(4), pp.460–7.

Humbert, P.O. et al., 2008. Control of tumourigenesis by the Scribble/Dlg/Lgl polarity module. *Oncogene*, 27(55), pp.6888–6907.

Igaki, T. et al., 2009. Intrinsic tumor suppression and epithelial maintenance by endocytic activation of Eiger/TNF signaling in Drosophila. *Developmental Cell*, 6(3), pp.247–253.

Jeanes, A., Gottardi, C.J. & Yap, A.S., 2008. Cadherins and cancer : how does cadherin dysfunction promote tumor progression ? *Oncogene*, 27(1), pp.6920–6929.

Johnston, L.A. et al., 1999. Drosophila myc Regulates Cellular Growth during Development. *Cell*, 98(6), pp.779–790.

Kajita, M. et al., 2010. Interaction with surrounding normal epithelial cells influences signalling pathways and behaviour of Src-transformed cells. *Journal of Cell Science*, 123(2), pp.171–180.

Kane, C.D. & Greenhalgh, D.G., 2000. Expression and localization of p53 and bcl-2 in healing wounds in diabetic and nondiabetic mice. *Wound Repair and Regeneration*, 8(1), pp.45–58.

Karimian, A., Ahmadi, Y. & Yousefi, B., 2016. Multiple functions of p21 in cell cycle, apoptosis and transcriptional regulation after DNA damage. *DNA Repair*, 42, pp.63–71.

Khalil, A. a & Friedl, P., 2010. Determinants of leader cells in collective cell migration. *Integrative biology : quantitative biosciences from nano to macro*, 2(11–12), pp.568–574.

Khromov, A. et al., 2009. Phosphorylation-dependent Autoinhibition of Myosin Light Chain Phosphatase Accounts for Ca $^{2+}$ Sensitization Force of Smooth Muscle Contraction. *Journal of Biological Chemistry*, 284(32), pp.21569–21579.

Kim, J.H. et al., 2011. High cleavage efficiency of a 2A peptide derived from porcine teschovirus-1 in human cell lines, zebrafish and mice. *PLoS ONE*, 6(4), pp.1–8.

Kim, Y.H. et al., 2017. Senescent tumor cells lead the collective invasion in thyroid cancer. *Nature Communications*, 8(May), pp.1–14.

Kolahgar, G. et al., 2015. Cell Competition Modifies Adult Stem Cell and Tissue Population Dynamics in a JAK-STAT-Dependent Manner. *Developmental Cell*, pp.1–13.

Kucinski, I. et al., 2017. Chronic activation of JNK JAK/STAT and oxidative stress signalling causes the loser cell status. *Nature Communications*, 8(1).

Kumar, M. et al., 2001. Systematic determination of the packaging limit of lentiviral vectors. *Human gene therapy*, 12(15), pp.1893–1905.

Kuo, L.J. & Yang, L.-X., 2008. Gamma-H2AX - a novel biomarker for DNA double-strand breaks. *In vivo (Athens, Greece)*, 22(3), pp.305–9.

de la Cova, C. et al., 2004. Drosophila Myc Regulates Organ Size by Inducing Cell Competition. *Cell*, 117(1), pp.107–116.

de la Cova, C. et al., 2014. Supercompetitor status of drosophila Myc cells requires p53 as a Fitness sensor to reprogram metabolism and promote viability. *Cell Metabolism*, 19(3), pp.470–483.

Labernadie, A. et al., 2017. A mechanically active heterotypic E-cadherin / N-cadherin adhesion enables fibroblasts to drive cancer cell invasion. , 19(November 2016).

Lämmermann, T. & Sixt, M., 2009. Mechanical modes of “amoeboid” cell migration. *Current Opinion in Cell Biology*, 21(5), pp.636–644.

Lamouille, S., Xu, J. & Derynck, R., 2014. Molecular mechanisms of epithelial–mesenchymal transition. *Nature Reviews Molecular Cell Biology*, 15(3), pp.178–196.

Lampson, M.A. et al., 2000. Demonstration of insulin-responsive trafficking of GLUT4 and vpTR in fibroblasts. *Journal of Cell Science*, 113(22), pp.4065–4076.

Leckband, D.E. & de Rooij, J., 2014. Cadherin Adhesion and Mechanotransduction. *Annual Review of Cell and Developmental Biology*, 30(1), pp.291–315.

Leong, W.F., Chau, J.F.L. & Li, B., 2009. p53 Deficiency Leads to Compensatory Up-Regulation of p16INK4a. *Molecular Cancer Research*, 7(3), p.354 LP-360.

Levayer, R., Dupont, C. & Moreno, E., 2016. Tissue Crowding Induces Caspase-Dependent Competition for Space. *Current Biology*, 26(5), pp.670–677.

Levayer, R., Hauert, B. & Moreno, E., 2015. Cell mixing induced by myc is required for competitive tissue invasion and destruction. *Nature*, 524(7566), pp.476–480.

Li, J., Poi, M.J. & Tsai, M.-D., 2012. The Regulatory Mechanisms of Tumor Supressor p16INK4 and Relevance to Cancer. , 50(25), pp.5566–5582.

Li, L. et al., 2013. Collective cell migration: Implications for wound healing and cancer invasion. *Burns & Trauma*, 1(1), p.21.

Li, W. & Baker, N.E., 2007. Engulfment Is Required for Cell Competition. *Cell*, 129(6), pp.1215–1225.

Lohia, M., Qin, Y. & Macara, I.G., 2012. The Scribble polarity protein stabilizes E-cadherin/p120-catenin binding and blocks retrieval of E-cadherin to the Golgi. C. Gottardi, ed. *PloS one*, 7(11), p.e51130.

Lujambio, A., 2016. To clear, or not to clear (senescent cells)? That is the question. *BioEssays*, 38, pp.S56–S64.

Marinari, E. et al., 2012. Live-cell delamination counterbalances epithelial growth to limit tissue overcrowding. *Nature*, 484(7395), pp.542–5.

Mark, S. et al., 2010. Physical model of the dynamic instability in an expanding cell culture. *Biophysical Journal*, 98(3), pp.361–370.

Marusyk, A. et al., 2010. Irradiation selects for p53-deficient hematopoietic progenitors. *PLoS Biology*, 8(3).

Matsubayashi, Y. et al., 2004. ERK Activation Propagates in Epithelial Cell Sheets and Regulates Their Migration during Wound Healing. *Current Biology*, 14(8), pp.731–735.

Mayor, R. & Etienne-Manneville, S., 2016. The front and rear of collective cell migration. *Nature Reviews Molecular Cell Biology*, 17(2).

Merino, M.M. et al., 2015. Elimination of Unfit Cells Maintains Tissue Health and Prolongs Lifespan. *Cell*, (160), pp.1–16.

Meyer, S.N. et al., 2014. An ancient defense system eliminates unfit cells from developing tissues during cell competition. *Science*.

Miaczynska, M., Pelkmans, L. & Zerial, M., 2004. Not just a sink: Endosomes in control of signal transduction. *Current Opinion in Cell Biology*, 16(4), pp.400–406.

Mirzayans, R. et al., 2012. New insights into p53 signaling and cancer cell response to DNA damage: Implications for cancer therapy. *Journal of Biomedicine and Biotechnology*, 2012.

Morata, G. & Ripoll, P., 1975. Minutes: Mutants of Drosophila autonomously affecting cell division rate. *Developmental Biology*, 42(2), pp.211–221.

Moreno, E. & Basler, K., 2004. dMyc Transforms Cells into Super-Competitors. *Cell*, 117(1), pp.117–129.

Moreno, E., Basler, K. & Morata, G., 2002. Cells compete for decapentaplegic survival factor to prevent apoptosis in Drosophila wing development. *Nature*, 416(6882), pp.755–759.

Muñoz-Espín, D. & Serrano, M., 2014. Cellular senescence: from physiology to pathology. *Nature Reviews Molecular Cell Biology*, 15(7), pp.482–496.

Nakagawa, S. & Huibregtse, J.M., 2000. Human Scribble (Vartul) Is Targeted for Ubiquitin-Mediated Degradation by the High-Risk Papillomavirus E6 Proteins and the E6AP Ubiquitin-Protein Ligase. *Molecular and Cellular Biology*, 20(21), pp.8244–8253.

Navarro, C. et al., 2005. Junctional recruitment of mammalian Scribble relies on E-cadherin engagement. *Oncogene*, 24(27), pp.4330–4339.

Neto-Silva, R.M., de Beco, S. & Johnston, L.A., 2010. Evidence for a growth stabilizing regulatory feedback mechanism between Myc and Yorkie, the Drosophila homolog of Yap. *Developmental Cell*, 19(4), pp.507–520.

Nieman, M.T. et al., 1999. N-cadherin promotes motility in human breast cancer cells regardless of their E-cadherin expression. *The Journal of cell biology*, 147(3), pp.631–44.

Nikolic, D.L. et al., 2006. Role of boundary conditions in an experimental model of epithelial wound healing. *Am J Physiol Cell Physiol*, 08544, pp.68–75.

Norman, M. et al., 2012. Loss of Scribble causes cell competition in mammalian cells. *Journal of Cell Science*, 125(1), pp.59–66.

Oertel, M. et al., 2006. Cell competition leads to a high level of normal liver reconstitution by transplanted fetal liver stem/progenitor cells. *Gastroenterology*, 130(2), p.507–20; quiz 590.

Ohoka, a. et al., 2015. EPLIN is a crucial regulator for extrusion of RasV12-transformed cells. *Journal of Cell Science*, 128(4), pp.781–789.

Ohsawa, S. et al., 2011. Elimination of oncogenic neighbors by JNK-mediated engulfment in Drosophila. *Developmental cell*, 20(3), pp.315–28.

de Oliveira Gonzalez, A.C. et al., 2016. Wound healing - A literature review. *Anais Brasileiros de Dermatologia*, 91(5), pp.614–620.

Omelchenko, T. et al., 2003. Rho-dependent formation of epithelial "leader" cells during wound healing. *Proceedings of the National Academy of Sciences of the United States of America*, 100(19), pp.10788–10793.

Ossovskaya, V.S. et al., 1996. Use of genetic suppressor elements to dissect distinct biological effects of separate p53 domains. *Proceedings of the National Academy of Sciences*, 93(19), p.10309.

Paek, A.L. et al., 2016. Cell-to-Cell Variation in p53 Dynamics Leads to Fractional Killing. *Cell*, 165(3), pp.631–642.

Pagliarini, R. a & Xu, T., 2003. A genetic screen in Drosophila for metastatic behavior. *Science (New York, N.Y.)*, 302(5648), pp.1227–31.

Pearson, H.B. et al., 2011. SCRIB expression is deregulated in human prostate cancer , and its deficiency in mice promotes prostate neoplasia. *The Journal of Clinical Investigation*, 121(11), pp.4257–4267.

Petitjean, L. et al., 2010. Velocity fields in a collectively migrating epithelium. *Biophysical Journal*, 98(9), pp.1790–1800.

Plutoni, C., Bazellières, E. & Gauthier-Rouvière, C., 2016. P-cadherin-mediated Rho GTPase regulation during collective cell migration. *Small GTPases*, 7(3), pp.156–163.

Portela, M. et al., 2010. Drosophila SPARC is a self-protective signal expressed by loser cells during cell competition. *Developmental Cell*, 19(4), pp.562–573.

Poujade, M. et al., 2007. Collective migration of an epithelial monolayer in response to a model wound. *Proceedings of the National Academy of Sciences of the United States of America*, 104(41), pp.15988–93.

Powell, E., Piwnica-Worms, D. & Piwnica-Worms, H., 2014. Contribution of p53 to metastasis. *Cancer Discov*, 4(4), pp.405–414.

Prober, D.A. & Edgar, B.A., 2000. Ras1 promotes cellular growth in the Drosophila wing. *Cell*, 100(4), pp.435–446.

Qiao, Y.N. et al., 2014. Myosin phosphatase target subunit 1 (MYPT1) regulates the contraction and relaxation of vascular smooth muscle and maintains blood pressure. *Journal of Biological Chemistry*, 289(32), pp.22512–22523.

Qin, Y. et al., 2005. The mammalian Scribble polarity protein regulates epithelial cell adhesion and migration through E-cadherin. *The Journal of cell biology*, 171(6), pp.1061–71.

Ran, F. et al., 2013. Genome engineering using the CRISPR-Cas9 system. *Nature protocols*, 8(11), pp.2281–308.

Rausch, S. et al., 2013. Polarizing cytoskeletal tension to induce leader cell formation during collective cell migration. *Biointerphases*, 8(1), p.36.

Reffay, M. et al., 2014. Interplay of RhoA and mechanical forces in collective cell migration driven by leader cells. *Nat Cell Biol*, 16(3), pp.217–223.

Reffay, M. et al., 2011. Orientation and polarity in collectively migrating cell structures: Statics and dynamics. *Biophysical Journal*, 100(11), pp.2566–2575.

Rhiner, C. et al., 2010. Flower forms an extracellular code that reveals the fitness of a cell to its neighbors in Drosophila. *Developmental cell*, 18(6), pp.985–98.

Riahi, R. et al., 2015. Notch1-Dll4 signalling and mechanical force regulate leader cell formation during collective cell migration. *Nature communications*, 6, p.6556.

Ribeiro, A.S. et al., 2010. Extracellular cleavage and shedding of P-cadherin: A mechanism underlying the invasive behaviour of breast cancer cells. *Oncogene*, 29(3), pp.392–402.

Rodrigues, A.B. et al., 2012. Activated STAT regulates growth and induces competitive interactions independently of Myc, Yorkie, Wingless and ribosome biogenesis. *Development*, 139(21), pp.4051–4061.

Roger, L., Gadea, G. & Roux, P., 2006. Control of cell migration: a tumour suppressor function for p53? *Biology of the cell / under the auspices of the European Cell Biology Organization*, 98(3), pp.141–52.

Rosen, P. & Misfeldt, D.S., 1980. Cell density determines epithelial migration in culture. *Proceedings of the National Academy of Sciences*, 77(8), pp.4760–4763.

Saito, M. et al., 2012. Classical and desmosomal cadherins at a glance. *Journal of Cell Science*, 125(11), pp.2547–2552.

Sancho, M. et al., 2013. Competitive interactions eliminate unfit embryonic stem cells at the onset of differentiation. *Developmental Cell*, 26(1), pp.19–30.

Sander, J.D. & Joung, J.K., 2014. CRISPR-Cas systems for editing, regulating and targeting genomes. *Nature Biotechnology*, 32(4), pp.347–350.

Scarpa, E. et al., 2015. Cadherin Switch during EMT in Neural Crest Cells Leads to Contact Inhibition of Locomotion via Repolarization of Forces. *Developmental Cell*, 34(4), pp.421–434.

Schindelin, J. et al., 2012. Fiji: an open-source platform for biological-image analysis. *Nature methods*, 9(7), pp.676–82.

Senoo-Matsuda, N. & Johnston, L.A., 2007. Soluble factors mediate competitive and cooperative interactions between cells expressing different levels of Drosophila Myc. *Proceedings of the National Academy of Sciences of the United States of America*, 104(47), pp.18543–18548.

Shih, W. & Yamada, S., 2012. N-cadherin-mediated cell-cell adhesion promotes cell migration in a three-dimensional matrix. *Journal of Cell Science*, 125(15), pp.3661–3670.

Simpson, P. & Morata, G., 1981. Differential mitotic rates and patterns of growth in compartments in the Drosophila wing. *Developmental Biology*, 85(2), pp.299–308.

Su, W.H. et al., 2013. Polarity protein complex scribble/lgl/dlg and epithelial cell barriers. *Advances in Experimental Medicine and Biology*, 763, pp.149–170.

Suijkerbuijk, S.J.E. et al., 2016. Cell competition drives the growth of intestinal adenomas in Drosophila. *Current Biology*, 26(4), pp.428–438.

Sullivan, K.D. et al., 2017. Mechanisms of transcriptional regulation by p53. *Cell Death and Differentiation*, 25(1), pp.133–143.

Tamori, Y. et al., 2010. Involvement of Lgl and Mahjong/VprBP in cell competition. *PLoS biology*, 8(7), p.e1000422.

Tamori, Y. & Deng, W.-M., 2011. Cell competition and its implications for development and cancer. *Journal of genetics and genomics = Yi chuan xue bao*, 38(10), pp.483–95.

Tamori, Y. & Deng, W.M., 2013. Tissue Repair through Cell Competition and Compensatory Cellular Hypertrophy in Postmitotic Epithelia. *Developmental Cell*, 25(4), pp.350–363.

Taniuchi, K. et al., 2005. Overexpressed P-cadherin/CDH3 promotes motility of pancreatic cancer cells by interacting with p120ctn and activating Rho-family GTPases. *Cancer Research*, 65(8), pp.3092–3099.

Theveneau, E. et al., 2013. Chase-and-run between adjacent cell populations promotes directional collective migration. *Nature Cell Biology*, 15(7), pp.763–772.

Theveneau, E. & Linker, C., 2017. Leaders in collective migration: are front cells really endowed with a particular set of skills? *F1000Research*, 6(0), p.1899.

Theveneau, E. & Mayor, R., 2012. Cadherins in collective cell migration of mesenchymal cells. *Current Opinion in Cell Biology*, 24(5), pp.677–684.

Tian, X. et al., 2011. E-Cadherin/beta-catenin complex and the epithelial barrier. *Journal of Biomedicine and Biotechnology*, 2011.

Tomasz, M., 1995. Mitomycin C: small, fast and deadly (but very selective). *Chemistry and Biology*, 2(9), pp.575–579.

Tse, J.M. et al., 2012. Mechanical compression drives cancer cells toward invasive phenotype. *Proceedings of the National Academy of Sciences*, 109(3), pp.911–916.

Villa del Campo, C. et al., 2014. Cell competition promotes phenotypically silent cardiomyocyte replacement in the mammalian heart. *Cell Reports*, 8(6), pp.1741–1751.

Vincent, J.-P. et al., 2011. Steep differences in wingless signaling trigger Myc-independent competitive cell interactions. *Developmental cell*, 21(2), pp.366–74.

Vousden, K.H. & Lane, D.P., 2007. p53 in Health and Disease. *Nature Reviews Molecular Cell Biology*, 8(4), pp.275–283.

Wagstaff, L. et al., 2016. Mechanical cell competition kills cells via induction of lethal p53 levels. *Nature Communications*, 7, p.11373.

Wang, C. et al., 2013. APC loss-induced intestinal tumorigenesis in Drosophila: Roles of Ras in Wnt signaling activation and tumor progression. *Developmental Biology*, 378(2), pp.122–140.

Wang, W. et al., 2015. p53/PUMA expression in human pulmonary fibroblasts mediates cell activation and migration in silicosis. *Scientific Reports*, 5(March), pp.1–12.

Wang, Y., Huang, S. & VP, S., 1998. Cardiac muscle cell hypertrophy and apoptosis induced by distinct members of the p38 mitogen-activated protein kinase family. *J Biol Chem*, 273(4), pp.2161–2168.

Watanabe, H. et al., 2018. Mutant p53-Expressing Cells Undergo Necroptosis via Cell Competition with the Neighboring Normal Epithelial Cells. *Cell Reports*, 23(13), pp.3721–3729.

Westendorf, C. et al., 2010. Live cell flattening - traditional and novel approaches. *PMC Biophys*, 3(1), p.9.

Wu, J.C., Gregory, C.W. & DePhilip, R.M., 1993. P-cadherin and E-cadherin are co-expressed in MDCK cells. *Biochemical and Biophysical Communications*, 195(3), pp.1329–1335.

Wyman, J. et al., 2013. Multiplex Genome Engineering Using CRISPR/Cas Systems. *Science*, 339(February), pp.819–824.

Yamaguchi, N. et al., 2015. Leader cells regulate collective cell migration via Rac activation in the downstream signaling of integrin β1 and PI3K. *Scientific Reports*, 5, p.7656.

Yan, X. et al., 2015. N-cadherin, a novel prognostic biomarker, drives malignant progression of colorectal cancer. *Molecular medicine reports*, 12(2), pp.2999–3006.

Yao, Z. & Sherif, Z.A., 2016. The effect of epigenetic silencing and TP53 mutation on the expression of DLL4 in human cancer stem disorder. *Oncotarget*, 7(39).

Yap, A.S., Duszyc, K. & Viasnoff, V., 2017. Mechanosensing and Mechanotransduction at Cell–Cell Junctions. *Cold Spring Harbor Perspectives in Biology*, p.a028761.

Zelenka, P.S. & Arpitha, P., 2008. Coordinating cell proliferation and migration in the lens and cornea. *Seminars in Cell and Developmental Biology*, 19(2), pp.113–124.

Zerbino, D.R. et al., 2018. Ensembl 2018. *Nucleic Acids Research*, 46(D1), pp.D754–D761.

Zhan, L. et al., 2008. Deregulation of Scribble promotes mammary tumorigenesis and reveals a role for cell polarity in carcinoma. *Cell*, 135(5), pp.865–878.

Zhang, G. et al., 2017. p53 Pathway Is Involved in Cell Competition During Mouse Embryogenesis. *Proceedings of the National Academy of Sciences of the United States of America*, 114(3), pp.498–503.

Zhang, H.M. et al., 2005. Gamma Interferon-Inducible Protein 10 Induces HeLa Cell Apoptosis through a p53-Dependent Pathway Initiated by Suppression of Human Papillomavirus Type 18 E6 and E7 Expression. *Molecular and Cellular Biology* , 25(14), pp.6247–6258.

Ziosi, M. et al., 2010. dMyc functions downstream of Yorkie to promote the supercompetitive behavior of hippo pathway mutant cells. *PLoS genetics*, 6(9), p.e1001140.

Appendix 1: Publications

---

nature COMMUNICATIONS

ARTICLE

Received 26 Feb 2016 | Accepted 18 Mar 2016 | Published 25 Apr 2016

DOI: 10.1038/ncomms11373 OPEN

Mechanical cell competition kills cells via induction of lethal p53 levels

Laura Wagstaff[1], Maja Goschorska[1], Kasia Kozyrska[1], Guillaume Duclos[2], Iwo Kucinski[1], Anatole Chessel[3,†], Lea Hampton-O'Neil[1,†], Charles R. Bradshaw[1], George E. Allen[1], Emma L. Rawlins[1], Pascal Silberzan[2], Rafael E. Carazo Salas[3] & Eugenia Piddini[1]

Cell competition is a quality control mechanism that eliminates unfit cells. How cells compete is poorly understood, but it is generally accepted that molecular exchange between cells signals elimination of unfit cells. Here we report an orthogonal mechanism of cell competition, whereby cells compete through mechanical insults. We show that MDCK cells silenced for the polarity gene *scribble* (*scrib*^{KD}) are hypersensitive to compaction, that interaction with wild-type cells causes their compaction and that crowding is sufficient for *scrib*^{KD} cell elimination. Importantly, we show that elevation of the tumour suppressor p53 is necessary and sufficient for crowding hypersensitivity. Compaction, via activation of Rho-associated kinase (ROCK) and the stress kinase p38, leads to further p53 elevation, causing cell death. Thus, in addition to molecules, cells use mechanical means to compete. Given the involvement of p53, compaction hypersensitivity may be widespread among damaged cells and offers an additional route to eliminate unfit cells.

[1] The Wellcome Trust/Cancer Research UK Gurdon Institute and Zoology Department, University of Cambridge, Tennis Court Road, Cambridge CB2 1QN, UK. [2] Laboratoire PhysicoChimie Curie, Institut Curie, Paris Sciences et Lettres Research University – Sorbonne Universités, Université Pierre et Marie Curie – Centre National de la recherche Scientifique – Equipe labellisée Ligue Contre le Cancer, 75005 Paris, France. [3] Pharmacology Department, University of Cambridge, Tennis Court Road, Cambridge CB2 1PD, UK. † Present addresses: LOB, Ecole Polytechnique, CNRS, INSERM, Université Paris-Saclay, 91128 Palaiseau cedex, France (A.C.); Faculty of Medical and Veterinary Sciences, University of Bristol, Bristol BS8 1TD, UK (L.H.-O.). Correspondence and requests for materials should be addressed to E.P. (email: e.piddini@gurdon.cam.ac.uk).

Cell competition is a remarkable phenomenon, conserved from arthropods to mammals, that causes the elimination of relatively less fit cells from tissues, helping to maintain overall tissue health[1–10]. Despite important advances[11–16], the mechanisms that lead to the elimination of unfit cells are still little understood and it is unclear whether one or multiple pathways lead to cell killing[17–22].

It has recently been reported that Madin–Darby canine kidney (MDCK) epithelial cells silenced for the polarity gene *scribble* (*scrib*^{KD} cells) are eliminated in the presence of wild-type MDCK cells[23], while they are viable on their own[23]. However, the mechanisms by which *scrib*^{KD} cells are killed by wild-type cells are largely unknown. We therefore took advantage of this recent observation to investigate the mechanisms of cell competition.

Here we show that *scrib*^{KD} cells are out-competed by wild-type cells through mechanical insults rather than molecular exchange. We find that *scrib*^{KD} cells are hypersensitive to compaction and that this is due to elevation of baseline p53 levels, which is both necessary and sufficient to induce hypersensitivity to crowding and confer a mechanical loser status. We further show that on contact with wild-type cells, *scrib*^{KD} cells become compacted into a high-density arrangement and that compaction is not only required but also sufficient to eliminate *scrib*^{KD} cells. We also delineate the mechano-transduction cascade that leads to *scrib*^{KD} cell death. Specifically, we show that *scrib*^{KD} cells' compaction causes activation of the Rho-associated kinase (ROCK), which in turn activates p38 leading to further p53 elevation and cell death. Overall, this work demonstrates that mechanical forces can be responsible for the elimination of cells during cell competition and that p53 levels play a key role both in instructing the mechanical loser status and in the execution of mechanical cell competition.

Results

Compaction of *scrib*^{KD} cells induces mechanical competition. It has previously been shown that *scrib*^{KD} MDCK cells are eliminated when co-cultured with wild-type MDCK cells through cell death and delamination (see ref. 23 and Supplementary Fig. 1a and Supplementary Movie 1, left), while monocultures of *scrib*^{KD} cells are viable (see ref. 23 and Supplementary Fig. 1b and Supplementary Movie 1, right). To investigate the mechanisms of *scrib*^{KD}-mediated cell competition, we first asked whether it is mediated by soluble factors, as in other cases of *in vitro* cell competition[6,24]. Growth rate (doubling time) profiles showed that *scrib*^{KD} cells in pure cultures divide, albeit at a reduced rate, to reach a steadily maintained number (Supplementary Fig. 1d), whereas under competing conditions, their numbers collapse following initial growth (Fig. 1a). Interestingly, we found that the growth rate of *scrib*^{KD} cells is not affected by conditioned medium from competing cultures (Fig. 1b and Supplementary Fig. 1c). Similarly, in transwell systems that allow exchange of solutes but prevent cell contact, *scrib*^{KD} cells grown together with co-cultures of competing (wild-type/*scrib*^{KD}) cells grew comparably to *scrib*^{KD} cells grown with other *scrib*^{KD} cells (Fig. 1c and Supplementary Fig. 1c). This indicated that soluble factors are not sufficient to induce cell competition and that cell contact is required. We hypothesized that cell contact enables molecular interactions essential for cell competition, as observed by others[11,12]. However, to our surprise, we found that sustained contact with wild-type cells is not sufficient for elimination of *scrib*^{KD} cells (Fig. 1d, black arrow and Supplementary Movie 2) and that *scrib*^{KD} clones are efficiently eliminated only when fully surrounded by wild-type cells (Fig. 1d, white arrow and Supplementary Movie 2). This suggested that a type of exchange other than molecular signalling (which would be enabled by contact) may be needed, and prompted us to look for differences between *scrib*^{KD} clones that were surrounded and peripheral clones that were simply contacted.

One striking feature of surrounded clones, which is not shared by peripheral clones, is that they reach a dramatically higher cell density than confluent *scrib*^{KD} pure cultures (Fig. 1e–g and Supplementary Fig. 1e). *scrib*^{KD} cells acquire a flattened morphology upon gene silencing[23,25], which at confluence results in a much lower ($\sim$1/3) final density compared with wild-type cells (Fig. 1e–g). However, *scrib*^{KD} clones surrounded by wild-type cells do not flatten and reach a density that is $\sim$4.5-fold higher than that of pure *scrib*^{KD} cultures (Fig. 1e–g). Furthermore, competing *scrib*^{KD} cells are taller than when grown in single cultures (Fig. 1h–j). Together, this indicates that as a result of their interaction with wild-type cells, *scrib*^{KD} cells become more compacted than in their default state and this correlates with and precedes their elimination.

We next asked whether cell compaction plays a role in *scrib*^{KD} cell elimination, by assessing its effect on *scrib*^{KD} cells in complete absence of wild-type cells. To that end, we used micropatterns to form *scrib*^{KD} microcultures of a defined, homogenous density and size ($\varnothing = 800\,\mu$m, ref. 26). When plated at high density, control cells that had not undergone *scribble* silencing (without tetracycline, $-$TET) continued to grow until they reached a maximal density of 61 ± 4 cells per $10{,}000\,\mu m^2$, which they maintained homeostatically (Fig. 1k,l and Supplementary Movie 3, left), as previously shown[27,28]. Remarkably, *scrib*^{KD} cultures ($+$TET) instead saw their numbers and densities drop (Fig. 1m,n, dark green and Supplementary Movie 3, right), due to a combination of increased cell death and extrusion, the same two events that lead to the elimination of *scrib*^{KD} cells during cell competition (Supplementary Movie 1, left and ref. 23). Notably, *scrib*^{KD} cells seeded at a lower density maintained that initial density (Fig. 1n, light green) indicating that the drop in cell number observed at higher density is not a general response of *scrib*^{KD} cells to plating. This suggested that *scrib*^{KD} cells are hypersensitive to compaction. To test this directly, we seeded confluent monolayers of control ($-$TET) or *scrib*^{KD} ($+$TET) cells on stretched polydimethylsiloxane (PDMS) substrates, which we then released to induce cell compression[27]. Control cultures showed no increase in apoptosis upon compression (Fig. 1o–q). The *scrib*^{KD} cells, however, displayed a 3-fold increase in apoptosis over their uncompressed baseline cell death, which was already higher than control (Fig. 1p,q). Altogether, these experiments show that *scrib*^{KD} cells display hypersensitivity to cell density and cannot sustain levels of crowding normally reached by wild-type cells. They further indicate that compaction of *scrib*^{KD} cells into higher cell densities, like those imposed on them by wild-type cells during competition, is sufficient to induce cell death. This suggests that wild-type cells eliminate *scrib*^{KD} cells through crowding-induced compaction. We name this new mode of selective elimination of one cell population by another due to differential sensitivity to crowding 'mechanical cell competition', to contrast it with forms of cell competition that rely on molecular exchange.

Corralling promotes but is not needed for *scrib*^{KD} elimination. As shown in Fig. 1f,g, in subconfluent competing cultures, the density of *scrib*^{KD} cells surpasses that of surrounding wild-type cells. This indicates that their acquired density does not simply reflect the density of the mixed culture, but is the result of an active process. To understand how *scrib*^{KD} cells become compacted during competition, we plated cells at low density and observed what happens when wild-type and *scrib*^{KD} clones first come into contact. Strikingly, we saw that, on contact, both

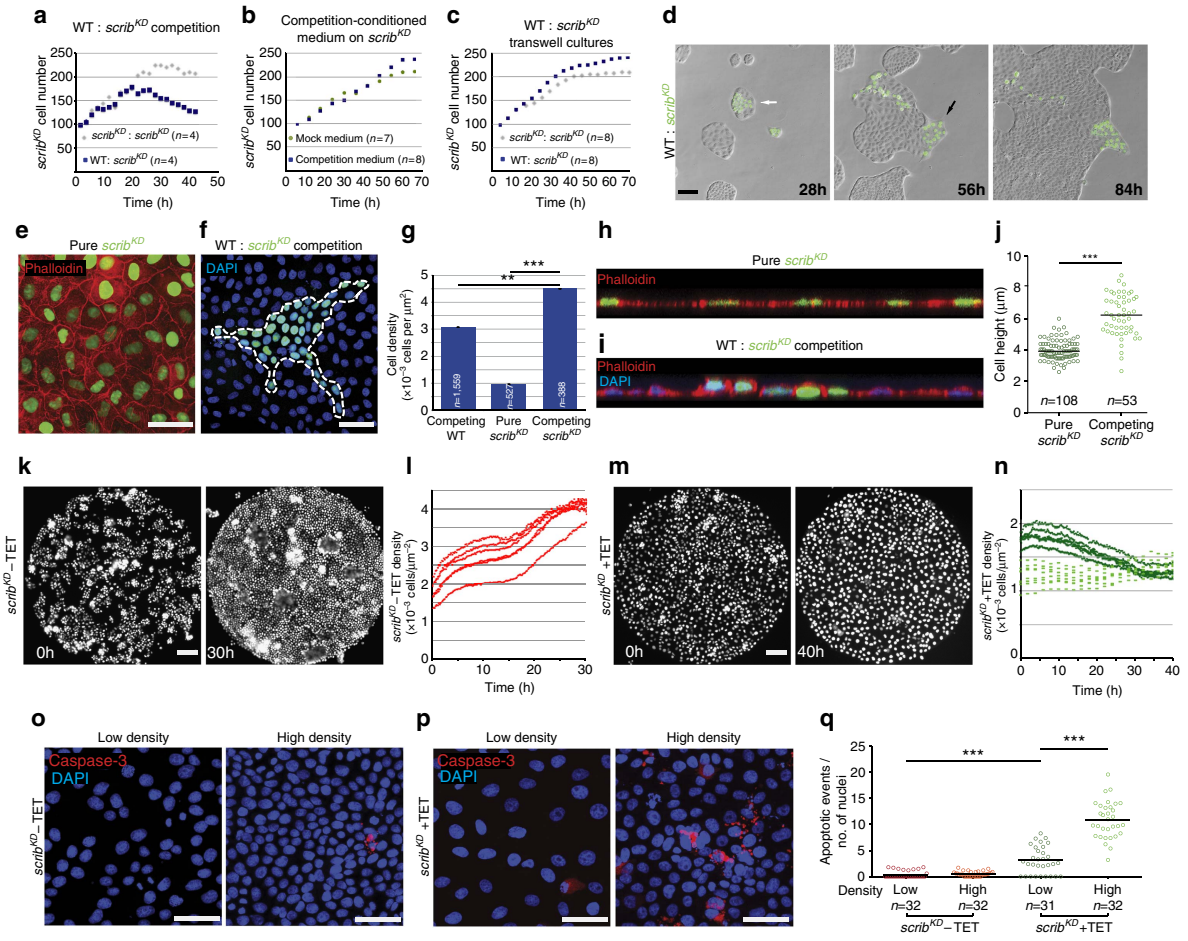

Figure 1 | Compaction of *scrib*^{KD} cells is both required and sufficient for their elimination. (**a**–**c**) Quantification showing growth rate of *scrib*^{KD} cells from time-lapse movies of: competition versus pure cultures (**a**), pure cultures in mock conditioned versus competition conditioned medium; two biological replicates (**b**) or transwell experiments, where *scrib*^{KD} cells were co-cultured across transwells with control or with competing cultures; three biological replicates (**c**). Each dot represents the average of *n* fields of cells. See also Supplementary Fig. 1c. (**d**) Time course of cell competition assay between unlabelled wild-type (WT) and GFP-labelled *scrib*^{KD} MDCK cells. Competition is observed in surrounded *scrib*^{KD} cells (white arrow), but not in cells that are only contacted (black arrow), see corresponding Supplementary Movie 2. (**e**) Confluent GFP-labelled *scrib*^{KD}cells stained with phalloidin. (**f**) Competing unlabelled WT and GFP-labelled *scrib*^{KD} cells counterstained with DAPI. (**g**) Quantification showing average (±s.e.m.) cell density values of confluent pure *scrib*^{KD} cells and subconfluent competing WT and *scrib*^{KD}cells as in **e** and **f**. (**h**,**i**) Confocal *xz* sections of representative GFP-labelled *scrib*^{KD}cells pure (**h**) or co-cultured with WT cells (**i**), stained with phalloidin (**h**,**i**) and DAPI (**i**). (**j**) Quantifications of cell height from images as in **h** and **i**. Black bars = median. (**k**,**m**) Representative stills from time lapse of GFP-labelled *scrib*^{KD} cells +/− TET growing on micropatterns (800 μm ∅), see corresponding Supplementary Movie 3. (**l**,**n**) Quantifications of cell density over time from movies as in **k** and **m**. Each dotted line corresponds to a different movie. (**o**,**p**) Cleaved Caspase-3 staining in WT (**o**) and *scrib*^{KD} (**p**) cells +/− compression (high density and low density, respectively). (**q**) Quantification of cell death events (cleaved Caspase-3) from images as in **o** and **p**. Data are pooled from three biological replicates. Black bars = mean; three biological replicates across two independent experiments. *n* = number of fields imaged in a single repeat (**a**–**c**,**q**) or *n* = number of cells (**g**,**j**). Scale bars, 100 μm (movie sequences) and 50 μm (immunofluorescence images) here and throughout all figures. $^{**}P<0.005$, $^{***}P<0.0005$ by KS test.

scrib^{KD} and wild-type cells engage in collective cell migration (Fig. 2a and Supplementary Movie 4). This behaviour was specific to wild-type/*scrib*^{KD} encounters, as it was not observed upon homotypic encounters of either cell population (Fig. 2b and Supplementary Movie 5). Interestingly, this migration was highly directional with *scrib*^{KD} cells always at the migrating front and, conversely, wild-type cells always at the back. We next characterized this migratory behaviour and assessed its contribution to cell compaction and elimination. First, we repeated the above experiment using a fluorescent nuclear label in each population to facilitate cell tracking (Fig. 2c). Kymograph analysis showed rapid activation of collective cell migration at the time of contact between wild-type and *scrib*^{KD} cells, with both populations moving synchronously (Fig. 2d, top and Fig. 2e). By

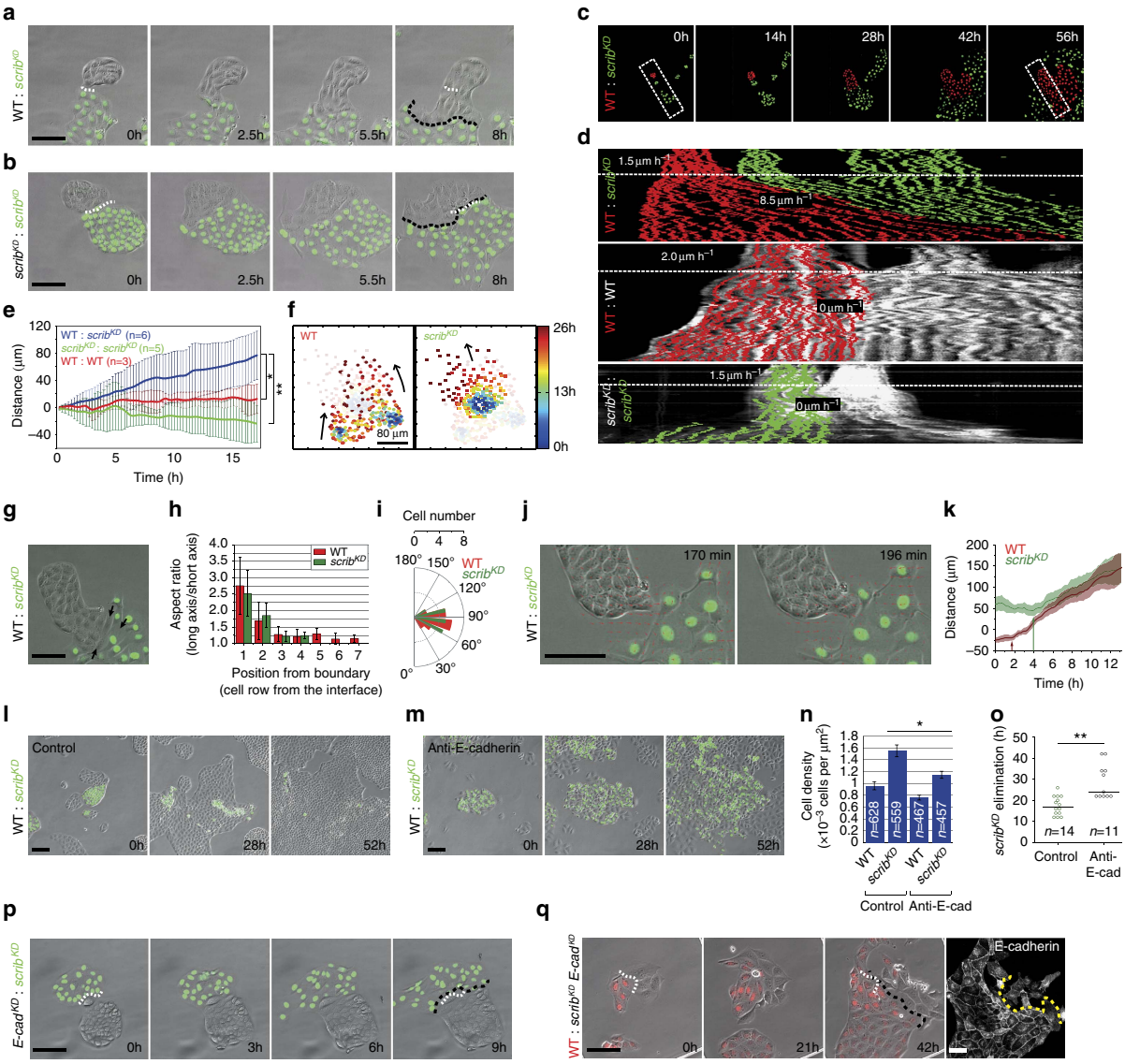

Figure 2 | Contact-induced migration promotes compaction and cell competition. (**a**,**b**) Stills from movies of wild-type (WT) and GFP-labelled *scrib*^{KD} co-cultures (**a**) or *scrib*^{KD} homotypic cultures (**b**), see Supplementary Movie 4,5. (**c**,**d**) Kymographs (**d**) from movies as in **c**. Velocities are shown before (above dashed white line) and after contact (below line). (**e**) Plot showing displacement of the line of contact between clones from movies as in **c**. The continuous line is the position of the front average ± s.d.; n = number of contact lines averaged. (**f**) Single-cell tracking of trajectories of WT and *scrib*^{KD} cells during competition. Heat-map representation shows time-resolved position of single cells. (**g**) Micrograph exemplifying cell shape change (arrows) after contact between WT and *scrib*^{KD} cells. (**h**) Bar plot representing aspect ratio of WT and *scrib*^{KD} cells as a function of distance from their contact point. n = 50 cells of each type from three movies; error bars = s.d. (**i**) Distribution of angles between a cell's long axis and its direction of motion; n (WT) = 18 cells; n (*scrib*^{KD}) = 17 cells. (**j**,**k**) PIV analysis of images at time of contact (see Supplementary Movie 6) (**j**); and quantification of cell displacements (**k**) shows WT cells begin migrating (arrows) before *scrib*^{KD} cells; n = 10 cells for each type from three independent movies. Coloured lines = mean; shaded areas = s.d. (**l**–**o**) Disrupting cell junctions by E-cadherin blocking antibody and calcium removal prevents contact-induced migration (**m**), compaction (**n**) and delays competition (**o**) compared with control (**l**), see Supplementary Movie 8; error bars = s.e.m. (**p**) E-cadherin knockdown in WT cells (*E-cad*^{KD}) prevents contact-induced migration. (**q**) E-cadherin knockdown in *scrib*^{KD} cells (*scrib*^{KD} *E-cad*^{KD}) prevents contact-induced migration, see Supplementary Movie 9. Right panel displays anti-E-cadherin immunofluorescence at end of movie (see Supplementary Fig. 2h,i). Five independent repeats; n = 10 events showing absence of directional migration, five were validated for E-cadherin levels and all five had WT levels. White dashed line = initial contact point; black dashed line = final contact point; yellow dashed line separates WT from *scrib*^{KD} *E-cad*^{KD} cells. *P < 0.05, **P < 0.005 by KS test.

contrast, similar kymographs of homotypic collisions did not show significant cell displacement (Fig. 2d, centre and bottom; and Fig. 2e). To further characterize the features of this collective cell migration, we carried out single-cell tracking of both cell populations before and after contact. The analysis of individual cell trajectories shows that single-cell movement is faster and more persistent for both wild-type and *scrib*^{KD} cells upon heterotypic collision (Fig. 2f and Supplementary Fig. 2a–d). We

then looked more closely at the dynamic interplay between wild-type and *scrib*^{KD} cells at the onset of migration. Interestingly, analysis of cell shape at the interface between the two populations revealed that both wild-type and *scrib*^{KD} cells become elongated at the site of contact (Fig. 2g,h), indicating that they are under anisotropic stress. Moreover, the cells in both populations move in the direction of their short axis (Fig. 2i), suggesting that they could be locally compressed. This could be the result of wild-type cells beginning migration and locally 'piling up' against the *scrib*^{KD} cells. In agreement with this, particle image velocimetry (PIV) and single-cell tracking revealed that wild-type cells begin migrating towards *scrib*^{KD} cells on average $\sim$2 h before the *scrib*^{KD} cells start migrating away (Fig. 2j,k and Supplementary Movie 6). Together, the chronology of these events and the local cellular deformations suggest that cells might engage in a behaviour similar to the 'chase and run' migration reported for other cell types[29]. These experiments do not distinguish whether *scrib*^{KD} cells are pushed by wild-type cells or, conversely, whether *scrib*^{KD} cells self-compact to avoid closer interaction wild-type cells. However, it is clear that as migration progresses, *scrib*^{KD} cells become corralled by wild-type cells and are compacted and eliminated (Supplementary Movie 7), indicating that this behaviour may facilitate compaction and outcompetition of *scrib*^{KD} cells.

To directly test the relevance of directional cell migration in the elimination of *scrib*^{KD} cells, we next sought to disrupt this behaviour. Adhesion molecules play an important role in collective cell migration[30] and have also been implicated in 'chase and run' among mesenchymal cells[29]. In addition, *scribble* downregulation has previously been shown to induce intracellular accumulation of E-cadherin[23,31] and we found that it causes an increase of both total and cell surface E-cadherin levels (Supplementary Fig. 2e–g). We therefore reasoned that targeting E-cadherin-mediated adhesion might disrupt directional migration between the wild-type and *scrib*^{KD} cells. We undertook two separate approaches and found that either blocking E-cadherin function in both populations, through a combination of low calcium and addition of a blocking antibody (Fig. 2l–o and Supplementary Movie 8), or silencing E-cadherin only in wild-type cells (*E-cad*^{KD} (ref. 32); Fig. 2p) was sufficient to inhibit directional migration. Interestingly, disruption of E-cadherin inhibited active cell compaction (Fig. 2l,m, Supplementary Movie 8 and quantification in Fig. 2n) and resulted in delayed elimination of *scrib*^{KD} cells (Fig. 2l,m, Supplementary Movie 8 and quantification in Fig. 2o). However, it did not rescue the *scrib*^{KD} cells from cell competition, since they were eventually eliminated as the culture became progressively more crowded due to proliferation (Fig. 2l,m and Supplementary Movie 8).

Having established that E-cadherin-mediated adhesion is involved in contact-induced migration between wild-type and *scrib*^{KD} cells, we next asked whether the upregulation of E-cadherin observed in *scrib*^{KD} cells (Supplementary Fig. 2e–g) plays a role in this directional cell movement. We therefore generated an inducible double *scrib*^{KD} *E-cadherin* knockdown cell line (*scrib*^{KD} *E-cad*^{KD}) and specifically selected clones that displayed partial silencing, enough to bring E-cadherin down to wild-type levels (Fig. 2q, right panel and Supplementary Fig. 2h,i). Indeed, partial downregulation of E-cadherin inhibited contact-induced migration, suggesting that high E-cadherin levels in the *scrib*^{KD} cells are required for this process (Fig. 2q and Supplementary Movie 9). As expected, these clones were still outcompeted by wild-type cells (Supplementary Fig. 2j). In contrast, we found that E-cadherin upregulation alone is not sufficient to cause contact-induced migration, as cells over-expressing E-cadherin at levels comparable to those of *scrib*^{KD} cells (Supplementary Fig. 2k) did not engage in directional cell migration with wild-type cells upon contact (Supplementary Fig. 2l). Altogether, we conclude that directional cell migration, by enabling corralling and active compaction of *scrib*^{KD} cells, promotes but is not required for mechanical cell competition, and that E-cadherin is necessary for corralling and active compaction but it does not impact on loser cell status.

p53 is activated in *scrib*^{KD} cells before cell competition. Key to the outcompetition of *scrib*^{KD} cells is their hypersensitivity to compaction (Fig. 1k–q). To identify genes and pathways involved in this behaviour, we carried out transcriptional profiling of *scrib*^{KD} cells (*scrib*^{KD} + TET) and compared it with the transcriptomes of control MDCK cells (*scrib*^{KD} − TET) and, importantly, of an isolate of *scrib*^{KD} cells that is resistant to cell competition (*scrib*^{RES}). Despite maintaining *scribble* gene knockdown (Supplementary Fig. 3a), the *scrib*^{RES} cells do not display elevated E-cadherin (Supplementary Fig. 3b), do not engage in contact-induced migration with wild-type cells (Supplementary Fig. 3c) and are not outcompeted in cell competition assays (Supplementary Fig. 3d and Supplementary Movie 10). Notwithstanding these fundamental differences, we observed that the *scrib*^{KD} transcriptome is still substantially closer to *scrib*^{RES} (with 523 differentially expressed genes) than to control (*scrib*^{KD} − TET) cells (with 1,645 differentially expressed genes; Fig. 3a, left and Supplementary Data 1 and 2). This allowed us to rule out all genes that are differentially expressed in *scrib*^{KD} versus wild-type cells but are similarly expressed between *scrib*^{KD} and *scrib*^{RES}, as these are clearly not sufficient to induce cell competition. Instead, we focused on the small intersection of 306 genes that are differentially expressed between wild-type and *scrib*^{KD} cells but are also different between *scrib*^{KD} and *scrib*^{RES} cells (Fig. 3a and Supplementary Data 3).

Gene Ontology term enrichment analysis highlighted p53 signalling as the top functionally enriched pathway (Fig. 3a, middle). A number of known p53 target genes were moderately upregulated in *scrib*^{KD} cells, suggesting p53 activation (Fig. 3a, right). Consistent with this, we found that p21 (a known p53 target[33] and the most highly upregulated p53 target in our gene list; Fig. 3a) is specifically upregulated upon *scribble* knockdown in *scrib*^{KD} cells (Fig. 3b, Supplementary Fig. 3e and Supplementary Fig. 4d,e) but not in *scrib*^{RES} cells (Fig. 3b) and that p53 levels are higher in *scrib*^{KD} cells than in wild-type cells (Fig. 3c,d and Supplementary Fig. 3f), confirming pathway activation. Thus, *scrib*^{KD} cells have high baseline p53 activity and this correlates with their loser status.

p53 is further elevated in *scrib*^{KD} cells by compaction. Next we asked whether cell competition affects p53 activity. Interestingly, we found that in competing conditions, p53 levels in *scrib*^{KD} cells increase above their already elevated baseline level, in a way that correlates with the degree of cell compaction (Fig. 3c–e; $r = 0.56$ by non-parametric Spearman correlation). This suggested that compaction increases p53 levels or, conversely, that higher p53 levels enable compaction. To distinguish between these two possibilities, we looked at how compression alone affects p53, using deformable PDMS substrates as before (Fig. 1o–q). Importantly, we found that compression alone causes an increase in p53 levels (Fig. 3f,g), as seen during competition. This indicates that cell competition induces further p53 activation in the *scrib*^{KD} cells via compaction-induced mechanical stress.

Given that p53 is upregulated during cell competition, we next sought to ask whether it contributes to this process. Therefore we mutated p53 in *scrib*^{KD} cells by CRISPR-mediated mutagenesis (*scrib*^{KD} *p53*$^{-/-}$ cells, Supplementary Fig. 4a,b). The *scrib*^{KD}

$p53^{-/-}$ cells failed to upregulate p21 following ultraviolet irradiation (Supplementary Fig. 4b) or *scribble* knockdown (Supplementary Fig. 4c–e), confirming functional p53 inactivation. Strikingly, we found that p53 inactivation in $scrib^{KD}$ $p53^{-/-}$ cells was sufficient to partially rescue their low homeostatic cell density (Fig. 3h) and their hypersensitivity to compaction (Fig. 3i). Remarkably, genetic (using $scrib^{KD}$ $p53^{-/-}$ cells) or chemical (using the inhibitor Pifithrin-α) inhibition of

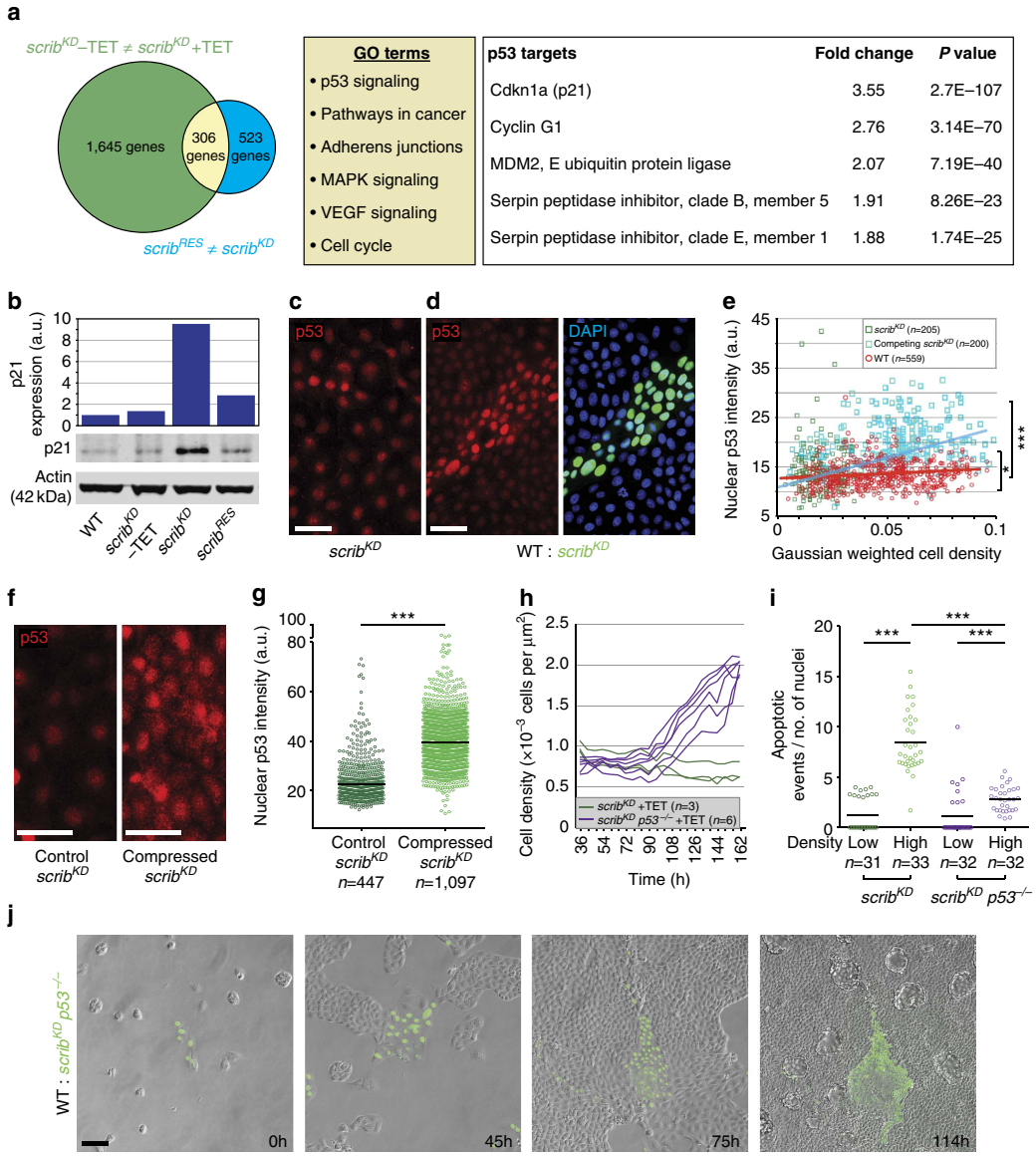

Figure 3 | p53 is activated in $scrib^{KD}$ cells before competition and further p53 elevation upon compaction causes competition-induced cell death. (**a**) Left, transcriptional profiling of $scrib^{KD}$ cells without tetracycline (TET) versus $scrib^{KD}$ cells with TET (green) and of $scrib^{KD}$ cells with TET versus $scrib^{KD}$ cells resistant to competition ($scrib^{RES}$) with TET (blue), and corresponding intersection of differentially expressed genes (yellow). Middle, list of pathways functionally enriched in the yellow intersection. Right, list of p53 targets found in this intersection and corresponding fold change difference between $scrib^{KD}$ cells $-/+$TET. Three biological replicates for $scrib^{KD}$ cells $-/+$TET and two biological replicates for $scrib^{RES}$ cells $+$TET. (**b**) Western blot against p21 with LICOR quantifications and normalization to Actin. (**c**,**d**) p53 staining of pure $scrib^{KD}$ cells (**c**) and of co-cultures of GFP-labelled $scrib^{KD}$ and wild-type (WT) cells (**d**). (**e**) Graph showing single-cell nuclear p53 intensity plotted against cell density from images as in **c** and **d**; $^{*}P<0.05$ by KS test comparing p53 levels in pure $scrib^{KD}$ versus WT; $^{***}P<0.0005$ by KS test comparing competing $scrib^{KD}$ versus WT. Non-parametric Spearman correlation; red line = WT cells; blue line = competing $scrib^{KD}$ cells. (**f**,**g**) p53 staining in pure $scrib^{KD}$ cells on PDMS substrate $+/-$ compression (**f**) and quantification showing single-cell nuclear p53 intensity (**g**) from images as in **f**; black bars = median. (**h**) Time-resolved density measurement of growing $scrib^{KD}$ cells and $scrib^{KD}$ $p53^{-/-}$ cells. (**i**) Quantification of cell death (cleaved Caspase-3) for $scrib^{KD}$ cells versus $scrib^{KD}$ $p53^{-/-}$ cells on PDMS substrate $+/-$ compression; black bars = mean; data from three biological replicates across two independent experiments. (**j**) Stills from time-lapse movies of WT and GFP-labelled $scrib^{KD}$ $p53^{-/-}$ co-cultures, see corresponding Supplementary Movie 11; n = cell number in **e** and **g** or n = number of imaged fields of cells in **h** and **i**. a.u. = arbitrary units, here and throughout all the figures. $^{*}P<0.05$, $^{***}P<0.0005$ by KS test.

p53 in *scrib*^{KD} cells was also sufficient to prevent their outcompetition (Fig. 3j and Supplementary Movie 11; Supplementary Fig. 4f). Furthermore, *scrib*^{KD} *p53*$^{-/-}$ cells maintained high E-cadherin levels (Supplementary Fig. 4g) and still displayed contact-induced migration (Supplementary Fig. 4h), demonstrating again that corralling is not sufficient for competition. Altogether, we conclude that high baseline p53 activity in *scrib*^{KD} cells is associated with their loser status and is required for them to acquire a low homeostatic cell density and hypersensitivity to compaction, two key features of the mechanical loser status.

Interestingly, though it has long been established that *scribble*$^{-/-}$ cells are eliminated by cell competition in *Drosophila*[34,35], when we tested whether this might happen via mechanical insults in wing imaginal discs we found that, unlike in MDCK cells, *scribble*$^{-/-}$ wing disc cells did not upregulate E-cadherin (Supplementary Fig. 5a,b) and their outcompetition was not rescued by p53 inhibition (Supplementary Fig. 5c). It is possible that *scribble*$^{-/-}$ cells are not eliminated by mechanical cell competition in *Drosophila* or that the function of Scribble or p53 may not be conserved in this process. Alternatively and perhaps more likely, mechanical cell competition may be redundant with other mechanisms of cell competition that have been described to target *scribble*$^{-/-}$ cells in that system[36,37].

ROCK activates p38 leading to p53 elevation and cell death. We next wondered how mechanical stress might lead to p53 activation. A potential candidate was p38 signalling, as it is required for *scrib*^{KD} cell competition[23], is known to promote p53 activity[38–40] and has also been involved in the response to mechanical stress[41]. Consistent with an involvement of p38, we found that compression alone causes an increase in active phosphorylated (T180/Y182) p38 (ref. 38; P-p38) in *scrib*^{KD} cells (Fig. 4a,b) and that chemical inhibition of this pathway partially rescues both the homeostatic density of *scrib*^{KD} cells (Fig. 4c) and their compaction hypersensitivity (Fig. 4d). Moreover, the upregulation of p53 in competing *scrib*^{KD}cells was reduced by p38 inhibition (Fig. 4e). We conclude that in *scrib*^{KD} cells, compression induces p53 via activation of p38.

We next asked how compression of *scrib*^{KD} cells causes p38 activation. We monitored cytoskeletal changes induced by compression and found that both cortical Actin (by phalloidin staining) and active phosphorylated-myosin (P-Myosin) are upregulated in compacted *scrib*^{KD} cells during competition (Fig. 4f,g). Since the cytoskeletal regulator ROCK[42] is one of the main kinases responsible for Myosin phosphorylation, this suggested that ROCK might be activated. Indeed P-Myosin upregulation was reduced in the presence of a ROCK inhibitor (Supplementary Fig. 6a,b) and the ROCK target phospho-MYPT1 (ref. 43; p-MYPT1) was also elevated in compacted *scrib*^{KD} cells (Fig. 4h), indicating that ROCK is activated in compacted *scrib*^{KD} cells. This was potentially relevant because ROCK has been shown to phosphorylate p38 (ref. 44). Thus, to ask whether ROCK is upstream of p38 activation, we compressed pure cultures of *scrib*^{KD} cells in the presence or absence of a ROCK inhibitor and looked at P-p38 levels. ROCK inhibition led to a partial reduction of P-p38 levels, thus placing ROCK upstream of p38 signalling (Fig. 4i,j). In addition, ROCK inhibition was sufficient to partially rescue the homeostatic density of *scrib*^{KD} cells (Fig. 4k) and compression-induced cell death (Fig. 4l). Importantly, inhibition of ROCK was also sufficient to prevent the out-competition of *scrib*^{KD} cells, with no appreciable cell death observed even though cells were compacted far beyond standard competition densities (Fig. 4m and Supplementary Movie 12). Altogether, these experiments indicate that mechanical cell competition is caused by compaction-induced ROCK activation, which activates p38, leading to p53 elevation and cell death. Interestingly, ROCK has also been implicated in apical extrusion of dying or crowded MDCK cells[45,46]. However, in the case of Scribble competition, ROCK has a different function, as it is involved in p53 activation and cell death. In addition, while in that context ROCK was activated by S1P2 and Piezo signalling[45,46], inhibition of these pathways had no effect on Scribble cell competition (Supplementary Fig. 7a,b), suggesting a distinct upstream activation mechanism.

p53 activation turns wild-type cells into mechanical losers. Finally, we decided to address how *scribble* knockdown earmarks cells as losers. Our data indicated that a loser cell status is not an obligate outcome of *scribble* silencing, as we could isolate *scrib*^{KD} cells that are competition resistant (*scrib*^{RES} cells; Supplementary Fig. 3d). Instead, our data showed that p53 is necessary for competition and that mild p53 elevation is required for *scrib*^{KD} cells to acquire key features of the mechanical loser status (Fig. 3h,i). This prompted us to investigate whether p53 might actually be sufficient to induce the mechanical loser status and cell competition. Nutlin-3, a chemical inhibitor of the E3 ubiquitin ligase MDM2 (Mouse Double Minute 2 (ref. 47)), activates p53 in a dose-dependent manner. This allowed us to establish conditions to induce mild p53 activation in wild-type MDCK cells. Strikingly, low-level p53 activation was sufficient to induce cell flattening (Fig. 5a) and to lower the homeostatic density of wild-type cells (Fig. 5b). Remarkably, Nutlin-3 treatment was also sufficient to induce compaction hypersensitivity (Fig. 5c). Thus, mild p53 activation is sufficient to induce in wild-type cells all the features that we observed in *scrib*^{KD} cells that are hallmarks of their mechanical loser status. Therefore, we next asked whether differential p53 levels are sufficient to induce mechanical cell competition. To test this, we generated a p53 knockout cell line (*p53*$^{-/-}$), which we then co-cultured with wild-type cells. Not surprisingly, simply mixing wild-type and *p53*$^{-/-}$ cells was not sufficient to induce competition (Supplementary Fig. 8a). Strikingly however, mild p53 activation in wild-type cells, by Nutlin-3 addition at sublethal doses, caused the elimination of these cells specifically in the co-culture, but not when they were cultured alone (Fig. 5d, Supplementary Fig. 8b and Supplementary Movie 13). Importantly, p53-induced cell competition was indistinguishable from *scribble* cell competition, as it resulted in loser cell compaction (Fig. 5e) and only caused elimination when cells were compacted by *p53*$^{-/-}$ cells (Fig. 5d). Overall, these results demonstrate that mild elevation of p53 is sufficient to phenocopy Scribble cell competition and induce both hypersensitivity to cell crowding and the mechanical loser status in otherwise wild-type cells.

To demonstrate the existence of p53-mediated mechanical cell competition beyond the MDCK experimental paradigm, we turned to primary cultures of epithelial cells, specifically to mouse tracheal epithelial cells (MTECs), and looked for evidence of this process. Under normal conditions, confluent MTEC monolayers show little proliferation or change in cell density (Fig. 5f,g, compare first and second time points, and Supplementary Movie 14, left, before Nutlin-3 addition). Interestingly however, when we induced mild elevation of p53 (by Nutlin-3 treatment) in these cultures, we found that this results in a 26% average reduction in cell density, accompanied by cell extrusion, suggesting acquired hypersensitivity to crowding (Fig. 5f,g, compare before and after Nutlin-3 addition, and Supplementary Movie 14, left, after Nutlin-3 addition). To test whether differential levels of p53 could induce cell competition in MTECs, we mixed Tomato-labelled wild-type MTECs (MTEC Tomato; from *Rosa*26R-nTomato-nGFP mice[48]) either with unlabelled wild-type MTECs or with unlabelled p53 null MTECs (MTEC *p53*$^{-/-}$;

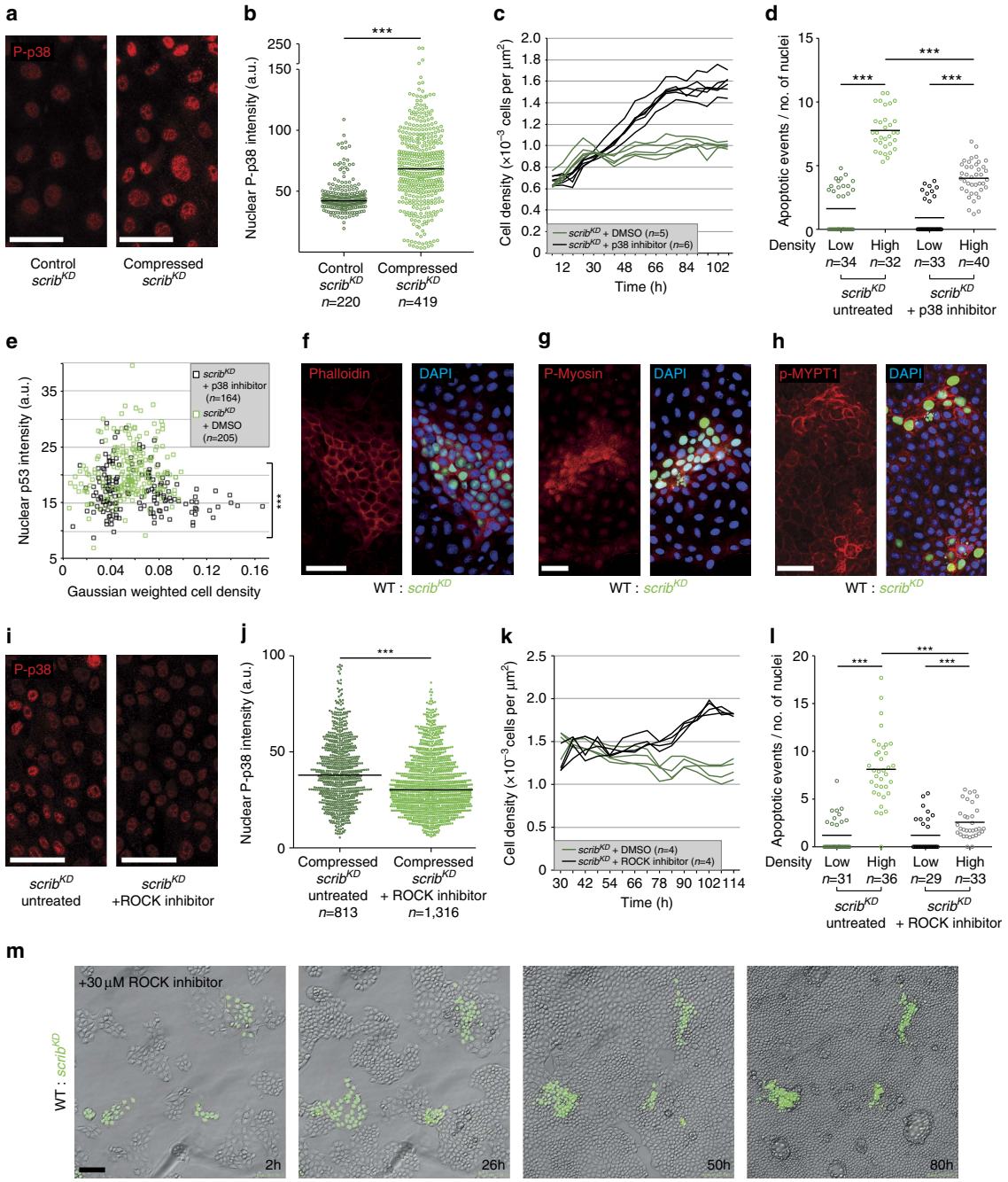

Figure 4 | During mechanical cell competition ROCK activates p38 leading to p53 elevation. (**a**) Phosphorylated p38 (P-p38) staining in pure *scrib*^{KD} cells +/− compression. (**b**) Single-cell nuclear P-p38 intensity from images as in **a**; black bars = median. (**c**) Time-resolved density measurement of growing *scrib*^{KD} cells +/− p38 inhibitor. (**d**) Quantification of cell death (cleaved Caspase-3) of *scrib*^{KD} cells with or without compression and +/− p38 inhibitor; black bars = mean; pooled data from three biological replicates across two independent experiments. (**e**) Single-cell nuclear p53 signal intensity in competing *scrib*^{KD} cells +/− p38 inhibitor, plotted against cell density. (**f**-**h**) F-Actin (phalloidin-stained, **f**), phosphorylated Myosin-II (P-Myosin, **g**) and phosphorylated MYPT1 (p-MYPT1, **h**) are elevated in compacted GFP-labelled *scrib*^{KD} cells compared with wild-type (WT) cells during competition. (**i**) P-p38 staining in compressed *scrib*^{KD} cells +/− ROCK inhibitor. (**j**) Single-cell nuclear P-p38 intensity from images as in **i**; black bars = median. (**k**) Time-resolved density measurement of growing *scrib*^{KD} cells +/− ROCK inhibitor; two independent repeats. (**l**) Quantification of cell death (cleaved Caspase-3) in *scrib*^{KD} cells with or without compression and +/− ROCK inhibitor; black bars = mean; pooled data from three biological replicates across two independent experiments. (**m**) Stills from time-lapse movies of WT and GFP-labelled *scrib*^{KD} co-cultures treated with ROCK inhibitor (30 μM), see corresponding Supplementary Movie 12; *n* = cell number in **b**,**e** and **j** or *n* = number of imaged fields of cells in **c**,**d**,**k** and **l**. ***$P<0.0005$ by KS test.

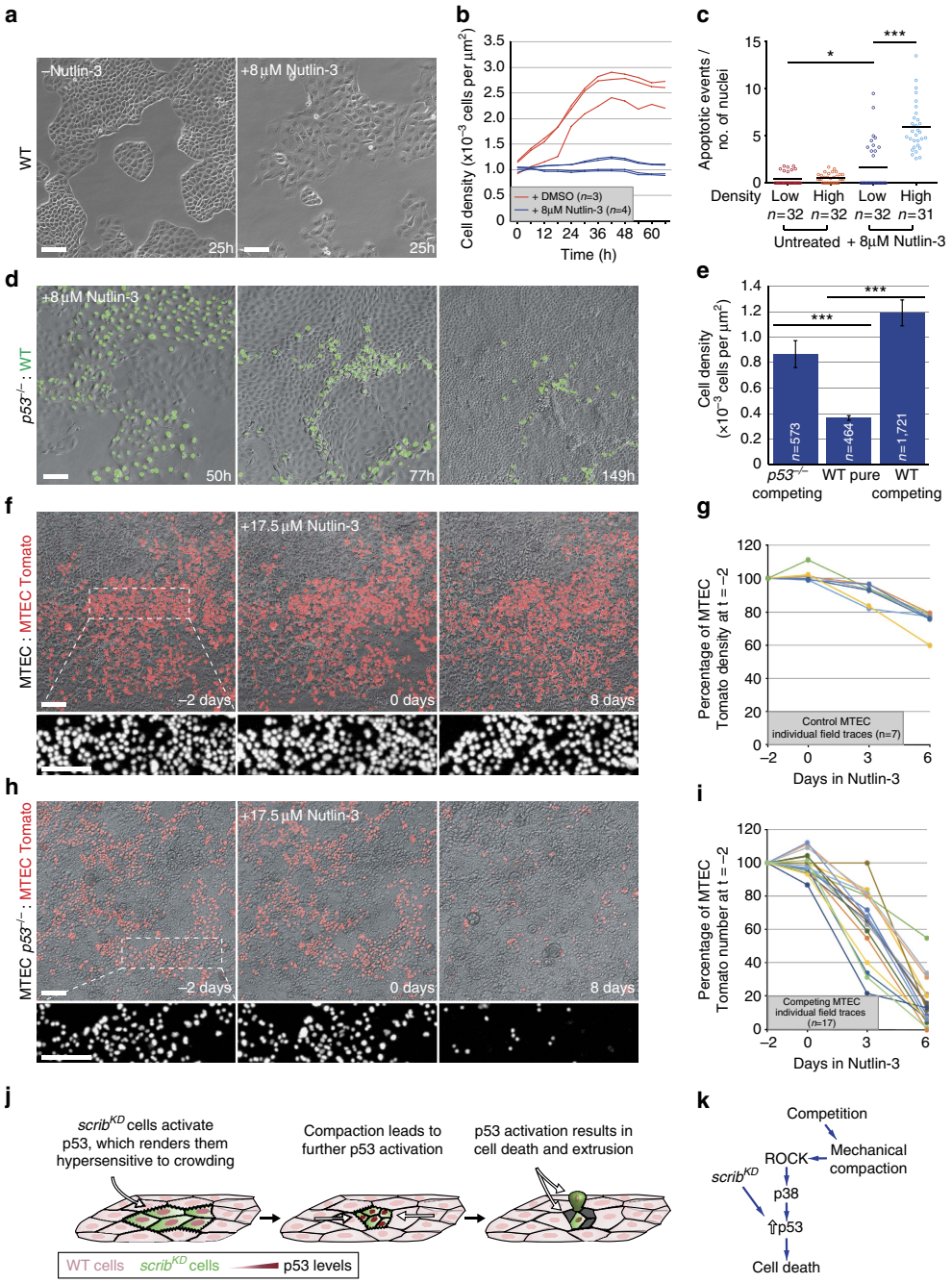

Figure 5 | p53 activation is sufficient to induce crowding hypersensitivity and mechanical cell competition. (**a**) Addition of Nutlin-3 (8 μM) causes flattening of wild-type (WT) MDCK cells; $n = 4$ fields per repeat. (**b**) Time-resolved cell density measurement of growing WT MDCK cells +/− Nutlin-3 (8 μM). (**c**) Quantification of cell death (cleaved Caspase-3) of WT MDCK cells with and without compression and +/− Nutlin-3 (8 μM); black bars = mean; three biological replicates from two independent experiments. (**d**) Stills from time-lapse movies of WT and $p53^{-/-}$ MDCK co-cultures with Nutlin-3 (8 μM) see corresponding Supplementary Movie 13. (**e**) Cell density measurement from movies as in **d**; mean ± s.e.m. (**f**) Stills from time-lapse movies of primary cultures of unlabelled and Tomato-labelled WT MTECs (see corresponding Supplementary Movie 14). Nutlin-3 (17.5 μM) was added at $t = 0$. (**g**) Time-resolved cell density measurement from movies as in **f** of WT MTECs before and after Nutlin-3 (17.5 μM) addition. (**h**) Stills from time-lapse movies of primary cultures of unlabelled $p53^{-/-}$ and Tomato-labelled WT MTECs (see corresponding Supplementary Movie 15). Nutlin-3 (17.5 μM) was added at $t = 0$. (**i**) Time-resolved measurement of cell number from movies as in **h** of WT MTECs before and after Nutlin-3 (17.5 μM) addition. (**j**,**k**) Model of mechanical cell competition of $scrib^{KD}$ cells; n = cell number in **e** or n = number of imaged fields of cells in **b**,**c**,**g** and **i**. For **c** and **e**, data are pooled from three biological replicates. $^{*}P < 0.05$, $^{***}P < 0.0005$ by KS test.

from p53 null mice). Before Nutlin-3 addition, the proportion of wild-type (Tomato) MTECs in the monolayer did not change for several days when co-cultured with either $p53^{-/-}$ cells or more wild-type cells (Fig. 5f–i, first two time points, and Supplementary Movie 14, before Nutlin-3 addition). However and strikingly, Nutlin-3 addition induced robust cell competition specifically in wild-type/$p53^{-/-}$ MTEC co-cultures, causing the number of wild-type cells to plummet within 6 days to ~17% of their starting number, with pronounced cell death and fragmentation (Fig. 5h,i and Supplementary Movie 14, right). Thus, mild p53 elevation is sufficient to induce crowding hypersensitivity and mechanical cell competition in MTEC cultures.

Discussion

In summary, our work demonstrates that in addition to molecular signals, cells use mechanical means to compete (see model in Fig. 5j,k), a concept that had previously only been speculated about and proposed on theoretical grounds[19,49]. We show that hypersensitivity to crowding provides an additional route to the loser cell status, leading to mechanical cell competition and the elimination of loser cells. One interesting prediction of our findings is that they suggest that competition could take place between genetically identical cells if they are endowed with differential sensitivity to mechanical stress or if they reside in tissues with varying mechanical properties[50,51], a hypothesis that should be investigated. In addition, given the involvement of p53, a general sensor of cell stress, we suggest that mechanical cell competition may be widespread among the damaged cells. Moreover, future work should also examine the implications of our findings on the behaviour of cancer cells. Since *p53* is one of the most commonly mutated genes in cancer[52], our findings suggest that its loss could enable neoplastic cells (*scribble* is a tumour-suppressor gene[53,54]) to evade mechanical cell competition. Identifying the physiological contexts where mechanical cell competition plays a role may help better understand tissue biology and potentially cancer formation.

Note added in proof: Evidence of mechanical competition in *Drosophila* was reported just prior to acceptance of this work[55].

Methods

Antibodies and materials. For immunofluorescence we used:

Rabbit anti-p53 antibody (1:750, Cell Signaling Technology #9382), rabbit anti-p21 antibody (1:200, Santa Cruz sc-397). In functional tests, both antibodies show an increase in staining intensity +ultraviolet-C treatment and a reduction or complete absence of staining in $scrib^{KD}$ $p53^{-/-}$ and $p53^{-/-}$ cells (Supplementary Fig. 4b). In addition, the anti-p21 antibody is documented to cross-react in canine. Mouse anti-E-cadherin antibody (1:600 total stain or 1:200 surface stain[56]), rabbit anti-E-cadherin antibody (1:500 total stain or 1:50 surface stain[57]), both documented to cross-react in canine. Rabbit anti-P-p38 MAPK (T180/Y182) antibody (1:50, Cell Signaling Technology #9215) was used as in Norman *et al.*[23] Rabbit anti-P-Myosin light chain (phospho S20) antibody (1:100, Abcam ab2480), predicted to cross-react with all mammals. Goat p-MYPT1 (Thr 853) (1:50, Santa Cruz sc-17432) antibody, documented to cross-react in canine. Rabbit anti-cleaved Caspase-3 antibody (1:200, Cell Signaling Technology #9661s), predicted to cross-react in canine based on 100% sequence homology. DAPI (1 μg ml^{-1} Invitrogen); Alexa Fluor conjugated secondary antibodies (1:1,000, Invitrogen); Alexa Fluor-568 and Alexa Fluor-647 conjugated phalloidin (1:40, Invitrogen).

For western blotting we used:

Rabbit anti-p53 antibody (1:1000, Cell Signaling Technology #9382), rabbit anti-p21 antibody (1:500, Santa Cruz sc-397). Goat anti-Scribble antibody (1:500, Santa Cruz sc-11048), functional tests show a decrease in signal intensity in $scrib^{KD}$ cells +TET and it is documented to cross-react in canine (Supplementary Fig. 3a). Mouse anti-E-cadherin antibody (1:1,000; (ref. 56)), rabbit anti-β-tubulin antibody (1:50,000, Abcam ab6046), HRP conjugated secondary antibodies (1:3,000, Bio-Rad) and IRDye infrared fluorescent dyes (1:10,000, LI-COR).

Inhibitors and treatments were used at the following concentrations: Pifithrin-α (Sigma) 10 μM, p38 inhibitor SB202190 (Calbiochem) 10 μM, ROCK inhibitor Y27632 (Sigma) 30 μM, Piezo inhibitor gadolinium III chloride (Sigma) 100 μM, S1P2 inhibitor JTE013 (Tocris Bioscience) 10 μM, tetracycline (Sigma) 5 μg ml^{-1} (except for pre-treating $scrib^{KD}$ cells for RNA-seq analysis where it was used at 10 μg ml^{-1}), doxycycline (Sigma) 1 μg ml^{-1}, Nutlin-3 (Cayman Chemicals) was added as specified.

Cell culture and plasmids. The cell lines used in this publication are not listed in the database of misidentified cell lines maintained by ICLAC. MDCK cell lines were authenticated in our laboratory by RNA sequencing, which confirmed their canine origin. All cell lines used in this publication have been tested in our laboratory and were found to be negative for mycoplasma infection (EZ PCR Mycoplasma Test Kit, Geneflow).

Wild-type MDCK, MDCK-pTR *E-cadherin* shRNA ($Ecad^{KD}$)[32] and MDCK-pTR *scribble* shRNA ($scrib^{KD}$) cells[23] were a kind gift from Yasuyuki Fujita. Wild-type and $E\text{-}cad^{KD}$ MCDK cells were cultured in DMEM (21885; Invitrogen) supplemented with 10% fetal bovine serum (FBS, Invitrogen) in a humidified incubator at 37 °C with 5% CO_2. The $scrib^{KD}$ cells were cultured as described for wild-type cells with the addition of blasticidin 50 μg ml^{-1} (Sigma) and G418 800 μg ml^{-1} (Invitrogen) to the culture media. To establish MDCK cell lines that stably express a nuclear green fluorescent protein (GFP) or red fluorescent protein (RFP) marker, we used a modified pGIPZ-turboGFP-Puro (Thermo Scientific) plasmid where we replaced turbo-GFP with either GFP-NLS or RFP-NLS. Selection following infection was carried out with puromycin (0.65 μg ml^{-1}, Sigma).

Resistant $scrib^{KD}$ MDCK cells ($scrib^{RES}$) were generated by culturing MDCK-pTR *scribble* shRNA cells in 5 μg ml^{-1} tetracycline for 20 days. The resulting final population was expanded in the absence of tetracycline and tested for efficient Scribble knockdown by western blotting.

The MDCK $p53^{-/-}$ and $scrib^{KD}$ $p53^{-/-}$ cells were generated using Cas9 D10A CRISPR technology. sgRNAs against canine TP53 were manually designed following published guidelines[58]

(p53_CRISPR#1_Fw: 5′-GCAGAAGTGGCTGGCATCCT-3′, p53_CRISPR#2_Fw: 5′-CCCTGGACCGGCCCCCTCC-3′).

sgRNAs were individually cloned into the PX461 vector[58] and the pair was co-transfected into recipient cells. Pools of both $p53^{-/-}$ and $scrib^{KD}$ $p53^{-/-}$ cells were generated by functional selection with Nutlin-3 (20–30 μM) for 5–7 days and either used immediately or expanded from single cells. p53 knockout was verified by functional tests.

To knock down E-cadherin expression in MDCK *scribble* shRNA cells ($scrib^{KD}$ $E\text{-}cad^{KD}$), the recipient cells were stably transfected with a modified version (pSUPERIOR.hygro + gfp *E-cadherin* shRNA) of a plasmid provided by Yasuyuki Fujita (pSUPERIOR.neo + gfp *E-cadherin* shRNA[32]). Selection was carried out with Hygromycin B (75 μg ml^{-1}, Invitrogen). To overexpress E-cadherin in wild-type MDCK cells, the E-cadherin-GFP cDNA[59] was introduced into a modified pTRIPZ-turboRFP-Puro plasmid (Thermo Scientific) in which turboRFP was replaced by RFP-NLS (pTRIPZ-RFP-NLS-Puro). The cells infected with the pTRIPZ ECAD-GFP-P2A-RFP-NLS construct express doxycycline-inducible E-cadherin-GFP and RFP-NLS as a single transcript. Selection following infection was carried out with puromycin (0.65 μg ml^{-1}, Sigma).

Primary mouse tracheal epithelial cells (MTECs) were obtained from 5-month-old animals from 26R-Tomato ($Gt(ROSA)26Sor^{tm1(CAG\text{-}tdTomato*,\text{-}EGFP*)Ees}$) and p53-null ($Trp53^{tm1Tyj}$) strains, both of C57BL/6 background, using a protocol adapted from published methods[60]. Tracheas were dissected from the larynx to the bronchial main branches and collected in ice-cold DMEM:F12 (11330-32; Invitrogen) supplemented with a solution of 100 units ml^{-1} penicillin and 100 μg ml^{-1} streptomycin (Invitrogen). The muscle, vascular tissue and glands were then removed and the trachea cut into three to four rings. Each fragment was washed in phosphate-buffered saline (PBS) and then incubated in Dispase (BD Biosciences) at 7.5 Caseinolytic Units in PBS (total volume 450 μl per trachea) for 25 min at room temperature (RT). Tracheal fragments were then transferred into ice-cold DMEM:F12 and the sheets of epithelial tissue were peeled off. The epithelial sheets and medium were transferred to an ice-cold 1.5 ml tube, and pelleted twice at 500 *g* for 3 min with a PBS wash in between. The pellets were resuspended in 0.05% TE (Invitrogen) supplemented with 5 mM EDTA for 30 min at 37 °C. Five hundred microlitres of DMEM:F12 supplemented with 5% FBS was added to stop the reaction. The cells were pelleted (500 *g*, 3 min), resuspended in MTEC/Plus media and plated on collagen-coated (50 μg ml^{-1} rat tail collagen I (BD Biosciences)/0.02 M acetic acid) 24-well tissue culture inserts (BD Falcon) in MTEC/Plus media at approximately 5×10^4 cells per insert. The MTEC cells were cultured in MTEC/Plus media consisting of: DMEM:F12 basal media supplemented with a solution of 100 units ml^{-1} penicillin and 100 μg ml^{-1} streptomycin, 10 μg ml^{-1} insulin (Invitrogen), 5.5 μg ml^{-1} transferrin (Invitrogen), 6.7 μg ml^{-1} selenium (Invitrogen), 0.1 μg ml^{-1} cholera toxin (Sigma), 25 ng ml^{-1} epidermal growth factor (R&D Systems), 30 μg ml^{-1} bovine pituitary extract (Invitrogen), 5% FBS, 15 mM HEPES and 0.01 μM freshly added retinoic acid (Sigma) in a humidified incubator at 37 °C with 5% CO_2.

Conditioned media and transwell assays. For competition-conditioned medium experiments, media were conditioned for 48 h by cultures of GFP-labelled $scrib^{KD}$ and wild-type cells with (competition condition) or without (mock condition) tetracycline. Recipient GFP-labelled $scrib^{KD}$ cells were pre-treated with tetracycline for 24 h and 10,000 cells per well were seeded into 24-well plates with 1 ml of conditioned medium. For transwell assays, GFP-labelled $scrib^{KD}$ cells (10,000 per well) were seeded at the bottom of a 24-well plate. Co-cultures at a ratio of 1:10 (GFP-labelled $scrib^{KD}$: wild-type or GFP-labelled $scrib^{KD}$: $scrib^{KD}$) were plated onto a transwell insert (3.0 μm pore size-polyester membrane, Corning) at 1,500 cells

per insert). All *scrib*^{KD} and GFP-labelled *scrib*^{KD} cells were pre-treated for 24 h with tetracycline before plating.

Fences system. Where applicable, immunofluorescence of cell competition was carried out in a 24-well plate using 'fences' (Aix Scientifics, http://www.aix-scientifics.co.uk/en/fences.html). The system allows two different populations of cells to be seeded on either side of a silicone barrier, thus allowing experimental and control conditions to be cultured, treated, imaged and (where applicable) stained within the same well/coverslip.

Cell competition and contact-induced migration assays. Cell competition assays on MDCK cells were carried out in 24-well plate fences. Control cultures were plated in the centre of the fence (1,000 cells per fence) at a ratio of 1:10 GFP-labelled *scrib*^{KD}: *scrib*^{KD}. Competition cultures were seeded on the outside of the barrier (8,000 cells per fence) at a ratio of 1:10, *scrib*^{KD}: wild-type cells. The fences were removed approximately 5 h after plating and the culture medium was replaced with or without addition of tetracycline. Twenty hours later, the culture medium was replaced with phenol red-free DMEM (+10% FBS and 1% L-glutamine, Invitrogen) with or without tetracycline. Where specified, the chemical inhibitors were also added at this point, except for the ROCK, Piezo and S1P2 inhibitors, which were added after an additional 24 h. Live imaging was started 2–4 h after the final media change and was continued for at least 50 h with regular media changes every 2–3 days.

For cell migration assays, the cells were seeded as for competition assays, except that they were plated at a lower density (1,000 cells in the centre of the fence, 2,000–5,000 cells in the outer chamber) and imaged more frequently (every 10 min to every 2 h). Alternatively, where specified, cells for competition or migration assays were plated on gridded tissue culture plates (μ-Dish 35 mm Grid-500, Ibidi) at 6,250 cells per plate. This allowed us to find specific clones of cells for immunofluorescence analysis after live imaging had finished. Co-cultures, unless otherwise specified, were plated at a ratio of 1:10 (*scrib*^{KD}: wild-type).

The MTEC cells were plated in collagen-coated tissue culture inserts and allowed to grow for approximately 2 weeks until they reached homeostatic density before commencing experiments. In control cultures, wild-type (unlabelled) cells were plated with wild-type *Rosa*26R-Tomato (nuclear red) cells (MTEC Tomato)[48] cells at a 2:1 ratio. In competition cultures, unlabelled p53-null cells (MTEC *p53*$^{-/-}$) and wild-type *Rosa*26R-Tomato cells (MTEC Tomato) were plated at a 2:1 ratio. Nutlin-3 was added at 17.5 μM on day 3 of live imaging. The medium was changed every 2 days.

Homeostatic cell density assays. These assays were carried out in 96-well plates. GFP-labelled *scrib*^{KD} and *scrib*^{KD} *p53*$^{-/-}$ cells (8,000–12,000 cells per plate) were pre-treated with tetracycline for 12 h before plating where applicable, in the presence or absence of inhibitors. Where applicable, Nutlin-3 was added 24 h after plating. The whole well was then imaged and the individual images were stitched together for further analysis to obtain data on total cell number and density. The plates were imaged every 6 h and cell culture medium and drug treatments were changed every 2 days.

Micropattern assays. For assays in micropatterns, GFP-labelled *scrib*^{KD} cells with or without tetracycline pre-treatment (72 h) were plated onto circular adhesive patterns (∅ 800 μm) within a PEG cell-repellent surface[26,61]. The cells were flushed with culture medium 5 h after plating and the medium was replaced with phenol red-free DMEM (+10% FBS and 1% L-glutamine, Invitrogen) with or without tetracycline. Cell culture medium and drug treatments were changed every 2 days.

PDMS-based cell compression assays. The GFP-labelled *scrib*^{KD} cells were plated onto a stretched flexible silicone substrate (Gel pak PF-60-X4, 150 μm thickness, Teltek), held in a custom-made chamber (GREM; http://www.jove.com/video/51193/stretching-micropatterned-cells-on-a-pdms-membrane). Before plating, the clamped membranes were coated with 25 μg ml^{-1} fibronectin/PBS (Sigma) for 1 h at 37 °C. The membranes were stretched precisely by 2 cm, which provided a 57% stretch over the resting length (unless otherwise specified). A PDMS rectangular chamber, with two compartments (6.6 × 13 mm each) was attached to the membrane with Baysilone paste (GE Bayer). Two densities (low and high) of tetracycline pre-treated or Nutlin-3 pre-treated (48 h) GFP-labelled *scrib*^{KD} cells were plated, one in each compartment. High-density cells were plated between 75,000 and 120,000 cells per compartment, forming a confluent monolayer; low-density cells were plated at 25,000–35,000 cells per compartment. The cells were allowed to adhere for 24 h and then the membrane was released to induce compression. The cells were fixed in 4% PFA/PBS (3 h after release for p53 staining, 1.5 h for P-p38 staining and 5 h for cleaved Caspase-3 staining) and processed for immunofluorescence. As per design, low- and high-density cells were stained and imaged from the same stretcher avoiding sample-to-sample variability. The p38 inhibitor was added one day before plating; the ROCK inhibitor was added 1 h before releasing the membrane.

E-cadherin-blocking experiments. To block E-cadherin-dependent junctions, 20 h after the addition of tetracycline, the cells were incubated in 10 mM EDTA/PBS for 5 min, followed by a 20 min incubation in calcium-free DMEM (Invitrogen). The cells were then cultured in calcium-free DMEM (+10% FBS and 1% L-glutamine, Invitrogen), supplemented with an anti-E-cadherin-blocking antibody (1:200; ref. 57). Live-image analysis was started 2–4 h after the final media change and continued for at least 50 h.

Immunofluorescence. For immunofluorescence, the cells were cultured on glass coverslips or on gridded dishes (μ-Dish 35 mm Grid-500, Ibidi). The cells were fixed for 10 min in 4% PFA/PBS, quenched for 10 min in 50 mM NH_4Cl/PBS and then permeabilized for 10 min with 0.1% Triton X-100/PBS. The cells were blocked in 2% BSA, 2% FBS/PBS for 30 min. Primary and secondary antibodies were diluted in blocking solution diluted 1:1 in PBS. The primary antibodies were incubated for a minimum of 1 h at RT, followed by washes in PBS; secondary antibodies were incubated for a minimum of 30 min at RT followed by washes in PBS. Coverslips were mounted with FluorSave (Millipore). For immunostaining against phosphorylated proteins, fixing solution was supplemented with PhosSTOP (1 tablet per 10 ml, Sigma), all PBS solutions were substituted with TBS, and blocking solution was substituted with 5% BSA/TBS. For surface immunostaining, the cells were washed in ice-cold phenol red-free DMEM (Gibco) and incubated with primary antibody diluted in ice-cold phenol red-free DMEM at 4 °C for 45 min. The cells were then washed in ice-cold PBS before fixation at RT in 4% PFA/PBS for 10 min. Secondary antibody staining was then carried out as outlined previously.

Western blotting. The cells were lysed in 1% SDS/PBS and 10–20 μg of protein was separated on a 4–12% gradient gel (Invitrogen) and transferred onto PVDF membrane for standard ECL blots (Anachem) or Immobilon FL PVDF for LI-COR blots (Millipore, 0.45 μm pore size). The membranes were blocked with 5% Marvel/0.05% Tween-20/PBS (PBST) for 1 h at RT, incubated in primary antibodies (in 2% Marvel/PBST) overnight at 4 °C, washed in PBST and incubated in secondary HRP-conjugated antibodies for ECL blots or Infrared fluorescent dyes (IRDye-800CW and IRDye-680RD) for LI-COR blots, diluted in 2% Marvel/PBST for 1 h at RT. After washes in PBST, the membranes were developed using standard ECL (GE Healthcare) or scanned with a LI-COR Odyssey CLx near-infrared fluorescence imaging system. Quantifications for LI-COR blots were carried out using Image studio lite (http://www.licor.com/bio/products/software/image_studio_lite/?gclid=COWG_Yze98MCFYvpwgodfR8Adg), using Actin to normalize the samples for loading. For original full blots, see Supplementary Fig. 9.

RNA-seq and differential expression analysis. RNA-seq libraries were prepared with the TrueSeq RNA sample preparation V2 kit (Illumina) according to the manufacturer's instructions, and sequenced on an Illumina HiSeq 2000 instrument in single-read mode at 36 or 40 base length. The resulting fastq files were filtered for low-quality reads (<Q20) and low-quality bases were trimmed from the ends of the reads (<Q20).

Genome-based RNA-seq mapping was carried out using *Canis lupus familiaris* 3.1 (NCBI/Dog Sequencing Consortium) as a reference genome. Transcript sequences were assigned to genome using BLAT[62]. The resulting mappings were filtered by a mismatch threshold (2%), as well as requiring 90% of the transcript to match the genome and all exons to match a single chromosome. This resulted in 21,571 transcripts mapping to the genome. This mapping was used as a junction file for Tophat 2 (ref. 63), which was used to map the RNA-seq reads to the genome. To provide gene names, transcript sequences were downloaded from the NCBI RefSeq database in March 2013 (24,538 sequences). Orthologues were found against the *Mus musculus* proteome (downloaded in January 2013—NCBI RefSeq) using Inparanoid[64]. The sequences were further annotated using InterProScan[65] to provide both InterPro Domains and Panther ontology terms[66]. For differential expression, read counts were generated by quantifying overlaps with transcript locations. These were then used to generate RPKMs. Comparisons were made between pairs of conditions, each with at least four replicates. For a transcript to be included, counts per million had to be above 10 for all samples in at least one condition and within 2-fold between replicates. Differentially expressed transcripts were then called using EdgeR[67]. Hits were selected applying the following thresholds: $P>0.05$ log FC (fold change) >0.5. Gene Ontology terms over-represented among these lists were found using David Bioinformatics Resources[68], in particular, KEGG pathway analysis.

Experiments in *Drosophila* wing discs. Flies were raised on a standard fly food containing yeast at 25 °C. The larvae were collected at wandering third instar stage. Clones in wing discs were induced either with en-FLP (Supplementary Fig. 5a,b) or with hs-FLP (with a 10-min heat-shock at 37 °C, 48–72 h before dissection; Supplementary Fig. 5c). For immunofluorescence, late third instar larvae were dissected in PBS followed by fixation in 4% formaldehyde/PBS solution for 20 min, permeabilization in 0.25% Triton X-100 PBS for 20 min and blocking in 4% FBS/PBS for 30 min. The primary and secondary antibodies were diluted in blocking solution. The primary antibodies were incubated overnight at 4 °C, followed by washes in 0.25% Triton X-100/PBS; secondary antibodies were incubated for a

minimum of 1 h at RT followed by washes in 0.25% Triton X-100/PBS. The wing discs were mounted in Vectashield (Vector Laboratories) and imaged on Leica SP5 or SP8 confocal microscopes. Optical sections were acquired with 0.8μm steps. The images were processed in ImageJ and Photoshop. Genotypes: Supplementary Fig. 5a,b en-flp, Act>STOP>Gal4, UAS-GFP/+; UAS-Scrib-RNAi, Supplementary Fig. 5c (left) hs-FLP, tub-Gal4, UAS-GFP/+; +/+, FRT82, tub-Gal80/ FRT82, scrib2 and Supplementary Fig. 5c (right) hs-FLP, tub-Gal4, UAS-GFP/+; UAS-p53DN/+, FRT82, tub-Gal80/ FRT82, scrib2. Antibodies used: anti-Scribble (1:2000, from Chris Doe lab), anti-E-Cadherin (DSHB DCAD2, 1:200). Both the antibodies were raised against *Drosophila* antigens and have been previously used in *Drosophila*.

Imaging and image analysis. Quantifications shown in the figures are from a single representative experiment of a minimum of three independent repeats per experiment, unless otherwise specified in the figure legend.

Fixed samples were imaged with a Leica SP5 or SP8 confocal microscope. For live imaging, the cells (kept at 37 °C and 5% CO_2) were imaged using a Nikon BioStation CT with a ×10 air objective with imaging frequency between every 10 min and every 6 h (as indicated in the movie time stamps), with media changes every 2–3 days. For each live imaging experiment, at least five fields were imaged by time lapse and analysed. Movie sequences or individual field time points that lost focus during the experiment were discarded from further analysis, as this precluded accurate cell counting.

For Fig. 1a–c and Supplementary Fig. 1d, quantifications of cell number over time were carried out using the open-source image analysis software Cell Profiler (http://www.cellprofiler.org/), using the nuclear GFP signal to segment cells.

To measure cell density in competition assays, the number of nuclei was manually counted using DAPI and/or nuclear GFP and divided by surface area, as calculated in Fiji (http://fiji.sc/Fiji; Fig. 1g and 2n, Fig. 5e, Supplementary Fig. 1e).

For Fig. 1k–n, cell number over time was quantified with the open-source image analysis software Icy[69], using Icy Protocols. The nuclei were detected using the wavelet-based spot detection plugins. Areas with cysts, where nuclei were not visible due to overexposure or because they were out of focus, and areas without cells were excluded from both cell counting and from area measurements on a frame by frame basis. For Fig. 3h, Fig. 4c,k and Fig. 5b, entire wells of a 96-well plate were imaged by tiling. Individual images were then stitched and processed as above.

Cell height (μm, Fig. 1h–j) was measured from apical to basal membranes using the open image analysis software Fiji.

Cell death in compression assays was quantified as the number of activated caspase-3 positive death events (Fig. 1o–q, Fig. 3i, Fig. 4d,l and Fig. 5c) divided by total number of DAPI-positive nuclei.

Kymographs were generated by first registering the hyperstack containing the different channels (bright-field, RFP and GFP) to remove any global motion or drift over time of the cells (Fig. 2d). The position of the centroid for each nucleus at each time point was extracted and the RFP and GFP channels were then projected on the same mean direction of motion by re-slicing the stacks and then projecting the maximum intensity of the centroid. For the control kymographs (GFP-labelled $scrib^{KD}$: $scrib^{KD}$; RFP-labelled WT: WT), this was done only using the bright-field channel and one fluorescent channel.

The directionality index of migrating cells (D = Euclidean distance/total distance, Supplementary Fig. 2b,d) was calculated after manual tracking of individual cell nuclei (>40 cells and >5 movies per condition) with the aid of ImageJ (http://imagej.nih.gov/ij/). Data analysis was performed with Matlab (MathWorks Inc.).

Analysis of cell shape and migratory features (Fig. 2g–k). The aspect ratio, which is defined as the ratio of the long axis to the short axis of cells, was measured from three independent movies by manually fitting the best fit ellipses to single cells. To plot the distribution of angles between the cell's long axis and the cell's direction of motion, we determined for each cell the orientation of the cell's long axis and calculated its angular deviation with respect to the cell's direction of motion (data were binned at 40° interval), by manual tracking. To measure the displacement of wild-type and $scrib^{KD}$ cells, we carried out PIV analysis, using a custom algorithm based on the MatPIV software package for MATLAB, and measured the displacement of individual cells within the first row of contact. Trajectories across different movies were adjusted so that the first time point where both populations formed a broad interface and moved concertedly was set at $t = 5$ h. Distance is the projected distance along the axis that joins both cell populations.

In Figs 3c–e and 4e, local density was measured for each cell by taking the sum of the Gaussian-weighted distances to all other cells within 50 μm using a Gaussian function with $\sigma = 20$.

Nuclear p53 (Fig. 3f,g), nuclear phospho-p38 (Fig. 4a,b,i,j) and nuclear p21 (Supplementary Fig. 4d) mean intensity was measured using Volocity (http://www.perkinelmer.co.uk/pages/020/cellularimaging/products/volocity.xhtml), using DAPI as a mask to segment the nuclei.

For Fig. 5f–I, quantifications of cell number over time were carried out in ImageJ (http://imagej.nih.gov/ij/), using the nuclear Tomato signal to segment cells.

In Supplementary Fig. 2h–i, E-cadherin staining intensity was measured using Fiji. The individual cells were manually selected on an average z stack projection and their integrated density values were recorded.

Statistical analysis. No statistical methods were used to predetermine sample size. Every experimental condition and treatment was carried out alongside a complete control set of experiments or no treatment control. The sample size was chosen to see a statistical difference between data sets. In the few instances where no difference was observed, sample size was at least as big as in conditions that had shown a difference. The experiments were not randomized and there was no blinding during experiments or analysis, as samples were marked. We carried out a minimum of independent three repeats for each experiment, unless otherwise specified in the figure legend.

The *t*-Test was used in Supplementary Fig. 1e and Supplementary Fig. 2b,d, where data were normally distributed and with equal variance. The Wicoxon rank-sum test was used in Supplementary Fig. 3f. Non-parametric Spearman correlation was used in Fig. 3e. Otherwise, the non-parametric KS test was used for all the statistical tests, removing the requirement for normally distributed data and equal variance. Throughout: $^{*}P<0.05$, $^{**}P<0.005$, $^{***}P<0.0005$.

References

1. Morata, G. & Ripoll, P. Minutes: mutants of drosophila autonomously affecting cell division rate. *Dev. Biol.* **42,** 211–221 (1975).
2. Moreno, E. & Basler, K. dMyc transforms cells into super-competitors. *Cell* **117,** 117–129 (2004).
3. la Cova, de, C., Abril, M., Bellosta, P., Gallant, P. & Johnston, L. A. Drosophila myc regulates organ size by inducing cell competition. *Cell* **117,** 107–116 (2004).
4. Oertel, M., Menthena, A., Dabeva, M. D. & Shafritz, D. A. Cell competition leads to a high level of normal liver reconstitution by transplanted fetal liver stem/progenitor cells. *Gastroenterology* **130,** 507–520 (2006).
5. Rhiner, C. *et al.* Persistent competition among stem cells and their daughters in the Drosophila ovary germline niche. *Development* **136,** 995–1006 (2009).
6. Sancho, M. *et al.* Competitive interactions eliminate unfit embryonic stem cells at the onset of differentiation. *Dev. Cell* **26,** 19–30 (2013).
7. Clavería, C., Giovinazzo, G., Sierra, R. & Torres, M. Myc-driven endogenous cell competition in the early mammalian embryo. *Nature* **500,** 39–44 (2013).
8. Tamori, Y. & Deng, W.-M. Tissue repair through cell competition and compensatory cellular hypertrophy in postmitotic epithelia. *Dev. Cell* **25,** 350–363 (2013).
9. Martins, V. C. *et al.* Cell competition is a tumour suppressor mechanism in the thymus. *Nature* **509,** 465–470 (2014).
10. Villa Del Campo, C., Clavería, C., Sierra, R. & Torres, M. Cell competition promotes phenotypically silent cardiomyocyte replacement in the Mammalian heart. *Cell Rep.* **8,** 1741–1751 (2014).
11. Rhiner, C. *et al.* Flower forms an extracellular code that reveals the fitness of a cell to its neighbors in Drosophila. *Dev. Cell* **18,** 985–998 (2010).
12. Meyer, S. N. *et al.* An ancient defense system eliminates unfit cells from developing tissues during cell competition. *Science* **346,** 1258236 (2014).
13. Merino, M. M. *et al.* Elimination of unfit cells maintains tissue health and prolongs lifespan. *Cell* **160,** 461–476 (2015).
14. Levayer, R., Hauert, B. & Moreno, E. Cell mixing induced by myc is required for competitive tissue invasion and destruction. *Nature* **524,** 476–480 (2015).
15. Mamada, H., Sato, T., Ota, M. & Sasaki, H. Cell competition in mouse NIH3T3 embryonic fibroblasts is controlled by the activity of Tead family proteins and Myc. *J. Cell Sci.* **128,** 790–803 (2015).
16. Li, W. & Baker, N. E. Engulfment is required for cell competition. *Cell* **129,** 1215–1225 (2007).
17. de Beco, S., Ziosi, M. & Johnston, L. A. New frontiers in cell competition. *Dev. Dyn.* **241,** 831–841 (2012).
18. Vivarelli, S., Wagstaff, L. & Piddini, E. Cell wars: regulation of cell survival and proliferation by cell competition. *Essays Biochem.* **53,** 69–82 (2012).
19. Vincent, J.-P., Fletcher, A. G. & Baena-Lopez, L. A. *Mechanisms and mechanics of cell competition in epithelia* 14, 581–591 (Nature Publishing Group, 2013).
20. Baillon, L. & Basler, K. Reflections on cell competition. *Semin. Cell Dev. Biol.* **32,** 137–144 (2014).
21. Moreno, E. Cancer: Darwinian tumour suppression. *Nature* **509,** 435–436 (2014).
22. Levayer, R. & Moreno, E. Mechanisms of cell competition: themes and variations. *J. Cell Biol.* **200,** 689–698 (2013).
23. Norman, M. *et al.* Loss of Scribble causes cell competition in mammalian cells. *J. Cell Sci.* **125,** 59–66 (2012).
24. Senoo-Matsuda, N. & Johnston, L. A. Soluble factors mediate competitive and cooperative interactions between cells expressing different levels of Drosophila Myc. *Proc. Natl Acad. Sci. USA* **104,** 18543–18548 (2007).

25. Qin, Y., Capaldo, C., Gumbiner, B. M. & Macara, I. G. The mammalian Scribble polarity protein regulates epithelial cell adhesion and migration through E-cadherin. *J. Cell Biol.* **171,** 1061–1071 (2005).
26. Deforet, M., Hakim, V., Yevick, H. G., Duclos, G. & Silberzan, P. Emergence of collective modes and tri-dimensional structures from epithelial confinement. *Nat. Commun.* **5,** 3747 (2014).
27. Eisenhoffer, G. T. *et al.* Crowding induces live cell extrusion to maintain homeostatic cell numbers in epithelia. *Nature* **484,** 546–549 (2012).
28. Marinari, E. *et al.* Live-cell delamination counterbalances epithelial growth to limit tissue overcrowding. *Nature* **484,** 542–545 (2012).
29. Theveneau, E. *et al. Chase-and-run between adjacent cell populations promotes directional collective migration* 15, 763–772 (Nature Publishing Group, 2013).
30. Theveneau, E. & Mayor, R. Cadherins in collective cell migration of mesenchymal cells. *Curr. Opin. Cell Biol.* **24,** 677–684 (2012).
31. Lohia, M., Qin, Y. & Macara, I. G. The Scribble polarity protein stabilizes E-cadherin/p120-catenin binding and blocks retrieval of E-cadherin to the Golgi. *PLoS ONE* **7,** e51130 (2012).
32. Hogan, C. *et al. Characterization of the interface between normal and transformed epithelial cells* 11, 460–467 (Nature Publishing Group, 2009).
33. Zilfou, J. T. & Lowe, S. W. Tumor suppressive functions of p53. *Cold Spring Harb. Perspect. Biol.* **1,** a001883 (2009).
34. Brumby, A. M. & Richardson, H. E. scribble mutants cooperate with oncogenic Ras or Notch to cause neoplastic overgrowth in Drosophila. *EMBO J.* **22,** 5769–5779 (2003).
35. Igaki, T., Pagliarini, R. A. & Xu, T. Loss of cell polarity drives tumor growth and invasion through JNK activation in Drosophila. *Curr. Biol.* **16,** 1139–1146 (2006).
36. Igaki, T., Pastor-Pareja, J. C., Aonuma, H., Miura, M. & Xu, T. Intrinsic tumor suppression and epithelial maintenance by endocytic activation of Eiger/TNF signaling in Drosophila. *Dev. Cell* **16,** 458–465 (2009).
37. Ohsawa, S. *et al.* Elimination of oncogenic neighbors by JNK-mediated engulfment in Drosophila. *Dev. Cell* **20,** 315–328 (2011).
38. Cuadrado, A. & Nebreda, A. R. Mechanisms and functions of p38 MAPK signalling. *Biochem. J.* **429,** 403–417 (2010).
39. Huang, C., Ma, W. Y., Maxiner, A., Sun, Y. & Dong, Z. p38 kinase mediates UV-induced phosphorylation of p53 protein at serine 389. *J. Biol. Chem.* **274,** 12229–12235 (1999).
40. Bulavin, D. V. *et al.* Phosphorylation of human p53 by p38 kinase coordinates N-terminal phosphorylation and apoptosis in response to UV radiation. *EMBO J.* **18,** 6845–6854 (1999).
41. Hofmann, M. *et al.* Mechanical pressure-induced phosphorylation of p38 mitogen-activated protein kinase in epithelial cells via Src and protein kinase C. *Biochem. Biophys. Res. Commun.* **316,** 673–679 (2004).
42. Amano, M., Nakayama, M. & Kaibuchi, K. Rho-kinase/ROCK: a key regulator of the cytoskeleton and cell polarity. *Cytoskeleton* **67,** 545–554 (2010).
43. Wilkinson, S., Paterson, H. F. & Marshall, C. J. Cdc42–MRCK and Rho–ROCK signalling cooperate in myosin phosphorylation and cell invasion. *Nat. Cell Biol.* **7,** 255–261 (2005).
44. Nakagawa, K. *et al.* Cyclic compression-induced p38 activation and subsequent MMP13 expression requires Rho/ROCK activity in bovine cartilage explants. *Inflamm. Res.* **61,** 1093–1100 (2012).
45. Rosenblatt, J., Raff, M. C. & Cramer, L. P. An epithelial cell destined for apoptosis signals its neighbors to extrude it by an actin- and myosin-dependent mechanism. *Curr. Biol.* **11,** 1847–1857 (2001).
46. Eisenhoffer, G. T. & Rosenblatt, J. Bringing balance by force: live cell extrusion controls epithelial cell numbers. *Trends Cell Biol.* **23,** 1–8 (2012).
47. Vassilev, L. T. *et al. In vivo* activation of the p53 pathway by small-molecule antagonists of MDM2. *Science* **303,** 844–848 (2004).
48. Prigge, J. R. *et al.* Nuclear double-fluorescent reporter for *in vivo* and *ex vivo* analyses of biological transitions in mouse nuclei. *Mamm. Genome* **24,** 389–399 (2013).
49. Shraiman, B. I. Mechanical feedback as a possible regulator of tissue growth. *Proc. Natl Acad. Sci. USA* **102,** 3318–3323 (2005).
50. Yu, H., Mouw, J. K. & Weaver, V. M. Forcing form and function: biomechanical regulation of tumor evolution. *Trends Cell Biol.* **21,** 47–56 (2011).
51. Friedl, P. & Alexander, S. Cancer invasion and the microenvironment: plasticity and reciprocity. *Cell* **147,** 992–1009 (2011).
52. Muller, P. & Vousden, K. H. Mutant p53 in cancer: new functions and therapeutic opportunities. *Cancer Cell* **25,** 304–317 (2014).
53. Bilder, D. Cooperative regulation of cell polarity and growth by Drosophila tumor suppressors. *Science* **289,** 113–116 (2000).
54. Zhan, L. *et al.* Deregulation of scribble promotes mammary tumorigenesis and reveals a role for cell polarity in carcinoma. *Cell* **135,** 865–878 (2008).
55. Levayer, R., Dupont, C. & Moreno, E. Tissue crowding induces caspase-dependent competition for space. *Curr. Biol.* **26,** 670–677 (2016).
56. Gumbiner, B. & Simons, K. A functional assay for proteins involved in establishing an epithelial occluding barrier: identification of a uvomorulin-like polypeptide. *J. Cell Biol.* **102,** 457–468 (1986).
57. Vestweber, D. & Kemler, R. Rabbit antiserum against a purified surface glycoprotein decompacts mouse preimplantation embryos and reacts with specific adult tissues. *Exp. Cell Res.* **152,** 169–178 (1984).
58. Ran, F. A. *et al.* Genome engineering using the CRISPR-Cas9 system. *Nat. Protoc.* **8,** 2281–2308 (2013).
59. Adams, C. L. Mechanisms of epithelial cell-cell adhesion and cell compaction revealed by high-resolution tracking of E-cadherin-green fluorescent protein. *J. Cell Biol.* **142,** 1105–1119 (1998).
60. You, Y., Richer, E. J., Huang, T. & Brody, S. L. Growth and differentiation of mouse tracheal epithelial cells: selection of a proliferative population. *Am. J. Physiol. Lung Cell Mol. Physiol.* **283,** L1315–L1321 (2002).
61. Tourovskaia, A., Barber, T., Wickes, B. T., Hirdes, D. & Grin, B. Micropatterns of chemisorbed cell adhesion-repellent films using oxygen plasma etching and elastomeric masks. *Langmuir* **19,** 4754–4764 (2003).
62. Kent, W. J. BLAT—the BLAST-like alignment tool. *Genome Res.* **12,** 656–664 (2002).
63. Trapnell, C., Pachter, L. & Salzberg, S. L. TopHat: discovering splice junctions with RNA-Seq. *Bioinformatics* **25,** 1105–1111 (2009).
64. Alexeyenko, A., Tamas, I., Liu, G. & Sonnhammer, E. L. L. Automatic clustering of orthologs and inparalogs shared by multiple proteomes. *Bioinformatics* **22,** e9–e15 (2006).
65. Zdobnov, E. M. & Apweiler, R. InterProScan—an integration platform for the signature-recognition methods in InterPro. *Bioinformatics* **17,** 847–848 (2001).
66. Thomas, P. D. *et al.* PANTHER: a library of protein families and subfamilies indexed by function. *Genome Res.* **13,** 2129–2141 (2003).
67. Robinson, M. D., McCarthy, D. J. & Smyth, G. K. edgeR: a Bioconductor package for differential expression analysis of digital gene expression data. *Bioinformatics* **26,** 139–140 (2010).
68. Huang, D. W., Sherman, B. T. & Lempicki, R. A. Systematic and integrative analysis of large gene lists using DAVID bioinformatics resources. *Nat. Protoc.* **4,** 44–57 (2008).
69. de Chaumont, F. *et al.* Icy: an open bioimage informatics platform for extended reproducible research. *Nat. Methods* **9,** 690–696 (2012).

Acknowledgements

This work was supported by a Cancer Research UK Programme Grant (E.P. and L.W. A12460), a Royal Society University Research fellowship to E.P. (UF0905080), a Wellcome Trust PhD studentship to I.K., a Cambridge Cancer Centre PhD studentship to M.G., a European Research Council (ERC) grant to R.E.C.S. (243283-SYSGRO), a BBSRC grant (R.E.C.S. and A.C. BB/K006320/1) and Core grant funding from the Wellcome Trust (092096) and CRUK (C6946/A14492). The 'Biology-Inspired Physics at Mesoscales' group is a member of the IPGG Labex. The laboratoire PhysicoChimie Curie is member of the Labex CelTisPhyBio Labex. We thank: Yasuyuki Fujita for providing *scrib*^{KD} and *E-cad*^{KD} MDCK cells and an E-cadherin shRNA construct; Richard Butler, Nicola Lawrence and Alex Sossick for help with microscopy and image analysis; Nicolas Carpi and Matthieu Piel for advice on the use of stretchers; James Nelson for E-cadherin constructs and discussions; Silvia Vivarelli for cloning pGIPZ-GFP-NLS and pGIPZ-RFP-NLS and researchers cited in methods for reagents. We apologize to the researchers whose work could not be cited due to space limitations.

Author contributions

E.P. conceived and led the project. E.P. and LW designed the experimental strategy with help from RECS. M.G. characterized the role of ROCK and S1P2 and carried out assays in MTECs with help from E.L.R. M.G. and L.W. carried out the PDMS assays. K.K. carried out all cloning and, with help from M.G. and L.W., characterized the contribution of E-cadherin to contact-induced migration and loser status. M.G., C.R.B. and G.E.A. carried out RNAseq and data analyses. I.K. and L.W. carried out conditioned media and transwell experiments. I.K. carried out all *Drosophila* work. G.D. and P.S. generated micropatterns and analysed directional cell migration. A.C. and R.E.C.S. developed an algorithm for time-resolved cell density measurements of cell density. L.H.-O. and L.W. characterized *scrib*^{RES} cells and p21 expression. All the other experiments were carried out by L.W. E.P. and L.W. prepared the manuscript with help from K.K., M.G., R.E.C.S. and other co-authors.

Additional information

Accession codes: The RNAseq data generated in this study have been deposited into the GEO (Gene Expression Omnibus) database under the accession code GSE79042.

Supplementary Information accompanies this paper at http://www.nature.com/naturecommunications

Competing financial interests: The authors declare no competing financial interests.

How to cite this article: Wagstaff, L. *et al.* Mechanical cell competition kills cells via induction of lethal p53 levels. *Nat. Commun.* 7:11373 doi: 10.1038/ncomms11373 (2016).

Title

p53 instructs leader cell behavior during collective cell migration

Authors

Kasia Kozyrska [1,2], Laura Wagstaff [1], Maja Goschorska [2], Medhavi Vishwakarma [2] and Eugenia Piddini [2]*

Affiliations

[1] The Wellcome Trust/Cancer Research UK Gurdon Institute and Zoology Department, University of Cambridge, Tennis Court Road, Cambridge CB2 1QN, UK.

[2] School of Cellular and Molecular Medicine, University of Bristol, Biomedical Sciences Building, University Walk, Bristol BS8 1TD, UK.

* Correspondence to: eugenia.piddini@bristol.ac.uk

Abstract

Upon wounding, epithelial cells migrate across the wound to close the gap. Leader cells at the front of migrating sheets drive this migratory process. However, how leader cells emerge from a seemingly homogeneous cell population is not fully understood. Here, by characterizing leaders emerging from MDCK monolayers, we identify the activity of the stress sensor p53 as the instructive signal for leader behaviour. p53 is necessary and sufficient to instruct leader cell fate and it does so by activating a single target gene, the cell cycle inhibitor $p21^{WAF1/Cip1}$. On wound closure, leader cells maintaining high p53 are eliminated by cell competition to preserve tissue health. Overall, our data indicate that injury itself instructs the emergence of leader cells by damage-induced p53 activation.

One Sentence Summary

Cell damage drives wound closure by inducing the activity of p53 and $p21^{WAF1/Cip1}$ in leader cells, which drive cell migration.

Main Text

Epithelial cells are normally non-migratory. However, when the integrity of an epithelial monolayer is compromised by injury or wounding, epithelial cells extend and migrate over the exposed area to seal the open space quickly (*1-3*). This process is driven by leader cells, which are located at the edge of the migrating front and guide the collective migration of epithelial sheets (*3-5*). Collective cell migration in wound closure has been actively studied to understand the cellular interactions and the biophysics underpinning wound closure (*1*, *4-7*) and to identify the features of leader cells that allow them to orchestrate this process (*3*, *8-10*). Several groups have shown that leader cells are morphologically distinct from followers and have different cytoskeletal properties (*3*, *10-13*).

Despite their distinctive characteristics, leader cells originate from the same epithelial cells as follower cells, begging the question of how they emerge. It is currently unknown how cells are singled out and instructed to become leaders from a seemingly homogeneous population of epithelial cells. Studies have proposed that geometrical cues at the wound edge itself may induce asymmetry and that this may be sufficient to instruct the leader cell fate (*9*, *14-16*). However, only a few cells at the wound edge become leaders suggesting that additional factors - cell intrinsic or cell extrinsic - are required.

MDCK kidney epithelial cells have been used extensively as a model to investigate leader cells and the mechanisms of wound closure, as they are a versatile system where wound healing can be studied by mechanically scratching epithelial cell monolayers or by releasing confluent monolayers from physical barriers. While imaging growing colonies of wild-type MDCK cells, we observed the spontaneous emergence of cells with a distinctive flattened morphology (Fig. 1A, yellow arrow). These flat cells often became migratory upon contact with colonies composed of cells with standard epithelial morphology, leading the entire colony with them in a behavior reminiscent of leader cell migration at wound sites (Fig. 1A and B and Movie 1). As these cells appear spontaneously in the absence of wounds, we termed them ‘spontaneous leaders’. Given their leader-like behavior, we thought that characterizing these cells might offer an orthogonal strategy to identify the mechanisms that allow leader cells to emerge.

Leader cells have been reported to have increased surface area, frequent binucleation, and lower division rates compared to normal epithelial cells (*3*, *17*). Interestingly, spontaneous leaders shared these same features, as they often did not divide during the entire span of our movies (> 48 hours) and tended to be binucleated (fig. S1A and B). We therefore asked if binucleation was sufficient to induce the leader status. Treating MDCK cells with the myosin inhibitor blebbistatin (*18*) prevents cytokinesis while still allowing karyokinesis to proceed (*19*). To facilitate the identification of blebbistatin-induced binucleated cells (BBCs) through visualization of their nuclei, we treated cells expressing nuclear GFP with blebbistatin and co-cultured these with untreated, unlabeled wild-type cells. Notably, the resulting BBCs were morphologically similar to spontaneous leaders and behaved as leaders themselves (fig. S1C and Movie 2).

The ‘tetraploidy checkpoint’ triggered upon cytokinesis failure has been shown to induce cell cycle arrest in a p53-dependent manner (*20*). p53 levels were indeed elevated in BBCs (fig. S1D), so we asked what the p53 status of spontaneous leaders was. Live imaging on optically clear gridded cell culture dishes allowed us to identify and track spontaneous leaders (Fig. 1C, first three panels) and locate them again following fixation. Immunostaining against p53 revealed that spontaneous leaders have significantly higher nuclear p53 levels than neighboring non-leader cells (Fig. 1C, rightmost panel and D).

We next asked if elevated nuclear p53 is instructive for leader cell fate. We treated wild-type MDCK cells expressing nuclear GFP with mitomycin C (MMC), an irreversible DNA damaging

agent (*21*), to permanently stabilize p53 (fig. S1E). After extensive washes to prevent MMC carryover, we co-seeded MMC-treated, GFP-labelled cells with untreated, unlabeled wild-type cells (Fig. 1E). Strikingly, MMC treatment was sufficient to trigger the leader phenotype and to induce the formation of migrating 'fingers' of untreated follower cells led by MMC-treated cells (Fig. 1F, fig. S1F, and Movie 3), suggesting that p53 elevation is sufficient to trigger the leader phenotype.

Cytokinesis failure and MMC treatment arrest cell division, due to the high levels of p53 (*22*, *23*). To ask whether cell cycle arrest was necessary for spontaneous leader fate, we sought conditions that allowed us to elevate p53 without inducing cell cycle arrest. Nutlin-3 is an Mdm2 inhibitor that stabilizes p53 in a dose-dependent manner (*24*). This allowed us to use concentrations that cause p53 elevation at levels that reduce, but do not arrest, cell cycle progression (fig. S1G and H), as we have done previously (*25*). We co-cultured GFP-labelled wild-type cells with *p53* knockout (*p53KO*) cells (*25*) in the presence of Nutlin-3, which created a discontinuity in p53 activity between the two populations. Under these conditions, p53 activation was still sufficient to confer a leader phenotype (Fig. 1G, fig. S1I, and Movie 4), indicating that cell cycle arrest is not required for cells to become leaders. Altogether, these experiments indicate that p53 elevation is sufficient to instruct the leader cell fate.

To test whether p53 is also necessary for leader cell migration, we generated two independent *p53KO* clones expressing nuclear GFP (*p53KO* C6 and C14). Sequencing of the p53 locus showed that both alleles were disrupted (Fig. 1H) and no p53 protein was detected upon induction of binucleation (fig. S1J-L). We then treated *p53KO* cells with MMC to test if they acquired leader behavior. Notably, MMC-treated *p53KO* cells behaved as leaders in just under 20% of cases, whereas MMC-treated wild-type cells acted as leaders in 80% of cases (Fig. 1I and J, and Movie 5). Indeed, cell tracks from representative movies showed that MMC-treated cells, if wild-type, migrate alongside wild-type cells upon contact (Fig. 1K) and cover long distances (Fig. 1M, gray tracks), as leader-follower pairs. However, this is not observed if the MMC-treated cells are *p53KO* (Fig. 1L and Fig. 1M, green tracks). Functional ablation of *p53* was also sufficient to reduce drastically the incidence of leader behavior in BBCs (fig. S1M and N). Taken together, these data demonstrate that p53 is both necessary and sufficient to induce leader cell behavior in MDCK cells.

We next wondered which factors downstream of p53 were responsible for the leader phenotype. Considering that spontaneous leaders, BBCs, and MMC-treated cells are cell cycle arrested, and that Nutlin-3 treated leaders divide less frequently than untreated controls, we hypothesized that effectors of p53 involved in cell cycle arrest might be involved. One of the main p53 target genes involved in cell cycle arrest is Cyclin-Dependent Kinase Inhibitor 1A (CDKN1A), also known as $p21^{WAF1/Cip1}$ (from here on referred to as p21) (*26*). Nuclear p21 was indeed upregulated in spontaneous leaders (Fig. 2A and B). To ask whether p21 was involved in leader cell behavior, we generated a clonal MDCK cell line overexpressing p21 (p21OE) in a doxycycline (DOX)-inducible manner. Overexpression of p21 resulted in cell cycle arrest, as expected, but also caused cells to flatten and take on a leader-like morphology (fig. S2A and B). Strikingly, when p21OE cells were co-cultured with wild-type cells, they behaved as leaders upon contact with wild-type cells (Fig. 2C and Movie 6), indicating that p21 overexpression is sufficient for leader cell behavior.

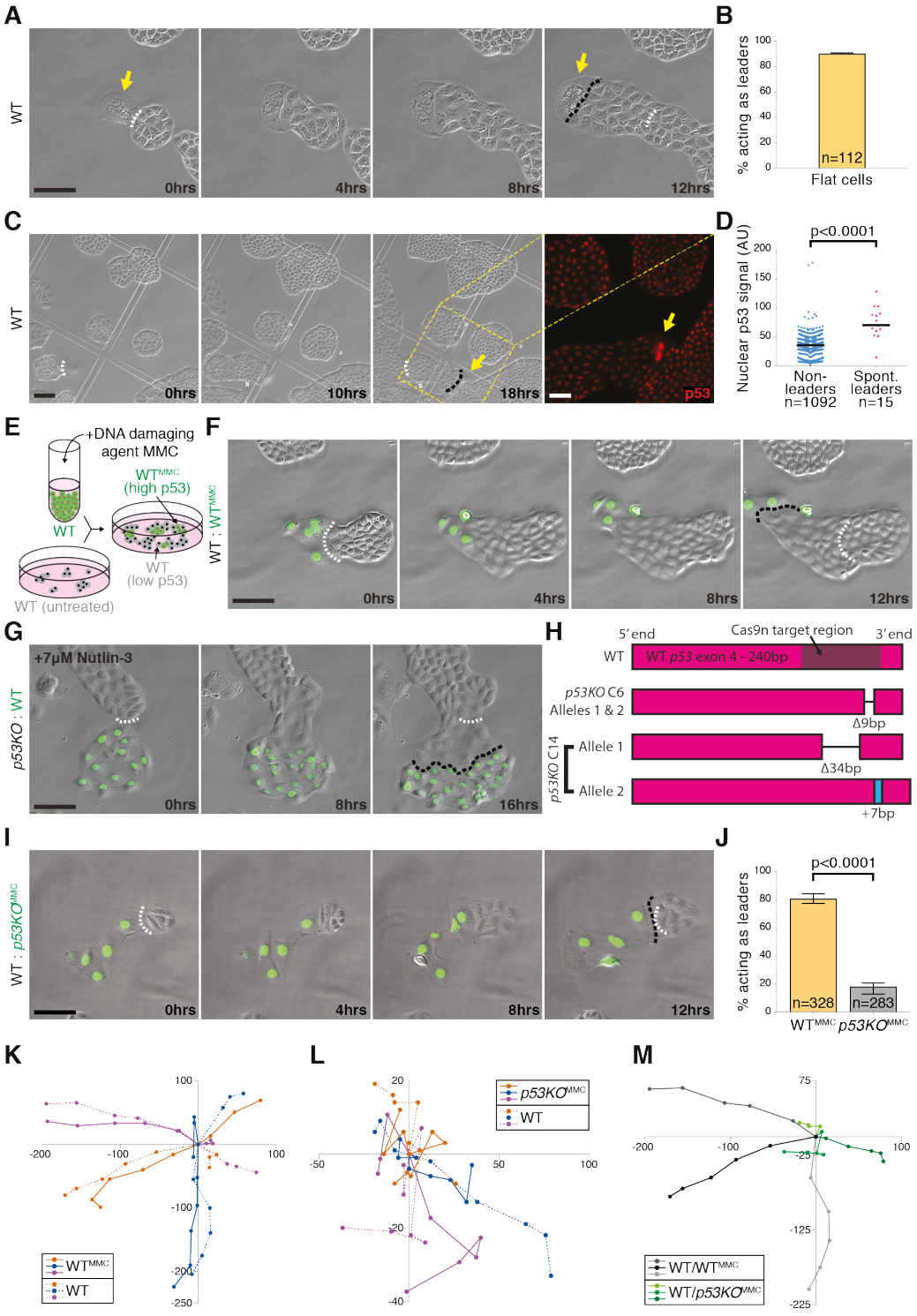

Fig. 1. p53 instructs leader cell behavior. (**A**) Movie stills of wild-type MDCK cultures shows spontaneously emerging flattened cells (yellow arrow displaying leader behavior. (**B**) Frequency at which cells with flattened morphology act as leaders. (**C**) Movie stills (first three panels) showing the migration of a spontaneous leader (yellow arrows). Fourth panel shows p53 immunostaining of the field indicated (dotted lines). (**D**) Quantification of single-cell nuclear p53 intensity of spontaneous leaders and surrounding non-leaders. (**E**) Experimental design for co-culture of untreated and MMC-treated cells (F). (**F**) Movie stills of co-cultures of wild-type cells expressing nuclear GFP and treated with MMC and unlabeled wild-type cells. (**G**) Movie stills of co-cultures of unlabeled *p53KO* cells and wild-type cells expressing nuclear GFP, treated with Nutlin-3. (**H**) Schematic representation of the

canine *p53* exon 4 sequence, targeted for CRISPR/Cas9-mediated mutagenesis. Gene disruptions in *p53KO* clones 6 and 14 (C6 and C14, respectively) are as indicated. (**I**) Movie stills from co-cultures of unlabeled wild-type cells and MMC-treated *p53KO* cells expressing nuclear GFP. (**J**) Percentage of MMC-treated wild-type or *p53KO* cells acting as leaders. (**K-L**) Cell tracks of pairs of untreated wild-type and MMC-treated wild-type cells (K) or untreated wild-type and MMC-treated *p53KO* cells (L); 0,0 coordinate indicates time of contact. (**M**) Cell tracks of wild-type cells upon contact by MMC-treated wild-type (gray) or *p53KO* cells (green).

Black bars = median in (D); n = number of cells in (B), (D), and (J). Data from one representative repeat of three biological replicates in (D), or pooled from three biological replicates in (B) and (J). Error bars = ±SEM in (B) and (J).

Here and throughout all figures:
White dashed line = initial contact point; black dashed line = final contact point. Scale bars 100μm (movie sequences) and 50μm (confocal images). P values obtained using the K-S test. DAPI = 4′,6-diamidino-2-phenylindole.

We next wanted to ask whether p21 is also necessary for leader fate. Using CRISPR/Cas9 technology, we generated two *p21* knockout clones (*p21KO* E9 and G5); bi-allelic disruption of the *p21* loci was verified by sequencing (Fig. 2D) and loss of functional p21 protein was confirmed by p21 immunofluorescence in the presence of Nutlin-3 (fig. S2C). Importantly, *p21KO* cells treated with MMC were substantially less likely to behave as leaders (Fig. 2E and F, fig. S2D, and Movie 7), demonstrating that p21 is necessary for the leader cell fate. Indeed, cell tracks from representative movies showed that *p21KO* MMC-treated cells do not migrate alongside wild-type cells upon contact (Fig. 2H) and do not cover long distances (Fig. 2I, green tracks) as leader-follower pairs, unlike control wild-type MMC-treated cells (Fig. 2G and Fig. 2I, gray tracks). Taken together, this demonstrates that p53 activation drives the spontaneous leader cell phenotype in MDCK cells by upregulating p21.

Having identified p53/p21 as a new pathway driving leader cell migration, we next asked whether this pathway induces leader cell behavior using the same factors required in leaders induced by wounding or barrier release. Wound-induced leaders upregulate Rac1, integrin β1 (ITGβ1), and phosphoinositide 3-kinase (PI3K) and require their activities to drive cell migration (*12*). We therefore tested whether these genes were also upregulated and required in spontaneous leaders and in p53/p21-induced leaders. Spontaneous leaders indeed showed upregulation of both PI3K and ITGβ1 compared to followers (fig. S3A and B). This was specifically due to p53 activation, as leaders generated by MMC treatment also showed high levels of both PI3K and ITGβ1 compared to neighboring untreated, wild-type followers (Fig. 3A and B). In addition, leaders induced by p21 overexpression alone showed PI3K and ITGβ1 upregulation (Fig. 3C and D). Furthermore, chemical inhibition of PI3K and Rac1 stalled the progress of actively migrating MMC-generated leaders (Fig. 3E-G and Movie 8), indicating that these pathways are also essential for p53/p21-mediated leader cell migration. Altogether, these results indicate that PI3K and ITGβ1 activation are downstream of p53 and p21 and that spontaneous leaders use the same mechanisms as wound induced leaders to drive collective cell migration.

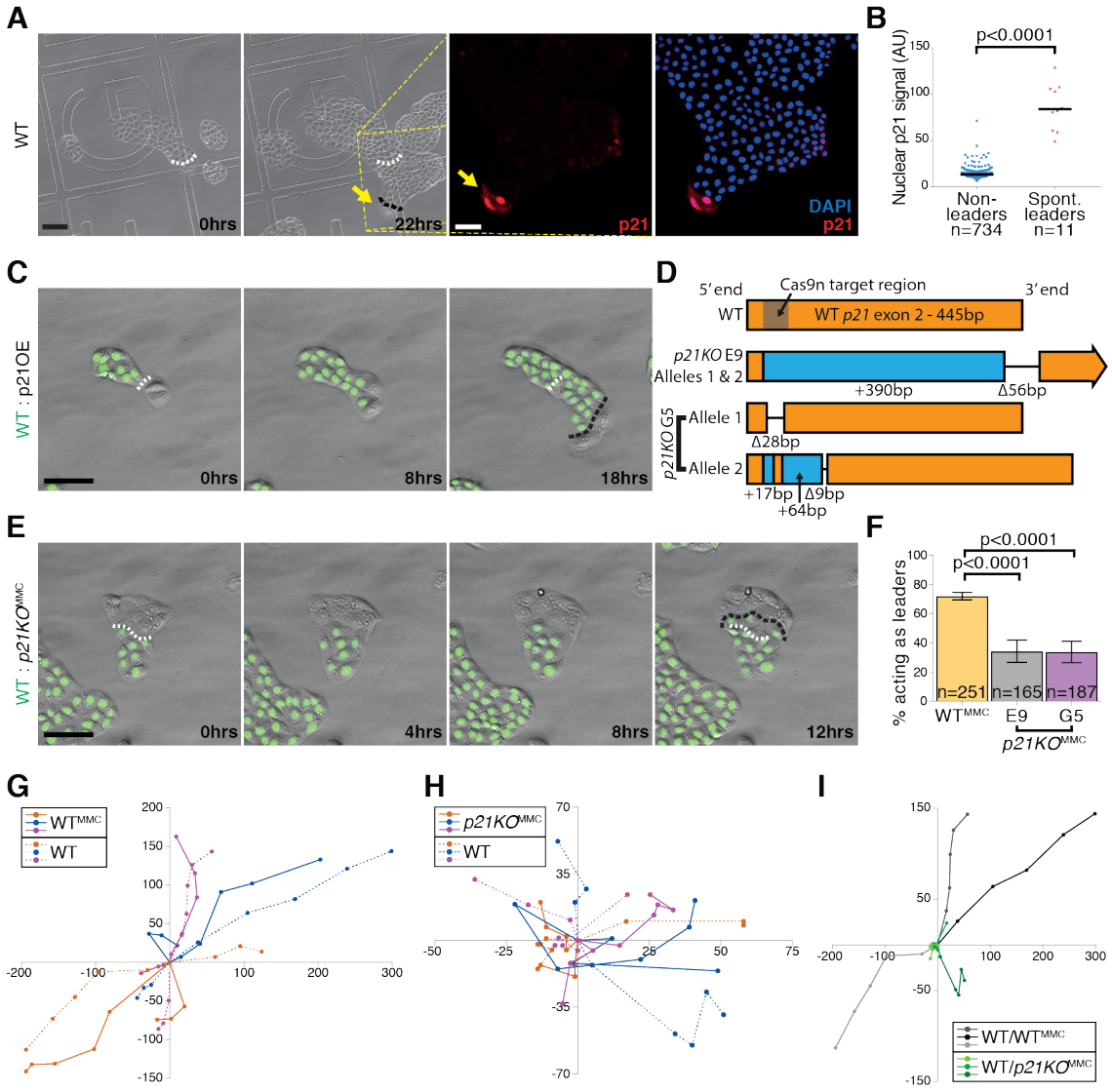

Fig. 2 p21 drives leader cell migration. (**A**) Movie stills (first two panels) of a migrating spontaneous leader (yellow arrows). Last two panels show confocal images of the same spontaneous leader following p21 immunostaining. (**B**) Quantification of single-cell nuclear p21 intensity of spontaneous leaders and surrounding non-leaders. (**C**) Movie stills from co-cultures of wild-type cells expressing nuclear GFP and unlabeled cells inducibly overexpressing p21 (p21OE). (**D**)Schematic representation of the canine *p21* exon 2 sequence, which was targeted for CRISPR/Cas9-mediated mutagenesis. Gene disruption in *p21KO* clones E9 and G5 are as indicated. (**E**) Movie stills of wild-type cells expressing nuclear GFP co-cultured with MMC-treated unlabeled *p21KO* cells. (**F**) Percentage of MMC-treated wild-type or *p21KO* cells acting as leaders. (**G-H**) Coordinates of pairs of untreated wild-type and MMC-treated wild-type cells (G) or untreated wild-type and MMC-treated *p21KO* cells (H) plotted over time after they first establish contact at point 0,0. (**I**) Cell tracks of pairs of untreated wild-type and MMC-treated wild-type cells (G) or untreated wild-type and MMC-treated *p21KO* cells (H); 0,0 coordinate indicates time of contact. (**I**) Cell tracks of wild-type cells upon contact by MMC-treated wild-type (gray) or *p21KO* cells (green).

Black bars = median in B; n = number of cells in (B) and (F). Data from one representative repeat of three biological replicates in (B), or pooled from three biological replicates in (F). Error bars = ±SEM in (F).

Since p53/p21-induced leaders share the same molecular mechanisms as wound-induced leaders to drive migration, we wondered whether p53 and p21 might also play a role in the migration of

wound-generated leaders. Strikingly, we found that leader cells emerging from scratched epithelial monolayers show high levels of both p53 (Fig. 4A and B) and p21 (Fig. 4 C and D). Importantly, leaders induced by barrier release (fig. S4A) also showed elevated levels of p53 (fig. S4B and C) and p21 (fig. S4D and E). This suggested that the p53/p21 pathway might be a general driver of leader cell migration in MDCK cells. We next sought to demonstrate that this pathway plays an active role during MDCK wound healing. We reasoned that, if that were true, then inhibiting p53 should slow down the speed of wound healing, whereas activating p53 should accelerate wound closure. Thus, we generated MDCK cells that inducibly express the canine version of the p53 peptide inhibitor GSE-22 (*27*). Notably, inhibiting p53 function was sufficient to reduce the migration speed of scratched monolayers (Fig. 4E-G). Next, we used laser-induced DNA damage (*28*) to elevate p53 at sub-lethal doses in specific regions of interest at the wound edge. Following epithelial scratching, we exposed only the first row of cells at the edge of the migrating front to laser-induced DNA damage (Fig. 4H and fig. S4F). Remarkably, inducing p53 in edge cells was sufficient to accelerate both cell migration and wound closure (Fig. 4I-K and Movie 9). Altogether, these data demonstrate that p53 and its target gene p21 are the signals activated at damaged wounds that instruct leader cell fate.

We next investigated what happens to leader cells once the wound is closed. Our interest was sparked by our recent observation that p53 elevation in MDCK cells causes mechanical cell competition: cells with high p53 acquire hypersensitivity to cell crowding and behave as mechanical losers, undergoing cell extrusion and apoptosis when compacted by cells with low p53 (*25*). Since the data in Fig. 4A and B indicate that high p53 is a hallmark of scratch-induced leaders, we wondered whether these might be eliminated upon wound closure, when they are compacted by follower cells. Remarkably, both spontaneous leaders (fig. S4G and H) and wound-induced leaders (Fig. 4L and M, and Movie 10) were extruded at high rates upon compaction. This indicates that leader cells behave as mechanical losers and are removed from repaired epithelial sheets if they still display high p53 elevation at the time of wound closure.

Understanding how leader cells emerge in damaged epithelia is important to understand the process driving wound healing and to identify interventions that could accelerate and improve wound repair. Our work identifies p53 as a key cell determinant that is both necessary and sufficient to instruct leader cell fate. As we show, p53 induces the transcriptional activation of p21, which in turn is sufficient to induce PI3K and ITGβ1 (Fig. 4N and O), both of which are required for leader cell migration (*12*). p53 is a general stress sensor and its activation constitutes a signaling node where multiple types of cellular damage converge. Here we show that cells with pre-existing damage may behave as leaders if exposed at the colony edge, as we observe in the case of spontaneous leaders. Notably, p53 can be activated by mechanical damage (*29*). We therefore suggest that, in the case of epithelial wounding, injury itself causes the emergence of leader cells by mechanically inducing p53 elevation. Our findings show that p53 orchestrates wound closure by playing multiple key roles (Fig. 4N and O). Firstly, it detects wounding through mechanical stress. Secondly, by juxtaposition of cells with high (leaders) and low (followers) p53, it provides the symmetry breaking that drives directional cell migration across the wound. Lastly and equally importantly, it induces leader cell clearance at wound closure, as injured leader cells with persistent p53 are eliminated as mechanical losers, providing a means to eliminate injured cells and fully reinstate epithelial health.

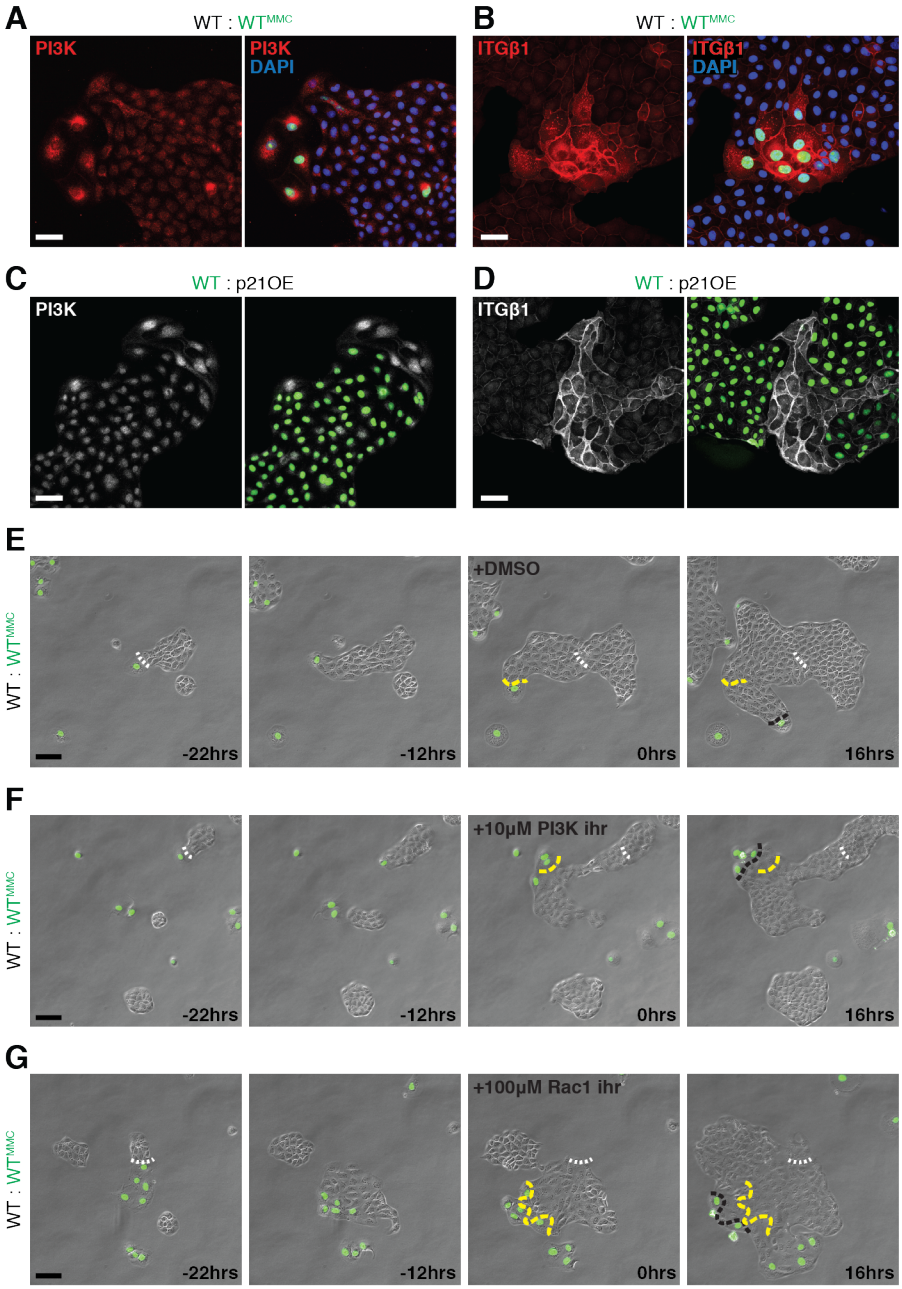

Fig. 3. The function of canonical leader cell markers is preserved in p53- and p21-driven leaders. (**A-B**) Confocal images of co-cultures of unlabeled wild-type cells and MMC-treated wild-type cells expressing nuclear GFP immunostained against phosphoinositide 3-kinase (PI3K; A) and integrin β1 (ITGβ1; B). (**C-D**) Confocal images of co-cultures of wild-type cells expressing nuclear GFP and unlabeled p21OE cells immunostained against (PI3K; C) and (ITGβ1; D). (**E-G**) Movie stills of co-cultures of unlabeled wild-type cells and MMC-treated wild-type cells expressing nuclear GFP. Following 22 hours DMSO (E) or PI3K inhibitor LY294002 (F), or Rac1 inhibitor Z62954982 (G) were added and the migration was followed for another 16 hours. White dashed line = initial contact point; yellow dashed line = contact point at addition of inhibitor; black dashed line = final contact point.

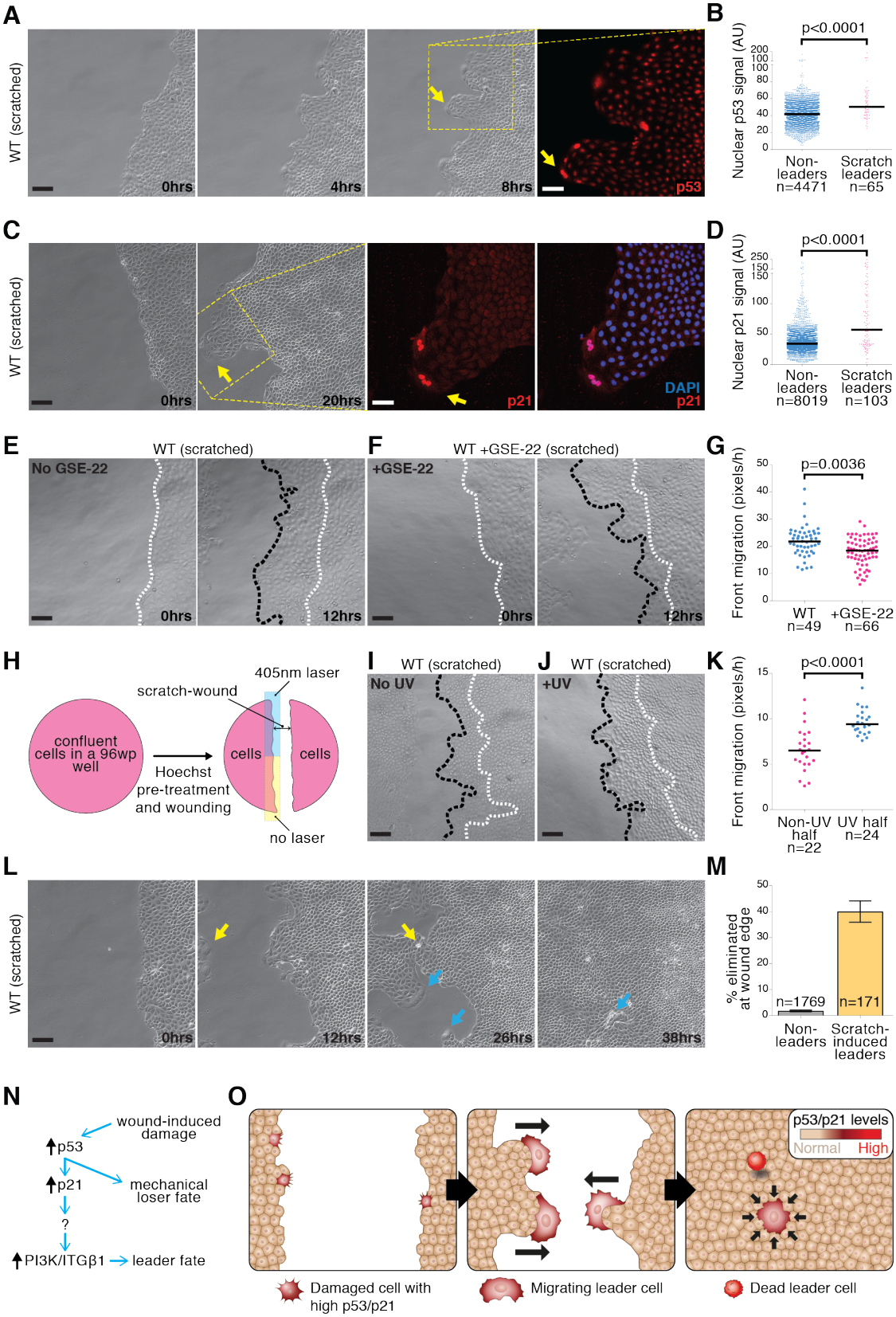

Fig. 4. p53 drives leader cell migration and leader cell outcompetition during wound healing. (**A**) Movie stills show emergence of leader cells (yellow arrow) following a scratch-wound to a MDCK monolayer (first three panels). Last panel shows p53 immunostaining of the field indicated (dotted lines) (**B**) Quantification of single-cell nuclear p53 intensity of scratch-induced leaders and surrounding non-leaders. (**C**) Movie stills wild-type MDCK

monolayer following a scratch (first two panels). Last two panels shows p21 immunostaining of the field indicated (dotted lines); yellow arrow points at leaders. (**D**) Quantification of single-cell nuclear p21 intensity of scratch-induced leaders and surrounding non-leaders. (**E-F**) Representative movie stills of control cultures (E) or cultures induced to overexpress GSE-22 (F). (**G**) Speed of migrating front from movies as in (E) and as in (F). (**H**) Experimental design to induce localized p53 activation at the edge of migrating wounds. (**I-J**) Movie stills of non-irradiated (I) or irradiated (J) wild-type cultures following a scratch-wound. (**K**) Speed of migrating front from movies as in (I) and as in (J). (**L**) Movie stills following the closure of a wild-type scratch-wound. Leaders (yellow and blue arrows) are eliminated. (**M**) Quantification of the frequency of leader cells eliminated at wound closure, compared to non-leader cells present at the wound edge. (**N-O**) Diagrams summarizing the function of p53/p21 in wound healing.

Black bars = median in (B), (D), (G), and (K); n = number of cells in (B), (D), and (M); n = number of fields in (G) and (K). Data from one representative repeat of three biological replicates in (B), (D), (G), and (K), or pooled from three biological replicates in (M). Error bars = ±SEM in (M).

References

1. V. Lecaudey, D. Gilmour, Organizing moving groups during morphogenesis. *Curr. Opin. Cell Biol.* **18**, 102–107 (2006).

2. C.-C. Liang, A. Y. Park, J.-L. Guan, In vitro scratch assay: a convenient and inexpensive method for analysis of cell migration in vitro. *Nature Protocols*. **2**, 329–333 (2007).

3. M. Poujade *et al.*, Collective migration of an epithelial monolayer in response to a model wound. *Proc. Natl. Acad. Sci. U.S.A.* **104**, 15988–15993 (2007).

4. S. Begnaud, T. Chen, D. Delacour, R.-M. Mège, B. Ladoux, Mechanics of epithelial tissues during gap closure. *Curr. Opin. Cell Biol.* **42**, 52–62 (2016).

5. V. Hakim, P. Silberzan, Collective cell migration: a physics perspective. *Rep Prog Phys*. **80**, 076601 (2017).

6. M. Reffay *et al.*, Interplay of RhoA and mechanical forces in collective cell migration driven by leader cells. *Nature Publishing Group*. **16**, 217–223 (2014).

7. L. Petitjean *et al.*, Velocity fields in a collectively migrating epithelium. *Biophys. J.* **98**, 1790–1800 (2010).

8. E. Theveneau, R. Mayor, Cadherins in collective cell migration of mesenchymal cells. *Curr. Opin. Cell Biol.* **24**, 677–684 (2012).

9. R. Riahi *et al.*, Notch1-Dll4 signalling and mechanical force regulate leader cell formation during collective cell migration. *Nature Communications*. **6**, 6556 (2015).

10. R. Mayor, S. Etienne-Manneville, The front and rear of collective cell migration. *Nat Rev Mol Cell Biol*. **17**, 97–109 (2016).

11. M. Reffay *et al.*, [Collective cell migration: a fair sharing between leader cells and supracellular coordination]. *Med Sci (Paris)*. **30** (2014), pp. 736–738.

12. N. Yamaguchi, T. Mizutani, K. Kawabata, H. Haga, Leader cells regulate collective cell migration via Rac activation in the downstream signaling of integrin β1 and PI3K. *Sci Rep*. **5**, 7656 (2015).

13. E. Theveneau, C. Linker, Leaders in collective migration: are front cells really endowed with a particular set of skills? *F1000Res*. **6**, 1899 (2017).

14. S. Mark *et al.*, Physical model of the dynamic instability in an expanding cell culture. *Biophys. J.* **98**, 361–370 (2010).

15. S. Rausch *et al.*, Polarizing cytoskeletal tension to induce leader cell formation during collective cell migration. *Biointerphases*. **8**, 32 (2013).

16. A. Ravasio *et al.*, Gap geometry dictates epithelial closure efficiency. *Nature Communications*. **6**, 7683 (2015).

17. M. Reffay *et al.*, Orientation and polarity in collectively migrating cell structures: statics

and dynamics. *Biophys. J.* **100**, 2566–2575 (2011).

18. M. Kovács, J. Tóth, C. Hetényi, A. Málnási-Csizmadia, J. R. Sellers, Mechanism of blebbistatin inhibition of myosin II. *J. Biol. Chem.* **279**, 35557–35563 (2004).

19. A. F. Straight *et al.*, Dissecting temporal and spatial control of cytokinesis with a myosin II Inhibitor. *Science*. **299**, 1743–1747 (2003).

20. P. R. Andreassen, O. D. Lohez, F. B. Lacroix, R. L. Margolis, Tetraploid state induces p53-dependent arrest of nontransformed mammalian cells in G1. *Mol. Biol. Cell*. **12**, 1315–1328 (2001).

21. M. M. COHEN, M. W. SHAW, EFFECTS OF MITOMYCIN C ON HUMAN CHROMOSOMES. *J. Cell Biol.* **23**, 386–395 (1964).

22. J. S. Lanni, T. Jacks, Characterization of the p53-dependent postmitotic checkpoint following spindle disruption. *Molecular and Cellular Biology*. **18**, 1055–1064 (1998).

23. S. G. Kang *et al.*, Mechanism of growth inhibitory effect of Mitomycin-C on cultured human retinal pigment epithelial cells: apoptosis and cell cycle arrest. *Curr. Eye Res.* **22**, 174–181 (2001).

24. L. T. Vassilev *et al.*, In vivo activation of the p53 pathway by small-molecule antagonists of MDM2. *Science*. **303**, 844–848 (2004).

25. L. Wagstaff *et al.*, Mechanical cell competition kills cells via induction of lethal p53 levels. *Nature Communications*. **7**, 11373 (2016).

26. V. Dulić *et al.*, p53-dependent inhibition of cyclin-dependent kinase activities in human fibroblasts during radiation-induced G1 arrest. *Cell*. **76**, 1013–1023 (1994).

27. V. S. Ossovskaya *et al.*, Use of genetic suppressor elements to dissect distinct biological effects of separate p53 domains. *Proc. Natl. Acad. Sci. U.S.A.* **93**, 10309–10314 (1996).

28. M. W. Berns, R. S. Olson, D. E. Rounds, In vitro production of chromosomal lesions with an argon laser microbeam. *Nature*. **221**, 74–75 (1969).

29. S. Hashimoto *et al.*, Role of p53 in human chondrocyte apoptosis in response to shear strain. *Arthritis Rheum.* **60**, 2340–2349 (2009).

Materials and Methods

Antibodies and drugs

For immunofluorescence we used: rabbit anti-p53 (1:750, 9382, Cell Signalling Technology), rabbit anti-p21 (1:200, sc-397, Santa Cruz Biotechnology), rat anti-ITGβ1 (1:200, AIIB2, DSHB), mouse anti-PI3K (1:200, 610045, BD Biosciences), rabbit anti-γH2AX (Ser 139) (1:200, 9718, Cell Signalling Technology), Alexa Fluor conjugated antibodies (1:1,000; ThermoFisher Scientific).

Treatments used: Rac1 inhibitor Z62954982 (100 μM in DMSO, 553512, Merck), PI3K inhibitor LY294002 (10 μM in DMSO, L9908, Merck), Nutlin-3 (concentration as specified in DMSO, CAY10004372, Cambridge Bioscience), mitomycin C (7.5 μg/ml in water, M4287, Merck), doxycycline (1 μg/ml in water, D9891, Merck), puromycin (0.65 μg/ml in water, P9620, Merck), Hoechst 33342 (3 μg/ml in water, H3570, Thermo Fisher Scientific), DAPI (1 μg/ml in water, D3571, Thermo Fisher Scientific).

Cell culture and plasmids

MDCK cells were maintained in DMEM (21885, Thermo Fisher Scientific) supplemented with 10% foetal bovine serum (FBS; P30-3305, FBS Standard, South America, PAN Biotech) in a humidified incubator at 37°C and 5% CO_2. The origin of the MDCK wild-type and MDCK wild-type GFP-NLS cells has been previously described in Wagstaff et *al.* 2016.

MDCK *p53KO* GFP-NLS clones 6 and 14 were constructed by infecting the MDCK *p53KO* pool (Wagstaff et *al.* 2016) with lentiviral construct pGIPZ-turboGFP-NLS-Puro (Wagstaff et *al.* 2016). Selection post infection was carried out in 0.65 μg/ml puromycin. The resulting GFP-NLS labelled pool was then plated at one cell per well in 96-well plates; the clones were expanded and verified by immunofluorescence, sequencing, and Western blotting.

MDCK *p21KO* clones G5 and E9 were generated using Cas9 D10A CRISPR technology. sgRNAs against canine *CDKN1A* were designed manually following published methods (Ran *et al.* 2013). Target sequences used: 5'-CGGCAAGCCTTGCTGCCATG(AGG)-3' and 5'-TGGACAGCGAGCAGCTGCGC(CGG)-3'. sgRNAs were cloned individually into PX461 vectors (Ran *et al.* 2013) and co-transfected as a pair into wild-type MDCK cells using Lipofectamine 2000 (Thermo Fisher Scientific). The transfected cells were treated with 11 μM Nutlin-3 for 6 days to enrich for non-growth-inhibited *p21KO* cells. The pool was then plated at one cell per well in 96-well plates; the resulting clones were expanded and verified by immunofluorescence and sequencing.

To overexpress p21, p21 cDNA was amplified from a cDNA library obtained from MDCK *scribble* shRNA cells treated with tetracycline to induce *scribble* knockdown, as these cells have been shown to express high levels of p21 (Wagstaff et *al.* 2016). The resulting PCR product was introduced into doxycycline-inducible pTRIPZ-RFP-NLS-Puro (Wagstaff et *al.* 2016) with a P2A peptide bridging the two proteins to make pTRIPZ-p21-P2A-RFP-NLS-Puro. MDCK wild-type cells were infected with the final construct, selected using 0.65 μg/ml puromycin, and then plated out in 96-well plates to isolate single clones that were verified by immunofluorescence.

The dominant negative GSE-22 peptide was first described for the rat in Ossovskaya et *al.* 1996. To overexpress the dominant negative GSE-22 peptide in MDCK cells, amino acids 302-381 of canine p53 (homologous to the original rat sequence) were amplified from the MDCK cDNA library used in p21 cloning above; a forward primer carrying an adaptor with three start ATG codons and a reverse primer containing three stop codons were used to account for all three reading frames, as was done in the original publication. The resulting PCR product was introduced into doxycycline-inducible pTRIPZ-GFP-NLS-Puro with a P2A peptide bridging the two proteins to make pTRIPZ-GSE-22-P2A-GFP-NLS-Puro. MDCK wild-type cells were infected with the final construct, selected using 0.65 μg/ml puromycin to generate a pool population.

Mitomycin C (MMC) assays

On day 1, 2,500 untreated wild-type MDCK cells (labelled with GFP-NLS or unlabeled, as appropriate) were seeded per well in 24-well plates. On day 2, a second population of MDCK cells was trypsinized, and $1x10^6$ of these were incubated in suspension in 5 ml complete media containing 7.5 μg/ml MMC for 1 hour at 37°C and 5% CO_2. The cells were then washed at least three times in complete media (spinning down the cells after each wash) to reduce MMC carryover, and then 5,000 MMC-treated cells were plated on top of the untreated population. Live imaging was begun on day 3; samples were imaged every 2 hours.

Spontaneous leader assays

5,000 wild-type MDCK cells were seeded in a 24-well plate or, if immunofluorescence was to be performed at end of live imaging, in a gridded tissue culture plate (μ-Dish 35 mm Grid-500, 81166, ibidi). Approximately 48 hours later, cells with the spontaneous leader morphology were manually selected on the Nikon BioStation CT and imaged every 2 hours. Where applicable, cells at the end of live imaging were fixed in 4% PFA (15713-S, Electron Microscopy Sciences) in PBS for 10 min at RT.

Wound healing and barrier release assays

27,000-33,000 wild-type MDCK cells were seeded in the middle of a 'fence' (Aix Scientifics, http://www.aix-scientifics.co.uk/en/fences.html) placed in a 24-well plate or straight into a well of a 96-well plate (no 'fence'). If immunofluorescence was to be performed after live imaging, we used optically clear plates (μ-Plate 24 well, 82406, ibidi or CellCarrier-96, 6005550, PerkinElmer). The 'fence' was removed approximately 5 hours after seeding and the culture medium changed. Approximately 20 hours later, a P1000 pipette tip was used to generate a scratch-wound through the middle of the now-confluent monolayer and the culture medium changed. Imaging of the wound edge was started approximately 1 hour after scratching and imaged every 1-2 hours.

UV irradiation experiments

On day 1, 25,000-30,000 wild-type cells per well were plated in an optically clear 96-well plate (CellCarrier-96, 6005550, PerkinElmer). The cells were left to adhere overnight. On day 2, a scratch-wound was generated through the middle of each well in the 96-well plate using a P1000 tip and returned to the 37°C / 5% CO_2 incubator for approximately 30 min. Cells were then treated in the incubator with 3 μg/ml Hoechst 33342 diluted in complete media for 10 min. The cells were then washed three times in complete media. UV irradiation along the top half of the wound edge was performed using a 20× air objective on a Leica SP8 confocal microscope, which was set up to keep the samples at 37°C / 5% CO_2 during imaging; the bottom half of the wound was not irradiated. UV treatment settings used: 30 frames at 100% 405 nm laser with the FRAP booster on. The samples were then imaged using the BioStation CT every hour for at least 24 hours. For γH2AX staining, samples were fixed and processed 2-4 hours after UV irradiation.

Blebbistatin-induced binucleated cell (BBC) generation

On day 1, 5,000 unlabeled wild-type MDCK cells were plated per gridded dish (μ-Dish 35 mm Grid-500, 81166, ibidi). Also on day 1, 12,000 GFP-NLS labelled WT MDCK cells were incubated with 37.5 μM blebbistatin in DMSO (B0560, Merck) in a 12-well plate. 16 hours later, on day 2, the cells were washed three times in PBS and left to recover for 4 hours in complete media. The cells were then harvested by trypsinization and large clumps removed using a 20 μm filter (04-0042-2315, CellTrics). Half of the recovered cells were plated per gridded dish. Imaging was started on day 3; cells were imaged every 2-4 hours.

Immunofluorescence

Depending on the assay, cells were cultured on glass coverslips or optically clear tissue culture dishes. Cells were fixed in 4% PFA (15713-S, Electron Microscopy Sciences) in PBS for 10 min at RT, quenched for 10 min at RT in 50 mM in NH_4Cl in PBS, and permeabilized for 10 min at RT in 0.1% Triton X-100 in PBS. Samples were blocked for at least 30 min in 2% bovine serum albumin (BSA; A2153, Sigma), 2% FBS in PBS at RT. Both primary and secondary antibodies were diluted in blocking solution diluted 1:1 with PBS. Primary antibody incubations were either a minimum of 1 hour at RT or overnight at 4°C. Following 4 x 5 min washes in PBS, secondary antibodies were incubated for 1 hour at RT, then washed 4 x 5 min in PBS. Coverslips were mounted in FluorSave (345789, Merck). Optically clear dishes were either flooded with FluorSave and sealed with a coverslip or imaged directly in the last PBS wash. For immunostaining against phosphorylated proteins, fixing solution was supplemented with PhosSTOP (1 tablet per 10ml, Sigma), all PBS-based solutions were substituted with TBS, and blocking solution was substituted with 5% BSA in TBS.

Imaging and image analysis

Imaging of fixed samples was done at RT on Leica SP5 or SP8 confocal microscopes using a 40× oil objective or on the PerkinElmer Opera LX system using a 20× water objective. UV irradiation experiments were done on a Leica SP8 confocal microscope set up to keep the samples at 37°C / 5% CO_2 during imaging. All live imaging was done on a Nikon BioStation CT system at 37°C / 5% CO_2 using 10× or 4× air objectives with an imaging frequency every 1-4 hours (indicated in movie time stamps); media was changed every 2–3 days.

Mean intensities of nuclear p53 and p21 were measured using DAPI as a mask to segment the nuclear volumes in Volocity (PerkinElmer).

Cell tracking was done by marking coordinates of cell nuclei over time using MtrackJ plugin in ImageJ. Cells from an untreated / MMC-treated pair were tracked starting from 8 hours (four time points) before, until 12 hours (six time points) after contact between the two was established, thereby making coordinate 0,0 a point when the two cells meet. Coordinates of cell tracks were analyzed in Microsoft Excel.

The migration speed of scratch-wound fronts was measured in FIJI by manually drawing freehand lines outlining the wound edge at the first and final time points. If any wound edges were not parallel to the y axis, the images were adequately rotated. The median x position for each line was recorded to calculate the median x displacement in pixels, which was then divided by the duration of the experiment in hours to generate a speed value in pixels/h.

All graphs were plotted using GraphPad Prism. Figures were made using Adobe Illustrator CS6.

Statistical analysis

All statistical analysis was performed using GraphPad Prism. All p values were obtained using the Kolmogorov-Smirnov (K-S) test.

Supplementary Figures

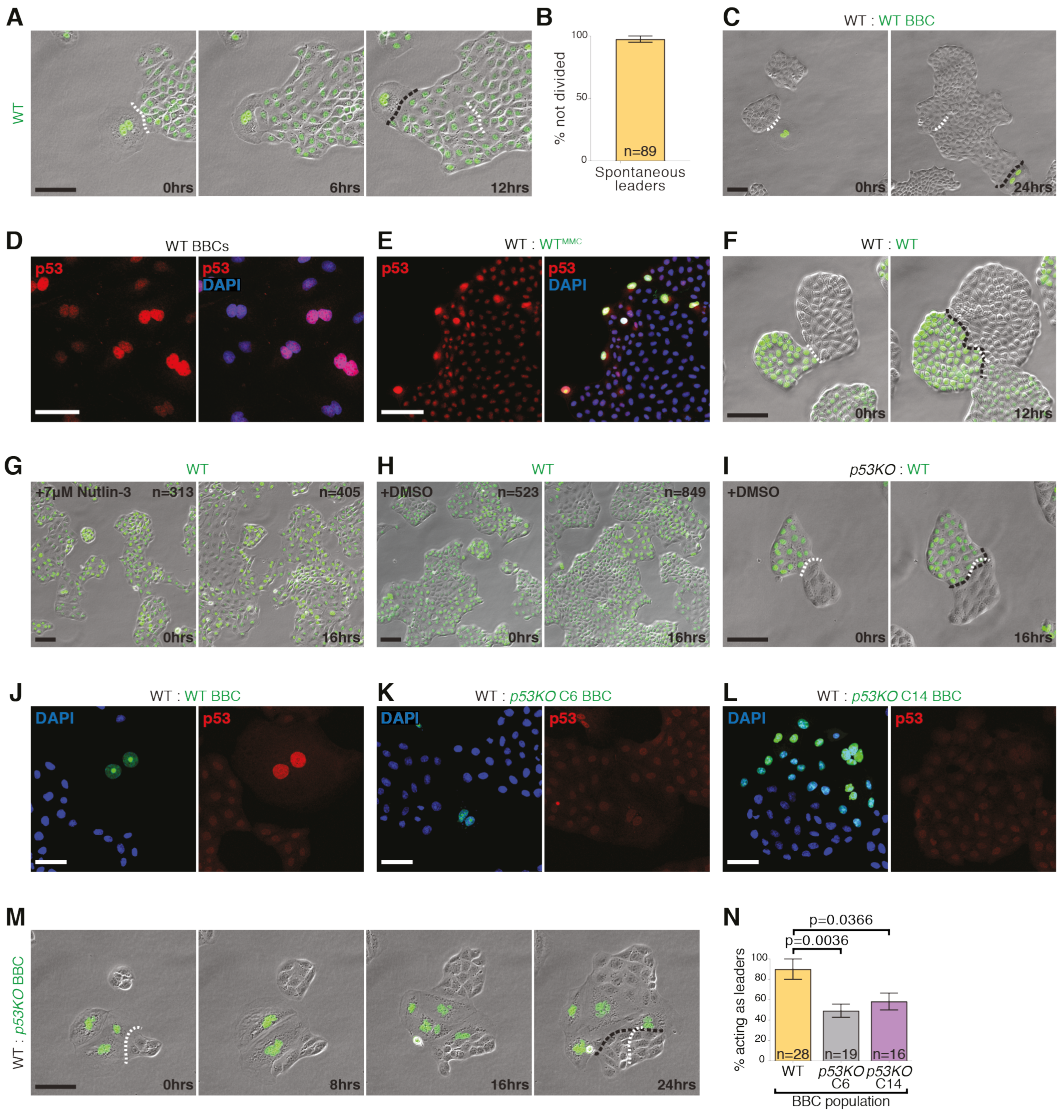

Fig. S1. Blebbistatin-induced binucleated cells (BBCs) behave as leaders and this behavior is driven by p53. (**A**) Time-course movie stills of a binucleated spontaneous leader emerging from a wild-type MDCK population that expresses nuclear GFP. (**B**) Quantification of the number of spontaneous leaders that did not divide during the course of movie acquisition. (**C**) BBCs, which had been generated from a population of wild-type cells expressing nuclear GFP, display leader behavior in the presence of unlabeled wild-type cells. (**D**) Confocal images of BBCs following p53 immunostaining show that they have elevated p53 levels compared to their mononucleated neighbors. (**E**) Confocal images of a co-culture of unlabeled wild-type cells and mitomycin C (MMC)-treated wild-type cells expressing nuclear GFP immunostained against p53. (**F**) Movie stills from co-cultures of unlabeled wild-type MDCKs and wild-type cells expressing nuclear GFP. There is no leader behavior if neither of the populations have been treated with MMC; control panels for Fig. 1F. (**G-H**) Wild-type cells expressing nuclear GFP still divide when treated with sub-lethal doses of Nutlin-3 (G), albeit at a slower rate than cells treated with the DMSO vector alone (H). (**I**) Movie stills from co-cultures of unlabeled *p53KO* MDCKs and wild-type cells expressing nuclear GFP in the presence of DMSO. There is no leader behavior in the absence of Nutlin-3; control panels for Fig. 1G. (**J-L**) Confocal images of p53 immunostaining of co-cultures of unlabeled wild-type cells and BBCs generated from cells expressing nuclear GFP, the latter being either wild-type (J) or *p53* knockout clones 6 (K) and 14 (L) (*p53KO* C6 and C14, respectively). (**M**) Movie stills from a co-culture of unlabeled wild-type cells and BBCs generated from *p53KO*

cells expressing nuclear GFP. (**N**) Quantification of the frequency of leader cell behavior of wild-type and *p53KO* BBCs in the presence of an untreated wild-type population.

n = number of cells in (B), (G), (H), and (N). Data pooled from three biological replicates in (B) and (N). Error bars = ±SEM in (B) and (N).

Here and throughout all figures:
White dashed line = initial contact point; black dashed line = final contact point. Scale bars 100μm (movie sequences) and 50μm (confocal images). P values obtained using the K-S test.

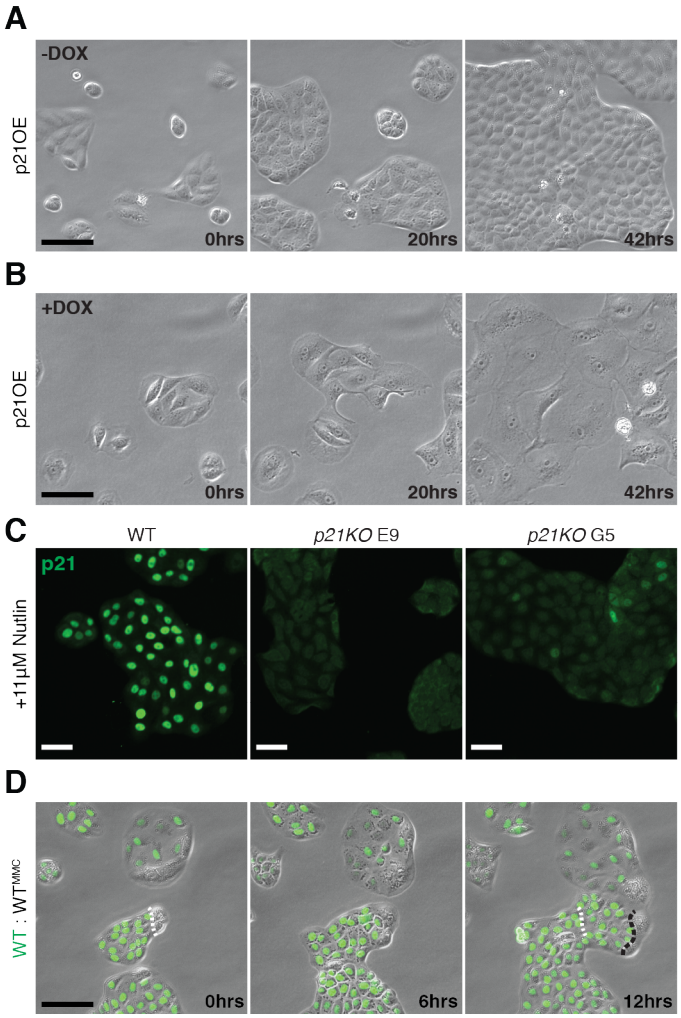

Fig. S2. Generation of cells overexpressing p21 and p21 knockout MDCKs. (**A-B**) A clonal cell line that overexpressed canine p21 (p21OE) in a doxycycline (DOX)-inducible manner was generated. Without DOX addition (A) the cells displayed normal MDCK morphology; upon addition of DOX (B) the cells stopped dividing and flattened. (**C**) Confocal images of p21 immunostaining after 24 hours of Nutlin-3 treatment of wild-type or *p21KO* clones E9 and G5. (**D**) Movie stills of co-cultures of MMC-treated unlabeled wild-type cells and untreated wild-type cells expressing nuclear GFP. Control panels for Fig. 2E.

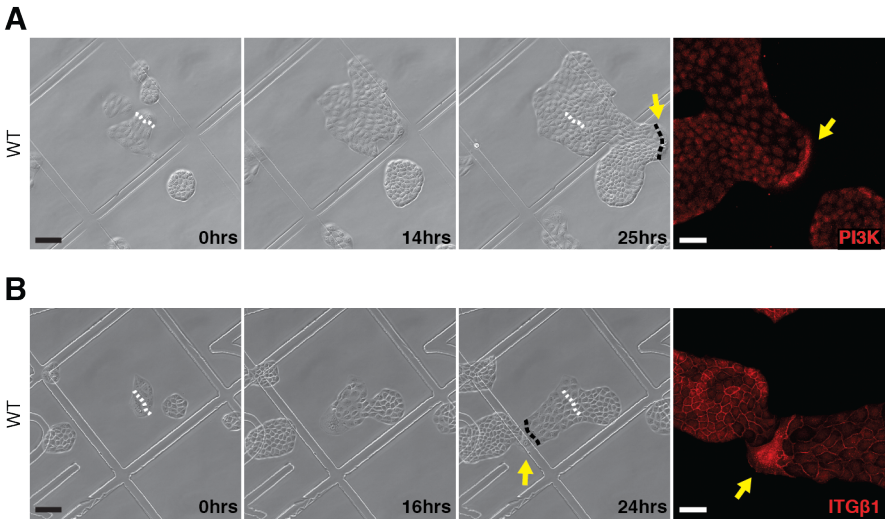

Fig. S3. Spontaneous leaders display elevation of canonical leader cell markers. (**A-B**) Movie stills (first three panels) following the migration of two spontaneous leaders (yellow arrows). Fourth panel shows confocal images of those same spontaneous leaders following immunostaining against phosphoinositide 3-kinase (PI3K) in (A) and integrin β1 (ITGβ1) in (B).

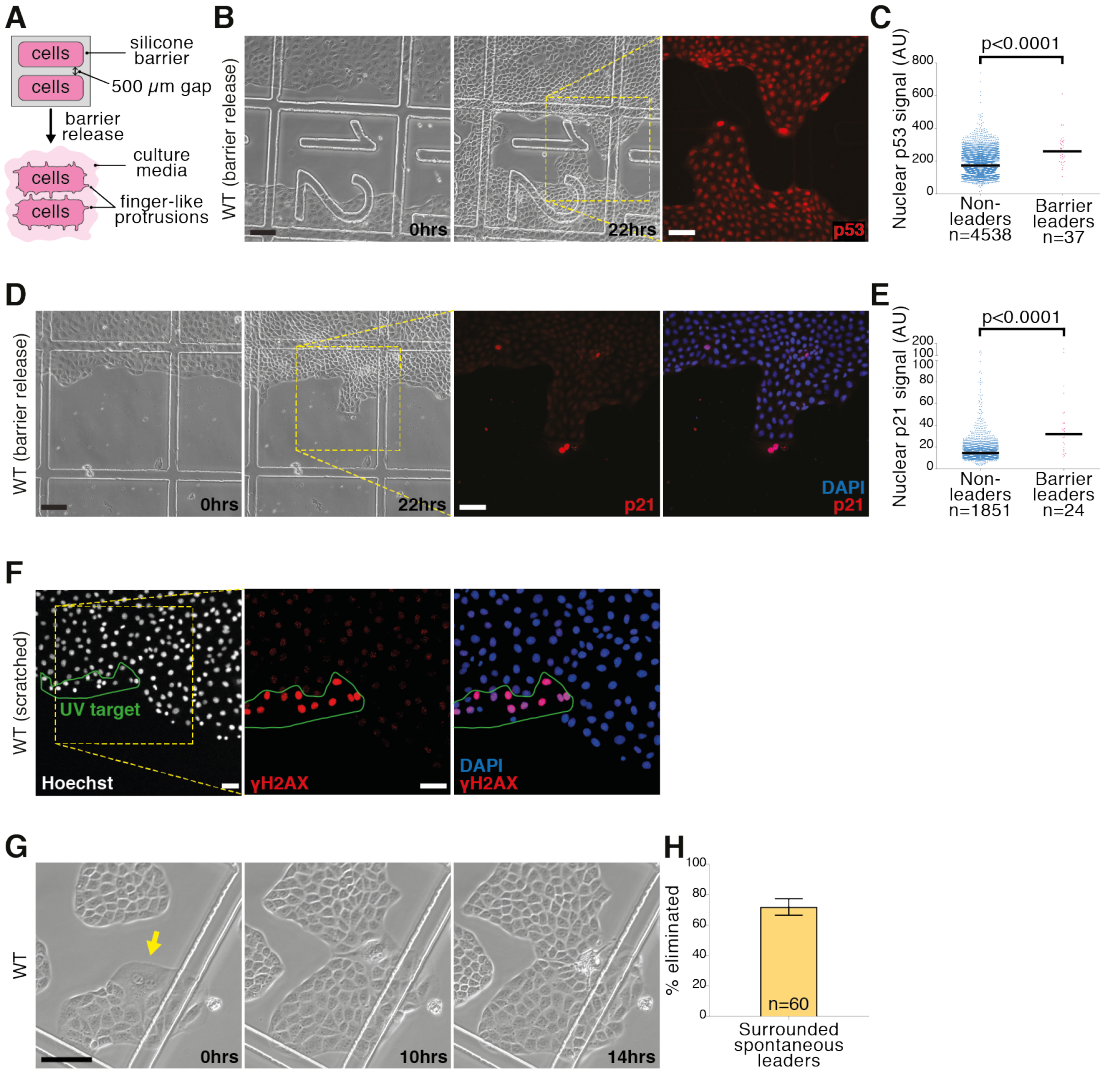

Fig. S4. Leaders generated by barrier release also display p53/p21 elevation; UV treatment that increases the speed of migration during wound healing also elevates DNA damage marker γH2AX; spontaneous leaders are mechanical losers. (**A**) Schematic of the barrier release experiment shown in (B). (**B**) Movie stills (first two panels) following the migration of leaders generated by barrier release. Last panel shows a confocal image of those same spontaneous leaders following p53 immunostaining. (**C**) Quantification of single-cell nuclear p53 intensity of barrier release-induced leaders versus surrounding non-leaders. (**D**) Movie stills (first two panels) following the migration of leaders generated by barrier release. Last two panels show confocal images of those same spontaneous leaders following p21 immunostaining. (**E**) Quantification of single-cell nuclear p21 intensity of barrier release-induced leaders versus surrounding non-leaders. (**F**) The first panel is a confocal image of a scratch-wound edge generated in a Hoechst-treated wild-type MDCK monolayer prior UV irradiation of the left half of the edge cells; the UV target region is marked using the green line. The last two panels are confocal images of a γH2AX immunostaining of the same scratch area approximately 2 hours post UV treatment. (**G**) Movie stills following the migration of a spontaneous leader (yellow arrow) that is eliminated once the local cell density increases. (**H**) Quantification of the number of spontaneous leaders that are eliminated when surrounded by wild-type neighbors.

Black bars = median in (C) and (E); n = number of cells in (C), (E), and (H). Data from one representative repeat of three biological replicates, (C) and (E), or pooled from three biological replicates, (H). Error bars = ±SEM in (H).

Movie Legends

Throughout all movies, the initial contact point is marked using a magenta asterisk.

1. A spontaneous leader emerging from a wild-type MDCK culture. (Fig. 1A)
2. A blebbistatin-induced binucleated cell (BBC) expressing nuclear GFP displays leader behavior following contact with untreated, unlabeled wild-type cells. (Fig. S1C)
3. MMC-treated wild-type cells expressing nuclear GFP become leaders when confronted with untreated, unlabeled wild-type cells (left movie). Untreated cells do not display leader behavior (right movie). (Fig. 1F and Fig. S1F)
4. In the presence of sub-lethal doses of Nutlin-3 (left movie), wild-type cells expressing nuclear GFP show leader behavior following contact with unlabeled cells lacking p53 (*p53KO*). There is no leader behavior in the absence of Nutlin-3 (right movie). (Fig. 1G and Fig. S1I)
5. Loss of p53 prevents leader behavior of MMC-treated cells expressing nuclear GFP following contact with untreated, unlabeled wild-type cells. (Fig 1I)
6. Unlabeled cells overexpressing p21 (p21OE) show leader behavior following contact with wild-type cells expressing nuclear GFP. (Fig. 2C)
7. MMC-treated, unlabeled wild-type cells become leaders when confronted with untreated wild-type cells expressing nuclear GFP (right movie) but knockout of p21 (*p21KO*) prevents this (left movie). (Fig. 2E and Fig. S2D)
8. MMC-treated cells expressing nuclear GFP show leader behavior following contact with untreated, unlabeled wild-type cells. This migration is stalled upon the addition of PI3K and Rac1 inhibitors (middle and right movies, respectively) but continues in the presence of the DMSO vector (left movie). Please note that the drug treatments are added at time = 0 hours, when the text appears in the top right corner of each movie. (Fig. 3E-G)
9. UV irradiation of cells at the wound edge (right movie) accelerates the speed of front migration, compared to a non-irradiated edge (left movie). The white line denotes initial front position; the black line denotes final front position. (Fig. 4I-K)
10. Scratch-induced leaders (cyan and magenta arrows) are often eliminated upon wound closure. (Fig. 4L)

Appendix 2: Plasmid maps

A

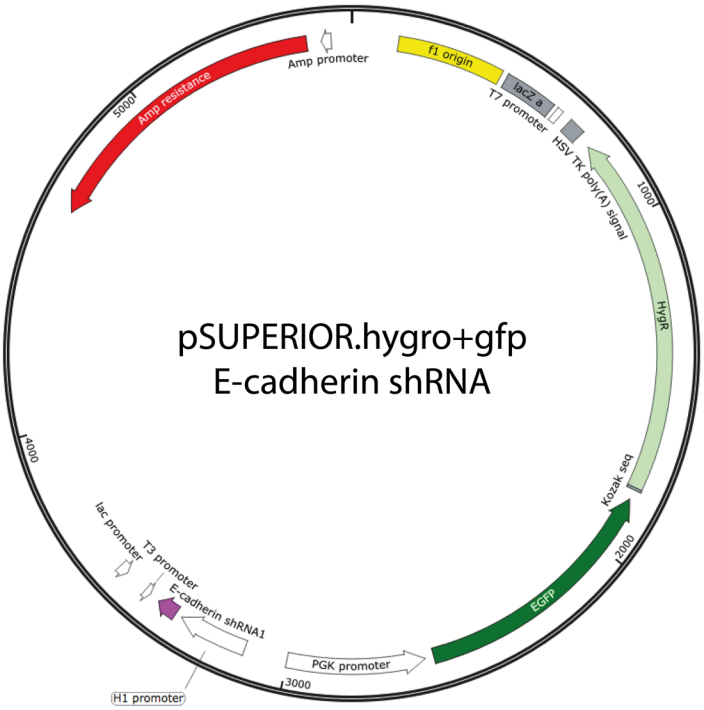

B

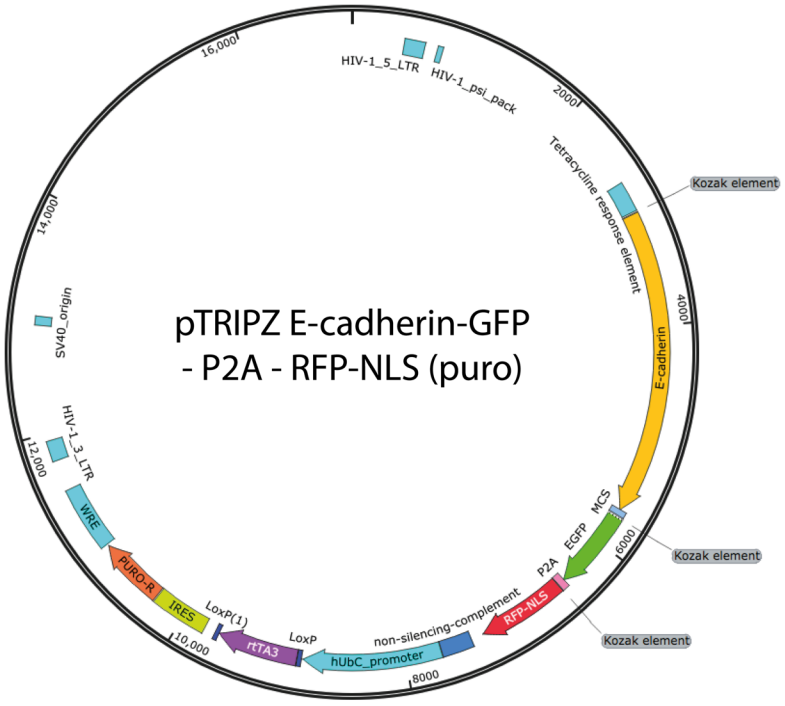

C

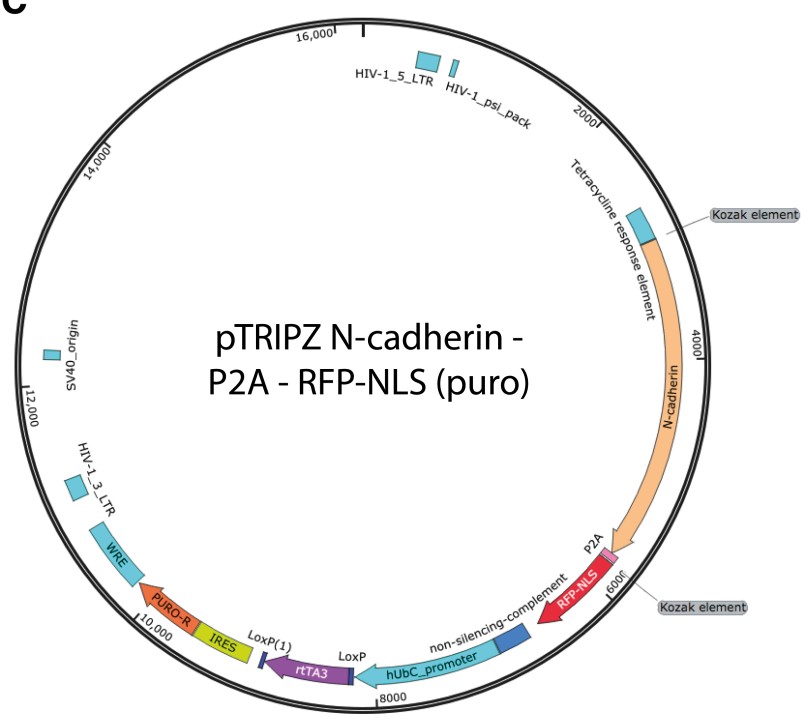
pTRIPZ N-cadherin -
P2A - RFP-NLS (puro)
16,000
HIV-1_5_LTR
HIV-1_psi_pack
2000
Tetracycline response element
Kozak element
4000
N-cadherin
P2A
RFP-NLS
6000
Kozak element
non-silencing-complement
hUbC_promoter
LoxP
rtTA3
LoxP(1)
IRES
PURO-R
10,000
WRE
HIV-1_3_LTR
12,000
SV40_origin
14,000
8000

D

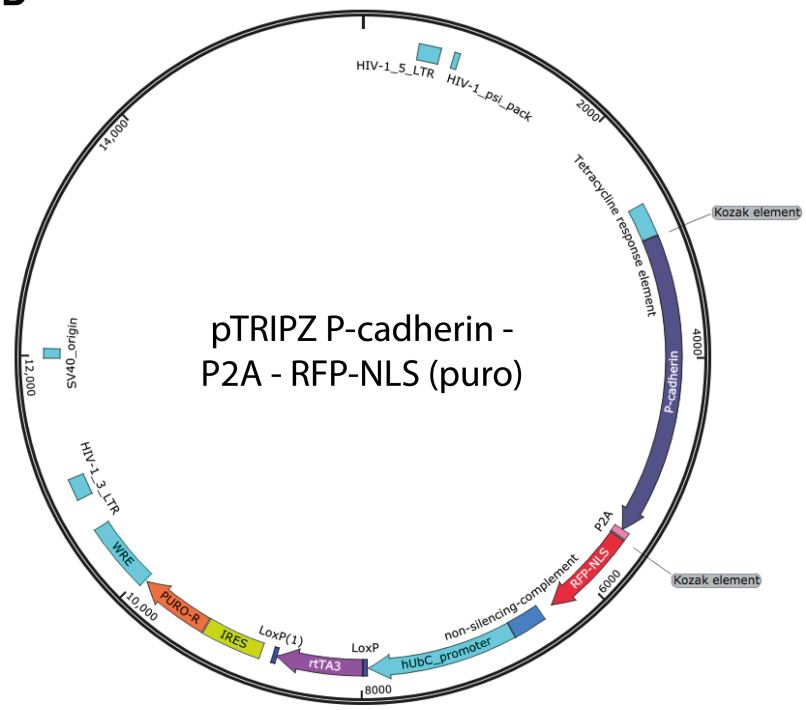
pTRIPZ P-cadherin -
P2A - RFP-NLS (puro)
HIV-1_5_LTR
HIV-1_psi_pack
2000
Tetracycline response element
Kozak element
4000
P-cadherin
P2A
RFP-NLS
6000
Kozak element
non-silencing-complement
hUbC_promoter
LoxP
rtTA3
LoxP(1)
IRES
PURO-R
10,000
WRE
HIV-1_3_LTR
12,000
SV40_origin
14,000
8000

E

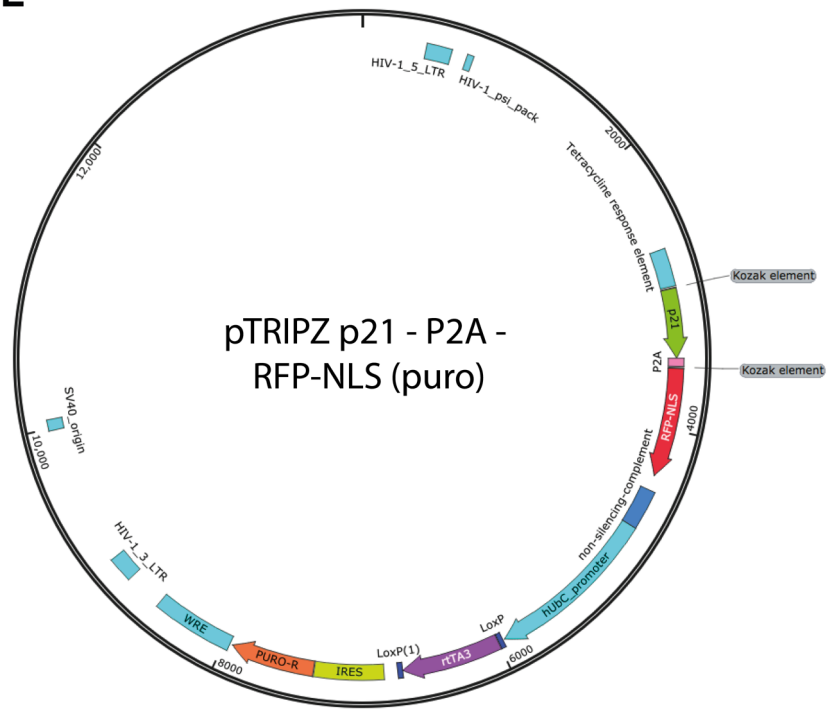
pTRIPZ p21 - P2A -
RFP-NLS (puro)
HIV-1_5_LTR
HIV-1_psi_pack
Tetracycline response element
p21
P2A
RFP-NLS
Kozak element
Kozak element
non-silencing-complement
hUbC_promoter
LoxP
rtTA3
LoxP(1)
IRES
PURO-R
WRE
HIV-1_3_LTR
SV40_origin
2000
4000
6000
8000
10,000
12,000

F

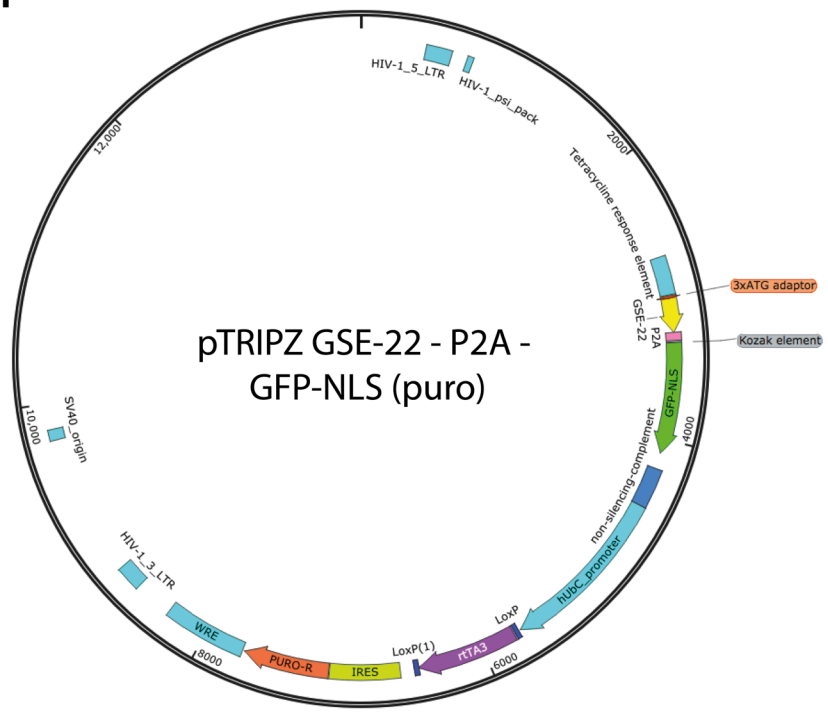
pTRIPZ GSE-22 - P2A -
GFP-NLS (puro)
HIV-1_5_LTR
HIV-1_psi_pack
Tetracycline response element
GSE-22
P2A
GFP-NLS
3xATG adaptor
Kozak element
non-silencing-complement
hUbC_promoter
LoxP
rtTA3
LoxP(1)
IRES
PURO-R
WRE
HIV-1_3_LTR
SV40_origin
2000
4000
6000
8000
10,000
12,000

G

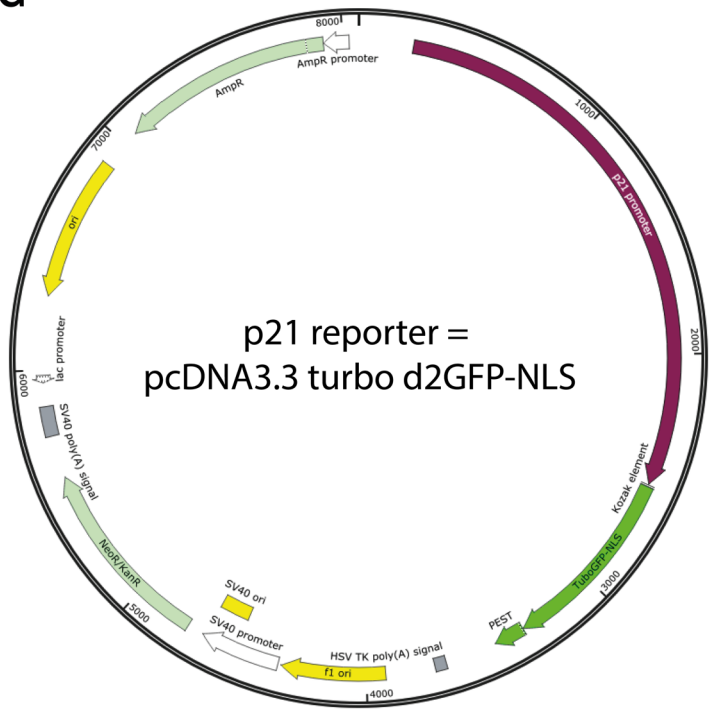
p21 reporter =
pcDNA3.3 turbo d2GFP-NLS
8000
AmpR promoter
AmpR
1000
p21 promoter
2000
Kozak element
d2GFP-NLS
3000
PEST
HSV TK poly(A) signal
4000
f1 ori
SV40 promoter
SV40 ori
5000
NeoR/KanR
SV40 poly(A) signal
6000
lac promoter
ori
7000

H

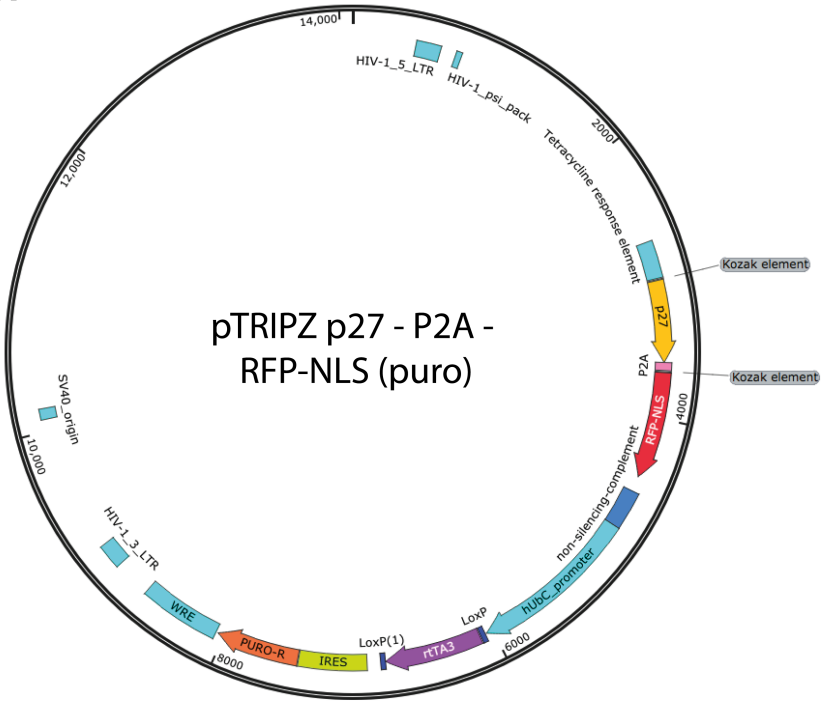
pTRIPZ p27 - P2A -
RFP-NLS (puro)
14,000
HIV-1_5_LTR
HIV-1_psi_pack
2000
Tetracycline response element
Kozak element
p27
P2A
Kozak element
RFP-NLS
4000
non-silencing-complement
hUbC_promoter
LoxP
6000
rtTA3
LoxP(1)
IRES
PURO-R
8000
WRE
HIV-1_3_LTR
10,000
SV40_origin
12,000

I

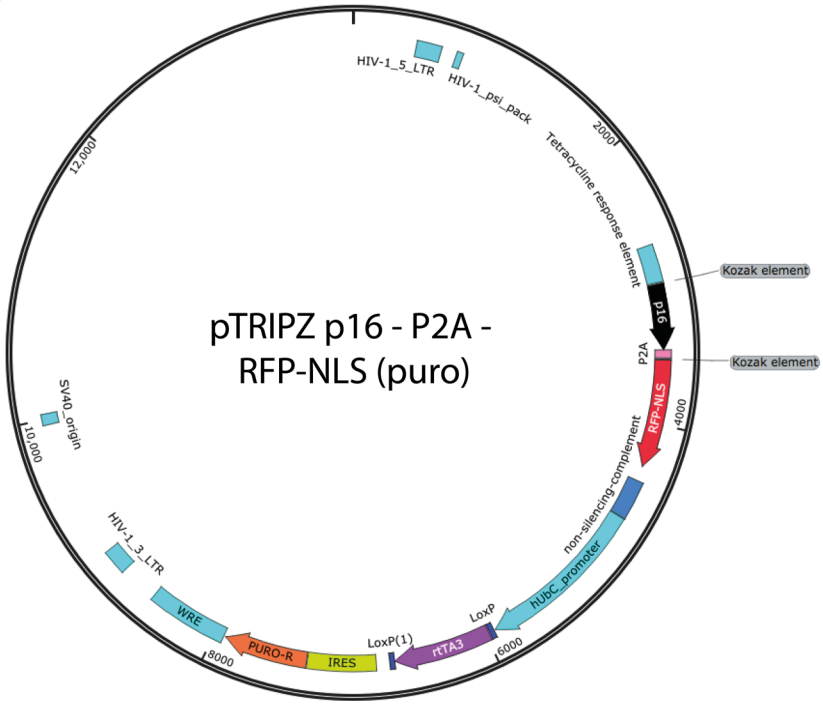
pTRIPZ p16 - P2A -
RFP-NLS (puro)
HIV-1_5_LTR
HIV-1_psi_pack
Tetracycline response element
Kozak element
p16
P2A
Kozak element
RFP-NLS
non-silencing-complement
hUbC_promoter
LoxP
rtTA3
LoxP(1)
IRES
PURO-R
WRE
HIV-1_3_LTR
SV40_origin
2000
4000
6000
8000
10,000
12,000

J

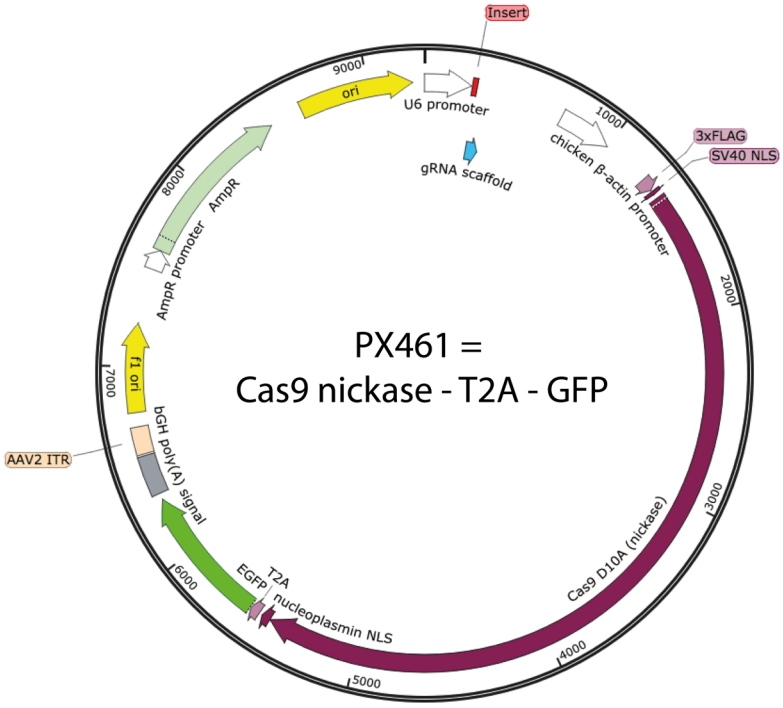
PX461 =
Cas9 nickase - T2A - GFP
Insert
ori
U6 promoter
gRNA scaffold
chicken β-actin promoter
3xFLAG
SV40 NLS
Cas9 D10A (nickase)
nucleoplasmin NLS
T2A
EGFP
bGH poly(A) signal
AAV2 ITR
f1 ori
AmpR promoter
AmpR
9000
1000
2000
3000
4000
5000
6000
7000
8000